

**Leaching of Ni-Cu-Fe-S Peirce Smith converter  
matte: Effects of the Fe-endpoint and leaching  
conditions on kinetics and mineralogy**

**RF van Schalkwyk**

*Thesis presented in partial fulfilment of the requirements for the Degree*

**Master of Science in Engineering  
(Extractive Metallurgy)**

*in the Faculty of Engineering  
at Stellenbosch University*

**Supervisor: Prof. G. Akdogan**

**December 2011**

## ***Declaration***

By submitting this thesis electronically, I declare that the entirety of the work contained therein is my own, original work, that I am the sole author thereof (save to the extent explicitly otherwise stated), that reproduction and publication thereof by Stellenbosch University will not infringe any third party rights and that I have not previously in its entirety or in part submitted it for obtaining any qualification.

11 / 11 / 2011

.....

Signature

.....

Date

*Copyright © 2011 Stellenbosch University*

*All rights reserved*

## ABSTRACT

In a first stage atmospheric leach at the Lonmin Marikana base metals refinery, nickel-copper-iron-sulphur Peirce Smith converter matte is leached in recycled electrolyte from the electrowinning section. The electrolyte contains sulphuric acid, copper and nickel sulphates, and a small amount of iron sulphate. The converter matte contains mostly nickel, copper and sulphur (typically 48 %, 28 % and 23 %, respectively), but also minor amounts (<5 %) iron and cobalt. The matte also contains platinum group elements (PGEs) and other precious metals totalling 0.2 – 0.7 % (platinum, palladium, iridium, rhodium, ruthenium, osmium and some gold). The predominant mineral phases are heazlewoodite, chalcocite and a nickel-copper alloy phase, as well as some entrained slag and spinel minerals. The purpose of the first stage leach is to extract nickel, while simultaneously precipitating copper and PGEs contained in the recycled electrolyte. Nickel, cobalt and iron are leached by acid and oxygen. Copper is precipitated by a redox reaction in which copper ions oxidise nickel from the matte. The purpose of this study was to determine the effects of key variables on the performance of the first stage leach (specifically on the removal of PGEs and copper from solution and the overall extraction of nickel) and to improve fundamental understanding of these effects.

Batch leaching tests were carried out to investigate the effects of the following factors: availability of oxygen, initial acid concentration, initial copper concentration, iron endpoint (iron content of the matte), solids/liquid ratio and stirring rate. Liquid samples were analysed with Atomic Absorption Spectroscopy (AA) to determine leaching kinetics. Characterisation of solid samples from leach tests by quantitative X-Ray diffraction (XRD) and scanning electron microscopy with an energy dispersive system (SEM-EDS) helped to improve understanding of the leaching mechanism.

The oxidative leaching mechanism entails an initial period in which the alloy phase is leached by acid and oxygen, while copper reacts with the nickel-copper-alloy and heazlewoodite phases (which react galvanically with each other) to form a chalcocite precipitate. In a second reaction period, heazlewoodite was transformed to millerite by acid leaching and the particle structure became more porous. The rate of copper

precipitation and nickel extraction were faster during the second reaction period than the first reaction period. Some copper leaching occurred once the leachable nickel (60 – 70 %) had been dissolved, provided that the solution was strongly acidic ( $\text{pH} < 2$ ).

The non-oxidative leaching mechanism entails a galvanic interaction, between the nickel-copper-alloy and heazlewoodite phases, in which nickel is leached from both phases and copper is precipitated as chalcocite. Leaching by acid was negligible in most non-oxidative tests. An initial fast period of copper precipitation was followed by a second slower period. The decrease in reaction rate can probably be linked to the decreasing availability of the nickel-copper-alloy phase. During non-oxidative leaching, the particle structure remained mostly intact. Copper precipitation kinetics under non-oxidative conditions was found to be slower than under oxidative conditions. The faster copper precipitation kinetics under oxidative conditions is most likely caused by an increase in porosity and reaction area as nickel is leached from the matte by acid and oxygen.

The initial acid concentration, solids/liquid ratio and Fe-endpoint were the most important factors determining reaction kinetics under oxidative conditions. Low initial acid concentrations (37 g/L) and a high solids/liquid ratio improved the extent of copper precipitation. Nickel extraction was enhanced by low solids/liquid ratios and high initial acid concentrations (74 g/L). Nickel extraction was significantly less (56 % less in one instance) when leaching high iron mattes (5.7 % Fe) rather than low iron mattes (< 1 % Fe). Copper precipitation was initially faster when leaching a high iron matte, but slower nickel leaching from high iron mattes led to an excess of available acid, which resulted in copper being leached. The results suggest that high iron mattes will lead to poor copper and PGE precipitation in the first stage leach and also to lower nickel extractions. Consequently, Peirce Smith converting at the plant must be carefully controlled to avoid high iron mattes.

Under non-oxidative conditions, the solids/liquid ratio and Fe-endpoint were the most important factors. The rate of copper precipitation was faster when a high iron matte was leached, so that a higher percentage copper was precipitated and more nickel was extracted from the matte.

## OPSOMMING

As 'n eerste stap in die Lonmin Marikana basis-metale veredelingsaanleg word nikkels-koper-yster-swawel Peirce-Smith-converter-mat geloog in elektroliet wat hersirkuleer word vanaf die aanleg se koper-elektroplaterings-afdeling. Die loging word by atmosferiese druk uitgevoer. Die elektroliet bevat swawelsuur, koper- en nikkels-sulfate en 'n klein hoeveelheid ystersulfaat. Die mat bevat hoofsaaklik nikkels, koper en swawel (tipies 48 %, 28 % en 23 %), maar ook klein hoeveelhede (< 5 %) yster en kobalt. Verder maak Platinum Groep Elemente (PGE's) en ander waardevolle metale (platinum, palladium, iridium, rhodium, ruthenium, osmium en goud) 0.2 % tot 0.7 % van die massa van die mat uit. In terme van minerale bestaan die materiaal hoofsaaklik uit heazlewoodite, chalcocite en 'n nikkels-koper allooifase, asook slak en spinel minerale, wat tydens Peirce-Smith-converting weens meesleuring in die mat rapporteer. Die doel van die eerste stadium loog is om nikkels op te los, terwyl koper en PGE's wat in die elektroliet voorkom presipiteer moet word. Nikkels, kobalt en koper word geloog in reaksies met suurstof en swawelsuur. Koper word presipiteer deur middel van 'n redoks reaksie waarin koper-ione nikkels in die mat oksideer. Die doel van hierdie studie was om die effekte van sleutelveranderlikes op die proses te bepaal (spesifiek hoe nikkels-loging en koper presipitasie affekteer word) en om fundamentele begrip van die veranderlikes en hul effekte te verkry.

Lot loogtoetse is uitgevoer op 'n laboratorium-skaal en die effekte van die volgende faktore is ondersoek: beskikbaarheid van suurstof, begin suurskonsentrasie, yster eindpunt (die ysterinhoud van die mat), vastestof/vloeistof verhouding en die roertempo. Vloeistof monsters geneem tydens loogtoetse is geanaliseer met behulp van Atoom Absorpsie Spektroskopie (AA) om kinetika te bepaal. Vastestof monsters is ook geneem tydens loogtoetse en kwantitatiewe X-straal diffraksie (XRD), asook skanderings-elektron-mikroskopie met 'n energie dispersie sisteem (SEM-EDS) is gebruik om die materiaal te karakteriseer en die logingsmeganisme te verduidelik.

Die oksidatiewe logingsmeganisme behels 'n aanvanklike periode waartydens die allooifase geloog word deur suur en suurstof, terwyl koper presipiteer om chalcocite

te vorm as gevolg van 'n reaksie waarin galvaniese interaksie tussen die nikkel-koper-allooi en heazlewoodite fases 'n belangrike rol speel. In 'n tweede reaksie periode is heazlewoodite gelooë deur suur om millerite te vorm. Tydens hierdie tweede fase het die partikel struktuur meer porieus geword. Die tempo van koper presipitasie en nikkel loging was vinniger tydens die tweede reaksie periode as tydens die eerste. Koper is gelooë indien die oplossing baie suur was ( $\text{pH} < 2$ ) en die loogbare nikkel (60 – 70 %) reeds opgelos het.

Die nie-oksidatiewe logingsmeganisme behels galvaniese interaksie tussen die nikkel-koper-allooi en heazlewoodite fases, wat lei tot koper presipitasie as chalcocite. Loging deur swawelsuur was onbeduidend. 'n Aanvanklike vinnige periode van koper presipitasie tydens nie-oksidatiewe toetse is gevolg deur 'n tweede stadiger periode. Die afname in reaksietempo kan waarskynlik verklaar word deur die afnemende beskikbaarheid van die nikkel-koper-allooi fase. Tydens nie-oksidatiewe loging het die partikel struktuur redelik onveranderd gebly. Koper presipitasie kinetika in nie-oksidatiewe toetse was stadiger as in oksidatiewe toetse.

Die belangrikste faktore wat kinetika in oksidatiewe toetse beïnvloed het was die suurkonsentrasie, vastestof/vloeistof verhouding en die yster-eindpunt. Lae begin-suurkonsentrasies (37 g/L) en 'n hoë vastestof/vloeistof verhouding het gelei daartoe dat meer koper uit die elektroliet herwin is. Nikkel ekstraksie was hoër indien die vastestof/vloeistof verhouding laag was en die begin suurkonsentrasie hoog (74 g/L). Nikkel ekstraksie was beduidend laer (56 % laer in een geval) wanneer hoë-yster mat (5.7 % Fe) gelooë is, eerder as lae yster mat (< 1 % Fe). Wanneer 'n hoë yster mat gelooë is, was koper presipitasie aanvanklik vinniger, maar weens stadige nikkel-ekstraksie-tempos was 'n oormaat van suur beskikbaar sodat koper uiteindelik gelooë is. PGE presipitasie is ook nadelig beïnvloed wanneer koper gelooë is en veral tydens toetse met hoë yster mat.

Die mees belangrike faktore wat nie-oksidatiewe loging beïnvloed het was die vastestof/vloeistof verhouding en die yster-eindpunt. Die tempo van koper presipitasie was vinniger in toetse met 'n hoë yster mat, sodat 'n hoër persentasie koper presipiteer het en meer nikkel opgelos het wanneer 'n hoë yster mat gelooë is.

## **Acknowledgements**

Lonmin Platinum - for providing funding and the initiative for this project

Prof. Jacques Eksteen and Mr. Nico Steenekamp from Lonmin Platinum – for providing information required for this thesis and for valuable inputs.

Prof. Guven Akdogan – for guidance, good advice and coffee.

All the administrative and technical personnel at the US Department of Process Engineering - for continuous assistance.

Family and friends – for love and support.

## Table of Contents

<b>Chapter 1</b>	<b>Introduction.....</b>	<b>1-1</b>
1.1	<b>Background .....</b>	<b>1-1</b>
1.1.1	Lonmin Marikana: Process description .....	1-1
1.1.2	First stage atmospheric leach .....	1-5
1.2	<b>Motivation .....</b>	<b>1-8</b>
1.3	<b>Document outline.....</b>	<b>1-9</b>
<b>Chapter 2</b>	<b>Literature Review.....</b>	<b>2-10</b>
2.1	<b>Introduction .....</b>	<b>2-10</b>
2.2	<b>Leaching chemistry and mechanisms .....</b>	<b>2-11</b>
2.2.1	Galvanic interaction in sulphide minerals.....	2-11
2.2.2	Thermodynamics and solution chemistry.....	2-13
2.2.3	Kinetic models .....	2-23
2.2.4	Cementation and metathesis mechanisms and kinetics .....	2-29
2.2.5	Catalysis: Iron and copper .....	2-33
2.3	<b>Key results from previous laboratory leaching investigations .....</b>	<b>2-35</b>
2.3.1	Oxidative leaching .....	2-35
2.3.2	Non-oxidative leaching.....	2-41
2.3.3	Section summary .....	2-43
2.4	<b>Chapter Conclusion.....</b>	<b>2-46</b>
<b>Chapter 3</b>	<b>Experimental methods and materials .....</b>	<b>3-47</b>
3.1	<b>Materials .....</b>	<b>3-47</b>
3.1.1	Chemical composition and mineralogy of converter matte.....	3-47
3.1.2	Milling procedure and particle size distribution .....	3-48
3.1.3	Spent composition .....	3-49
3.2	<b>Methodology.....</b>	<b>3-50</b>
3.2.1	Equipment.....	3-50
3.2.2	Experimental procedure.....	3-53



3.2.3	Analysis .....	3-54
<b>Chapter 4</b>	<b>Results and discussion.....</b>	<b>4-55</b>
<b>4.1</b>	<b>Experimental design.....</b>	<b>4-55</b>
<b>4.2</b>	<b>Oxidative leaching (OX).....</b>	<b>4-63</b>
4.2.1	Leaching kinetics and mineralogical changes with time in oxidative tests	4-63
4.2.2	Effect of solids/liquid ratio (OX).....	4-76
4.2.3	Effect of initial acid and copper concentrations (OX) .....	4-84
4.2.4	Effect of the Fe-endpoint (OX) .....	4-93
4.2.5	Effect of stirring rate (OX) .....	4-100
<b>4.3</b>	<b>Non-oxidative leaching (NOX).....</b>	<b>4-106</b>
4.3.1	Leaching kinetics and mineralogical changes with time in non-oxidative tests (NOX) .....	4-106
4.3.2	Effect of solids/liquid ratio (NOX) .....	4-117
4.3.3	Effect of initial acid and copper concentrations (NOX).....	4-121
4.3.4	Effect of the Fe-endpoint (NOX) .....	4-126
4.3.5	Effect of stirring rate (NOX).....	4-132
<b>4.4</b>	<b>Effect of oxygen .....</b>	<b>4-137</b>
<b>Chapter 5</b>	<b>Copper precipitation kinetics .....</b>	<b>5-144</b>
<b>Chapter 6</b>	<b>Conclusion.....</b>	<b>6-149</b>
<b>6.1</b>	<b>Oxidative leaching mechanism for low iron matte.....</b>	<b>6-149</b>
<b>6.2</b>	<b>Non-oxidative leaching mechanism for low iron matte .....</b>	<b>6-151</b>
<b>6.3</b>	<b>Effect of solid/liquid ratio .....</b>	<b>6-151</b>
<b>6.4</b>	<b>Effect of initial acid concentration .....</b>	<b>6-153</b>
<b>6.5</b>	<b>Effect of initial copper concentration.....</b>	<b>6-154</b>
<b>6.6</b>	<b>Effect of the Fe-endpoint.....</b>	<b>6-155</b>
<b>6.7</b>	<b>Effect of stirring .....</b>	<b>6-156</b>
<b>6.8</b>	<b>Effect of oxygen .....</b>	<b>6-158</b>

6.9	Copper precipitation kinetics.....	6-158
Chapter 7	Recommendations .....	7-160
Chapter 8	References .....	8-162
Appendix A:	Experimental procedure .....	8-168
Appendix B:	Calculations.....	8-171
Appendix C:	Repeatability.....	8-173
Appendix D:	Comparison of results not given in text.....	8-175
Appendix E:	Experimental data (concentrations, pH & XRD- analyses) .....	8-184
Appendix F:	Results from selected tests .....	8-216
Appendix H:	Size distribution of milled matte .....	8-228

## List of Tables

- Table 1-1 Typical Merensky and UG-2 concentrate for Lonmin Operations (Nell, 2004)
- Table 3-1 Chemical compositions of converter mattes used in this study. Analyses obtained with XRF.
- Table 3-2 Mineralogy of converter mattes used in this study. Analyses obtained with quantitative XRD.
- Table 3-3 Laboratory batch milling parameters
- Table 3-4 Comparison of size distribution of a batch of laboratory milled matte (Matte C), with milled material from Lonmin Marikana
- Table 3-5 Concentrations of dissolved base metals in diluted spent mixture used in tests (from AA analyses)
- Table 3-6 Concentrations of dissolved PGEs (ppm) in diluted spent mixture used in tests (Ir, and Rh from ICP-MS. Ru from ICP-OES)
- Table 4-1. List of experiments in this work
- Table 4-2. Summary of operating conditions from previously published works on batch leaching tests
- Table 4-3 Mineralogical changes during test 20. Test conditions: 74 g/L acid, 20 g/L  $\text{Cu}^{2+}$ , 150 g solids/L, 1100 rpm, 0.53 % Fe
- Table 4-4 Operating conditions for test 15 and 21
- Table 4-5. Operating conditions for tests 17, 20 and 22
- Table 4-6 Operating conditions for tests 18 and 19
- Table 4-7 Operating conditions for test 20 and 21
- Table 4-8 Operating conditions for 14, 15, 16 and 17
- Table 4-9 Mineralogical compositions of matte and residues from test 14, 15, 16 and 17
- Table 4-10 Operating conditions for test 20 and 23
- Table 4-11 Mineralogical changes during test 23. 74 g/L acid, 20 g/L  $\text{Cu}^{2+}$ , 150 g solids/L, 1100 rpm, 5.72 % Fe
- Table 4-12. Operating conditions for test 19 and 20

Table 4-13	Operating conditions for test 23 and 24
Table 4-14	Mineralogical changes in test 6. 74 g/L acid, 20 g/L Cu <sup>2+</sup> , 150 g solids/L, 1100 rpm, 0.83 % Fe
Table 4-15	Operating conditions for test 6 and 9
Table 4-16	Operating conditions for test 2 and 7
Table 4-17	Operating conditions for test 4 and 5
Table 4-18	Operating conditions for test 6 and 7
Table 4-19	Operating conditions for test 1 and 3
Table 4-20	Operating conditions for test 6 and 12
Table 4-21	Mineralogical changes during test 12. 74 g/L acid, 20 g/L Cu <sup>2+</sup> , 150 g solids / L, 1100 rpm, 5.72 % Fe
Table 4-22	Operating conditions for test 5 and 6
Table 4-23	Operating conditions for test 12 and 13
Table 4-24	Operating conditions for test 9 and 22
Table 4-25	Operating conditions for test 6 and 20
Table 4-26	Operating conditions for test 12 and 23

## List of Figures

- Figure 1-1 Simplified flowsheet of the Lonmin Marikana BMR  
(with permission of Lonmin Plc.)
- Figure 2-1 Schemating demonstrating a possible mechanism of galvanic interaction between NiS and Ni<sub>3</sub>S<sub>2</sub>
- Figure 2-2 Typical concentration and pH changes in a batch leach test of Ni-Cu-S matte with low initial acid concentration (Hofirek and Kerfoot, 1992)
- Figure 2-3 Stability diagram for Ni-Cu-S-H<sub>2</sub>O system (Redrawn from Lamya, 2007)
- Figure 2-4 Stability diagram for Cu-Ni-S-H<sub>2</sub>O system (Redrawn from Lamya, 2007)
- Figure 2-5 Stability diagram for Fe-Cu-Ni-S-H<sub>2</sub>O system  
(Redrawn from Lamya, 2007)
- Figure 2-6 Possible modes of solid state changes during leaching. Adapted from Sohn and Wadsworth (1979)
- Figure 3-1. Front view of assembled reactor setup
- Figure 3-2. Arrangement of parts within reactor vessel
- Figure 4-1. Oxidative tests to determine the effect of solids content on leaching, as well as interactions between solids content and stirring rate and between solids content and acid concentration.
- Figure 4-2. Non-oxidative tests to determine the effect of solids content on leaching.
- Figure 4-3 Oxidative tests to determine the effects of initial acid concentration and initial copper concentration
- Figure 4-4 Non-oxidative tests to determine the effects of initial acid concentration and initial copper concentration
- Figure 4-5 Oxidative tests to determine the effects of stirring rate and the Fe-endpoint.
- Figure 4-6 Non-oxidative tests to determine the effects of stirring rate and the Fe-endpoint

- Figure 4-7 Concentration changes with time in test 20.  
Test conditions: 74 g/L acid, 20 g/L  $\text{Cu}^{2+}$ , 150 g solids/L, 1100 rpm, 0.53 % Fe
- Figure 4-8 Changes in the masses of major phases with time in test 20.
- Figure 4-9 Solution pH as a function of time in test 20.
- Figure 4-10. Comparison of the number of moles nickel extracted and number of moles copper precipitated in test 20.
- Figure 4-11 PGE concentration changes with time in test 20.
- Figure 4-12 SEM images showing a residue particle from test 20
- Figure 4-13. Concentration changes with time in test 22.  
74 g/L acid, 20 g/L  $\text{Cu}^{2+}$ , 540 g solids/L, 1100 rpm, 1.05 % Fe.
- Figure 4-14. SEM images showing a particle sampled after 60 minutes in test 22.
- Figure 4-15 Comparison of metal extractions and copper precipitation during test 15 (80 g solids / L) and test 21 (150 g solids / L).
- Figure 4-16 Comparison of pH changes in test 15 (80 g solids / L) and 21 (150 g solids / L)
- Figure 4-17 Comparison of metal extractions and copper precipitation during test 17 (80 g solids/L), test 20 (150 g solids / L) and test 22 (540 g solids / L)
- Figure 4-18 Comparison of pH changes in tests 17, 20 and 22 (with respective solids contents of 80 g/L, 150 g/L and 540 g/L)
- Figure 4-19 Comparison of metal extractions and copper precipitation during test 18 (80 g solids / L) and test 19 (150 g solids / L).
- Figure 4-20. Comparison of metal extractions and copper precipitation during test 20 (74 g/L acid) and test 21 (37 g/L acid)
- Figure 4-21 Comparison of pH changes in test 20 (74 g/L acid) and test 21 (37 g/L acid)
- Figure 4-22 Comparison of metal extractions and copper precipitation during test 15, 16, 17 and 18
- Figure 4-23 Comparison of pH changes occurring in test 14, 15, 16 and 17
- Figure 4-24 Comparison of mass copper removed from solution in test 14, 15, 16 and 17
- Figure 4-25 Comparison of pH changes during test 20 (0.53 % Fe) and test 23 (5.72 % Fe)

- Figure 4-26 Comparison of metal extractions and copper precipitation during test 20 (0.53 % Fe) and 23 (5.72 % Fe).
- Figure 4-27 PGE concentration changes with time in test 23.
- Figure 4-28 Comparison of percentages Ru, Rh and Ir precipitated from solution after 240 minutes in test 6 (0.83 % Fe) and test 12 (5.72 % Fe)
- Figure 4-29 Masses of major phases as a function of time in test 20. 74 g/L acid, 20 g/L  $\text{Cu}^{2+}$ , 150 g solids/L, 1100 rpm, 0.53 % Fe
- Figure 4-30 Masses of major phases as a function of time in test 23. 74 g/L acid, 20 g/L  $\text{Cu}^{2+}$ , 150 g solids/L, 1100 rpm, 5.72 % Fe
- Figure 4-31 Comparison of metal extractions and copper precipitation during test 19 (500 rpm) and test 20 (1100 rpm)
- Figure 4-32 Comparison of pH changes during test 19 (500 rpm) and test 20 (1100 rpm)
- Figure 4-33 Comparison of metal extractions and copper precipitation during test 24 (500 rpm) and test 23 (1100 rpm)
- Figure 4-34 Comparison of pH changes in test 23 (1100 rpm) and test 24 (500 rpm)
- Figure 4-35 Concentration changes with time in test 6. 74 g/L acid, 20 g/L  $\text{Cu}^{2+}$ , 150 g solids/L, 1100 rpm, 0.83 % Fe
- Figure 4-36 Masses of major phases in the solid state as a function of time in test 6.
- Figure 4-37 Comparison of the number of moles nickel extracted and number of moles copper precipitated in test 6.
- Figure 4-38 PGE concentration changes with time in test 6.
- Figure 4-39 SEM images showing a residue particle from test 6
- Figure 4-40 Reactor boiling over during test 9 due to hydrogen evolution
- Figure 4-41 Comparison of the number of moles nickel extracted and number of moles copper precipitated in test 9.
- Figure 4-42 SEM images showing a particle from residue from test 9
- Figure 4-43 Comparison of metal extractions and copper concentrations as a function of time in test 6 (150 g solids / L) and test 9 (540 g solids / L)
- Figure 4-44 Comparison of metal extractions and copper concentrations as a function of time in test 2 (80 g solids / L) and 7 (150 g solids / L)
- Figure 4-45 Comparison of metal extractions and copper concentrations as a function of time in test 4 (80 g solids / L) and 5 (150 g solids / L)

- Figure 4-46 Comparison of metal extractions and copper precipitation in test 6 (74 g/L acid) and 7 (37 g/L acid)
- Figure 4-47 Comparison of copper precipitation and metal extractions in test 1, test 2 and test 3
- Figure 4-48 Comparison of copper precipitated (mass) in test 1, 2 and 3
- Figure 4-49 Comparison of metal extractions and copper precipitation in test 6 (0.83 % Fe) and test 12 (5.72 % Fe)
- Figure 4-50 Comparison of percentages Ru, Rh and Ir precipitated from solution in test 6 (0.83 % Fe) and test 12 (5.72 % Fe)
- Figure 4-51 SEM images of a particle sampled after 240 minutes in test 12
- Figure 4-52 Comparison of metal extraction and copper precipitation in test 5 (500 rpm) and test 6 (1100 rpm)
- Figure 4-53 SEM images of residue from test 5
- Figure 4-54 Comparison of metal extraction and copper precipitation during test 12 (1100 rpm) and test 13 (500 rpm)
- Figure 4-55 Comparison of metal extractions and copper concentrations during test 9 (non-oxidative) and test 22 (oxidative)
- Figure 4-56 Comparison of metal extraction and copper precipitation during test 6 (non-oxidative) and test 22 (oxidative).
- Figure 4-57 Comparison of percentage Ru, Rh and Ir precipitated after 240 mins in test 6 (non-oxidative) and test 22 (oxidative)
- Figure 4-58 Comparison of metal extraction and copper precipitation during test 12 (non-oxidative) and test 23 (oxidative)
- 
- Figure 5-1  $\text{Log} ([\text{Cu}^{2+}]_t / [\text{Cu}^{2+}]_0)$  as a function of time for test 6
- Figure 5-2 Shrinking core model fitted to data from test 6
- Figure 5-3  $\text{Log} ([\text{Cu}^{2+}]_t / [\text{Cu}^{2+}]_0)$  as a function of time during test 20



# Chapter 1 Introduction

---

## 1.1 Background

### 1.1.1 Lonmin Marikana: Process description

The world's largest platinum group element (PGE) reserves are located in the Bushveld Igneous Complex (BIC) in South Africa. A platinum bearing, nickel-copper-sulphide ore body, now known as the Merensky reef, was discovered in 1924 by Dr. Hans Merensky and Andries Lombaard on the farm Maandagshoek (see **Error! Reference source not found.**). Exploration of the complex led to the discovery of two more platinum rich ore bodies: the Upper Group 2 (UG2) chromitite and the Platreef (Cawthorn, 1999). Today there are many mining companies that operate in the Bushveld Igneous Complex, including the world's three largest platinum producers: Anglo Platinum, Impala Platinum and Lonmin Platinum.

At Lonmin's Marikana operations, located between Rustenburg and on the western limb of the bushveld igneous complex, ore from both the Merensky and UG2 reefs are processed. For many years, the Merensky reef was the primary source of ore from which PGEs were produced in South Africa. Processing of the UG2 reef, which underlies the Merensky reef by 40 to 140 metres in the western limb, is complicated by high concentrations  $\text{Cr}_2\text{O}_3$  (contained in chromite spinel minerals). The high gangue mineral content of UG2 ore leads to a large amount of slag forming in melting processes (Nell, 2004). Lonmin initiated mining of the UG2 in the 1970s and expansion into the UG2 deposit has gradually increased as the Merensky reef is depleted and PGE demand grows (Cawthorn, 1999).

The compositions of typical Merensky and UG-2 concentrates in the Lonmin process are shown in Table 1-1 (Nell, 2004). The large difference in Cr<sub>2</sub>O<sub>3</sub> content is evident.

Although the copper and nickel are present in much larger quantities than PGEs, operations at Lonmin Marikana are primarily aimed at producing PGEs, with winning of base metals being regarded as a secondary priority.

*Table 1-1 Typical Merensky and UG-2 concentrate analysis for Lonmin Operations (Nell, 2004)*

	Al <sub>2</sub> O <sub>3</sub> Mass %	CaO	Cr <sub>2</sub> O <sub>3</sub>	Cu+Ni	Fe	MgO	S	SiO <sub>2</sub>	PGE g/ton
<b>Merensky</b>	1.8	2.8	0.4	5.0	18.0	18.0	9.0	41.0	130
<b>UG-2 blend</b>	3.6	2.7	2.8	3.3	15.0	21.0	4.1	47.0	340

Ore is subjected to comminution and flotation processes to concentrate the valuable ore fraction, which then undergoes pyrometallurgical treatment. Gangue (SiO<sub>2</sub>, MgO, FeO and CaO) is removed with the slag during smelting in a three electrode submerged arc furnace. Smelting is followed by oxidation of the furnace matte in Peirce-Smith converters, with the purpose of lowering the iron and sulphur concentrations in the matte. Some Cr from the furnace feed reports as CrS in the furnace matte and is re-oxidised to FeCr<sub>2</sub>O<sub>3</sub> which is mostly removed with the slag during Peirce Smith converting. A Ni-Cu-S matte, which also serves as collector for PGEs, is produced and is granulated with water.

The matte commonly consists of three predominant phases: (1) A nickel sulphide phase which varies in composition, but has a primary mineral composition of heazlewoodite (Ni<sub>3</sub>S<sub>2</sub>). (2) A copper sulphide phase, consisting primarily of chalcocite (Cu<sub>2</sub>S). (3) A metal alloy phase, which mostly consists of Ni-Cu metal alloy, as well as Ni-Fe alloy. The platinum group metals have been found to concentrate in the alloy phase. In addition to the three major phases, a spinel phase in the form of (M<sup>2+</sup>)(M<sup>3+</sup>)<sub>2</sub>O<sub>4</sub> also occurs. Species that typically form are trevorite, (Ni,Fe<sup>2+</sup>)(Fe<sup>3+</sup>)<sub>2</sub>O<sub>4</sub>, and magnetite, Fe<sub>3</sub>O<sub>4</sub>.

The iron endpoint in the converting process can be defined as the residual iron content in the matte after Peirce Smith converting. Although the purpose of Peirce Smith converting is to remove iron, the iron endpoint needs to be carefully controlled.

The amount of iron which is oxidised and deported to the slag phase is proportional to the converter blow time. Plant experience indicates significant operational problems when the iron endpoint is too high (> 2 %), associated with poor nickel extraction in the first stage leach, high formation of Fe-slimes (jarosite) and severe solid-liquid separation problems, often with loss of PGEs due to entrainment in the mother liquor. When the iron content decreases below 1 %, nickel, cobalt and chromium are oxidized, leading to the formation of unwanted spinel phases and slag losses of pay-metals as oxides, as well as a depletion of the alloy phase. The formation of spinel increases slag viscosity and leads to poor separation of the matte and slag phases, leading to the loss of matte with the slag (J.J. Eksteen, 2011, Personal communication, Lonmin Platinum).

Converter matte is transferred to the base metals refinery (BMR), where it is milled in a closed circuit ball mill to a particle size of 90 % -75  $\mu\text{m}$ . Sherrit Gordon technology is used to selectively extract the different base metals from the matte and to produce nickel sulphate crystals, copper cathodes and a high grade PGE concentrate. Figure 1-2 shows a flowsheet of the Lonmin Marikana base metals refinery.

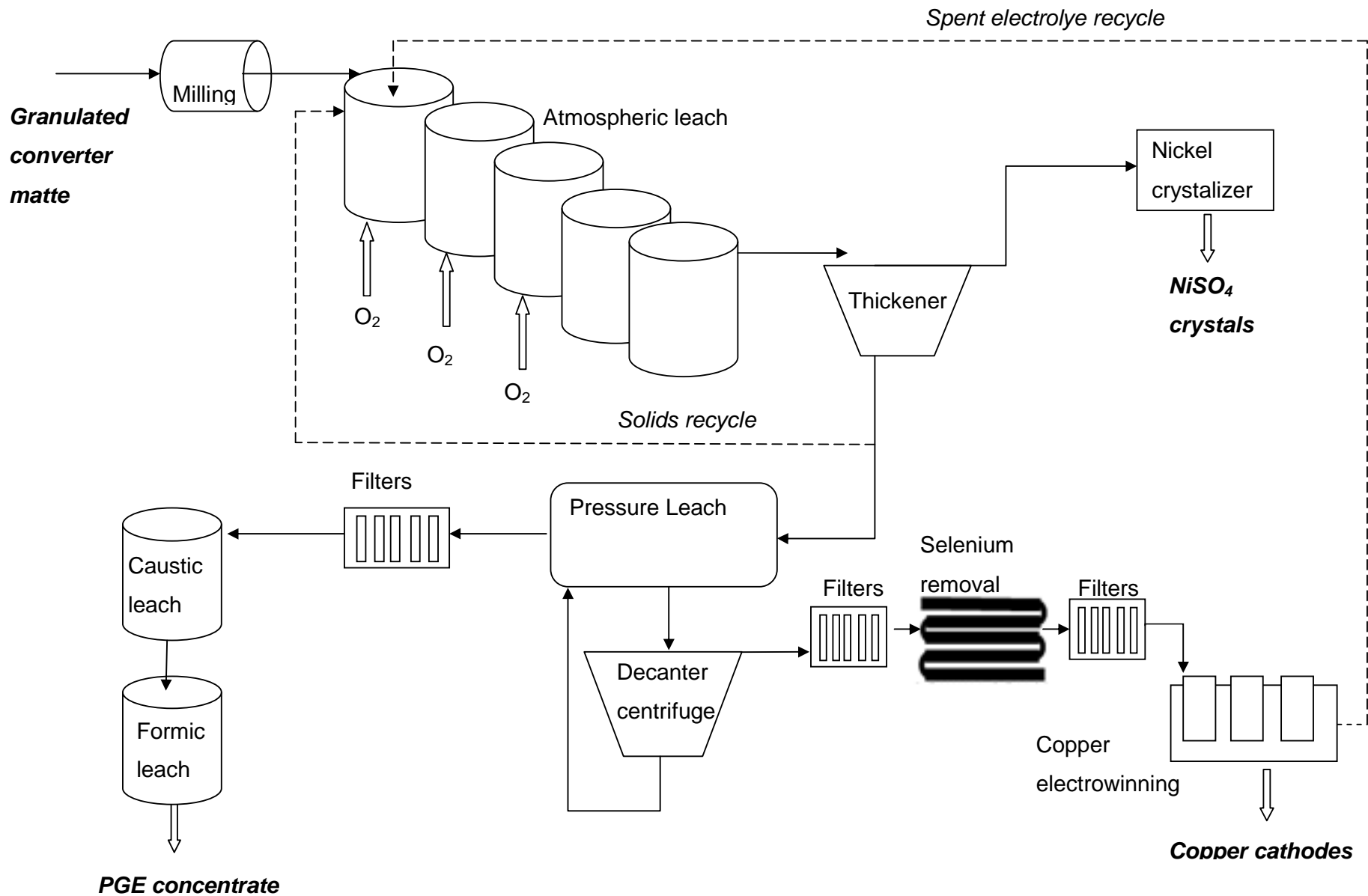


Figure 1-1 Simplified flowsheet of the Lonmin Marikana BMR (with permission of Lonmin Plc.)

The primary objective of the first stage leach is the dissolution of nickel to produce a concentrated copper and PGE containing solid residue. Cobalt and the remaining iron in the matte are also dissolved in the first stage leach. Spent electrolyte, which is recycled from the copper electrowinning section, contains sulphuric acid and dissolved nickel sulphate and copper sulphate, as well as some dissolved iron sulphate. Both sulphuric acid and  $\text{Cu}^{2+}$ -ions are utilised to dissolve metals by means of oxidation. In the process, copper that was not recovered in the copper electrowinning section is transported to the solid phase and thus recycled. In addition, Rh, Ru and Ir are found in spent and needs to be recovered by cementing / precipitating it on matte. The PGEs appear in solution due to 2<sup>nd</sup> and 3<sup>rd</sup> stage pressure leaches of the 1<sup>st</sup> stage leach residue. Recent work on pressure leaching at the Marikana plant was done by Dorfling et al. (2011).

The leach solution and solid residue from the first stage leach are separated in a thickener.  $\text{NiSO}_4$  crystals are produced from the liquid phase. The solid residue is transferred to autoclaves where copper is dissolved under pressure with sulphuric acid. Copper cathodes are produced in the electrowinning section from the autoclave leach liquor. The solid residue from the pressure leaching stage is subjected to a high pressure caustic leach to remove selenium, tellurium, arsenic and sulphur and an atmospheric formic leach to remove the remaining iron and nickel, thus producing a PGE concentrate.

### **1.1.2 First stage atmospheric leach**

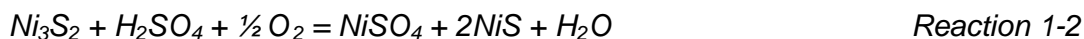
The first stage atmospheric leach at the Lonmin Marikana BMR is the focus of this project. The atmospheric leach consists of five continuously stirred tank reactors (CSTRs) in series. The purpose of the atmospheric leach is the dissolution of nickel from the granulated matte, with the simultaneous precipitation of copper from recycled spent electrolyte. Rhodium, ruthenium and iridium are assumed to follow the same behaviour as copper in the first stage leach (Steenekamp & Dunn, 1999). Platinum, palladium and gold are not leached in acidic sulphate media used in the first stage atmospheric leach or the subsequent pressure leach. Approximately 70 %

- 80 % of the nickel in the feed is usually dissolved, while copper is completely removed from solution.

Leaching takes place at temperatures of 75 – 85°C. Oxygen is required for acid leaching reactions and is sparged into the first three tanks in a decreasing relation of 60:30:10. The last two non-oxidative tanks provide residence time for copper removal from solution.

The chemistry involved with the leaching system is complex and will be discussed in more detail in Section 2.2. However, the following stoichiometry is generally used to describe the most important chemistry in the leach (Fugleberg et al., 1995: Reaction 1-1. Hofirek & Kerfoot, 1992: Reactions 1-2, 1-3, 1-4). Leaching of nickel takes place from both the sulphide and metal-alloy phases via an oxidative and non-oxidative mechanism: In the oxidative case, nickel is directly attacked by sulphuric acid and oxygen as shown in reactions 1-1 and 1-2.

Direct acid attack:



In the non-oxidative case, copper from solution is exchanged with nickel in the alloy phase (cementation, reaction 1-3) or with nickel in the sulphide phase (metathesis, reaction 1-4).

Cementation and metathesis:



Because of the acid consumed in reaction 1-1 and reaction 1-2, the pH level of the leaching solution will be slightly higher in each of the consecutive tanks. The pH level increases from approximately 0 in the first tank, to approximately 3 or 4 in the last tank.

In the operation of the first stage leach, the copper and acid in the spent, as well as the fresh converter matte entering the system can be regarded as the reactants. As such, the composition of the spent (acid and copper content) and the composition and mineralogy of the matte are important operating variables that will determine the ability of the first stage leach to operate optimally.

The mineralogical composition of the matte (mass relation between sulphides:alloy:spinel) has empirically been found to be linked to the iron endpoint (Sulphides : Alloy : Spinel) (J.J Eksteen, Personal communication, Lonmin Platinum; Thyse et al. (2010)) so that the iron endpoint consequently serves as an indicator of the matte leaching characteristics. In addition, the amount of iron in the matte will determine the amount of iron dissolved in the leaching circuit. It is suspected that variations in the Fe-endpoint can lead to inconsistent leaching behaviour, poor nickel recovery and incomplete precipitation of  $\text{Cu}^{2+}$  and platinum group elements (PGEs). Due to the exothermic nature of leaching reaction, temperature control is also closely linked to reaction rates and might be influenced by the iron endpoint.

In the case of spent electrolyte, the mode of operation is constrained by the chemistry of the copper electrowinning section. In the copper electrowinning section, copper is removed from solution and acid is generated in a one mole : one mole basis; thus two modes of operation are possible: a high copper/low acid mode and a low copper/high acid mode. In order to determine which mode is preferable, an understanding of the effects of copper and acid concentration on the complex chemistry in the atmospheric leach is required.

If the effects of the iron endpoint and spent composition are understood, as well as the interaction between them, it might be possible to improve control of the first stage leach, either by adapting the leaching conditions or by controlling the iron endpoint at a suitable level. Other operating conditions that might be adapted include:

1. The acid concentration, by adding extra fresh acid
2. The distribution of  $\text{O}_2$  amongst the tanks
3. The solid to liquid ratio, by increasing or decreasing the amount of thickener underflow which is recycled to the first tank

## 1.2 Motivation

The variable nature of ores in the mining industry leads to the challenge that continuous processes are operated with materials that are constantly changing in composition. A control strategy for the oxidative and non-oxidative steps of the first stage leach at the Lonmin Marikana BMR will be focused on operating conditions such as the mineralogy of matte (and the Fe-endpoint), as well as acid and copper concentrations and the availability of oxygen, to ensure that the primary goals of the first stage leach (nickel leaching, copper removal from solution and acid consumption from solution) are met.

This work is aimed at determining the importance of the iron endpoint, the acid concentration, the copper concentration and the availability of oxygen on the rates of metal leaching and copper removal reactions. Secondly the work aims to gain fundamental understanding into the mineralogy and solid state mechanisms operative during leaching. Thirdly, the work will highlight some aspects that should be taken into consideration if a kinetic model is constructed to describe the system. This knowledge will serve to improve fundamental understanding of the first stage leach and to improve control of the process.

The following key questions were identified:

1. What mechanisms (in terms of chemical reactions and mineralogical changes), are predominant during oxidative leaching, as well as non-oxidative leaching?
2. How does the rate of copper precipitation compare to the rate of acid leaching during oxidative leaching?
3. What is the effect of acid concentration on reaction kinetics?
4. What is the effect of copper concentration on reaction kinetics?
5. How does the Fe-endpoint influence reaction kinetics?
6. What is the effect of solid/liquid ratio and stirring rate on the rates of chemical reactions, specifically on the rate of copper precipitation?



## 1.3 Document outline

A review of literature relevant to the leaching of Ni-Cu-S mattes will be given in Chapter 2. The experimental methods used to address the problem statement will be discussed in Chapter 3. In Chapter 4, the effects of operating conditions on reaction kinetics and mineralogy will be discussed, along with the importance of these effects on the oxidative and non-oxidative sections of the first stage leach. The mechanisms operative (in terms of reaction mechanisms and solid state changes) during oxidative and non-oxidative leaching will also be discussed. Chapter 5 will give an introduction to kinetic modelling of the leaching system and reaction rate constants which were calculated for copper precipitation in selected tests. The conclusions from the study will be discussed in Chapter 6 and recommendations for further work are made in Chapter 7.

## Chapter 2 Literature Review

---

### 2.1 Introduction

In Section 2.2, some of the fundamental concepts underlying the leaching Ni-Cu-S mattes will be discussed. Pourbaix diagrams are commonly used to explain and predict the most stable aqueous and solid phases in leaching systems at different conditions. As these diagrams reflect thermodynamic equilibrium at the end state after a reaction, the two limiting features of Pourbaix diagrams are (1) that they give relatively little information with reference to meta-stable phases in the solid phase and (2) that they give no information on reaction kinetics. In order to aid understanding of the leaching chemistry and stable and meta-stable phases that form during leaching, galvanic interaction between mineral phases in the matte will be discussed in Section 2.2.1. In Section 2.2.2, Pourbaix diagrams and information from literature will be used to discuss the stoichiometry of Ni-Cu-S matte leaching and the reactions that might take place at different solution conditions (in terms of pH, Eh and available reactants). Possible kinetic models will be discussed in Section 2.2.3, while the cementation reaction and catalytic effects during leaching will be more closely investigated in respectively Sections 2.2.4 and 2.2.5.

In Section 2.3 results from previous laboratory investigations will be discussed. These investigations often focus on the effects of operating conditions, such as the initial acid and copper concentrations, on leaching kinetics.

The chapter will conclude with Section 2.4, which gives an overview of the preceding sections.

## 2.2 Leaching chemistry and mechanisms

### 2.2.1 Galvanic interaction in sulphide minerals

Peters (1984) and Hiskey and Wadsworth (1981) reviewed many of the electrochemical processes in the leaching of metal sulphides. Sulphide minerals are known to exhibit appreciable electronic conductivity. Hiskey and Wadsworth (1981) offer two contributing factors for this. Firstly, sulphides tend to be covalent in nature, resulting in non-localisation of charge and increased conductivity. Secondly, many sulphides have the ability to form non-stoichiometric compounds, with the result of increased conduction via electron holes or excess electrons.

The driving force behind a leaching reaction is the potential difference between the solid and the liquid phase (Holmes and Crundwell, 1995). The solution has a higher redox potential and consequently oxidises solid species with a lower redox potential. Due to their semi-conducting nature, charge transfer between sulphide phases in a mineral matrix is also possible, so that a constant mixed potential can be established throughout the solid. Since the potential difference between species in the solid phase and in solution is the driving force for leaching reactions, it follows that mineral phases that form galvanic couples in the solid phase will influence one another in terms of leaching behaviour.

In a galvanic couple, the mineral species with a lower redox potential will assume anodic behaviour, while the mineral species with a higher redox potential will assume cathodic behaviour, leading to enhanced leaching rates in the anodic mineral, with passivation of the cathodic mineral. This explains the preference for metals and alloys to be leached before sulphides. Provis et al. (2003) showed that galvanic couples exist between heazlewoodite and more highly oxidised sulphide phases, leading to slow leaching kinetics for other phases while heazlewoodite is still present in the material. A possible mechanism for this interaction is shown Figure 2-1. NiS has a higher potential when compared to the standard hydrogen electrode (V vs SHE) than Ni<sub>3</sub>S<sub>2</sub>, which means that the oxidation of Ni<sub>3</sub>S<sub>2</sub> is more favourable than the oxidation of NiS.

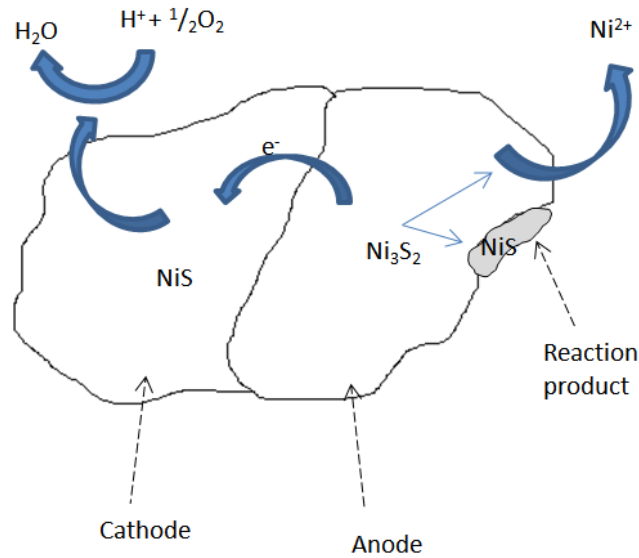


Figure 2-1 Schematic demonstrating a possible mechanism of galvanic interaction between NiS and Ni<sub>3</sub>S<sub>2</sub>

Galvanic interaction plays an important role in the leaching of Ni-Cu-S mattes not only in terms of leaching kinetics, but also in terms of the stabilisation of meta-stable phases. The dissolution of pure Ni<sub>3</sub>S<sub>2</sub> and Cu<sub>2</sub>S in sulphuric acid have been shown to be stepwise processes through a series of intermediates. (Rademan et al. (1999); Hiskey and Wadsworth (1981); Muir and Ho, (1996, 2006)) It has also been shown that the same steps are followed when Ni-Cu-S mattes are leached, with the onset of leaching for each intermediate phase corresponding to a stepped increase in the potential at which leaching takes place, which can be explained from the preceding discussion on the mixed potential of the solid phase. The complex leaching reactions that result from the formation of meta-stable phases are discussed further in Section 2.2.2.

The magnitude of a galvanic interaction is influenced by the potential difference between the mineral phases (the cell emf), as well as kinetic factors such as the resistance to conduction at the interface between the two phases (Hine, 1985). Holmes and Crundwell (1995) showed that the semi-conducting properties of minerals strongly affect the magnitude of galvanic interaction and consequently the rate of leaching.

Muir & Ho (1996) investigated the leaching behaviour of mattes with different compositions from seven different refineries around the world. It was found that the electrochemistry of the matte was modified in the presence of copper and alloy. Alloy was the easiest phase to leach from the matte and the reaction takes place at a lower potential than the leaching of Ni-S phases. The potential at which anodic dissolution of the alloy took place was higher in mattes with a larger copper content. Consequently, the ability of matte to cement copper from solution was decreased with increased copper content in the matte.

The mineral environment strongly influences galvanic interaction, but might also have other effects on kinetics. Linge (1976) showed that the leaching kinetics of copper from a chalcopyrite mineral concentrate was significantly influenced by the mineral environment of the chalcopyrite, but suggested that variation in leaching rates with varying mineral mixtures was caused by changes in the diffusivity within chalcopyrite lattice, rather than galvanic interaction.

## **2.2.2 Thermodynamics and solution chemistry**

The work of Hofirek and Kerfoot (1992) relates to the Rustenburg Base Metal Refiners. The description given by Hofirek and Kerfoot (1992) of the leaching chemistry is often cited in literature. The alloy and sulphide phases of the Ni-Cu-S matte are magnetically separated at the Rustenburg Base Metal Refiners and only the sulphide fraction is processed in the first stage leach. Hofirek and Kerfoot (1992) found that three stages, defined by the solution pH, were present when the matte is leached with an  $\text{H}_2\text{SO}_4\text{-CuSO}_4$  solution under oxidative conditions. Figure 2-2, which was adapted from Hofirek and Kerfoot (1992), shows the concentration changes in solution during a batch leaching experiment. The reaction stages are defined by the solution pH.

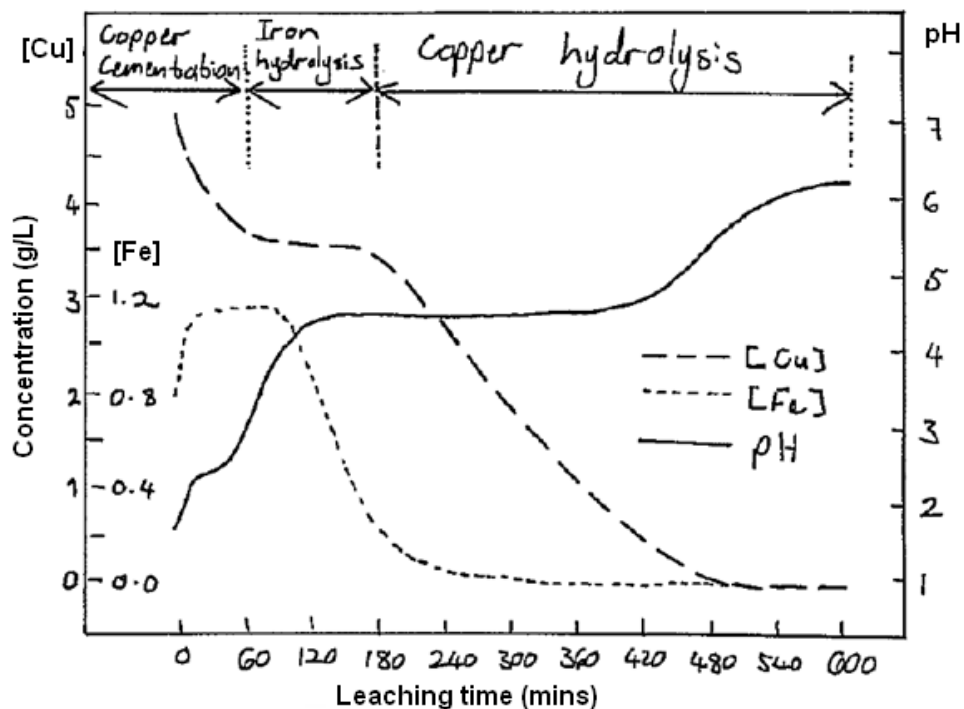


Figure 2-2 Typical concentration and pH changes in a batch leach test of Ni-Cu-S matte with low initial acid concentration (Redrawn, Hofirek and Kerfoot, 1992)

During the first stage of leaching ( $\text{pH} < 2.5$ ), nickel is dissolved from the matte via reaction with acid, while exchange reactions of nickel with copper lead to further dissolution of nickel with the simultaneous removal of copper from solution. During this stage,  $\text{Cu}_{1.96}\text{S}$ ,  $\text{NiS}$  and  $\text{Ni}_7\text{S}_6$  are formed as reaction products. The leaching reactions consume acid, which leads to a rise in the solution pH. Iron hydrolysis takes place in the pH range between 2.5 and 4.5, while any remaining copper will be removed from solution due to hydrolysis in the pH range of 4.5 – 6. The products of iron hydrolysis and copper hydrolysis are respectively ferric hydroxide  $\text{Fe}(\text{OH})_3 \cdot x\text{H}_2\text{O}$  or basic ferric sulphate  $\text{Fe}(\text{OH})\text{SO}_4$  and cupric sulphate  $\text{Cu}_3(\text{OH})_4\text{SO}_4$ .

Although significant dissimilarities can be found when comparing chemical mechanisms proposed by different authors in literature, the sequence described above is generally applicable and agrees well with predicted chemistry from Pourbaix diagrams. The rest of this chapter will give a more detailed discussion on the reactions operative at different solution conditions, as published in literature.

Pourbaix diagrams for Ni-Cu-S, Cu-Ni-S and Fe-Ni-Cu-S systems are respectively shown in Figure 2-3, Figure 2-4 and Figure 2-5. These diagrams were produced by Lamy (2007), using HSC software which was written by Roine (2002). Each diagram shows the predominant species (containing the main element) that will be found at a specific solution Eh (redox potential) and solution pH. The solution Eh, can be defined as the ability of the solution to remove electrons from species, or to act cathodically in electrochemical reactions. It should be noted that the predominant species at a set of conditions only indicates the most thermodynamically stable phase. Other phases might still be present and kinetic constraints might lead to completely different phases forming.

During the early stages of the leach, the leaching of metal constituents by sulphuric acid are predominant, while copper from solution can replace nickel and iron in the matte in exchange reactions. Figure 2-3 shows the predominance areas for Ni-containing species.

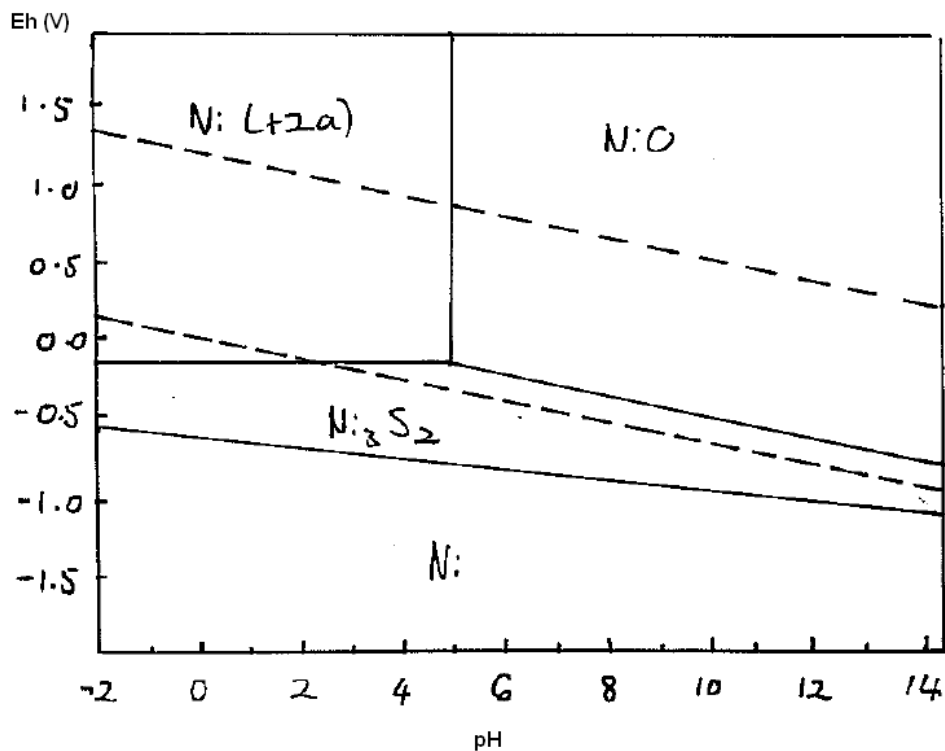
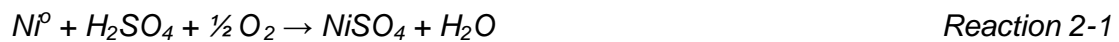


Figure 2-3 Stability diagram for Ni-Cu-S-H<sub>2</sub>O system at 80 °C (Redrawn, Lamy, 2007)

It can be seen that the dissolution of Ni from both the sulphide and the alloy phase is favoured under oxidative conditions ( $E_h > 0$ ) at a low solution pH ( $< 4.8$ ), where aqueous  $Ni^{2+}$  is the most predominant phase. Metallic nickel, being predominant at lower solution redox potentials, can be seen to be less stable under oxidative conditions than heazlewoodite. Therefore the alloy phase will be more subject to anodic dissolution than the sulphide phase.

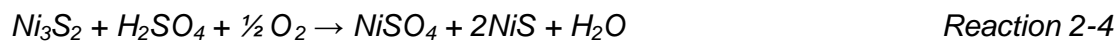
Leaching of nickel from the alloy phase takes place according to reaction 2-1. Fugleberg et al. (1995):



In the absence of oxygen, dissolution of of the nickel from the alloy can take place according to reaction 2-2, while dissolution from the sulphide phase can take place according to reaction 2-3. (Lamya, 2006)

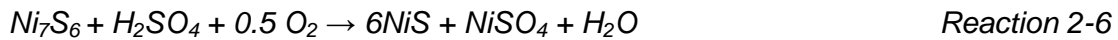
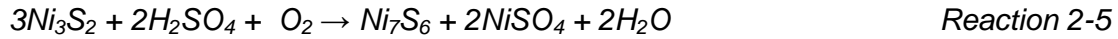


In the presence of oxygen, leaching of the nickel-sulphide phase is generally accepted to proceed according to reaction 2-4, with millerite forming as an intermediate product. (Llanos et al., 1974; Plasket and Romanchuk, 1978; Hofirek and Kerfoot, 1992; Fugleberg et al., 1995)

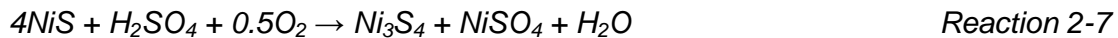




Hofirek and Kerfoot (1992) further noted that reaction 2-4 is an overall reaction that proceeds through the formation of godlevskite as an intermediate, with the complete reaction sequence given by reactions 2-5 and 2-6.



Fugleberg et al. (1995) noted that millerite can be converted to polydymite ( $Ni_3S_4$ ) under highly oxidative conditions (reaction 2-7).

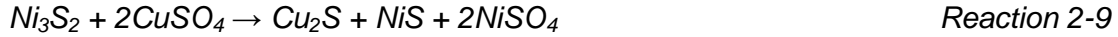


Plasket and Romanchuk (1978) also suggested that the direct dissolution of millerite (NiS) can proceed under highly oxidising conditions:

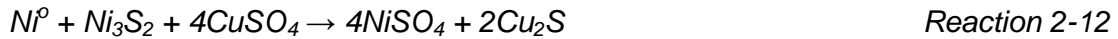


Dutrizac and Chen (1987) investigated pressure leaching of Ni-Cu mattes and found that millerite was not formed as an intermediary, but only found polydymite in a leach residue. Rademan et al. (1999) investigated the chemical reactions and mineralogical changes operative in the acid-oxygen pressure leach process at Impala Platinum, in order to clarify the mechanisms operative when leaching sulphide minerals. Rademan et al. (1999) showed that the mineral with the highest degree of symmetry in its structure will have the lowest free energy of formation and will exhibit the most resistance to leaching. Nickel and copper were found to be leached sequentially from the sulphide lattice, to form compounds with decreasing Ni:S and Cu:S ratios. For nickel, the series of intermediates were found to be  $Ni_3S_2$ - $Ni_6S_7$ -NiS- $Ni_3S_4$ .

Being more noble than nickel, copper from solution can exchange with nickel in the nickel sulphide matrix or with nickel from the alloy in respectively metathesis (reactions 2-9 and 2-10) and cementation reactions (reaction 2-11).



Rademan et al. (1999) suggested that the galvanic couple existing between the nickel alloy and the nickel sulphide phase might lead to a reaction of the following form:



Reactions 2-9 to 2-12 are responsible for the dissolution of nickel and the simultaneous removal of copper from solution. Cementation and metathesis will further be discussed in Section 2.2.4.

Copper leaching is undesirable in the atmospheric leach, but Figure 2-4 shows that metallic copper and  $Cu_2S$  can become unstable under oxidative solution conditions and low pH. Rademan et al. (1999) found that the following sequence of intermediates formed when copper sulphides are leached:  $Cu_2S$ - $Cu_{31}S_{16}$ - $Cu_{1.8}S$ - $CuS$ . The formation of  $Cu_{1.75}S$  and  $Cu_{1.95}S$  as intermediates have also been reported by Llanos et al. (1974).

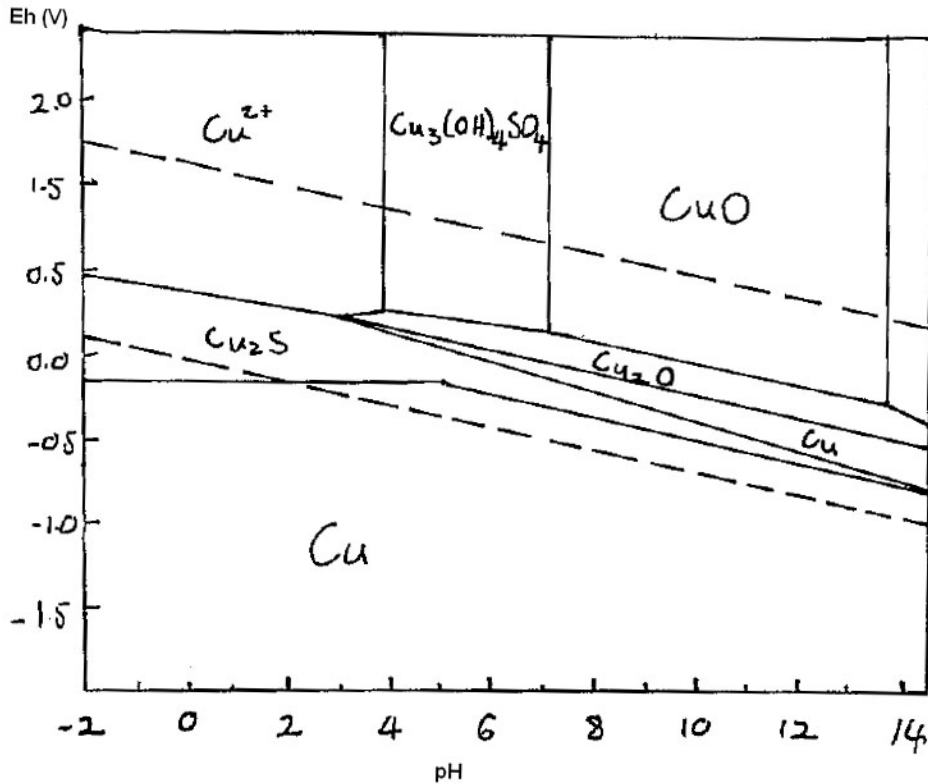
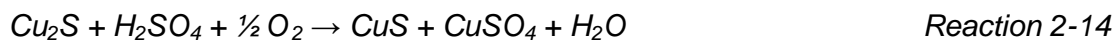


Figure 2-4 Stability diagram for Cu-Ni-S-H<sub>2</sub>O system at 80°C (Redrawn, Lamy, 2007)

Copper dissolution during atmospheric leaching is often associated with an excess of oxygen and has been reported by Plasket and Romanchuk (1978) and Symmens et al. (1979). Leaching of the alloy phase takes place according to reaction 2-13.



Hofirek and Kerfoot (1992) published reaction 2-14 for chalcocite leaching under pressurised conditions. The same reaction has been observed under atmospheric oxidative conditions by Plasket and Romanchuk (1978):

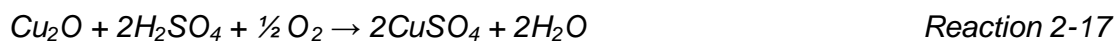


Plasket and Romanchuk (1978) also noted the dissolution of covellite under highly oxidising conditions during later stages of the leach (reaction 2-15):

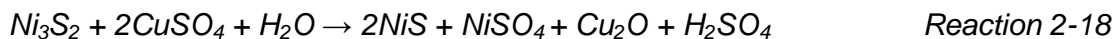


Rademan et al. (1999) suggested that the availability of oxygen is not the factor determining whether cementation or copper dissolution will take place. Instead, it was postulated that the availability of heazlewoodite for the cementation reaction to proceed is the key factor, with copper dissolution proceeding once all the heazlewoodite has been consumed.

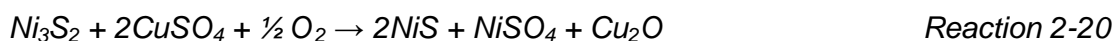
Cuprite was not found in the solid material used in this work, but its presence in both the matte and leach products have been mentioned in literature. Llanos et al. (1974) described the formation and subsequent dissolution of cuprite according to reaction 2-16 and reaction 2-17



Symmens et al. (1979) explains that cuprite forms as a product of a metathesis reaction (reaction 2-18). The metathesis reaction is followed by oxidation to form CuO (reaction 2-19):



A similar reaction was described by Llanos et al. (1974), in which oxygen participates in the interaction between nickel and copper:



In the higher pH ranges (4.5 to 6), copper hydrolysis takes place, accompanied by the formation of basic cupric sulphate (antlerite) and the removal of copper from solution. (Hofirek and Kerfoot, 1992):

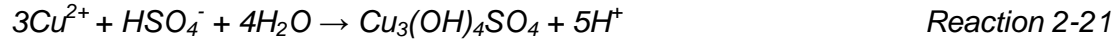


Figure 2-5 gives a Pourbaix diagram for an Fe-Cu-Ni-S system at 80 °C.

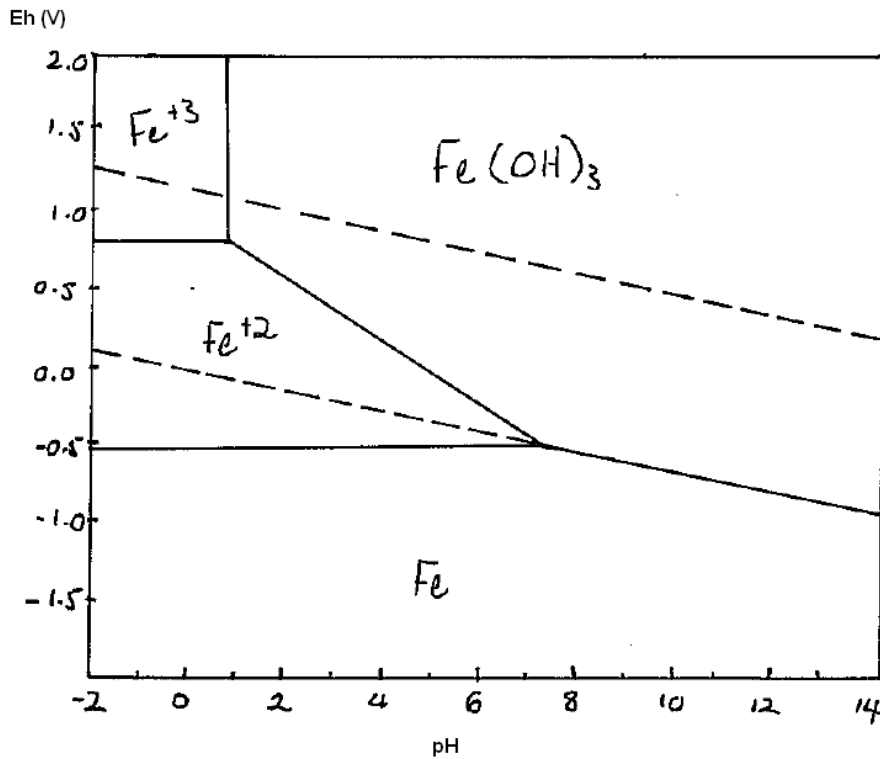
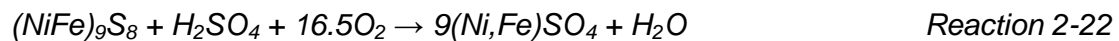


Figure 2-5 Stability diagram for Fe-Cu-Ni-S-H<sub>2</sub>O system at 80 °C (Redrawn, Lamya, 2007)

Iron in the matte in was found to be present mostly in the form of pentlandite ((NiFe)<sub>9</sub>S<sub>8</sub>). According to Knuutila et al. (1997), iron and nickel are leached from pentlandite via reaction 2-22.



It is likely that iron will also take part in exchange reactions with copper, which will be similar to the cementation and metathesis reactions given for nickel (reactions 2-9, 2-10 and 2-11).

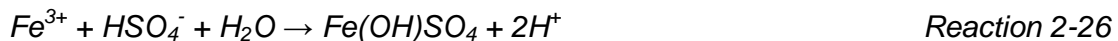
Although present in relatively small concentrations, iron has been reported to play an important role as catalyst and oxygen carrier to enhance the rates of leaching reactions. (Burkin, 2001; Mulak, 1987; Hofirek and Kerfoot, 1992) At a low pH, ferrous ions are oxidised to the ferric state according to reaction 2-23.



The ferric ion can act as oxidant in the leaching of heazlewoodite, which leads to the ferrous ion being continuously regenerated.



Reduction to the ferrous state ceases at pH values above 2 – 2.5 (Hofirek and Kerfoot, 1992). At pH values above 3.5, the ferric ion becomes unstable and hydrolysis commences:



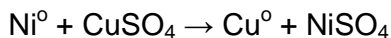
### 2.2.3 Kinetic models

According to Burkin (2001) leaching reactions can be broken down into the following steps:

1. Transport of reactants from solution to the solid-liquid interface
2. Adsorption of reactants to the surface
3. Reaction at the surface
4. Desorption of soluble reaction products
5. Transport of soluble products away from the reaction surface

In this sequence, step one and five are transfer processes and are dependent on the hydrodynamic conditions of leaching, or on material characteristics such as porosity. Steps two, three and four are chemically controlled processes, in which electron transfer is often the rate determining step.

In most dissolution reactions, the forward reaction is significantly favoured in terms of thermodynamics and the reverse reaction can be ignored (Hiskey and Wadsworth, 1981). Also, electrochemical reactions are often assumed to be first order reactions. (Provis et al., 2003) In the absence of deposit effects, reactions are described by a pseudo-first-order rate equation. If the cementation of copper onto metallic nickel powder is taken as an example, the rate of copper cementation can be represented by Equation 2-1



$$\frac{d[\text{Cu}^{2+}]}{dt} = -KA \frac{[\text{Cu}^{2+}]}{V}$$

*Equation 2-1*

By integrating and rearranging Equation 2-1, Equation 2-2 is obtained:

$$\log \left( \frac{[Cu^{2+}]_t}{[Cu^{2+}]_0} \right) = - \frac{KAt}{2.303 V_t} \quad \text{Equation 2-2}$$

Where

$V_t$  = volume of solution at time  $t$ .

$A$  = area of nickel powder available for reaction.

$[Cu^{2+}]_0$  = initial copper ion concentration.

$[Cu^{2+}]_t$  = copper ion concentration at sample time  $t$ .

$K$  = the rate constant

If a single rate-controlling mechanism is present, plotting the left side of Equation 2-2 as a function of time will yield a straight line with slope  $K/2.303$ , so that the rate constant can be determined. If more than one controlling mechanism is present the slope of the line will change with time.

If  $K$  is calculated from Equation 2-2, the apparent activation energy for a reaction can be determined from the Arrhenius equation (Fogler, 1995):

$$k_A(T) = Ae^{-E_a/RT} \quad \text{Equation 2-3}$$

Where

$A$  = pre-exponential or frequency factor

$E_a$  = activation energy, J/mol

$R$  = gas constant = 8.314 J/molK

$T$  = absolute temperature (K)

For transport controlled processes in which transport of the reactant from the solution phase to the solid/liquid interface is the rate-controlling step, the energy of activation should be in the range of 12 to 27 kJ/mol, which similar to the energy of activation for diffusion through a boundary layer in an aqueous solution (Burkin (2001)). For chemically controlled processes, the energy of activation will be substantially higher.



In heterogeneous reaction kinetics, the reaction area of the solid reactant plays a role similar to the concentration of a dissolved reactant that takes part in a homogeneous reaction. It follows that changes in the reaction area need to be taken into account when a large fraction of the solid reactant is consumed. Depending on the nature of the solids and the reactions taking place, several models exist that describe possible changes in the solid phase. These are shown in Figure 2-6, which was adapted from Sohn and Wadsworth (1979).

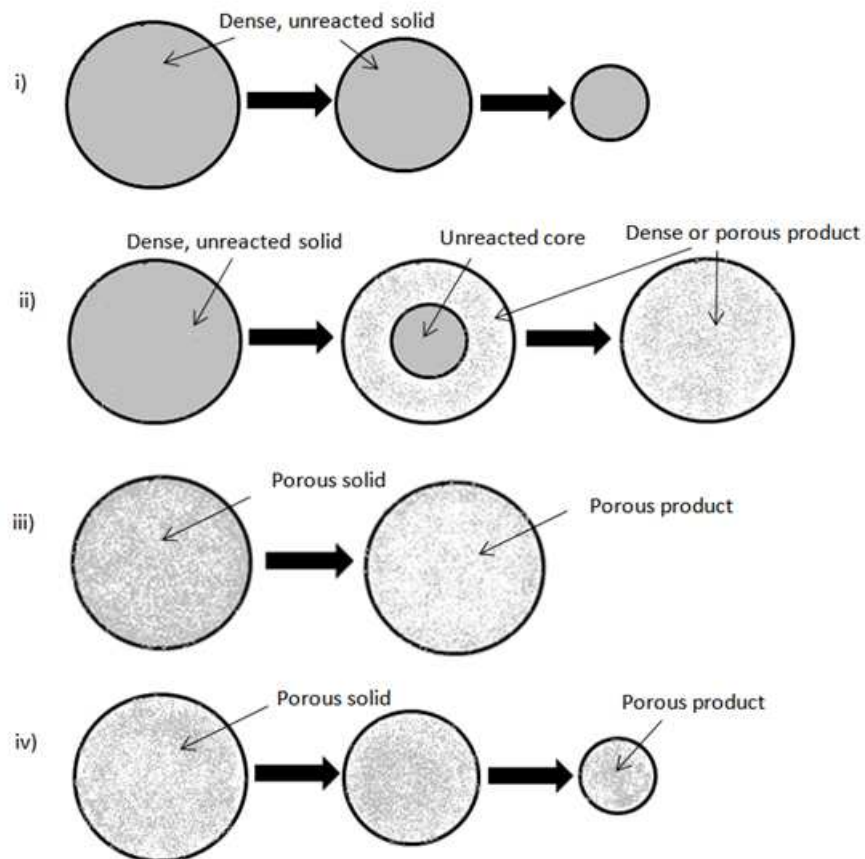


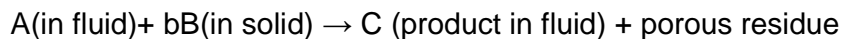
Figure 2-6 Possible modes of solid state changes during leaching. Adapted from Sohn and Wadsworth (1979)

- (i) Dense shrinking particle, no product layer
- (ii) Dense shrinking core with product layer
- (iii) Porous particle, uniform internal decomposition with no change in external geometry
- (iv) Porous particle undergoing internal and external decomposition

The first model shown in Figure 2-6 is the shrinking particle model and occurs in solid-liquid reaction processes where the solid dissolves with no solid product formation, or where the solid product continuously breaks away. The second model is the shrinking core model, in which reaction of the liquid with the solid leads to a porous 'ash layer', or to the formation of a product layer. Examples of particle passivation were given by Dutrizac (1978), as well as Dutrizac and Chen (1995). Dutrizac (1978) noted particle passivation due to the formation of elemental sulphur when leaching chalcopyrite in ferric-sulfuric acid solutions. Dutrizac and Chen (1995) noted that a passivating layer of elemental sulphur and  $\text{PbSO}_4$  can form when leaching galena ( $\text{PbS}$ ) in ferric sulphate media.

The derivation of kinetic expressions to describe the shrinking core model for different controlling mechanisms has been discussed by Levenspiel (1972), Sato and Lawson (1983), Gbor et al. (2000) and Herreros et al. (2002). The third and fourth model in Figure 2-6 are less commonly used to describe leaching kinetics and will not be discussed here. The equations given below were taken from Gbor et al. (2000).

The general reaction used in the development of the shrinking core model is of the following form:



Where  $b$  is the moles of species B consumed per mole of species A reacted.

In the shrinking core model, the overall reaction kinetics can be controlled either by mass transfer to the surface, the surface reaction, or diffusion of reactants and products through the solid layer, to the active reaction surface.

For a surface chemical reaction controlled process, the kinetics are described by the following equation:

$$1 - (1 - X_B)^{\frac{1}{3}} = k_r t \quad \text{Equation 2-4}$$

Where

$$k_r = \frac{bkC_{Ab}}{\rho R} = k'_r C_{Ab} \quad \text{Equation 2-5}$$

And

$k_r$  = first order reaction rate constant (m/s)

$C_{Ab}$  = concentration of A in the bulk of the fluid (mol/m<sup>3</sup>)

$\rho$  = molar density of B (mol/m<sup>3</sup>)

$R$  = radius of the solid particle (m)

$t$  = time (s)

$X_B$  is the fraction of B reacted

If a large excess of reactant B is available,  $C_{Ab}$  can be taken to be constant, but if  $C_{Ab}$  changes with time, the term for  $C_{Ab}$  should be included in Equation 2-4, leading to Equation 2-6.

$$1 - (1 - X_B)^{\frac{1}{3}} = k'_r DC_{Ab} t \quad \text{Equation 2-6}$$

For an internal diffusion-controlled process, equation 2-7 applies:

$$1 - 3(1 - X_B)^{\frac{2}{3}} + 2(1 - X_B) = k_d t = k'_d C_{Ab} t \quad \text{Equation 2-7}$$

Where

$$k_d = \frac{6bD_e C_{Ab}}{\rho R^2} = k'_d C_{Ab} \quad \text{Equation 2-8}$$

$D_e$  is the effective diffusion coefficient of A through the product layer. If  $b$ ,  $D_e$ ,  $\rho$  and  $R$  are assumed to be constant, it follows that  $k'_d$  can be determined experimentally by measuring  $C_{Ab}$  and  $X_B$ .

For a mixed control mechanism (surface chemical and product layer diffusion), Equation 2-9 applies:

$$[1 - 3(1 - X_B)^{2/3} + 2(1 - X_B)] + \alpha[1 - (1 - X_B)^{1/3}] = k_d t = k'_d C_{Ab} \quad \text{Equation 2-9}$$

Where

$$a = \frac{6D_e}{Rk} \quad \text{Equation 2-10}$$

And

$$k_d = \frac{6bD_e C_{Ab}}{\rho R^2} \quad \text{Equation 2-11}$$

Although  $k_d$ ,  $k_r$  and  $a$  are functions of fundamental characteristics of the material, their values are usually determined experimentally by means of curve fitting.

Semi-empirical models to describe the kinetics of Ni-Cu-S matte leaching have been developed by Rademan (1995), as well as Provis et al. (2003), for an acid-oxygen pressure leach. In the model developed by Provis et al. (2003), reaction equations were drawn up for sixteen reactions that were considered to be important in the leaching system. To describe the rate of change of the number of moles of species 'A' in solution, Equation 2-12 was used:

$$r_A = \frac{1}{V} \frac{dN_A}{dt} \quad \text{Equation 2-12}$$

In the model by Provis et al. (2003), all reactions were assumed to follow first-order kinetics, meaning that reactions were assumed to be linearly dependent on the concentration of dissolved reactants, as well as the oxygen partial pressure in reactions where oxygen is involved. The rate limiting step for all reactions was considered to either be chemical control or pore diffusion control. Reaction constants ( $k$ ) were determined by fitting the model to experimental data. For the leaching of the alloy from the matte, a shrinking core term was added to the rate

equation. In this instance, the shrinking core term was not intended to describe a change in the particle size, but rather a decrease in the amount of alloy, which is present as small inclusions that are leached out while the mineral matrix remains intact. For reaction 2-1 (given again below), the rate expression was expressed by Equation 2-13.



$$\frac{dN_{component\ i}}{dt} = v_{component\ i} k_2 C_{H^+} P_{O_2, eff} \left( \frac{N_{Ni\ alloy}}{N_{Ni\ alloy, (t=0)}} \right)^{2/3} \quad \text{Equation 2-13}$$

Rademan et al. (1999) found that  $Cu_2S$  and  $NiS$  will not be leached while  $Ni_3S_2$  and  $Ni$  alloy are still present, but this galvanic interaction was only addressed on an empirical level by the model of Provis et al. (2003).

Provis et al. (2003) reported that the model predicted experimental results satisfactorily, but suggested that mass transfer effects might be included on a fundamental level to improve the model performance.

Lamya (2007) developed a kinetic model similar to that of Provis et al. (2003) for the leaching of matte at atmospheric pressure under non-oxidative conditions.

## 2.2.4 Cementation and metathesis mechanisms and kinetics

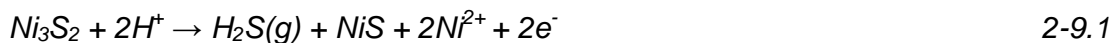
The generally accepted reaction equation for the metathesis reaction, with  $Cu_2S$  as reaction product, was given in Section 2.2.2. This reaction is given again below:



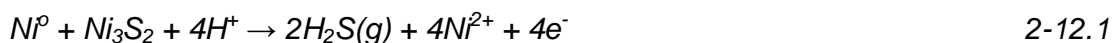
In addition to reaction 2-9, Rademan et al. (1999) suggested galvanic interaction between the alloy and heazlewoodite phases can take place and that reaction 2-12 might be operative when alloy phases are present in the matte.



Vydysh et al. (2005) noted that reaction 2-9 must be an overall reaction. Rademan et al. (1999) explained the cementation reaction of copper with heazlewoodite as a two step mechanism, in which hydrogen sulphide forms as an intermediate:



A similar mechanism to reaction 2-9 was suggested for the reaction of heazlewoodite and the nickel-alloy with copper in solution:

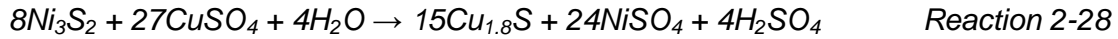
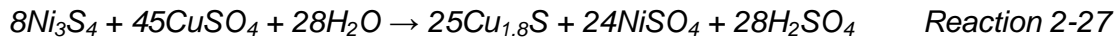


The reaction mechanisms suggested above is supported by observations by Hofirek and Kerfoot (1992), who noted that acid is required for metathesis reactions and that the rate of reaction increases with increased acid concentration.

Fugleberg et al. (1995) found that acid was formed in tests where cementation took place at 150 °C and concluded that the reaction of  $Cu^{2+}$  with millerite is not a simple exchange reaction, but is more likely to be an oxidation reaction of the form given below:



For polydymite and heazlewoodite, Fugleberg et al. (1995) suggested the following reactions:



In addition to the metathesis reaction, the cementation reaction of copper onto pure nickel is well-known. Many studies have been conducted to investigate cementation of copper ions onto different geometries and also onto different base materials. These include works by Demirkiran et al. (2007), Karavasteva (2005), Sędzimir (2002), Dönmez et al. (1999), Sahoo and Rao (1982), Annamalai and Murr (1979) and MacKinnon (1974).

The generally accepted reaction for cementation of copper onto nickel is given below:



For this reaction, first order kinetics is usually assumed, which means that the rate of cementation will decrease as a function of the copper concentration in solution. However, many authors have observed deviations from first order kinetics in leaching systems, which will be discussed in the following paragraphs.

Sędzimir (2002) observed that cementation rates can increase with time and explained the kinetics by the formation of a product layer on the particles. When metallic copper is cemented onto nickel, the cement copper and nickel assume a constant mixed potential. The cemented copper increases the reaction surface because the cementation reaction can proceed directly onto the cemented copper, without diffusion of ions from solution through the product layer. However, if the product layer is too dense, diffusion of the dissolved ions from the particle to the solution might become rate limiting.

Annamalai and Murr (1979) investigated copper cementation onto a rotating iron disk. It was found that the morphology of the copper deposit was a function of process parameters such as the temperature, stirring rate, initial copper concentration and solution pH. The cementation reaction was found to be controlled by surface reaction or pore diffusion at temperatures between 10 °C and 30 °C, with an activation energy of 95.77 kJ/mol. In the temperature range 30 – 60 °C, an activation energy of 33.22 kJ/mol was obtained, indicating that the reaction may be controlled by diffusion or surface reaction mechanisms. Cementation rates were retarded by high cupric ion concentrations, high stirring rates and low temperatures.

Lamya and Lorenzen (2005) investigated the cementation of copper onto matte and found a distinct increase in the reaction rate after some time. According to Lamya the cementation reaction followed a mixed control mechanism, with two distinct activation energies, namely 18.2 kJ/mol at 70 – 80 °C and 74.6 kJ/mol at 50 – 70 °C. From this it was concluded that the cementation reaction was probably controlled by a boundary layer diffusion mechanism at higher temperatures, while the surface reaction was controlling at low temperatures.

Mackinnon (1974) noted non-linear Arrhenius plots in the cementation of copper from a sulphuric acid solution onto nickel powder, but rather than enhanced leaching rates, particles were passivated by growing copper layer and diffusion of product ions through the deposit to become the rate controlling step. Cementation of copper onto nickel powder was diffusion controlled at high temperatures (>70°C),  $E_a = 11.72$  kJ/mol, but chemical reaction controlled at low temperatures (<70 °C),  $E_a = 78.66$  kJ/mol. Cementation reactions proceeded very poorly in the absence of acid. The effect of acid was attributed to the dissolution of nickel oxides and the consequent activation of the nickel surface for reaction.

Sahoo and Rao (1982) investigated cementation of copper from ferric chloride solution onto steel, iron, nickel and aluminium substrates. It was concluded that the pH had no significant influence on leaching kinetics.



Demirkiran et al. (2007) investigated the cementation for copper onto granulated zinc in a solution of water and hydrochloric acid. For a range of copper concentrations between 0.01 mol/L and 0.1 mol/L, it was found that an increase in initial copper concentration leads to an increased rate of cementation. The effect of pH was tested at pH values of 1,2,3,4 and 5. It was found that an increase in the pH from 1 to 4 will lead to increased reaction rates. Between 30 °C and 45 °C, an activation energy of 53.14 kJ/mol was found, indicating a surface controlled reaction. Between 45 °C and 55 °C an activation energy of 22.61 kJ/mol was found, indicating a diffusion controlled process.

Dönmez et al. (1999) investigated the kinetics of copper cementation from sulphate solutions, onto a rotating aluminum disc. The effect of the copper concentration was studied, using copper concentrations of 0.001, 0.01, 0.05 and 0.1 M. An increase in the cemented fraction was observed for lower copper concentrations and it was concluded that high reaction rates are favoured by low copper concentrations. This was explained by the larger surface area available per  $\text{Cu}^{2+}$  ion, at low concentrations. The effect of pH variations (pH 1 - 5) was also investigated. It was found that cementation rates decreased at pH values above 1. This was attributed to a possible decrease in the rate of surface oxide dissolution, which can lead to passivation of the reaction surface.

## 2.2.5 Catalysis: Iron and copper

It is a well-documented fact that iron and copper in solution can have a pronounced effect on the leaching kinetics of sulphide minerals. Several authors have shown an increase in the rate of chalcocite leaching due to increased copper and iron concentrations. (Grewal et al., 1992, Thomas et al., 1967, Mao & Peters, 1983, King et al., 1975, Dutrizac and MacDonald, 1973, Thomas and Ingraham, 1967) Grewal et al. (1992) explained the increased kinetics by means of the increased redox potential. Grewal et al. (1992) further found that increased iron concentration changed the morphology of copper sulphate that precipitated during leaching.

Hiskey and Wadsworth (1975) found that copper increased the kinetics of chalcopyrite in sulphuric acid solutions. However, above a threshold concentration, the formation of a  $\text{Cu}_2\text{S}$  layer on particles led to diffusion limitation and a decrease in reaction rates.

Iron and copper in solution have also been shown to have a catalytic effect on the leaching of heazlewoodite (Mulak, 1987; Hofirek and Kerfoot, 1992). In a sulphuric acid leach of heazlewoodite, Mulak (1987) found that extraction of nickel increased with 10 % with an increase of cupric and ferric ion concentration from 0.1 to 1.08 mM. Further addition of ions did not influence the dissolution rate.

In Section 2.2.4, it was mentioned that  $\text{H}_2\text{S}$  evolves spontaneously when heazlewoodite is leached in acidic solutions (Reaction 2-3). Pawlek (1969) showed experimentally that the addition of  $\text{H}_2\text{S}$  can suppress heazlewoodite leaching. There exists a concept that  $\text{H}_2\text{S}$  will be directly oxidised in the presence of  $\text{Cu}^{2+}$  or  $\text{Fe}^{3+}$  ions and that the particle surface will therefore remain active for leaching reactions. This corresponds closely to the metathesis mechanism in reaction 2-9, as reported by Rademan (1999). Similar reactions might be operative in which ferric ions accept electrons from evolved  $\text{H}_2\text{S}$  gas to form intermediate Fe-S products, which will subsequently be oxidised by oxygen again to reproduce catalytic ions (Mulak, 1987).

It has also been reported (Hofirek and Kerfoot, 1992) that cupric ions in solution have a catalytic effect on iron hydrolysis and that the rate of iron hydrolysis slows down markedly if no copper ions are present in solution. Symmens et al. (1979) reported similar results.

## 2.3 Key results from previous laboratory leaching investigations

Due to the complexity of the leaching system it is difficult to predict the outcome of a specific set of initial conditions purely from fundamental considerations (such as discussed in Section 2.2) Batch leaching tests at conditions approaching possible plant scenarios remain the most frequently used method to determine the effects of different operating variables for industrial leaching processes. Much of the leaching chemistry which was discussed in Section 2.2 comes from this body of work. This section will discuss the available literature in chronological order, after which an overview of the most important results will be given. Oxidative leaching studies will be discussed first (Section 2.3.1), followed by non-oxidative leaching (Section 2.3.2).

### 2.3.1 Oxidative leaching

Llanos et al. (1974) investigated the leaching behaviour of Ni-Cu-S mattes in the first stage atmospheric leach at the Port Nickel Refinery in Louisiana. The purpose of this first stage leach is the dissolution of nickel in an acidic copper sulphate solution, with the simultaneous removal of copper and iron from solution. In a typical test, milled matte containing 40.0 % Ni, 39.5 % Cu, 16.4 % S and 0.2 % Fe was leached at 75 °C in a solution containing 22 g/l  $\text{Cu}^{2+}$ , 32 g/l  $\text{Ni}^{2+}$  and 45 g/l free  $\text{H}_2\text{SO}_4$ . The reaction took place in an agitated vessel, with air provided as oxidant. The initial copper concentration, initial acid concentration and the pulp density were varied to determine their effects, while mattes containing respectively 6.5 % S, 13.0 % S and 19.6 % S were leached to determine the effect of matte metallisation.

Llanos et al. (1974) describe nickel dissolution as being controlled by copper cementation onto the matte during the first few minutes of the leach (reaction 2-1 and reaction 2-9), with cuprite forming as cementation product in the presence of oxygen (reaction 2-20). The presence of cuprite was confirmed by XRD analysis. In mattes high in copper and low in sulphur, metallic copper was initially leached from the matte (reaction 2-16). At a pH of about 2, cuprite formation caused rimming on

unreacted particles, leading to the cementation reaction slowing down. In the pH range from 2 to 3.9, nickel was leached from heazlewoodite (reaction 2-4) and it was found that oxygen transfer from the gas to the liquid phase became the rate limiting step. At pH values above 3.9, the rate at which acid was produced by copper hydrolysis determined the rate of nickel leaching.

Llanos et al. (1974) found that leaching time (defined as the time to remove all copper from solution and for the solution pH to reach a value of 5.3) was reduced significantly when the sulphur content of the matte was increased from 6.8 % to 19.6 %, but was not significantly influenced if the Ni/Cu ratio in the matte was varied, provided that the sulphur content of the matte did not change.

It was further found by Llanos et al. (1974) that leaching time increased when the ratio of nickel in the matte to reactants in solution was decreased. Therefore increasing the initial copper and acid concentrations led to longer leaching times and increased the total nickel extraction. The acid/copper ratio in the leach solution was found to have a smaller effect on nickel extraction than the total reactants available (moles  $H^+$  and  $Cu^{2+}$ ), although nickel extraction was found to be more sensitive to the initial acid concentration than to the initial copper concentration. Increasing the percentage solids decreased total leaching time, but led to lower nickel extractions.

Llanos et al. (1974) noted that the results discussed above only apply to tests in which the residual iron content in the fresh matte was less than 0.5 % and where the leach solution initially contained less 1 g/l Fe. Higher iron concentrations in either the matte or the solution increased the total leaching time.

The problem of high iron in matte was addressed by Symens, Queneau and Blandon (1976), who presented a patent for the treatment of mattes containing over 0.5 % and up to 20 % iron.

It was suggested by Symmens et al. (1976) that iron enters the  $Ni_3S_2$  lattice when a high iron matte is granulated by quenching from below the solidus-liquidus temperature, thus resulting in a  $(Ni,Fe)_3S_4$  phase which is less effective in consuming acid. This problem could be overcome by granulating the matte above the solidus-

liquidus temperature. The iron then apparently segregates as copper ferrite, which is less detrimental to reaction kinetics.

Symmens et al. (1976) further noticed that leaching stalls at pH 4 for high iron mattes (> 4 % Fe), or for leaching tests in which the initial Fe concentration was increased to 8 g/L, but that this problem could be overcome by replacing air with oxygen at pH 4. When using oxygen instead of air, iron precipitated from solution more quickly (Reactions 2-23 and 2-25) and the pH rapidly continued to rise up to pH 5.5, thus completing acid removal and copper removal via hydrolysis. It was also suggested that the solids content should be limited to avoid high iron concentrations in the leach solution.

Symmens et al. (1979) presented further work related to the leaching of high iron mattes (> 0.5 %), within the flowsheet of the Port Nickel refinery. The first stage atmospheric leach at the Port Nickel refinery employed oxygen and spent electrolyte to achieve three objectives: nickel extraction, copper precipitation from solution (cementation) and iron precipitation from solution (hydrolysis). The effects of the ratio of acid to copper in the electrolyte feed, the sulphur content of the matte and the percentage solids were investigated to determine the optimal conditions for treatment of high Fe matte.

In order to determine the effect of sulphur content of the matte, Symmens et al. (1979), compared the leaching behaviour of a high sulphur matte (40.7 % Ni, 34.3 % Cu, 19.6 % S, 2.1 % Fe, 3.0 % Slag) and a low sulphur matte (49.0 % Ni, 28.1 % Cu, 15.2 % S, 3.0 % Fe, 4.0 % Slag) at 80 °C. Leach solutions were used with initial acid concentrations in the range 38 – 80 g/L and initial copper concentrations in the range 21 – 48 g/L.

Like Llanos et al. (1974), Symmens et al. (1979) noticed the formation of cuprite ( $\text{Cu}_2\text{O}$ ) as cementation product (reaction 18) as well as the formation of  $\text{CuO}$  (reaction 19). Unlike Llanos et al. (1974), Symmens et al. (1979) observed faster copper removal from solution in low sulphur mattes and thus concluded that the cementation reaction proceeded mostly onto the alloy phase (which is more prominent in low sulphur mattes). In general, copper removal was rapid for low

sulphur matte, provided that the target nickel extraction (the percentage nickel that can be extracted if one mole of nickel can be extracted for each mole of acid and copper initially available in the leach solution) was lower than 74 %. Conversely, removal of iron from solution via hydrolysis was found to be slower for a low sulphur matte.

Symmens et al. (1979) found that copper precipitation in the pH range between 1.5 and 4 was accelerated when operating at a high  $\text{H}_2\text{SO}_4/\text{Cu}^{2+}$  ratio in the spent electrolyte. Less iron was precipitated via hydrolysis at increased  $\text{H}_2\text{SO}_4/\text{Cu}^{2+}$  ratios and this was attributed to the longer times required for the pH to increase and also to the quicker removal of  $\text{Cu}^{2+}$  ions from solution, since  $\text{Cu}^{2+}$  ions act catalytically in the hydrolysis of iron. Too much oxidation led to the dissolution of cement copper and too little oxidation led to slow iron hydrolysis. In order to achieve the goals of the Port Nickel first stage leach, it was concluded that it was practically feasible to operate at conditions where all the copper in solution was removed, while most of the iron was removed from solution. The set of conditions used to accomplish this was an  $\text{H}_2\text{SO}_4/\text{Cu}^{2+}$  ratio of 2 and an intermediate aeration rate.

Plasket and Romanchuk (1978) investigated the treatment of high-grade nickel-copper matte from Impala Platinum in a first stage acid oxidation leach. The purpose of the first stage leach was to obtain about 80 % nickel extraction, while producing a solution low in copper. The matte used in the study contained 44.7 – 48 % Ni, 1.2 % Co, 24.8 – 26.5 % Cu, 1.0 % Fe and 22.4 % S, while an electrolyte containing 20 g/L dissolved Cu, 25 g/L dissolved Ni and 60 - 120 g/L sulphuric acid was used.

The first stage leach in Plasket and Romanchuk's work (1978) was considered to proceed in three separate steps, namely copper cementation by heazlewoodite (reaction 2-9), acid dissolution of chalcocite and heazlewoodite (reaction 2-4 and reaction 2-14) and copper removal from solution via reaction with millerite (Reaction 2-10). Plasket and Romanchuk (1978) reported similar results to Symens et al. (1976) in the sense that overly oxidising conditions can prevent copper cementation from taking place. The third step of the first stage leach had to be carried out in the absence of oxygen to prevent the dissolution of covellite (reaction 2-15) and to ensure copper precipitation.

Hofirek and Kerfoot (1992) investigated the leaching chemistry of matte from Rustenburg Base Metal Refinerers. The matte was split into a metallic and non-metallic fraction and the leaching behaviour of the non-metallic (sulphide) fraction (38 – 45 % Ni, 27 – 32 % Cu, 0.5 % Co, 1.5 % Fe and 22.5 % S) was investigated at 75 – 80 °C. Major phases in the material were heazlewoodite and djurleite. The leach solution initially contained 100 g/L Ni, 5 g/L Cu and 1 g/L Fe, while the initial acid concentration was varied from 0 to 10 g/L..

Based on the initial acidity and acid/matte ratio, three possible modes of operation were defined:

Type 1: A leach in moderate or high acid solutions (acid concentration > 10 g/l, acid/matte ratio > 0.1 w/w), which is distinguished by copper being removed rapidly from solution via cementation, followed by iron hydrolysis. Copper hydrolysis was generally found to be absent. In this mode iron hydrolysis was found to be slow due to the absence of cupric ions that act catalytically in the oxidation of ferrous ions.

Type 2: An atmospheric leach in low acid solutions (acid concentration 1 – 10 g/l, acid/matte ratio < 0.1 w/w), which is characterised by the separate occurrence of cementation, iron hydrolysis and copper hydrolysis.

Type 3: An atmospheric leach in acid free solutions (pH > 2.5), which is characterised by the absence of cementation and simultaneous iron and copper hydrolysis.

Hofirek and Kerfoot (1992) found that copper rejection rate by metathesis was significantly faster than the rate of hydrolytic rejection. In agreement with what was previously reported by Symmens et al. (1979), Hofirek and Kerfoot (1992) found that the rate of metathesis increased with increased initial acid concentration. Metathesis only occurred at a pH below 2.5.

Fugleberg et al. (1995) carried out leaching test work in order to aid the development of the Hartley Platinum leaching process. A matte containing approximately 42 % Ni, 34 % Cu, 1 % Fe, 0.4 % Co and 22 % S was leached under pressure at a temperature of 150 °C, with acid levels ranging from 0 – 22 g/L.

Fugleberg et al. (1995) found that the metallic phase was the most reactive with the acid leaching of metallic nickel taking place first. Copper from the alloy was found to react with oxygen to form cuprite. (Reaction 2-16) Reactions involving the alloy phase were followed by the dissolution of nickel from the sulphide phase, to produce millerite, as well as the dissolution of chalcocite to produce covellite. Metathesis reactions were found to take place, but were mentioned only to take place at elevated temperatures (>100 °C). It was found that  $\text{Cu}^{2+}$  reacted with  $\text{Ni}_3\text{S}_2$ , NiS and  $\text{Ni}_3\text{S}_4$ , with the resulting copper sulphides being respectively  $\text{Cu}_{1.96}\text{S}$ ,  $\text{Cu}_{1.8}\text{S}$  and  $\text{Cu}_{1.8}\text{S}$ . The reaction rate for NiS was found to be much faster than for  $\text{Ni}_3\text{S}_2$  and  $\text{Ni}_3\text{S}_4$ , with the rate of  $\text{Ni}_3\text{S}_4$  being the slowest.

Vydysh et al. (2005) investigated the use of high copper converter matte (containing 25.42 % Ni, 48.9 % Cu, 0.72 % Co, 2.27 % Fe and 22.3 % S) for the removal of copper from a sulphuric acid/copper solution. The matte contained a copper sulphide, nickel sulphide and a metallic phase. The primary mechanism of nickel recovery was found to be leaching from the alloy phase and copper precipitation via exchange with nickel from the heazlewoodite lattice. All other conditions being the same, the introduction of additional acid did not influence nickel recovery. It was found that the key factor influencing nickel recovery was the ratio between the mass of converter matte to the amount of dissolved copper in the initial leach solution. In addition, it was found that nickel dissolution was higher for mattes which were low in sulphur, due to increased leaching of metallic nickel by sulphuric acid and oxygen. Nickel-extraction in low-sulphur mattes was consequently found to be less dependent on the initial copper concentration. The authors found that copper precipitation decreased dramatically for an initial matte/dissolved copper ratio of less than 17.78 kg/kg (which translates to 4.53 kg Ni / kg dissolved Cu). It was assumed that the hindrance was caused by kinetic, rather than thermodynamic constraints.



### 2.3.2 Non-oxidative leaching

In non-oxidative leaching, the amount of nickel that can be extracted is generally less due to the fact that acid-oxygen leaching reactions do not take place. The focus therefore shifts towards removal of copper from solution by means of cementation and metathesis, as well as the associated dissolution of nickel. Several studies on cementation are discussed in Section 2.2.4. This section will focus specifically on non-oxidative leaching with a milled Cu-Ni-S matte in a stirred batch reactor. Because the focus in many refining processes is on the dissolution of nickel, the body of work on the non-oxidative leaching of Ni-Cu-S mattes is much smaller than for oxidative leaching. Only the work of Lamy (2007) will be discussed.

Lamy (2007) investigated the non-oxidative leaching behaviour of Ni-Cu-S matte in a stirred batch reactor, using a  $\text{CuSO}_4\text{-H}_2\text{SO}_4$  solution. The purpose of the study was to understand the nature of the leaching process in the non-oxidative pre-leach step at Impala Platinum Refineries, where the purpose of the pre-leach is the removal of copper from solution with partial dissolution of nickel, iron and cobalt. Test work was carried out under atmospheric pressure and at temperatures of 60 °C, 70 °C and 80 °C. The matte contained 48.9 % Ni, 32.4 % Cu, 0.34 % Co, 0.67 % Fe and 20.7 % S Major phases were reported as 54 %  $\text{Ni}_3\text{S}_2$ , 33.%  $\text{Cu}_2\text{S-Cu}_{1.9}\text{S}$  and 11 % Ni-rich alloy.

Under non-oxidative conditions, Lamy (2007) assumed that metal leaching would be limited, especially from the sulphide phases. Nickel dissolution was considered to occur via cementation and metathesis reactions with the alloy phase (reaction 2-11) and nickel sulphide phase (reaction 2-9). Cementation of copper onto the alloy phase was substantiated by visible metallic copper remaining in the equipment after tests. After complete copper removal, the rate of leaching reactions increased and a sharp increase in the solution pH was observed. The increase in pH was attributed mainly to leaching of nickel from the alloy phase (reaction 2-2). SEM micrographs revealed holes of the same characteristic shape as the alloy phase in the leach residues, without disintegration of the sulphide matrix. It was postulated that a

galvanic couple exists between the Ni-alloy and the Ni-Cu sulphide minerals, in which the alloy has a lower rest potential and thus dissolves anodically.

One aspect of Lamy's work (2007) which is hard to understand is that the effects of operating variables on nickel dissolution and copper cementation were found to be different, in spite of the fact that nickel was assumed to mostly dissolve via reaction with copper. This might indicate that acid leaching played a larger role than suggested by Lamy (2007). The effects of temperature, stirring rate, particle size, pulp density, residence time, initial copper concentration and initial acid concentration were investigated and will be discussed below.

The kinetics of nickel dissolution were characterised with the shrinking core model for a reaction controlled by diffusion through surface layer (Equation 2-7). Diffusion control was further supported by an activation energy of 31 kJ / mol, as well as an increase in nickel extraction with increased stirring rates. The cementation reaction followed a mixed control mechanism, with two distinct activation energies: 18.2 kJ/mol at 70 – 80 °C and 74.6 kJ/mol at 50 – 70 °C. It was concluded that the rate of cementation was controlled by a boundary layer diffusion mechanism at higher temperatures, while the rate was controlled by a surface reaction mechanism at lower temperatures. The rate of cementation was found to be unaffected by the stirring rate. (Lamy, 2007)

A temperature increase from 50 °C to 60 °C led to a slight increase in nickel extraction (13.2 % to 16.9 %), but no significant increase was observed for temperatures above 60 °C, because the process was diffusion controlled. A significant increase in the cementation rate was observed as the temperature was increased from 60 °C to 80 °C. At 80 °C, all the copper could be removed from solution in 90 minutes, while 5 hrs was required for copper removal at 60 °C. (Lamy, 2007)

Lamy (2007), found that the rate and degree of metal dissolution were independent of the initial copper concentration in the range of 25 – 48 g/L, although the rate of cementation decreased as the initial copper concentration was increased from 25 – 36 g/L. MacKinnon and Ingraham (1970), observing similar results when copper was

cemented onto rotating aluminium discs, attributed the decreased reaction rates to activity changes brought on by the increased copper ion concentration, a rise in solution viscosity and the decrease in copper diffusivity with an increase in copper concentration.

An increase in the initial acid concentration from 90 g/L to 110 g/L had very little effect on the rate of nickel extraction or the percentage nickel extracted in 5 hrs, presumably because nickel leaching was mostly due to the cementation reaction (Lamya, 2007). However, iron and cobalt extractions increased with increased acid concentration. Cementation rates were found to decrease with an increase in the initial acid concentration from 90 – 110 g/L, presumably due to redissolution of some of the copper. Above 110 g/L, the cementation rate became independent of the acid concentration.

Copper cementation reached a maximum at a pulp density of 1.7 kg/L as the pulp density was increased from 1.6 – 1.75 kg/L. As the pulp density was increased from 1.6 – 1.7 kg/L, a slight decrease in nickel extraction was observed. The decreased copper cementation at pulp densities above 1.7 kg/L was attributed to poor mass transfer caused by the increased solids content in solution. (Lamya, 2007)

A semi-empirical kinetic model was developed by Lamya (2007) to describe leaching results, which is discussed in Section 2.2.3.

### **2.3.3 Section summary**

Work by Llanos et al. (1974), Symmens et al. (1976), Symmens et al. (1979), Plasket and Romanchuk (1978), Hofirek and Kerfoot (1992), Fugleberg et al. (1995) and Vidysh et al. (2005), in which the oxidative leaching behaviour of Ni-Cu-S converter mattes in  $\text{H}_2\text{SO}_4\text{-CuSO}_4$  media was investigated, was discussed in Section 2.3.1. With the exception of Fugleberg et al. (1995), all the results relate to leaching under atmospheric pressure. Work done by Lamya (2007), on non-oxidative leaching, was discussed in Section 2.3.2.

Hofirek and Kerfoot (1992) suggested a three step mechanism for the leaching of the sulphide fraction of matte: simultaneous leaching and cementation onto heazlewoodite takes place, followed by iron hydrolysis and copper hydrolysis. Although the general sequence (cementation and leaching followed by hydrolysis) is agreed on by other authors, other features have been suggested by Llanos et al. (1974) and Plasket and Romanchuk (1978). Llanos et al. (1974) found that cementation took place onto both the alloy and the sulphide phase, with cuprite forming as reaction product. This cuprite layer inhibited further reaction and thus solid-state diffusion became the rate limiting step in nickel leaching. As the pH increased above 2, nickel was leached from heazlewoodite and oxygen transfer became the rate limiting step. The formation of cuprite as cementation product was also noticed by Symmens et al. (1979). Plasket and Romanchuk (1978) described a three step leaching sequence, consisting of (1) cementation by heazlewoodite, (2) acid dissolution of chalcocite and heazlewoodite and (3) copper removal via reaction with millerite.

The effect of the sulphur content of the matte is difficult to describe from the available literature. It is unclear to what extent the alloy and nickel sulphide phases respectively react with copper and acid in solution. Llanos et al. (1974) observed slower acid consumption in low sulphur mattes, indicating that the sulphide phase is more reactive than the alloy phase. Fugleberg et al. (1995) found that the alloy phase is the most reactive in terms of nickel leaching, but suggested that metathesis took place onto NiS, Ni<sub>3</sub>S<sub>2</sub> and Ni<sub>3</sub>S<sub>4</sub> phases, with the kinetics being the fastest for NiS. Symmens et al. (1979) found that faster copper removal took place in low sulphur mattes, due to cementation mostly occurring onto the alloy phase. Vydish et al. (2005) found that the primary mechanisms responsible for nickel dissolution were leaching from the alloy phase and the metathesis reaction between heazlewoodite and copper. Vydish et al. (2005) further found that nickel dissolution was the highest for low sulphur mattes.

The importance of the matte/reactants ratio was mentioned by Llanos et al. (1974), Symmens et al. (1979), Hofirek and Kerfoot (1992) and Vydish et al. (2005). At too low densities, copper removal becomes problematic (Symmens et al. (1979); Vydish et al. (2005)) Vydish et al. (2005) suggested that the poor copper removal

at low densities was due to kinetic constraints, rather than thermodynamic constraints. Acid consumption was also found to be slow at low pulp densities (Llanos et al. (1974)). On the other hand, high densities led to poor nickel extractions (Llanos et al. (1974)). Hofirek and Kerfoot (1992) noted that the occurrence of iron and copper hydrolysis are dependent on the rate at which the solution pH changes and consequently on the initial matte/acid ratio.

The effects of initial acid and copper concentrations on leaching were discussed by Llanos et al. (1974), Symmens et al. (1979), Hofirek and Kerfoot (1992) and Vydysch et al. (2005). Llanos et al. (1974) noted that nickel extraction increased with increased initial copper and acid concentrations, but found that the final nickel extraction was more sensitive to the initial acid concentration. Similarly, Hofirek and Kerfoot (1992) and Symmens et al. (1979) found that the rate of copper removal increases with higher initial acid concentrations. Vydysch et al. (2005) found that nickel recovery was mainly due to reaction of the predominant heazlewoodite phase with copper in solution, while the alloy phase was leached out. Thus Vydysch et al. (2005) found that the initial acid concentration had little effect on nickel extraction, while higher initial copper concentrations were found to lead to higher nickel extractions.

The effect of iron on leaching was discussed by Llanos et al. (1974), Symmens et al. (1976) and Symmens et al. (1979). Llanos et al. (1974) found that acid consumption was slow when the initial Fe concentration was larger than 1 g/L or the matte Fe-content was more than 0.5 %. Symmens et al. (1976) suggested that the kinetics of leaching were slower for high iron mattes due to changes in the reactivity of heazlewoodite. Symmens et al. (1976) noticed that the pH stalled at 4 when the initial Fe concentration was larger than 8 g/L or the matte Fe content was larger than 4 %.

The effect of oxygen was discussed by Symmens et al.(1979) and Plasket and Romanchuk (1978). An excess of oxygen can interfere with copper removal via cementation, while increasing the rate of acid consumption and iron hydrolysis.

## 2.4 Chapter Conclusion

In this chapter, leaching mechanisms and chemistry has been discussed, as well as key results from previous investigations. Sulphide minerals show considerable intrinsic conductivity, which leads to the stabilisation of meta-stable phases and to galvanic interaction that strongly affects leaching chemistry. The leaching sequence for nickel sulphides has been shown to be  $\text{Ni}_3\text{S}_2$ - $\text{Ni}_6\text{S}_7$ - $\text{NiS}$ - $\text{Ni}_3\text{S}_4$ . If alloy is present in the matte, it will be more reactive than the sulphide phases and will likely be the first phase to be leached out. Copper from solution can be removed via exchange reactions with both the nickel-sulphide phase and the alloy phase, but the extent to which each phase respectively reacts with copper in solution is not clear from currently available literature. The leaching chemistry is well documented, although some differences exist when stoichiometric equations from different authors are compared.

Kinetic models were discussed that have previously been used to describe changes taking place during batch leaching tests. These models generally make use of first order kinetics, while galvanic and shrinking core effects were included empirically. Although models have previously been developed that were successful in describing the changes taking place in specific systems, it is not known if they will be effective at describing other systems. The interaction at play between acid concentration, copper concentration, matte mineralogy, catalytic effects, kinetic effects and galvanic interaction leads to a highly complex system in which effects cannot easily be isolated.

The difficulty in isolating effects is demonstrated by comparing previous results from laboratory leaching investigations, from which it is highly difficult to draw a clear conclusion on the effects of specifically the matte iron content, the initial copper concentration in solution and the initial acid concentration. When only element chemistry is available, the metallurgist is left with a highly convoluted problem which is in fact underspecified. Recent progress in quantitative mineralogy has made it possible to better quantify speciation and mineralogical changes with time, which leads to increased understanding of the system and better metallurgical decision making in an industrial context.

# Chapter 3 Experimental methods and materials

## 3.1 Materials

### 3.1.1 Chemical composition and mineralogy of converter matte

Granulated converter matte from five batches from the Lonmin Marikana BMR was used in this study. Chemical compositions of the matte (from XRF analysis) are shown in Table 3-1.

*Table 3-1 Chemical compositions of converter mattes used in this study. Analyses obtained with XRF*

Matte	Fe	Ni	Cu	S	Co
A	0.53	48.66	30.48	22.14	0.21
B	0.83	48.31	28.66	23.19	0.47
C	0.89	48.50	27.62	23.05	0.42
D	1.05	48.09	28.62	22.87	0.42
E	5.72	43.98	24.01	27.14	0.77

Matte E was used in tests where the effect of a high iron endpoint was tested. Due to limited amounts of matte available from each batch, matte A, B, C and D were interchangeably used as 'Low iron matte' in the experimental design. Matte A differs the most from other mattes in terms of iron and cobalt contents, and this variation will be taken into account where it might have been a factor.

The mineralogy of each batch of matte was determined by means of quantitative XRD analysis. Results are shown in Table 3-2. The mineralogy of granulated Ni-Cu-S converter matte produced at Lonmin Marikana has been thoroughly described by Thyse et al. (2010) and Thyse et al. (2011). Thyse et al. (2010) describe the matte as consisting of a cementing matrix of heazlewoodite ( $\text{Ni}_3\text{S}_2$ ), containing euhedral chalcocite grains ( $\text{Cu}_2\text{S}$ ), as well as a nickel-copper alloy phase.

Specifically, Thyse et al. (2010) investigated the effect of the Fe-endpoint on converter matte mineralization. When comparing mattes with iron endpoints of respectively 5.17 wt%, 0.99 wt% and 0.15 wt% Fe, it was reported that matte with an iron endpoint of 5.17 wt% was characterised by a significantly smaller relative abundance of alloy. The same major phases were observed in the current work. The high iron matte contained significantly less alloy than other mattes and also contained significant amounts of pentlandite and bornite.

*Table 3-2 Mineralogy of converter mattes used in this study. Analyses obtained with quantitative XRD*

Mineral phase	Matte:	Phase abundance (Mass %)				
		A	B	C	D	E
Ni-Cu	Ni-Cu	19.7	15.4	12.3	11.5	2.1
Heazlewoodite	Ni <sub>3</sub> S <sub>2</sub>	51.9	61.3	53.8	53.6	56.9
Godlevskite	Ni <sub>7</sub> S <sub>6</sub>	0	0	4.4	3	2.9
Millerite	NiS	0	0	0	2.5	0.4
Polydymite	Ni <sub>3</sub> S <sub>4</sub>	0	0	0	0	0
Pentlandite	(NiFe) <sub>9</sub> S <sub>8</sub>	0	0.5	0.7	0.5	9.1
Troilite	FeS	0.9	0	0.9	0.8	0.4
Magnetite	Fe <sub>3</sub> O <sub>4</sub>	1.5	1.4	1.2	1.8	1.1
Bornite	Cu <sub>5</sub> FeS <sub>4</sub>	0	0	0	0.5	11.7
Chalcocite	Cu <sub>2</sub> S	26	21.5	26.6	25.8	15.3
Djurleite	Cu <sub>31</sub> S <sub>16</sub>	0	0	0	0	0
Digenite	Cu <sub>9</sub> S <sub>5</sub>	0	0	0	0	0
Covellite	CuS	0	0	0	0	0
Cuprite	Cu <sub>2</sub> O	0	0	0.2	0	0
Antlerite	Cu <sub>3</sub> SO <sub>4</sub> (OH) <sub>4</sub>	0	0	0	0	0
Malachite	Cu <sub>2</sub> CO <sub>3</sub> (OH) <sub>2</sub>	0	0	0	0	0

### 3.1.2 Milling procedure and particle size distribution

The granulated matte was milled for 4 hours in a rubber-lined batch ballmill. The size distributions after different milling times were determined experimentally until a size distribution similar to milled matte from Lonmin Marikana was obtained. A size distribution similar to that in industry was desirable to investigate leaching behaviour similar to what can be expected in industry. Table 3-3 shows the milling parameters which were used to prepare solid material for test work.



*Table 3-3 Laboratory batch milling parameters*

Mill speed (rpm)	64 rpm
Mill volume	9 L
Mill charge(type)	Mixed steel balls
Mill charge (kg)	1.85 kg
Mass solids (kg)	12.5 kg
Mass water	1 kg
Milling time	4 hrs

In Table 3-4, the size distribution of a batch of matte milled in the laboratory is compared to the size distribution of material from the plant. The particle size distributions of the two mattes are very similar.

*Table 3-4 Comparison of size distribution of a batch of laboratory milled matte (Matte C) with milled material from Lonmin Marikana*

<b>Particle size (<math>\mu\text{m}</math>)</b>	<b>Particle size distribution (Vol %)</b>	
	<b>Laboratory (Matte C)</b>	<b>Plant material</b>
- 200 + 100	10.7	10.5
- 100 + 80	8.8	6.5
- 80 + 60	11.9	10.6
- 60 + 40	14.0	16.1
- 40	54.3	56.2

Particle size distribution from both samples determined with Saturn Digisizer 5200 V1.10.

The particle size distributions of three more batches of matte which were milled in the laboratory are given in Appendix H.

The specific surface area of a milled sample of matte was determined as  $2 \text{ m}^2/\text{g}$  by using an Accelerated Surface Area and Porosimetry System. This value will be used in calculations to determine kinetic rate constants.

### 3.1.3 Spent composition

Spent solution from Lonmin Marikana was diluted with water and used as leach solution. For tests in which higher acid or copper concentrations were required, the desired concentrations were obtained by adding 98 % sulphuric acid or copper sulphate pentahydrate crystals. The approach of diluting the entire mixture and adding specific reactants was used to ensure that the initial concentrations of all

other elements would be the same in all tests. Dilution of the spent solution also ensured that nickel would not reach its' saturation limit as leaching progressed.

The concentrations of acid and dissolved nickel, copper, iron and cobalt in the diluted spent are given in Table 3-5. The acid concentration in the spent solution was determined at the plant by a titration with sodium carbonate.

*Table 3-5 Concentrations of dissolved base metals in diluted spent mixture used in tests (from AA-analyses)*

	Ni (g/L)	Cu (g/L)	Fe (ppm)	Co (ppm)	Acid conc. (g/L)
<b>Concentration</b>	25.1	19.6	405	146	37

*Table 3-6 Concentrations of dissolved PGEs (ppm) in diluted spent mixture used in tests (Ir and Rh from ICP-MS. Ru from ICP-OES)*

	Pt (ppm)	Pd (ppm)	Ir (ppm)	Ru (ppm)	Rh (ppm)
<b>Concentration</b>	0	0	25.4	118.6	14.6

## 3.2 Methodology

### 3.2.1 Equipment

Leaching tests were carried out in a 6 L stainless steel stirred batch reactor. The reactor was scaled down geometrically from the reactors used at Lonmin Marikana. Garrison (1983) suggests that a diameter of at least 203 mm should be used on a pilot plant if wall effects are to be eliminated and mixing similar to the process from which the reactor was scaled down is to be obtained. This minimum diameter was used and the length of the reactor was subsequently chosen to obtain the same length / diameter ratio that applies to the plant reactors. The minimum diameter was chosen in order to minimise the material required for leach tests.

The setup, which was constructed for this project, is shown in Figure 3-1. The arrangement of parts within the reactor vessel is shown in Figure 3-2.

The temperature during experiments was kept at a constant setpoint of 85 °C ( $\pm 0.5$  °C), using a PID controller. A thermocouple was inserted in the leach solution to provide temperature readings and the temperature was controlled by on/off control of a 1500 W heating jacket fitted around the reactor vessel. Leaching reactions are exothermic and it was expected that heat generation might pose a problem. This was avoided by using a cooling coil inserted in the leaching solution, with a constant flow of cooling water.

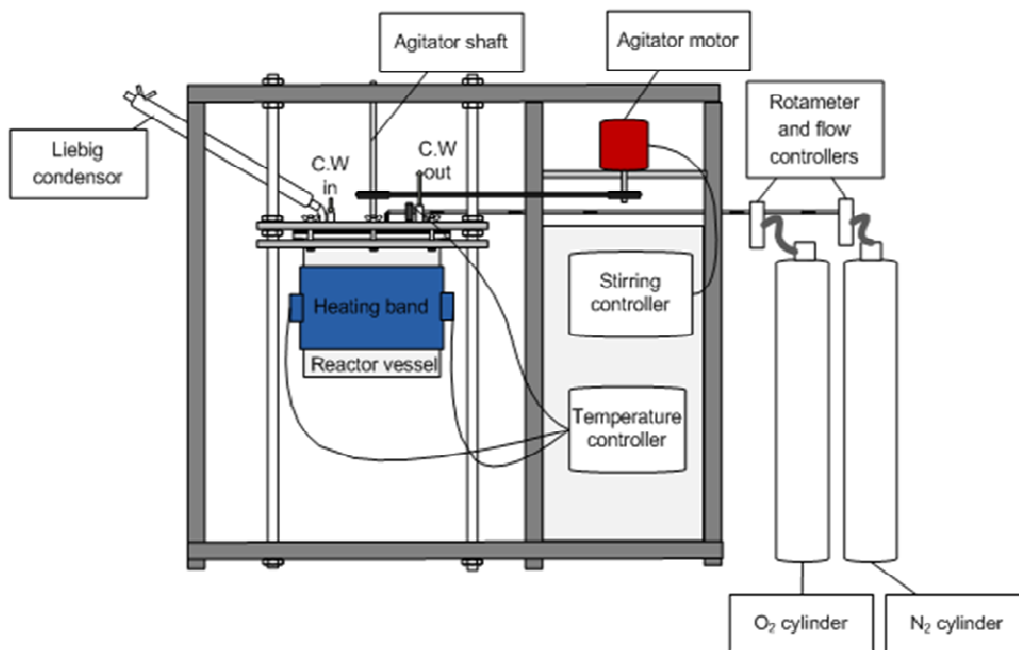


Figure 3-1 Front view of assembled reactor setup. Locations of gas supply, temperature and stirring controls, agitator motor, heating jacket and Liebig condenser are shown.

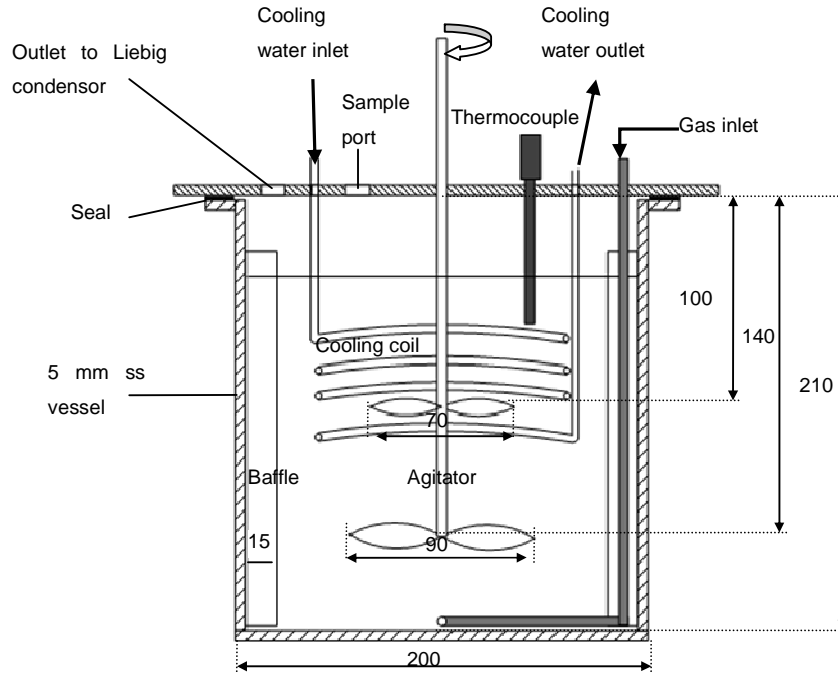


Figure 3-2 Arrangement of parts within reactor vessel. Dimensions are given in mm.

Agitation was provided by a stirrer outfitted with a pitched three-blade impeller at the top and a larger pitched four-blade impeller at the bottom (See Figure 3-2). Pitched blade impellers were used to provide axial lift and solid suspension. The bottom impeller also had the function of radial gas dispersion. The reactor was fitted with four baffles to promote turbulent mixing.

The reactor was covered during tests. (See Appendix A for schematic of disassembled reactor setup). A gas inlet was provided so that oxygen or nitrogen could be sparged into the solution from directly below the impeller. Nitrogen was used during non-oxidative tests to keep the system as free of oxygen as possible. The gas flowrate was controlled and measured with a rotameter. The gas flowrate was kept constant at 0.2 L/min. This flowrate was obtained by scaling down from the plant flowrate according to Equation 3-1.

$$\text{Scaled gas flow} = \text{Plant gas flow} \frac{V_{\text{liquid,scaled}}}{V_{\text{liquid,plant}}} \quad \text{Equation 3-1}$$

Where

$V_{\text{liquid, scaled}}$  is the liquid volume in the laboratory reactor

$V_{\text{liquid, plant}}$  is the liquid volume in a reactor at the plant

A gas outlet was provided in the cover and a Liebig condenser was used to minimise evaporation. Samples could be taken through a port in the cover which was otherwise closed with a plug.

### 3.2.2 Experimental procedure

A detailed experimental procedure is given in Appendix A. After filling the reactor with leaching solution, the stirrer was started and the temperature was increased to 85 °C. In non-oxidative tests, the nitrogen flowrate was set approximately 30 minutes before leaching started in order to flush the air from the volume between the liquid and the reactor cover. In oxidative tests, the oxygen flowrate was set approximately 10 minutes before the test started. When the reactor had stabilised at the correct temperature, the milled matte was fed through a port in the reactor cover.

A pipette was used to periodically take 15 ml samples from the reactor. Samples were immediately filtered to remove all particles larger than 0.2 µm, in order to prevent further reaction. The solids collected from samples were washed with distilled water, dried and kept for analysis. Liquid samples were kept at a temperature of 40 – 50 °C in a water bath while the pH and redox potential of liquid samples were noted. Immediately after measuring pH and redox potential, liquid samples were diluted with a nitric acid solution to prevent precipitation reactions from taking place.

The reactor was weighed at the beginning and end of tests to determine the mass of liquid that evaporated during tests. The final pulp was filtered in a pressure filter. The filter cake was washed with distilled water, after which the solids were dried at approximately 45 °C. Samples from the dry residue were taken for analysis.

### 3.2.3 Analysis

The following analysis techniques and equipment were used in this study:

#### Liquid samples:

- Dissolved nickel, cobalt, iron and copper concentrations in liquid samples was determined using atomic absorption spectroscopy (Varian SpectrAA-250 Plus).
- ICP-OES was used to determine the ruthenium content of liquid samples
- ICP-MS was used to determine the rhodium and iridium content of liquid samples.
- The solution redox potential was measured using a Ag/AgCl, KCl electrode.

#### Solid samples:

- The specific surface area of matte particles was determined using an ASAP 2010 (Accelerated Surface Area and Porosimetry System) from Micromeritics Instrument Corporation, using the BET theory.
- XRF analyses of solid samples were performed with a Panalytical AXIOS 2.4 kWatt instrument fitted with a Rh X-ray tube, to determine the Cu, Ni, Fe, S and Co content.
- To determine the mineralogy of leach residues, XRD analysis of solid samples were done using a PANalytical X'Pert Pro powder diffractometer with X'Celerator detector. X'Pert Highscore plus software was used to identify the phases.
- SEM-EDS analysis with JEOL JSM-7001F FEG SEM produced high resolution images of particles on polished mounts. EDS provided analysis of grain compositions. An accelerating voltage of 10 kV and emission current of 90  $\mu$ A was used.

## Chapter 4 Results and discussion

---

### 4.1 Experimental design

Experiments carried out during the course of this study are listed in Table 4-1. The list of tests is divided into an oxidative and non-oxidative block. This division will also apply when discussing results, with oxidative tests falling under Section 4.2 and non-oxidative tests under Section 4.3. Some of the results that will be discussed in Sections 4.2 and 4.3 have also been published by Van Schalkwyk et al. (2011).

Under oxidative conditions, copper removal reactions together with oxygen dependent acid leaching reactions are responsible for nickel leaching. For each oxidative test, a corresponding non-oxidative test was carried out. Comparison of oxidative and non-oxidative tests raises the possibility of gaining a better understanding into copper removal and acid leaching kinetics and mechanisms. Exceptions are test 17, for which a corresponding non-oxidative test was not carried out, as well as tests 8, 10 and 11, for which corresponding oxidative tests were not carried out. Tests 8, 10 and 11 are not directly comparable to other tests, but their results will be included in Appendix E.

In addition to the effect of oxygen, five more factors were investigated:

1. the solids/liquid ratio
2. initial acid concentration
3. initial copper concentration
4. Fe-endpoint
5. stirring rate

In this chapter, different selections of tests from Table 4-1 will be discussed to deal with each of the five factors listed above.

Table 4-1 List of experiments in this work

<b>Test</b>	<b>Fe-endpoint</b>	<b>Initial acid conc.</b>	<b>Initial Cu<sup>2+</sup> conc.</b>	<b>Stirring rate</b>	<b>Solids/liquid ratio</b>	<b>Target extraction</b>	<b>nickel</b>	<b>Cu<sup>2+</sup>/Ni ratio</b>
	<b>[Mass %]</b>	<b>[g/L]</b>	<b>[g/L]</b>	<b>[rpm]</b>	<b>[g/L]</b>	<b>[Mass %]</b>		
<b>Non-oxidative</b>								
1	0.86	37	40	1100	80		93	0.93
2	0.86	37	20	1100	80		46	0.46
3	0.86	74	37	1100	80		86	0.86
4	0.83	74	20	500	80		48	0.48
5	0.83	74	20	500	150		25	0.25
6	0.67	74	20	1100	150		25	0.25
7	0.89	37	20	1100	150		25	0.25
8	1.39	<5	10	1100	150		13	0.13
9	1.05	74	20	1100	540		7	0.07
10	1.39	10	20	1100	615		15	0.15
11	1.39	90	25	205	732		6	0.06
12	5.72	74	20	1100	150		28	0.28
13	5.72	74	20	500	150		28	0.28
<b>Oxidative</b>								
14	0.86	37	40	1100	80		100	1.0
15	0.86	37	20	1100	80		88	0.5
16	0.86	74	40	1100	80		100	0.9
17	0.86	74	20	1100	80		100	0.5
18	0.83	74	20	500	80		100	1.1
19	0.83	74	20	500	150		86	0.25
20	0.53	74	20	1100	150		97	0.29
21	0.53	37	20	1100	150		64	
22	1.05	74	20	1100	540		24	0.07
23	5.72	74	20	1100	150		95	0.28
24	5.72	74	20	500	150		95	0.28



The test matrix shown in Figure 4-1 will be discussed in Section 4.2.2 to show the effect of the solids/liquid ratio on oxidative leaching. Corresponding non-oxidative tests, as shown in Figure 4-2, will be discussed in Section 4.3.2. It was suspected that the solids/liquid ratio, initial acid concentration and stirring rate could all affect copper precipitation rates. For this reason, the three factors were investigated together. The effect of the solids/liquid ratio on oxidative leaching was tested at two stirring rates (500 rpm and 1100 rpm), as well as two acid levels (37 g/L and 74 g/L). The initial copper concentration was fixed at 20 g/L and low iron mattes were used.

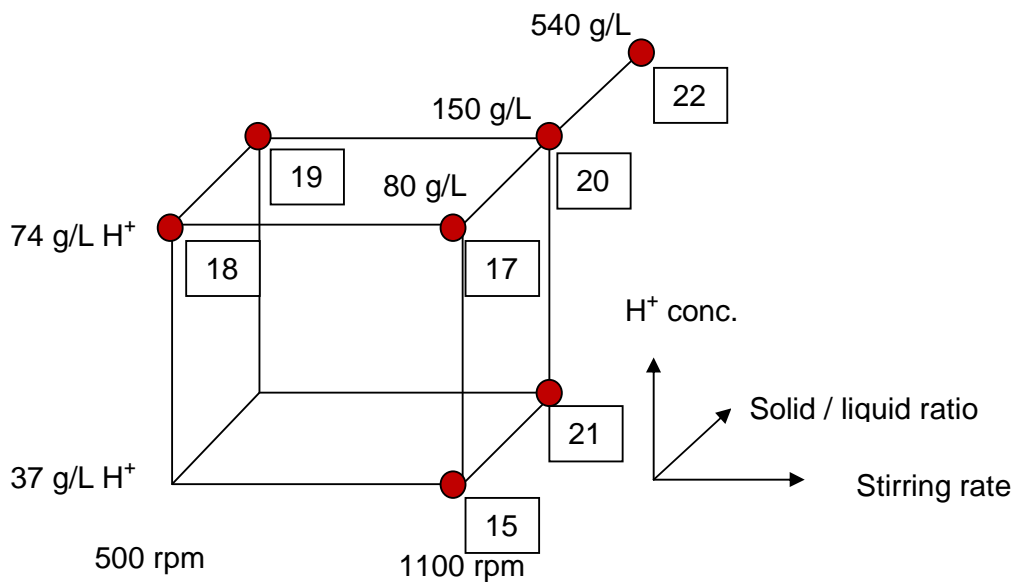


Figure 4-1 Oxidative tests to determine the effect of solids content on leaching, as well as interactions between solids content and stirring rate, and solids content and acid concentration. Low iron mattes were used in all tests and an initial copper concentration of 20 g/L.

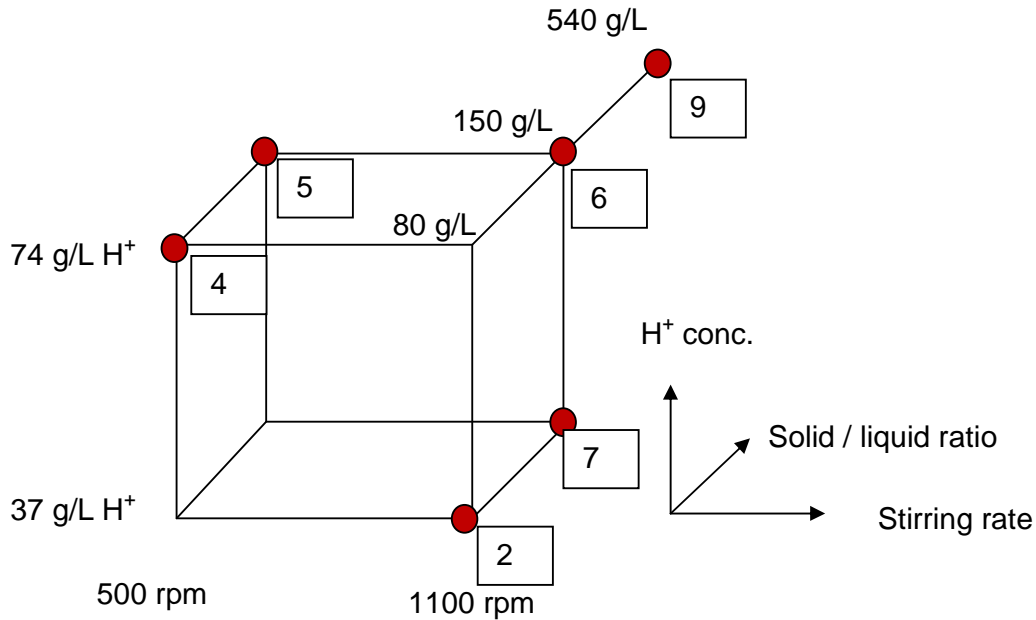


Figure 4-2 Non-oxidative tests to determine the effect of solids content on leaching. Tests correspond to the oxidative tests shown in Figure 4-1. Low iron mattes were used in all tests and an initial copper concentration of 20 g/L.

Three levels of solid/liquid ratios were used in tests: 80 g/L, 150 g/L and 540 g/L, which corresponded to pulp densities of 1190 g/L, 1240 g/L and 1520 g/L. The highest pulp density approaches the pulp density in the first stage leach (1600 g/L), as well as the pulp densities at which Lamy (2007) carried out test work on non-oxidative leaching (1600- 1750 g/L). At a solids content of 540 g/L, complete copper removal is possible, but the extent to which nickel can be leached is limited by the available reactants in solution. At 150 g solids/L, a substantial amount of copper can be removed, while still obtaining a reasonable percentage nickel extraction. At a solids content of 80 g/L, the available copper and acid in solution were in excess and more than 90 % of the nickel in the matte could theoretically be leached under oxidative conditions. On the other hand, complete copper removal was impossible at 80 g solids / L.

The initial copper and acid concentrations were based on the concentrations in spent electrolyte received from Marikana, as well as values used in literature. The concentrations are higher than that used in the continuous process at the Lonmin Marikana plant, but working at low concentrations in batch tests will lead to the

reactants being very quickly depleted. In the batch tests, the high and low levels were chosen as 74 g/L and 37 g/L for acid and 40 g/L and 20 g/L for copper. The operating ranges for acid and copper concentrations are comparable to several works from literature. These are summarised in Table 4-2. The work done by Hofirek and Kerfoot (1992) was carried out in a much lower concentration regime. Non-oxidative leaching was previously carried out by Lamy (2007) and conditions from this work are also shown in Table 4-2.

*Table 4-2 Summary of operating conditions from previously published works on batch leaching tests*

<b>Author</b>	<b>Oxidative/Non-oxidative</b>	<b>Cu<sup>2+</sup></b>	<b>H<sub>2</sub>SO<sub>4</sub></b>
Current work	Oxidative and non-oxidative	20 – 40 g/L	37 – 74 g/L
Llanos et al. (1974)	Oxidative	22 g/L	
Symmens et al. (1979)	Oxidative	21 – 48 g/L	38 – 80 g/L
Plasket and Romanchuk (1978)	Oxidative	20 g/L	60 – 120 g/L
Hofirek and Kerfoot (1992)	Oxidative	5 g/L	0 – 10 g/L
Lamy (2007)	Non-oxidative	25 – 48 g/L	90 – 110 g/L

Experiments carried out to investigate the effects of the initial acid and copper concentrations are shown in Figure 4-3 and Figure 4-4. For oxidative tests, it is possible to determine some of the interactions between the initial acid concentration, solids content and initial copper concentration. The effect of initial acid and copper concentrations will be discussed in Section 4.2.3 (oxidative) and Section 4.3.3 (non-oxidative).

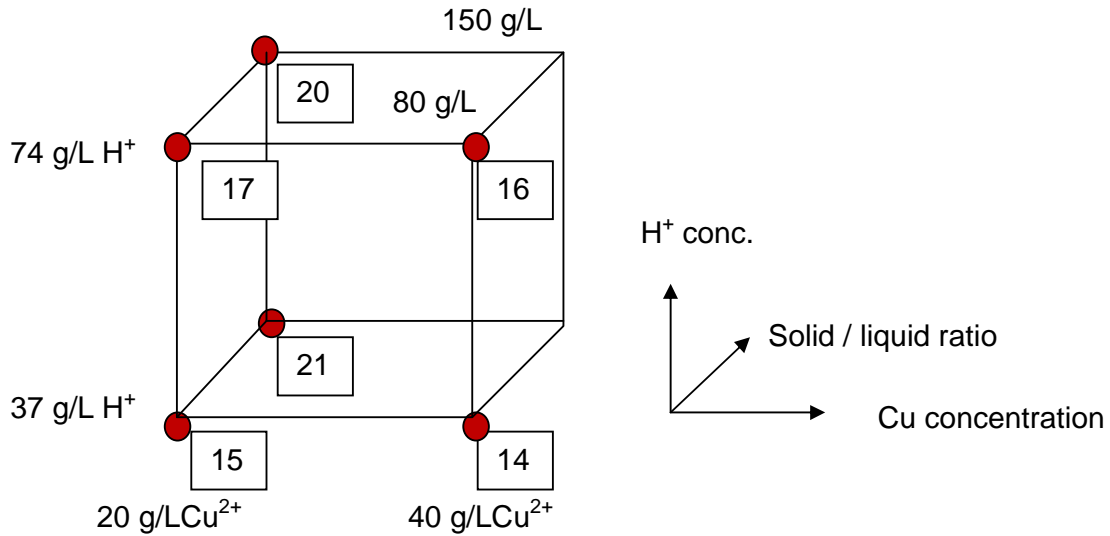


Figure 4-3 Oxidative tests to determine the effects of initial acid concentration and initial copper concentration. Low iron mattes were used in all tests and a stirring rate of 1100 rpm

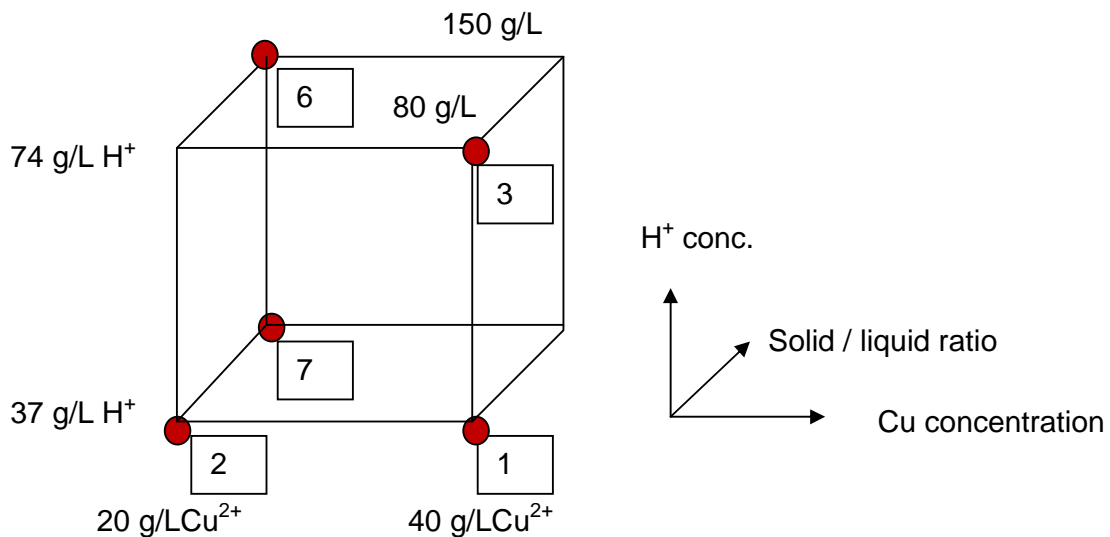


Figure 4-4 Non-oxidative tests to determine the effects of initial acid concentration and initial copper concentration. Corresponding oxidative tests shown in Figure 4-3. Low iron mattes were used in all tests and a stirring rate of 1100 rpm

Figure 4-5 and Figure 4-6 respectively show the oxidative and non-oxidative tests carried out to determine the effect of stirring rate. The high level stirring rate (1100 rpm) was chosen to ensure full solids suspension at the highest pulp density of 1520 g/L. The lower stirring (500 rpm) was chosen to produce less turbulent conditions in the reaction. It was suspected that lower stirring rates which might improve copper precipitation reactions.

The effect of stirring rate was investigated to give an indication of the kinetic controlling mechanisms of leaching and cementation reactions. In order to determine whether controlling mechanisms might be dependent on the matte composition, the effect of stirring rate on high and low iron mattes were tested. The effect of stirring rate on oxidative and non-oxidative leaching is discussed under heading 4.2.5 and 4.3.5.

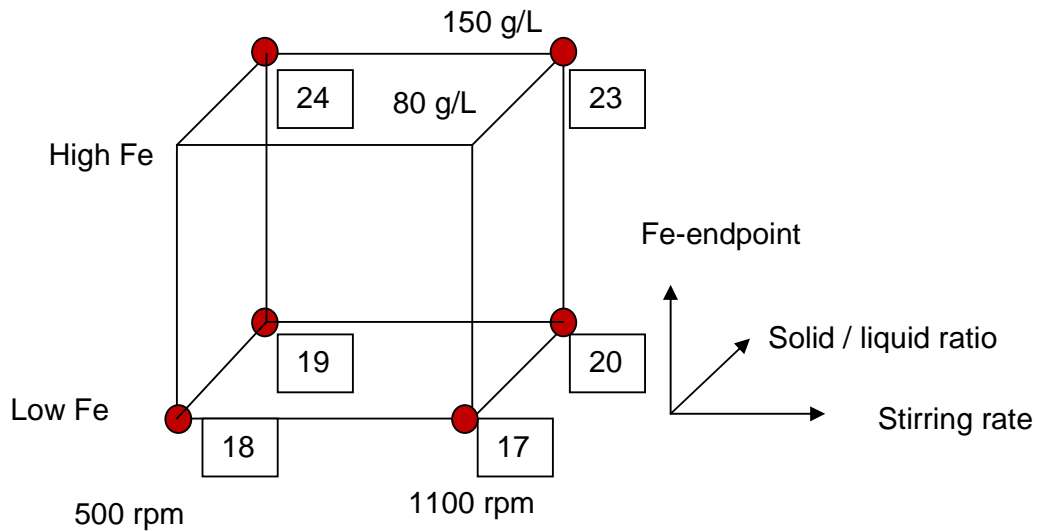


Figure 4-5 Oxidative tests that will be compared to determine the effects of stirring rate and the Fe-endpoint. In all tests the initial copper concentration was 20 g/L and the initial acid concentration was 74 g/L.

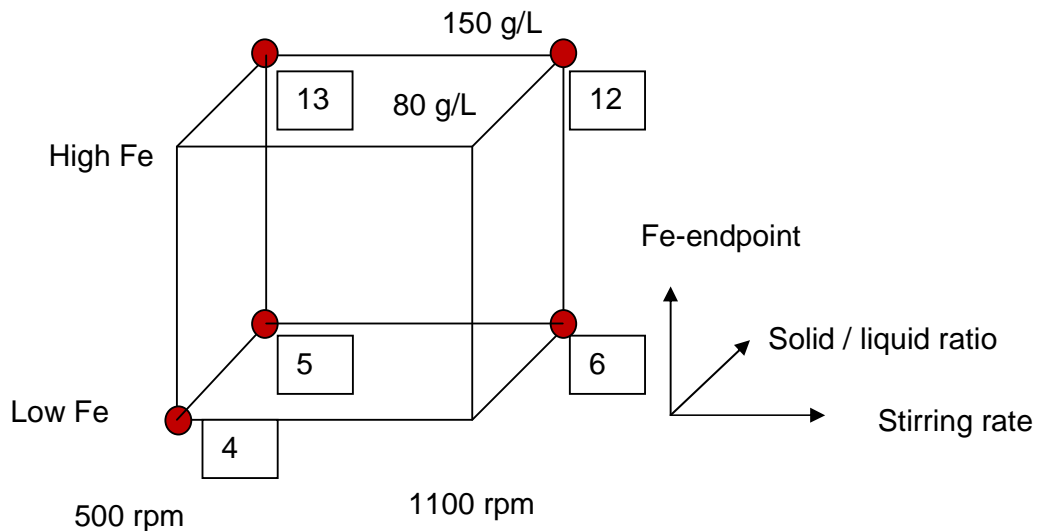


Figure 4-6 Non-oxidative tests to determine the effects of stirring rate and the Fe-endpoint. In all tests the initial copper concentration was 20 g/L and the initial acid concentration was 74 g/L.

Some of the tests shown in Figure 4-5 and Figure 4-6 will also be discussed in Section 4.2.4 and 4.3.4, to demonstrate the effect of the Fe-endpoint. In the case of oxidative leaching, tests 19, 20, 23 and 24 will be discussed. Tests 5, 6, 12 and 13 will be discussed to show the effect of the Fe-endpoint on non-oxidative leaching.

## **4.2 Oxidative leaching (OX)**

### **4.2.1 Leaching kinetics and mineralogical changes with time in oxidative tests**

In this section, the concentration changes and mineralogical changes in an oxidative batch leach test with a low iron matte will be described. Residue samples from all oxidative tests were analysed by quantitative XRD and solid samples taken periodically throughout tests were also used to determine changes in the mineralogy as leaching progressed during tests 19, 20, 21 and 22. Of these tests, test 20 will be described as a general example, while similarities with other tests will be highlighted. SEM-EDS analysis of samples from tests 20 and 22 will also be discussed at the end of this section. The results for tests 19, 21 and 22 are given in Appendix F. Deviations from test 20 that resulted from changes in operating conditions will be discussed in more detail Sections 4.2.2 – 4.2.5.

Concentration changes in solution occurring during test 20 are shown in Figure 4-7. The masses of major mineral phases as a function of time are shown in Figure 4-8. The mineralogical compositions of samples taken at different time intervals are given in Table 4-3. Figure 4-9 shows pH changes during the test and Figure 4-10 shows a comparison of the number of moles copper and acid consumed for nickel leaching. The number of moles acid which reacted was estimated as the difference between the copper precipitation and nickel extraction curves. The following discussion regarding the mechanism of leaching in test 20 will refer to these respective tables and figures.

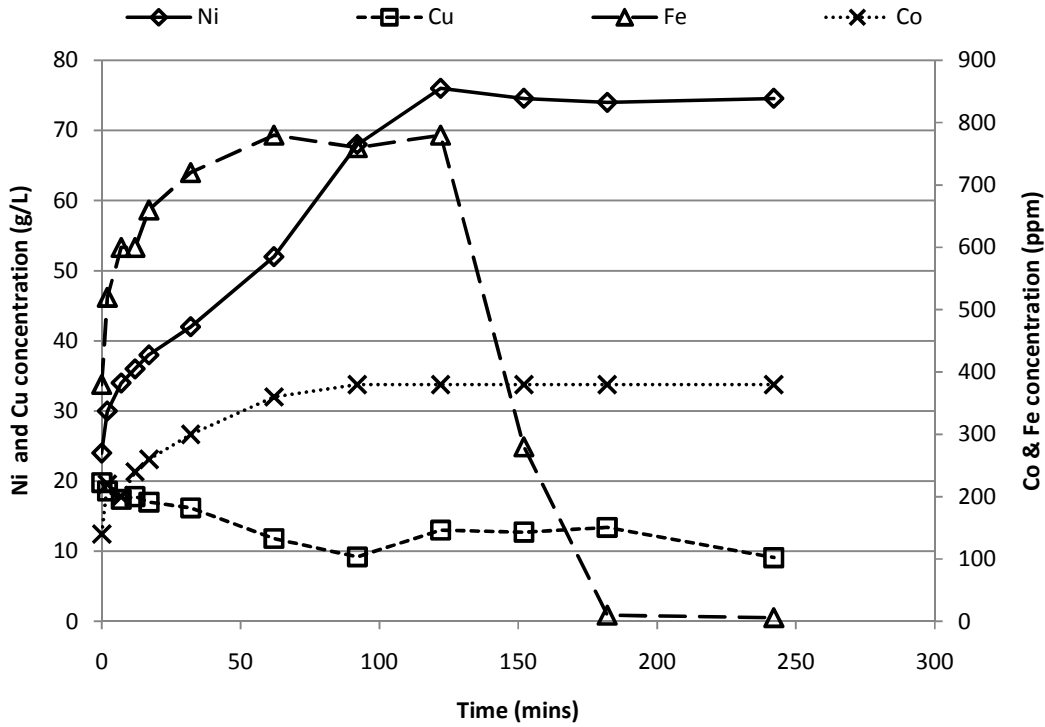


Figure 4-7 Concentration changes with time in test 20. 74 g/L acid, 20 g/L  $Cu^{2+}$ , 150 g solids/L, 1100 rpm, 0.53 % Fe

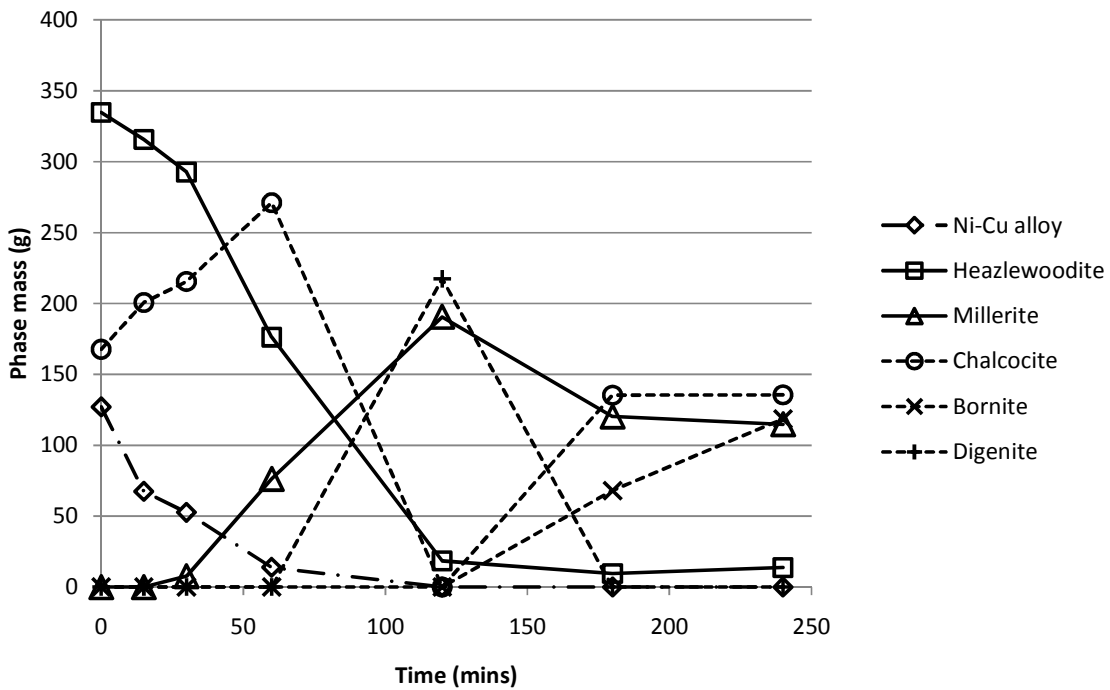


Figure 4-8 Changes in the masses of major phases with time in test 20. 74 g/L acid, 20 g/L  $Cu^{2+}$ , 150 g solids/L, 1100 rpm, 0.53 % Fe



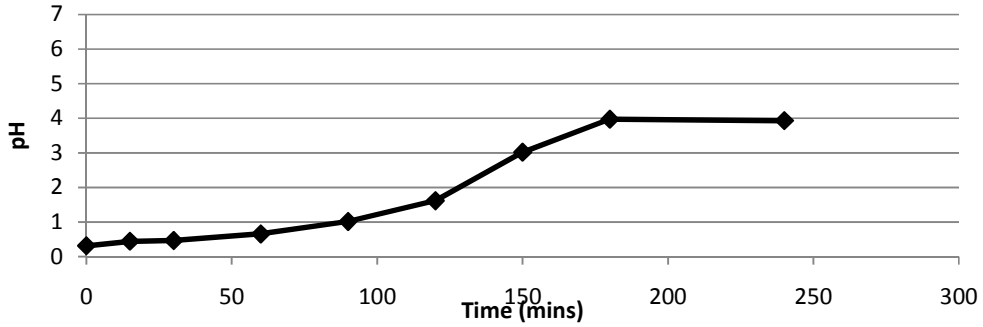


Figure 4-9 Solution pH as a function of time in test 20. 74 g/L acid, 20 g/L  $\text{Cu}^{2+}$ , 150 g solids/L, 1100 rpm, 0.53 % Fe

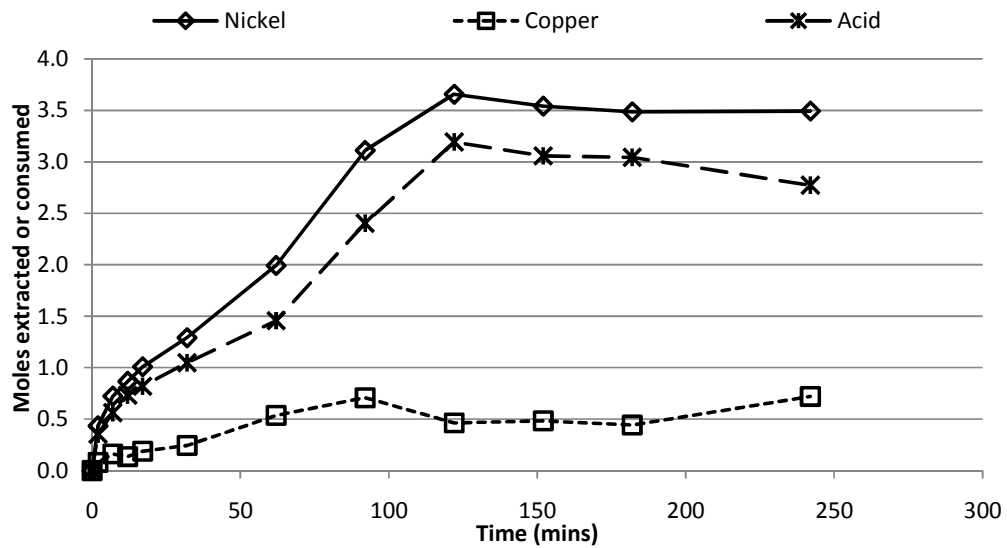


Figure 4-10 Comparison of the number of moles nickel extracted and number of moles copper precipitated in test 20.

Table 4-3 Mineralogical changes during test 20. 74 g/L acid, 20 g/L  $\text{Cu}^{2+}$ , 150 g solids/L, 1100 rpm, 0.53 % Fe

Mineral	Sample time:	Mass %						
		0	15	30	60	120	180	240
<b>Ni-Cu</b>	Ni-Cu	19.7	11.3	9.0	2.5	0	0	0
<b>Heazlewoodite</b>	$\text{Ni}_3\text{S}_2$	51.9	53.0	50.2	31.5	4.0	2.0	2.8
<b>Godlevskite</b>	$\text{Ni}_7\text{S}_6$	0	0	0	0	0	15.1	9.1
<b>Millerite</b>	NiS	0	0	1.3	13.6	41.7	25.6	23.6
<b>Polydymite</b>	$\text{Ni}_3\text{S}_4$	0	0	0	0	0	8.0	4.6
<b>Pentlandite</b>	$(\text{NiFe})_9\text{S}_8$	0	0.5	0.5	2.0	4.3	4.1	4.8
<b>Troilite</b>	FeS	0.9	1.1	1.1	0.5	0.9	1.8	2.7
<b>Magnetite</b>	$\text{Fe}_3\text{O}_4$	1.5	0.5	0.8	1.4	1.5	0	0
<b>Bornite</b>	$\text{Cu}_5\text{FeS}_4$	0	0	0	0	0	14.5	24.4
<b>Chalcocite</b>	$\text{Cu}_2\text{S}$	26.0	33.7	37.0	48.5	0	28.9	27.9
<b>Djurleite</b>	$\text{Cu}_{31}\text{S}_{16}$	-	-	-	-	-	-	-
<b>Digenite</b>	$\text{Cu}_9\text{S}_5$	-	0	0	0	47.5	0	0
<b>Covellite</b>	CuS	-	-	-	-	-	-	-
<b>Cuprite</b>	$\text{Cu}_2\text{O}$	-	-	-	-	-	-	-
<b>Antlerite</b>	$\text{Cu}_3\text{SO}_4(\text{OH})_4$	-	-	-	-	-	-	-
<b>Malachite</b>	$\text{Cu}_2\text{CO}_3(\text{OH})_2$	-	-	-	-	-	-	-

From Figure 4-8 it can be seen that the initial rate at which the mass of alloy decreased was fast (0 – 30 mins). Figure 4-10 shows the number of moles nickel extracted and copper precipitated. It can be seen that the moles nickel extracted during the first 30 minutes was much higher than the number of moles copper precipitated, indicating that nickel extraction probably took place due to leaching of the alloy phase by oxygen and acid (reaction 2-1). Heazlewoodite also decreased during the first 30 minutes, but formation of godlevskite and millerite did not take place, indicating that leaching of heazlewoodite by acid (reactions 2-4 and 2-5), did not take place.

The substantial increase in the chalcocite mass during the first 30 minutes indicates that copper from solution exchanged with nickel from the nickel-sulphide matrix (metathesis). Reaction 2-9, which is commonly postulated in literature, cannot be the mechanism responsible for metathesis, because experimental data shows that millerite formation did not take place during the first 30 minutes of the test. Metathesis probably took place via a galvanic interaction between heazlewoodite and the alloy phase, such as suggested by Rademan et al. (1999) (reaction 2-12). In

test 19, 21 and 22, similar initial stages of chalcocite formation were noted which were accompanied by a decrease in the alloy and heazlewoodite masses. Formation of pure metallic copper was generally not observed, indicating that the exchange of nickel from the alloy with dissolved copper (cementation; reaction 2-11), was limited.

In Figure 4-7 inflection points can be seen at 30 minutes in the nickel extraction curve, as well as in the copper concentration curve, after which the rates of copper precipitation and nickel extraction increased, along with the rate at which the heazlewoodite mass decreased (Figure 4-8). The slow kinetics with which heazlewoodite initially reacted might be explained by galvanic inhibition due to the presence of the alloy phase. Increased nickel leaching in the second period (after 30 minutes) can be attributed to the reaction of acid with heazlewoodite (reaction 2-4), which is supported by the formation of millerite. Results from test 20 (as well as results from test 19) show that millerite was formed before godlevskite was formed, showing that the reaction of heazlewoodite to form millerite does not need to progress through godlevskite as an intermediate (reactions 2-5 and 2-6). Godlevskite formation was also observed in tests 18, 21 and 22. The metathesis reaction (reaction 2-12) and chalcocite growth continued up to 60 minutes in test 20, but in tests 19, 21 and 22, chalcocite formation slowed down substantially after the initial period of nickel extraction, indicating that the second period of nickel extraction is dominated by acid leaching.

In tests 20, 14, 15, 16 and 17 nickel leaching reached a maximum, although enough copper and acid were still available for nickel leaching to continue. From these results, the maximum leacheable nickel can be determined to be approximately 55 – 66 % of the nickel originally present in the matte. In test 20 a nickel extraction of 65.3 % was achieved. Cobalt often reached a maximum percentage extraction at approximately the same time as nickel.

In the period between 90 and 150 minutes in test 20, copper was leached. Copper leaching also occurred in tests 14, 15, 16, 17 and 19. In many tests copper leaching started shortly before nickel leaching reached a maximum, suggesting that copper leaching starts once the leachable nickel has been extracted. In test 20, copper

leaching was limited and chalcocite was converted to digenite. The complete conversion of chalcocite to digenite between 60 and 120 minutes indicates that solid state changes can occur rapidly throughout the solid particles. In tests where copper extraction took place to a larger extent (tests 16 and 17), it was found that leaching of chalcocite led to the formation of covellite.

Iron precipitation occurred after 120 minutes. At the same time, copper was precipitated from solution. Precipitated iron, together with copper and sulphur, formed bornite. The simultaneous occurrence of iron precipitation with bornite formation and growth was also seen in tests 21 and 22. In test 21, this period was also associated with an increase in nickel extraction rate. To a lesser extent, troilite and pentlandite were also formed as iron was integrated into the nickel sulphide matrix. Other examples of bornite, troilite and pentlandite formation can be found in tests 14 and 15.

During the last 120 minutes of test 20, millerite was transformed to godlevskite and polydymite through a solid state reaction. The nickel concentration did not change during this time. Nickel extraction slowed down substantially when all the heazlewoodite had been converted to millerite.

The kinetics of PGE precipitation in tests 20, 21 and 22 were analysed. Changes in iridium, rhodium and ruthenium concentrations with time during test 20 are illustrated in Figure 4-11. The amounts of platinum and palladium in the starting leach solution were negligible and these elements did not dissolve during the test. PGEs were almost entirely precipitated from solution in all tests.

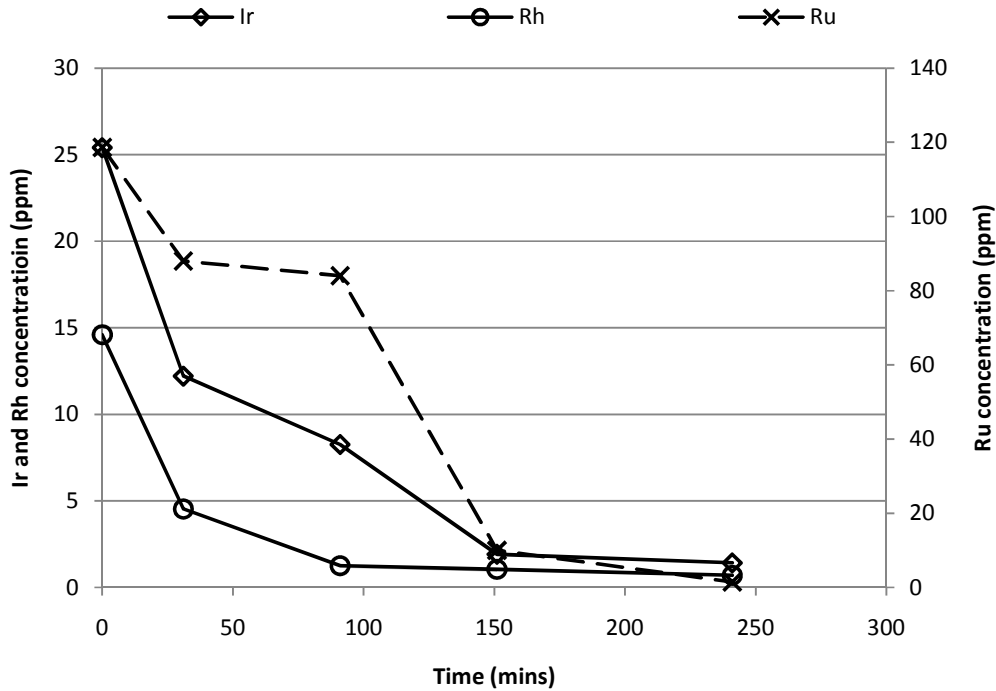


Figure 4-11 PGE concentration changes with time in test 20. 74 g/L acid, 20 g/L  $\text{Cu}^{2+}$ , 150 g solids/L, 1100 rpm, 0.53 % Fe

Representative solid samples from tests 20 and 22 were analysed with a scanning electron microscope equipped with energy dispersive X-ray spectroscopy to improve understanding of solid state changes during leaching. The relative abundances of phases in the residue from test 20, as determined with quantitative XRD analysis were 2.8 % heazlewoodite, 9.1 % godlevskite, 23.6 % millerite, 4.6 % polydymite, 4.8 % pentlandite, 2.7 % magnetite, 24.4 % bornite and 27.9 % chalcocite. SEM-images of particles from the residue sample are shown in Figure 4-12.

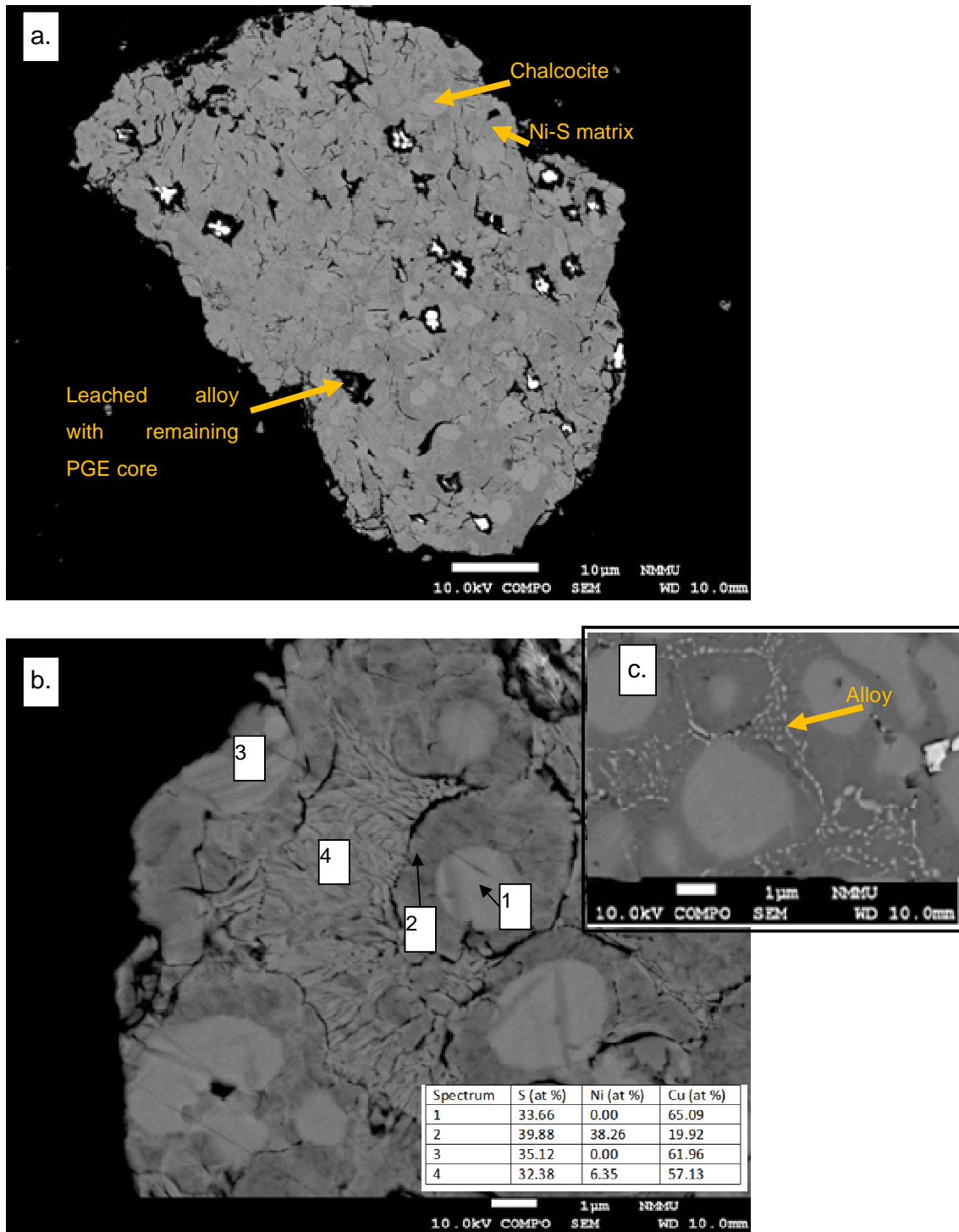


Figure 4-12 (a and b): SEM images of a residue particle from test 20, showing evidence of copper substitution and disintegration of the nickel-sulphide matrix. (c): veinlike alloy structures in residue of test 6

When considering Figure 4-12 (a), holes with the characteristic shape of the alloy phase are apparent. It is also of interest that the PGE-containing core, which is typically associated with the alloy phase (Thyse et al. (2010)), remained unleached. The image shows euhedral chalcocite grains (lighter areas) embedded in a cementing nickel-sulphide matrix. Analyses of six chalcocite grains showed little variation in chemical composition with an average composition 63.2 at % copper and 35.1 at % sulphur (Ranges: 59.9 – 64.7 at % Cu, 33.4 – 38.1 at % S). On the other hand, the composition of the nickel sulphide matrix shows significant variation after leaching, leading to the variation in greyscale as shown at location 2 in image (b). Analysis of eight areas similar to location 2 shows that the nickel to copper ratio changes from one area to the next, while the relative abundance of sulphur remains fairly constant. The average composition over the eight areas was 39.5 at % Ni, 19.1 at % Cu and 39.2 at % S. (Ranges: 24.5 – 50.7 at % Ni, 4.1 – 35.5 at % Cu, 36.2 – 41.1 at % S).

In Figure 4-12, the veinlike structure (location 4 on image b) appears to be a newly formed copper sulphide phase, which is formed as copper replaces nickel in the heazlewoodite matrix. The porous appearance of these areas is probably caused by nickel leaching. Analyses of seven similar areas show an average composition similar to chalcocite, but with some residual nickel: 7.6 at % Ni, 52.7 at % Cu and 34.7 at % S (Ranges: 3.3 – 12.9 at % Ni, 38.4 – 59.4 at % Cu, 30.4 – 46.3 at % S). Image (c) shows a micrograph of a residue particle from test 6, in which a veinlike alloy structure is indicated. Similar alloy structures were probably present in the matte at the start of test 20. The similarity in appearance suggests that the veinlike structure in image (b) might have its origin in alloy structures such as shown in image (c). It is possible that copper from the alloy replaces nickel in the adjacent nickel sulphide matrix as the alloy dissolves, leading to the formation of structures such as shown in image (b).

Concentration changes occurring during test 22 are shown in Figure 4-13. The test conditions for test 22 were the same as for test 20, with the exception that the solids content was higher (540 g/L). SEM-images of particles from a solid sample taken after 60 minutes in test 22 are illustrated in Figure 4-14. The concentration changes up to 60 minutes, together with phase changes in the solid state indicate that the

solid sample was taken before the second stage of nickel leaching (as discussed for test 20), during which acid leaching of the heazlewoodite matrix would have been more prominent and the nickel leaching rate would have increased. The relative abundances of respectively the Ni-Cu alloy, heazlewoodite and chalcocite were 12.0 %, 53.7 % and 25.5 % at the start of test 22 and 6.8 %, 52.4 % and 34.5 % after 60 minutes.

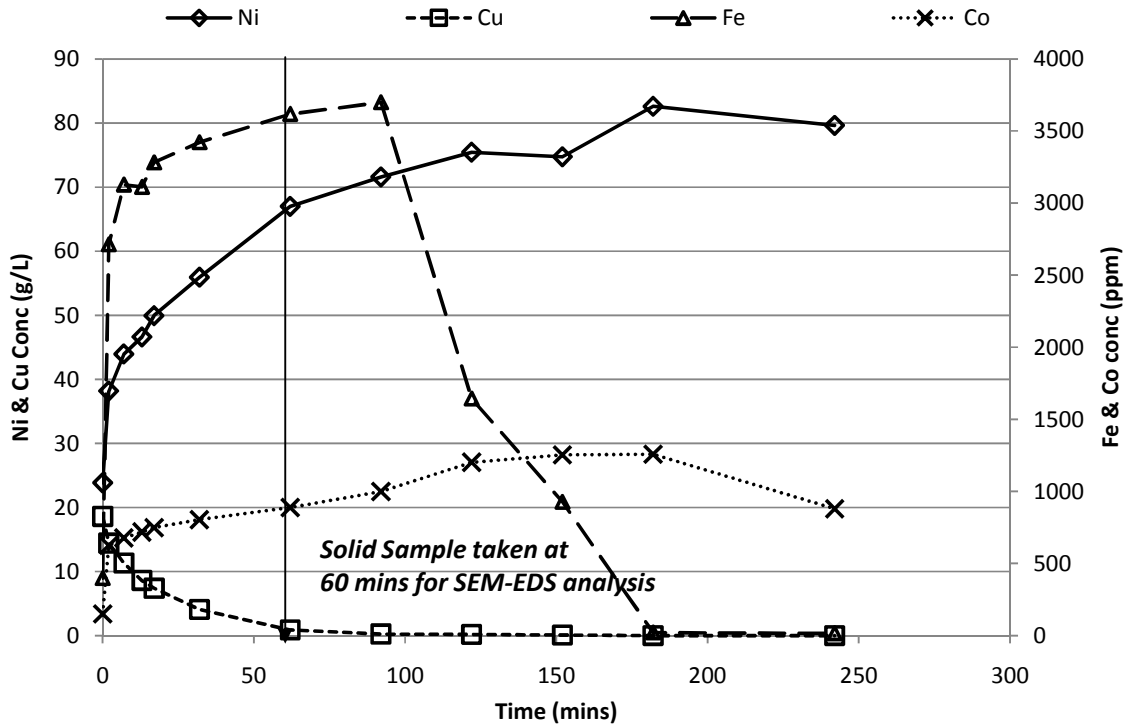


Figure 4-13 Concentration changes with time in test 22. 74 g/L acid, 20 g/L  $\text{Cu}^{2+}$ , 540 g solids/L, 1100 rpm, 1.05 % Fe.



In Figure 4-14, image (a) shows a solid particle at 10  $\mu\text{m}$  bar, while the marked area is enlarged and shown at 1  $\mu\text{m}$  bar in image (b). Alloy grains were left intact or partially leached out. Analysis of eight alloy grains showed an average composition of 69.7 at % Ni (60.3 - 73.2 at %) and 26.6 at % Cu (21.8 – 36.2 at %), with the relative abundances of all other elements being less than 1 % (It should be noted that the analyses were done on the alloy surrounding the PGE-containing core). The heazlewoodite matrix shows some evidence of disintegration, but, unlike the residue from test 20, the nickel sulphide matrix contained only a small amount of copper. The average composition of the nickel sulphide, determined from analyses of ten areas, was 62.2 at % Ni (57.8 – 68.9 at %), 2.5 at % Cu (0 – 5.8 at %) and 33.3 at % S (30.8 – 35.1 at %). The small percentage copper in the heazlewoodite matrix suggests that copper which is precipitated during the first stage is not integrated into the nickel sulphide matrix. Rather, evidence of growth in the existing chalcocite phases was found (as shown in image (b)). Analyses of four chalcocite grains showed an average composition of 67.8 at % Cu (59.7 at % - 70.6 at %) and 28.6 at % S (27.8 – 29.3 at %).

When comparing the SEM-EDS analyses of samples from tests 20 and 22, it appears that copper precipitation during different reaction stages leads to different mineralogical formations. In test 22, where only one stage of nickel leaching was visible, copper precipitation led to the growth of chalcocite grains, while the nickel sulphide matrix remained pure of copper. However, when nickel leaching progressed further, such as during test 20, copper was also included in the disintegrating nickel sulphide matrix. Images from both samples suggest that the reactions took place to the same extent throughout the particles: no signs of shrinking core effects (such as an inhibiting product layer) were seen.

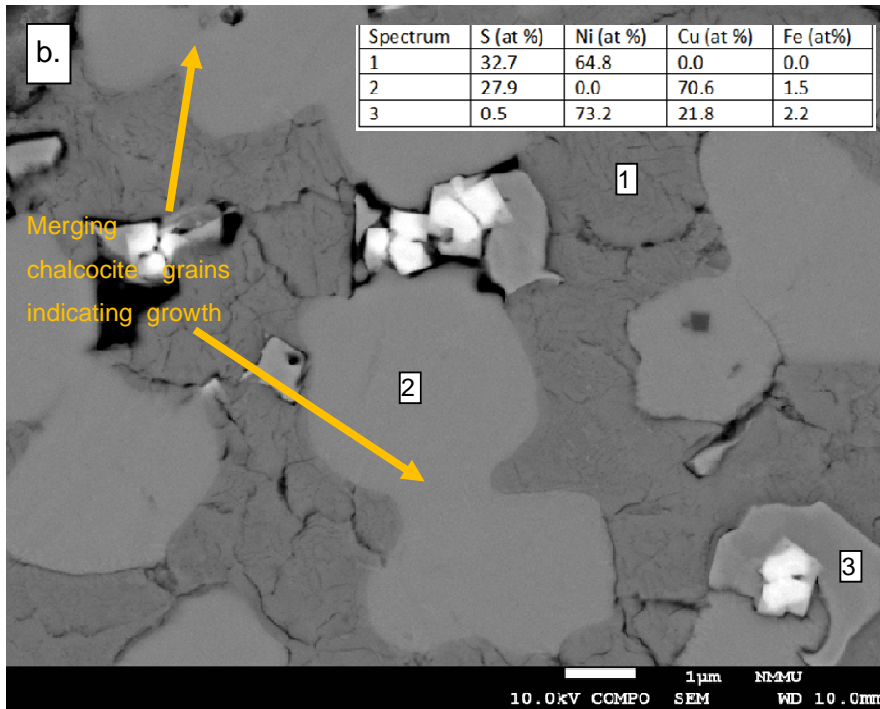
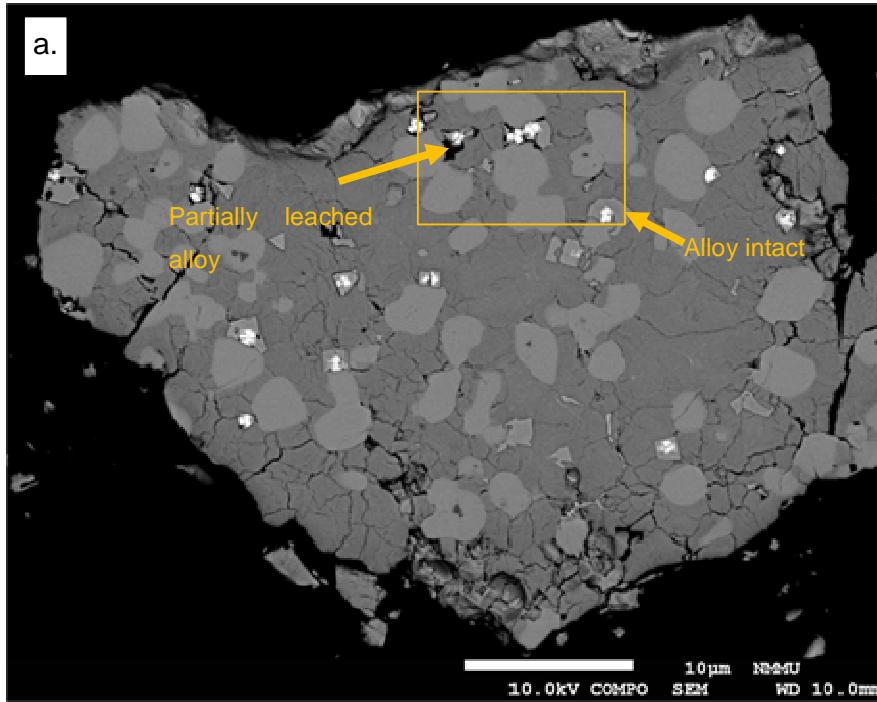


Figure 4-14 (a and b): SEM image of a particle sampled after 60 minutes in test 22 , showing alloy leaching and heazlewoodite disintegration

From the results discussed in the preceding text, the following generalised mechanism for oxidative leach tests can be derived: In a first reaction stage, alloy was leached by acid (reaction 2-1), while metathesis took place according to reaction 12, which was proposed by Rademan et al. (1999) and involves galvanic interaction between the alloy and heazlewoodite phases. In a second reaction stage, the rate at which heazlewoodite is consumed increases and millerite is formed. During this second stage, acid leaching of heazlewoodite (reaction 2-4) is probably the dominant mechanism responsible for nickel leaching. Chalcocite is formed during both reaction stages. Rademan et al. (1999) reported that chalcocite formed a barely visible deposit on the edges of particles and veins during pressure leaching of Ni-Cu-S converter matte. In the current work, copper precipitation leads to the growth of existing chalcocite grains and to the integration of copper into the heazlewoodite matrix during later stages. Cuprite formation (which is reported as a prominent feature in literature: Llanos et al. (1974), Symmens et al. (1979), Fugleberg et al. (1995)) was not observed by means of quantitative XRD or SEM analyses. Copper leaching can occur when the heazlewoodite content of the solid phase becomes limited, leading to the formation of digenite or chalcocite. Similar results were previously reported by Rademan et al. (1999). Nickel leaching came to a stop or slowed down substantially when most of the nickel had been converted from heazlewoodite to phases with lower Ni:S ratios. If the solution pH rose sufficiently, iron precipitation occurred. Copper precipitation was found to increase in some instances when iron precipitation occurred, this was accompanied by the formation of bornite and to a lesser extent troilite and pentlandite.

The solution redox potential, relative to a Ag/AgCl electrode, was measured in many of the oxidative tests. Typically, the value at the start of a test was between 450 to 500 mV. In the first 15 to 30 minutes of leaching tests, the solution redox potential decreased quickly, after which it stabilised at values ranging between 270 and 390 mV. The pH increased as acid was consumed in tests and often reached a plateau at a value of 4 (Tests 14, 15, 20 and 22)

## 4.2.2 Effect of solids/liquid ratio (OX)

The effect of the solids/liquid ratio on oxidative leaching will be demonstrated by comparing three sets of tests (Refer to Figure 4-1). In the first set of tests (tests 15 and 21), the solids contents were respectively 80 g/L and 150 g/L. The stirring rate was 1100 rpm and the initial acid concentration was 37 g/L. In the second set of tests (Tests 17, 20 and 22), the solids contents were respectively 80 g/L, 150 g/L and 540 g/L. The stirring rate was 1100 rpm and the initial acid concentration was 74 g/L. The solids/liquid ratios for the third set of tests (Tests 18 and 19), were respectively 80 g/L and 150 g/L. The stirring rate was 500 rpm and the initial acid concentration was 74 g/L. Tests 17 and 20 differ from tests 15 and 21 in terms of acid concentration and from tests 18 and 19 in terms of stirring rate.

### Comparison of tests 15 and 21

Operating conditions for tests 15 and 21 are given in Table 4-4. pH changes in the two tests are compared in Figure 4-16. More acid was consumed in the high solids test. The pH rose to a value of 6.5 during the 150 g solids/L test and to 4 in the 80 g solids/L test. Test 21 (150 g solids/L) was stopped after 150 minutes due to the rapid rise in pH. The rates of metal extraction and copper precipitation are compared in Figure 4-15. In the test with the higher solids content, the rates and extents of nickel, cobalt and iron extractions were lower. Copper removal was initially fast in both tests, but the second stage was much slower in the 80 g solids/L test than in the 150 g solids/L test. XRD analyses of solid samples from test 21 show that the second period of copper removal is associated with a rapid decrease in the mass of heazlewoodite. In test 15 (for which an XRD analysis is only available for the residue), the heazlewoodite was probably leached out faster than in test 21, so that a second period of copper removal did not occur.

Table 4-4 Operating conditions for tests 15 and 21

Test	Solids/Liquid [g/L]	Gas	Fe-endpoint [Mass %]	Init. Cu conc [g/L]	Init. Acid conc. [g/L]	Stirring [rpm]
15	80	O <sub>2</sub>	0.89	20	37	1100
21	150	O <sub>2</sub>	0.53	20	37	1100

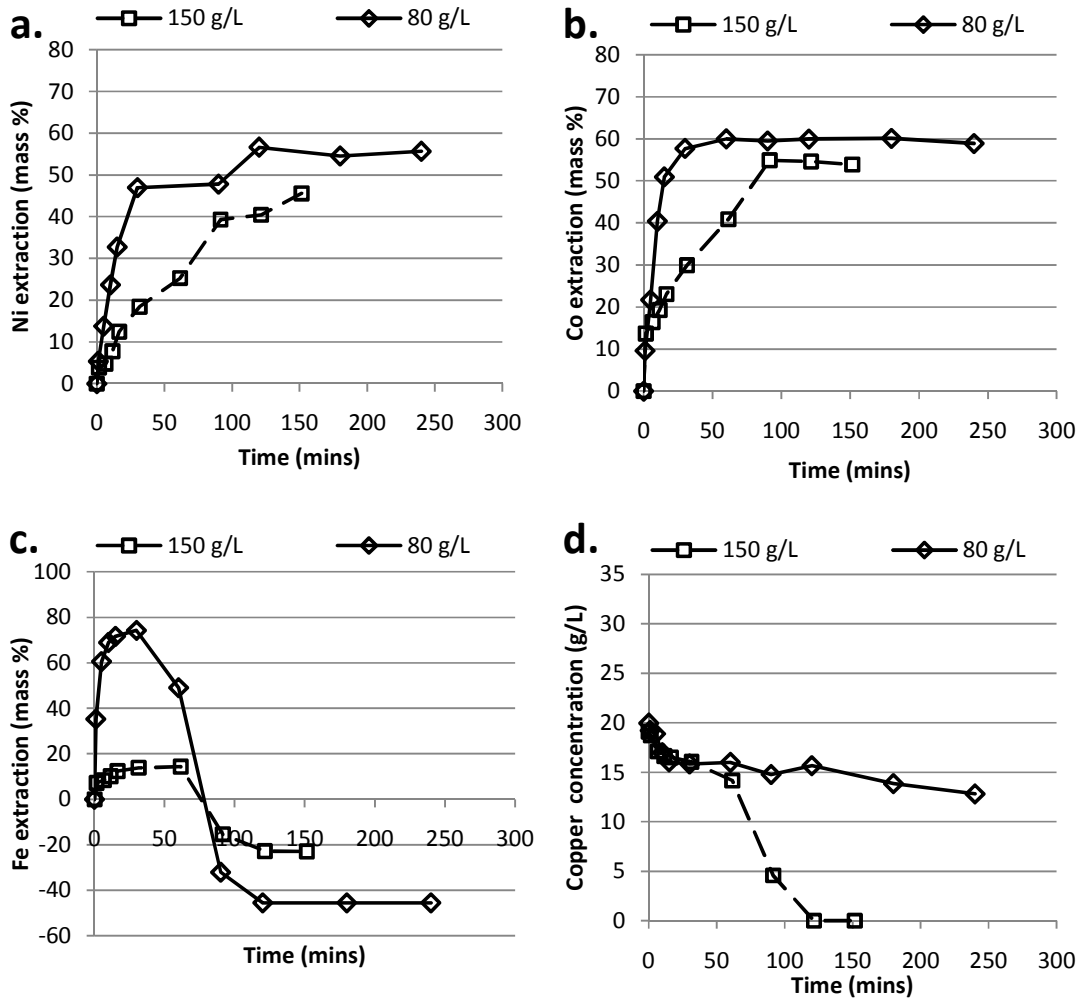


Figure 4-15 Comparison of metal extractions and copper precipitation during test 15 (80 g solids / L) and test 21 (150 g solids / L).

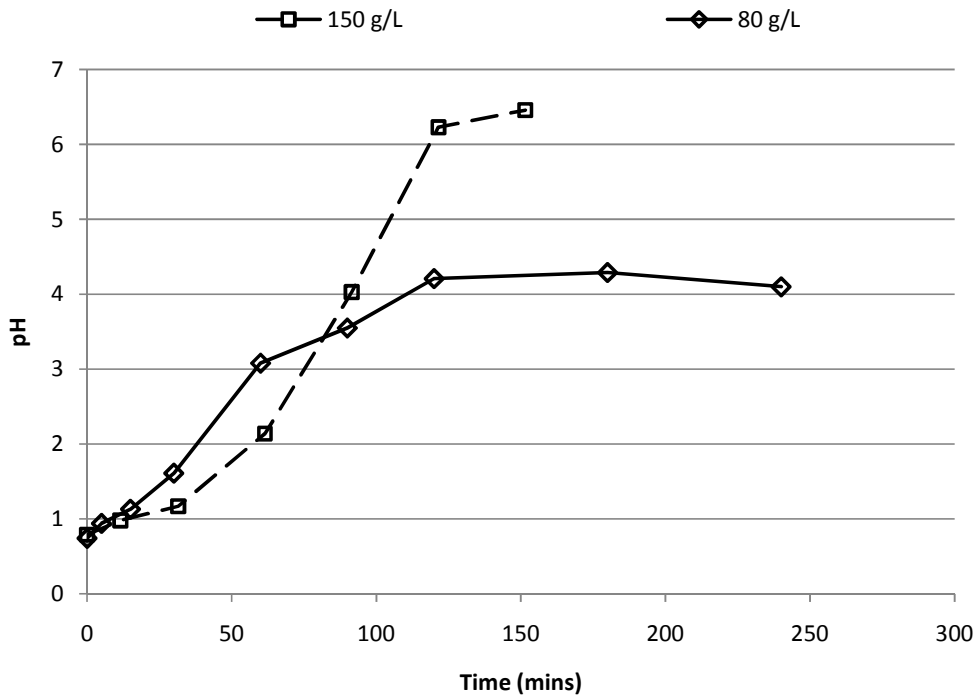


Figure 4-16 Comparison of pH changes in test 15 (80 g/L) and 21 (150 g/L)

Comparison of tests 17, 20 and 22

Operating conditions for tests 17, 20 and 21 are given in Table 4-5. Metal extractions with respect to time, as well as changes in the copper concentrations during the three tests are compared in Figure 4-17. Solution pH as a function of time during the tests are shown in Figure 4-18. Acid consumption and the rate at which the pH increased was higher at higher solids contents (Figure 4-18).

The nickel extraction rate was higher with a solids content of 80 g/L (test 17) than with a solids content of 150 g/L (test 20), although a higher final extraction was obtained in the 150 g/L test. The initial rate of cobalt extraction was the same in tests 17 and 20. (The highest cobalt extraction was achieved in the 150 g/L test, but it should be noted that the matte only contained 0.21 % Co, while the mattes used in the 80 g/L test and the 540 g/L tests both contained 0.42 % Co.) The effect of the solid/liquid ratio on cobalt and nickel leaching rates was less pronounced when comparing test 17 to test 20 than when comparing test 15 to 21. This can be attributed to the fact that the acid concentration was lower in tests 15 and 21, which

meant that the available acid became limiting when the solids content was increased.

When comparing results from tests 17 and 20 with test 22, the rates and extents of nickel extraction were significantly higher in the 80 g/L and 150 g / L tests than in the 540 g solids / L test. In the 540 g/L test, the availability of reactants in solution was the limiting factor in nickel leaching, while the availability of nickel in the matte was the limiting factor in the tests with lower solids/liquid ratios. From the lower density tests, it can be seen that only 60 % to 70 % of the nickel in the converter matte was readily leachable.

More copper was precipitated from solution in the 150 g solids/L test (test 20) than in the 80 g solids/L test (test 17). Copper was leached in both tests, but to a larger extent in the 80 g solids/L test, where the solution pH was lower. At a solids content of 540 g/L, copper was removed rapidly from solution in a single reaction stage.

Table 4-5 Operating conditions for Tests 17, 20 and 22

Test	Solids/Liquid [g/L]	Gas	Fe-endpoint [Mass %]	Init. Cu conc [g/L]	Init. Acid conc. [g/L]	Stirring [rpm]
17	80	O <sub>2</sub>	0.89	20	74	1100
20	150	O <sub>2</sub>	0.53	20	74	1100
22	540	O <sub>2</sub>	1.05	20	74	1100

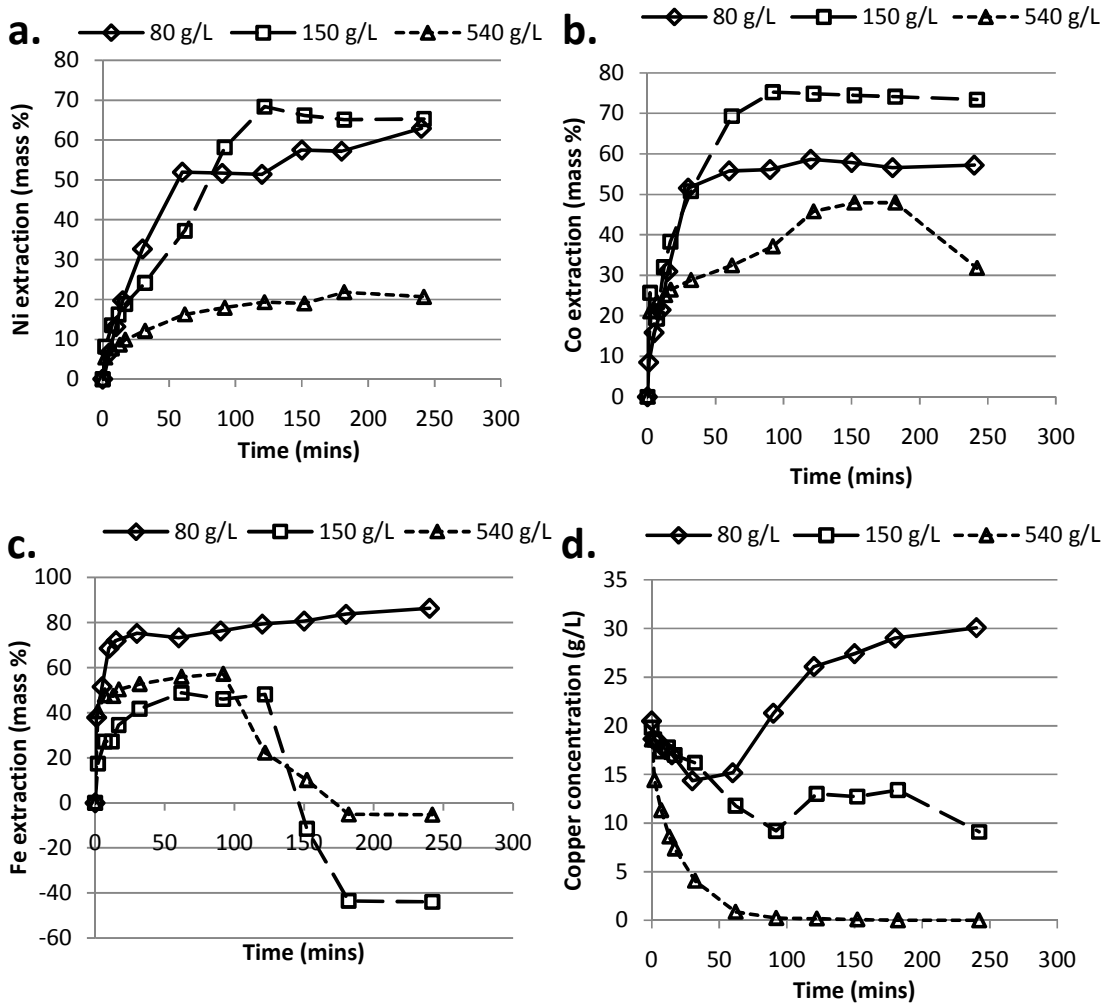


Figure 4-17 Comparison of metal extractions and copper precipitation during test 17 (80 g solids / L), test 20 (150 g solids / L) and test 22 (540 g solids / L)



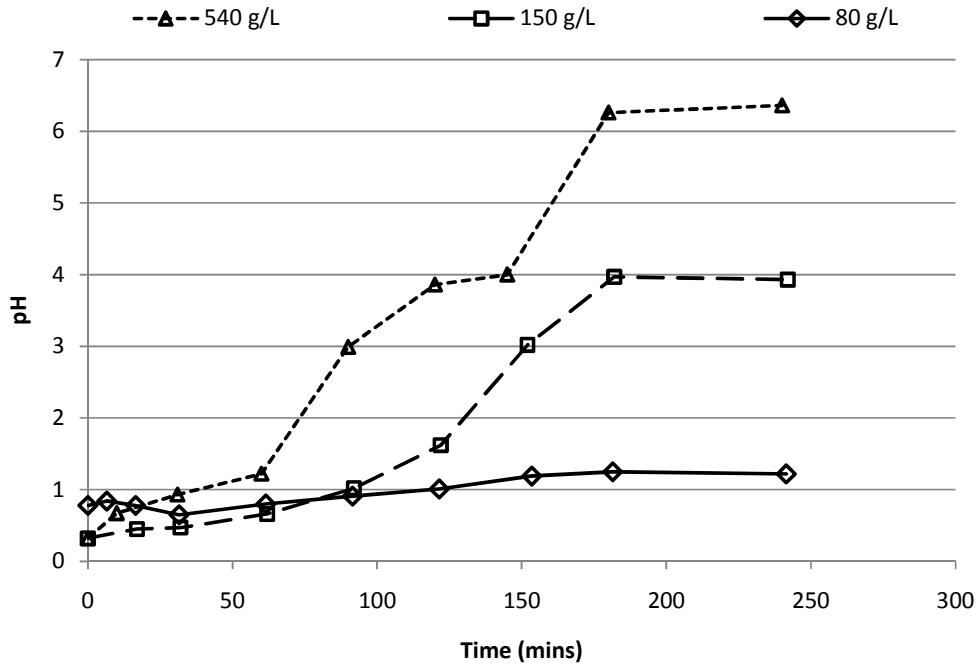


Figure 4-18 Comparison of pH changes in Tests 17, 20 and 22 (with respective solids contents of 80 g/L, 150 g/L and 540 g/L)

The initial rate of iron leaching was much faster at a solids content of 80 g/L than at 150 g/L or 540 g/L, probably due to the increase in available reactants in relation to the iron in the matte. In the 150 g solids / L and the 540 g / L tests, the pH reached a plateau at a value of 4. Iron precipitation took place while the pH was at this value.

Comparison of tests 18 and 19

Tests 18 and 19 were carried out with a stirring rate of 500 rpm, with respective solid/liquid ratios of 80 g/L and 150 g/L. Test conditions are given in Table 4-6 and results are shown in Figure 4-19. Due to slow reaction rates at the low stirring rate, significant pH changes did not occur in either test.

Table 4-6 Operating conditions for tests 18 and 19

Test	Solids/Liquid [g/L]	Gas	Fe-endpoint [Mass %]	Init. Cu conc [g/L]	Init. Acid conc. [g/L]	Stirring [rpm]
18	80	O <sub>2</sub>	0.83	20	74	500
19	150	O <sub>2</sub>	0.83	20	74	500

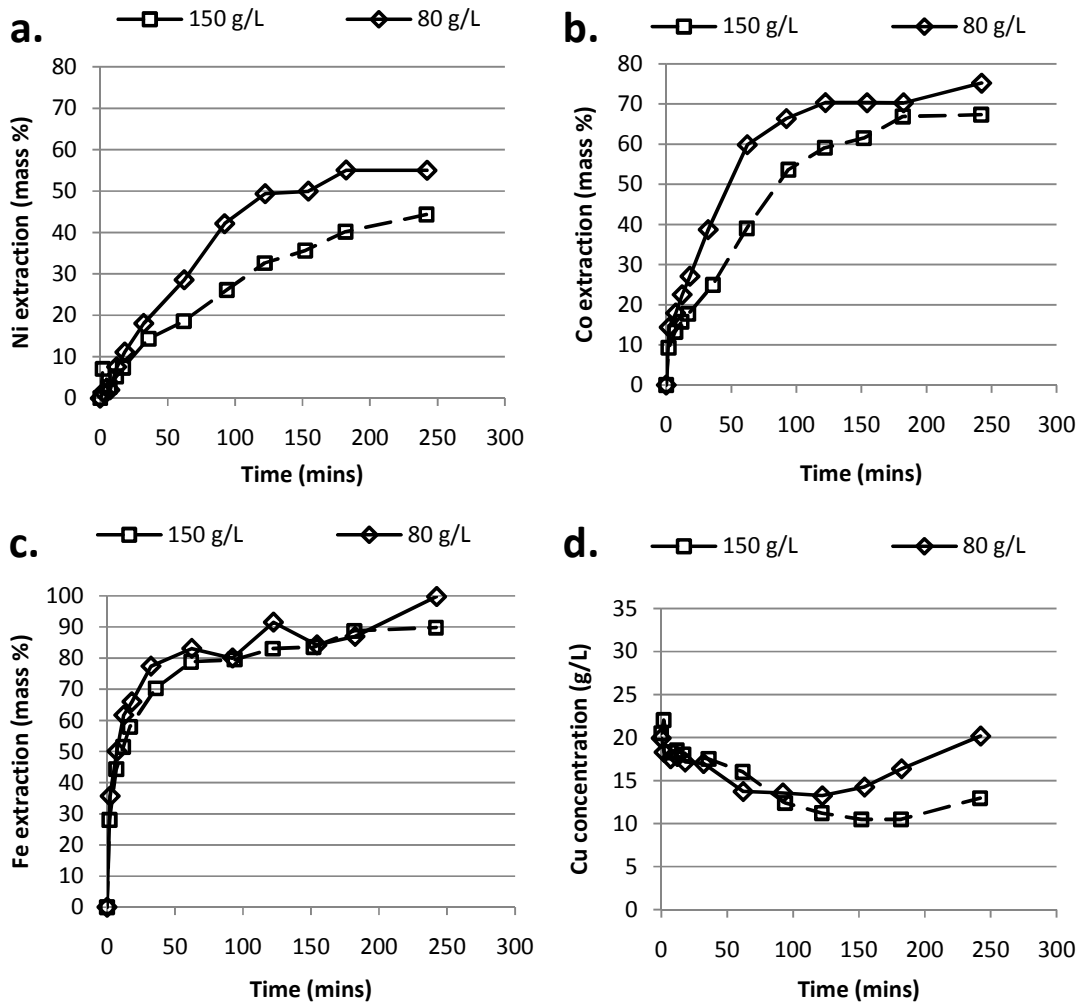


Figure 4-19 Comparison of metal extractions and copper precipitation during test 18 (80 g solids / L) and test 19 (150 g solids / L)

The rates and extents of nickel and cobalt extraction were higher in the 80 g solids / L test (Test 18) than in the 150 g solids / L test (Test 19). These results are in agreement with results for tests 15 and 21. Iron extractions were similar at the two densities. Copper leaching took place in both tests, but more copper was removed from solution in the 150 g solids / L test in the period before copper leaching started.

## Section review

The results from the three sets of tests show that nickel and cobalt extraction rates are lower at higher solid/liquid ratios. This effect was less noticeable when the initial acid concentration was high and the solution was highly agitated (tests 17 and 20). At a lower acid content (tests 15 and 21), extractions at a solids content of 150 g/L (test 21) were probably limited by the acid available to participate in reactions. At a lower stirring rate (tests 18 and 19), extractions at a higher solids content (test 19) were probably also limited by the availability of acid, but this was further aggravated by poor mass transfer.

Acid consumption was higher in high solids tests, which meant that the pH increased to a higher value. This led to iron precipitation in tests with higher solids contents.

Less copper was precipitated at lower solids contents. The second stage of copper removal was influenced to a larger extent than the first reaction stage. At a low solid/liquid ratio, copper precipitation is limited because the available heazlewoodite is quickly leached out by acid. The excess of acid available with a low solids/liquid ratio also meant that copper was leached more easily.

Vydysh et al. (2005) found that copper removal decreased dramatically if the ratio of nickel in the matte to the initial copper in solution was smaller than 4.53 g Ni / g Cu<sup>2+</sup>. The decrease was attributed to a kinetic, rather than thermodynamic effect. Vydysh et al. (2005) used initial acid concentrations of 25 – 55 g/L. The Ni/Cu<sup>2+</sup> ratio in the current work was 1.94 g/g in tests 15, 17 and 18, 3.65 g/g in tests 19, 20 and 21 and 13.0 g/g in test 22. The results from test 21 show that complete copper removal was possible at a Ni/Cu<sup>2+</sup> ratio of 3.65 g/g, but copper precipitation at lower ratios was limited.

Results from tests with 150 g solids / L or 80 g solids / L show that only 60 % - 70 % nickel was readily leachable, although acid was available for further nickel leaching. Mineralogical analysis of samples taken at time intervals throughout the tests can be found in the Appendix. Disintegration of the nickel sulphide matrix led to the formation of large amounts of millerite in all tests. At low solid content, millerite and

polydymite formed, while godlevskite and millerite formed at higher solids contents. Chalcocite was formed as copper cementation product, while digenite or covellite were formed as copper leaching products, depending on the extent of copper leaching. In tests where iron precipitation took place, bornite, and to a lesser extent pentlandite and troilite, were formed.

### **4.2.3 Effect of initial acid and copper concentrations (OX)**

In this section, two sets of tests will be compared to demonstrate the effects of initial acid and copper concentrations. The first set of tests to be discussed will be tests 20 and 21, in which the solids content was 150 g/L and the initial acid concentrations were respectively 74 g/L and 37 g/L. After discussion of tests 20 and 21, tests 14, 15, 16 and 17 will be compared, in which the solids content was 80g/L. Different initial acid and copper concentrations were used in the four tests. By comparing the effects of initial acid concentration at two densities, the effects of the two factors (solids/liquid ratio and acid concentration) can be compared, especially with respect to copper precipitation.

#### Comparison of tests 20 and 21

The operating conditions for tests 20 and 21 are given in Table 4-7. The solution pH as measured in the two tests, are compared in Figure 4-21. The pH rose more quickly in the low acid test, which was stopped when the pH reached a value of 6.5 after 150 minutes. Metal extractions are compared in Figure 4-20 (a, b and c). The rates and extents of nickel, cobalt and iron extraction were higher in the high acid test.

Table 4-7 Operating conditions for Tests 20 and 21

Test	Solids/Liquid [g/L]	Gas	Fe-endpoint [Mass %]	Init. Cu conc [g/L]	Init. Acid conc. [g/L]	Stirring [rpm]
20	150	O <sub>2</sub>	0.53	20	74	1100
21	150	O <sub>2</sub>	0.53	20	37	1100

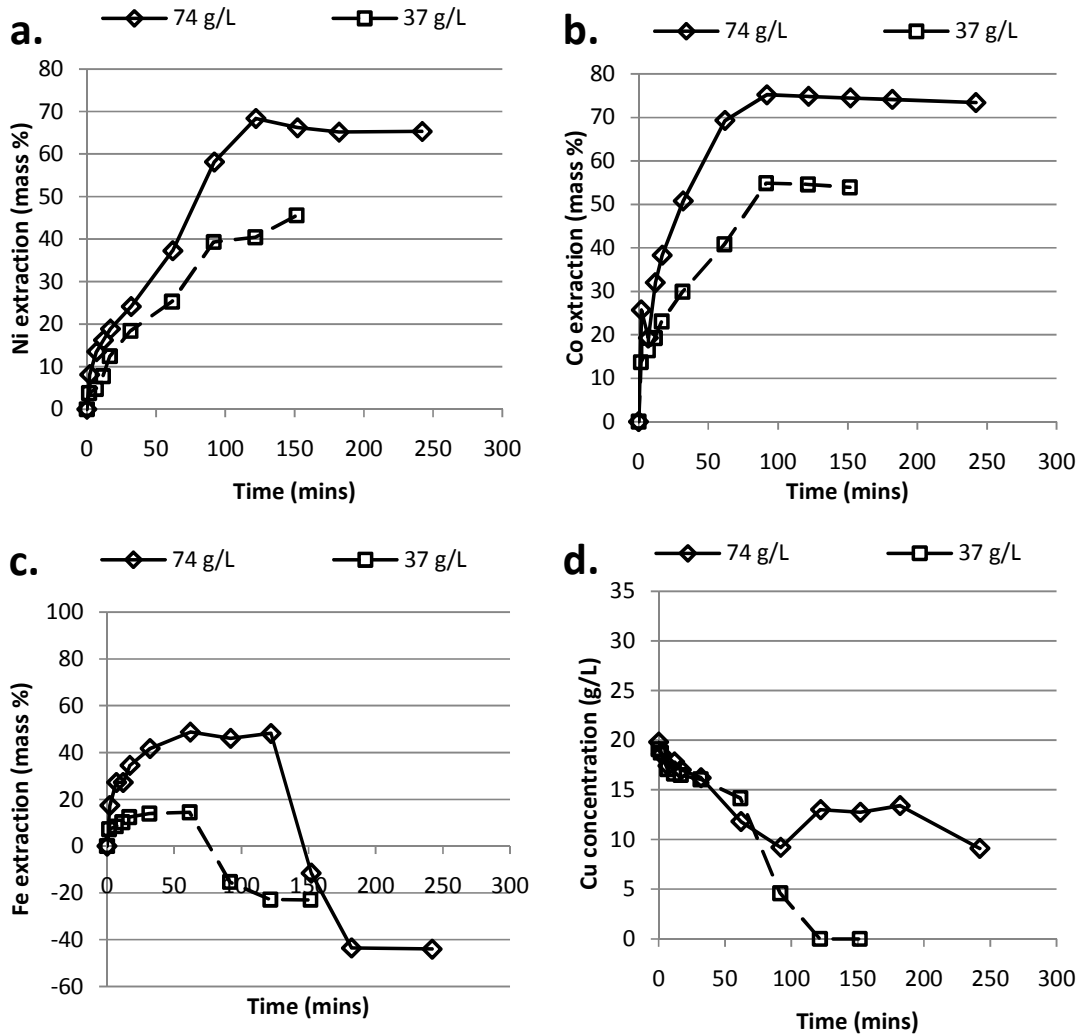


Figure 4-20 Comparison of metal extractions and copper precipitation during test 20 (74 g/L acid) and test 21 (37 g/L acid)

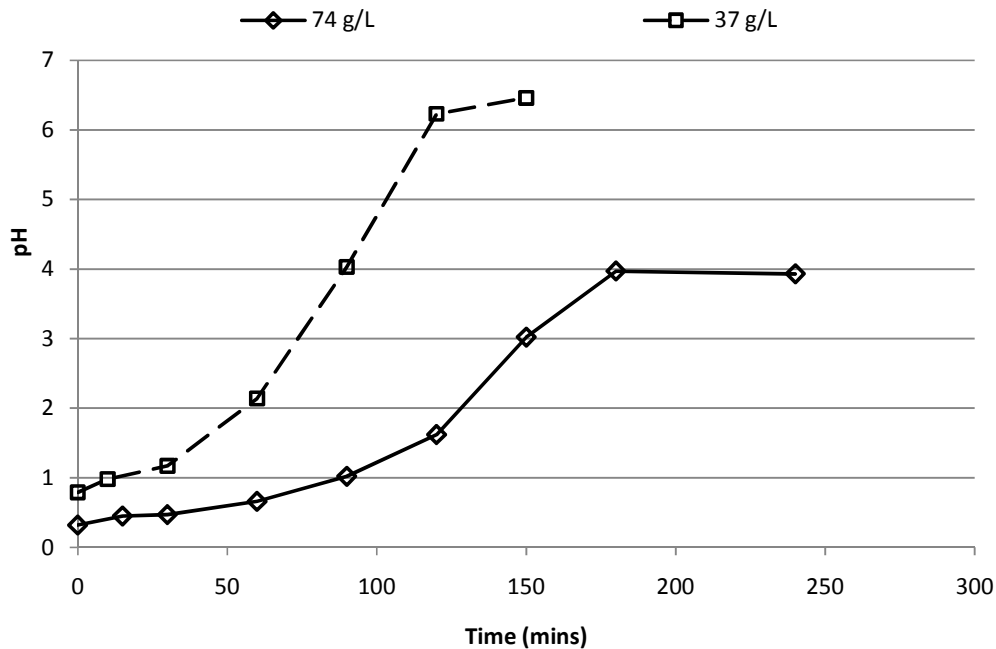


Figure 4-21 Comparison of pH changes in test 20 (74 g/L acid) and test 21 (37 g/L acid)

In both tests, two stages of copper precipitation could be distinguished (Figure 4-20-d). The first stage of copper precipitation was completed after 30 minutes in the high acid test (test 20) and after 60 minutes in the low acid test (test 21). The onset of the second reaction stage occurred at an earlier stage in the high acid test; this can probably be attributed to quicker leaching of the alloy phase (see discussion of results for test 20 heading in Section 4.2.1 and mineralogical analysis of samples from test 21 in Appendix F). During the second reaction stage, copper precipitation was slower in the high acid test, due to copper leaching taking place. Chalcocite was formed in both tests, but digenite was only formed in the high acid test, in which copper leaching took place.

Nickel leaching from the heazlewoodite matrix led to the formation of millerite and godlevskite in tests 20 and 21. A higher percentage nickel was extracted in the high acid test (test 20), so that polydymite was also formed. Copper was leached in the high acid test when the heazlewoodite had nearly been depleted (< 5 %). In the low acid test, copper leaching did not take place, although the relative abundance of heazlewoodite was less than 5 % after 150 minutes. In the low acid test, the solution

pH had probably increased to a value where copper leaching was not thermodynamically favoured, before the heazlewoodite was leached out. Iron precipitation occurred in both tests and was accompanied by the formation of bornite, pentlandite and troilite.

#### Comparison of tests 14, 15, 16 and 17

Operating conditions for tests 14, 15, 16 and 17 are given in Table 4-8. pH measurements from the tests are compared in Figure 4-23. The pH increased at a faster rate and to a higher level in the low acid tests (tests 14 and 15) than in the high acid tests (tests 16 and 17). Consequently, iron precipitation only took place in tests 14 and 15, as shown in Figure 4-22-c. The rate at which the pH increased was the fastest in test 15, in which the initial acid and copper concentrations were low.

The rates and extents of nickel extraction in tests 14, 16 and 17 were nearly identical, but nickel extraction was faster in test 15. The faster nickel extraction in test 15 can probably be attributed to an increase in the rate of nickel leaching by acid, which is also the cause for the faster increase in solution pH.

Cobalt extraction was higher when the copper concentration was increased (14 vs 15, 16 vs 17), or when the initial acid concentration was decreased (14 vs 16, 15 vs 17). The combination of these two factors led to the highest cobalt extraction test 14, where the initial acid concentration was low and the initial copper concentration was high. The initial rate of cobalt extraction was not affected by copper or acid concentrations.

The initial rates of iron extraction in the four tests were unaffected by initial acid and copper concentrations.

Table 4-8 Operating conditions for tests 14, 15, 16 and 17

Test	Solids/Liquid [g/L]	Gas	Fe-endpoint [Mass %]	Init. Cu conc [g/L]	Init. Acid conc. [g/L]	Stirring [rpm]
14	80	O <sub>2</sub>	0.89	40	37	1100
15	80	O <sub>2</sub>	0.89	20	37	1100
16	80	O <sub>2</sub>	0.89	40	74	1100
17	80	O <sub>2</sub>	0.89	20	74	1100

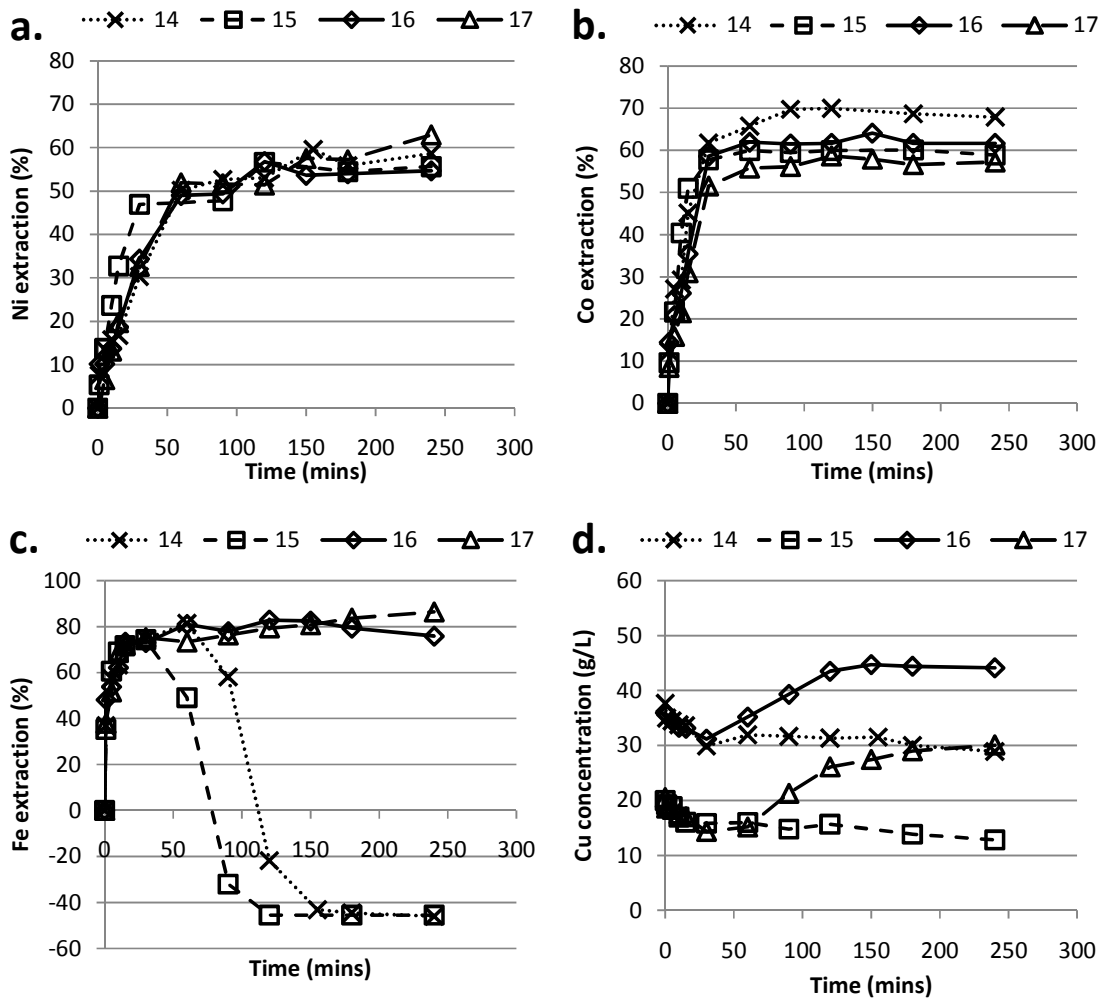


Figure 4-22 Comparison of metal extractions and copper precipitation during tests 15, 16, 17 and 18



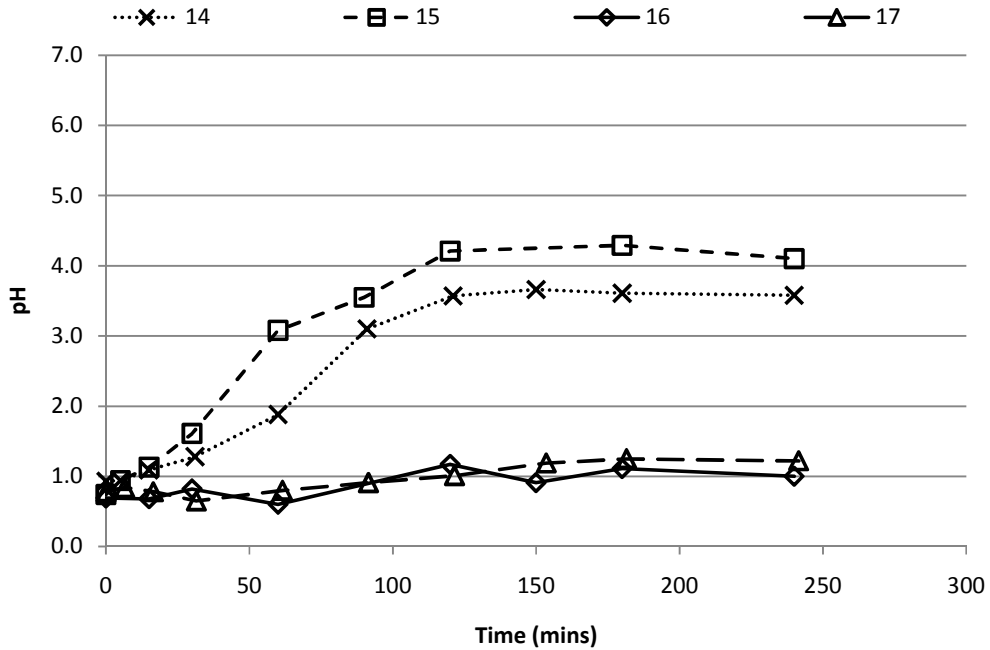


Figure 4-23 Comparison of pH changes occurring in tests 14, 15, 16 and 17 (operating conditions listed in Table 4-8)

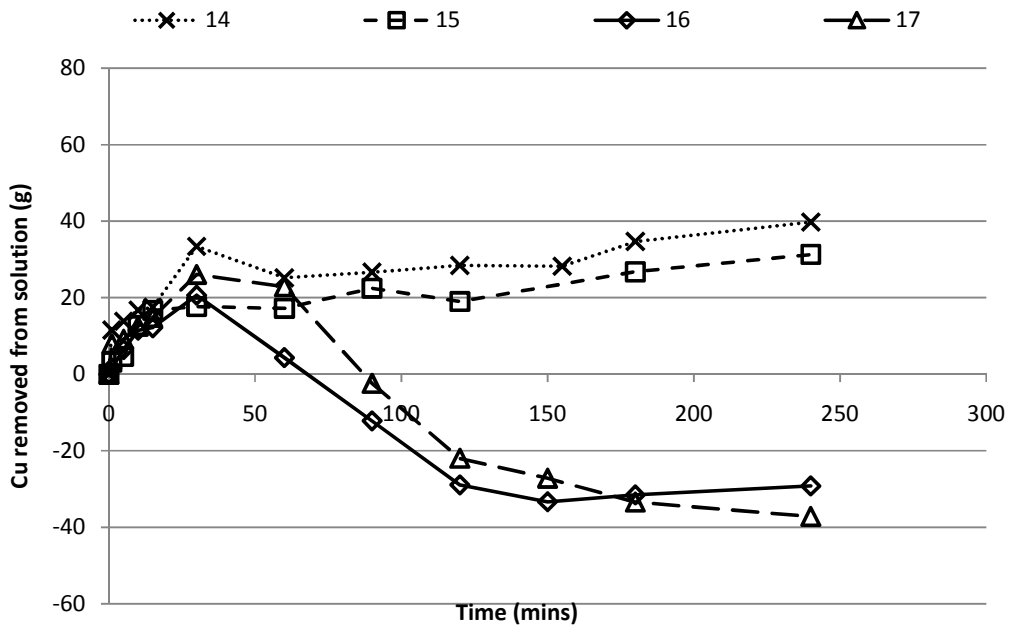


Figure 4-24 Comparison of mass copper removed from solution in tests 14, 15, 16 and 17 (operating conditions listed in Table 4-8). Negative trends indicate copper leaching.

The mass of copper removed from solution during tests 14, 15, 16 and 17 is illustrated in Figure 4-24. Significant copper leaching took place in the high acid tests (tests 16 and 17), with copper leaching starting at an earlier stage in test 16 (high acid, high copper) than test 17 (high acid, low copper). Copper was also leached to some extent in test 14 (low acid, high copper) between 30 and 60 minutes, but not in test 15 (low acid, low copper). These results indicate that higher copper concentrations increase the tendency for copper to be leached. Increased copper concentrations might lead to decreased diffusivity of dissolved copper ions at the solid/liquid interface, leading to decreased rates of copper precipitation in copper-nickel exchange reactions.

The mineralogical compositions of residues from tests 14, 15, 16 and 17, along with the mineralogical composition of the matte which was used as starting material, are given in Table 4-9. The residues from the two high acid tests (tests 16 and 17) were very similar, indicating that the influence of the initial copper concentration was limited. In tests 16 and 17, covellite formed due to copper leaching, while millerite and polydymite formed due to nickel leaching.

The residues from the two low acid tests (tests 14 and 15) differed significantly from the residues from high acid tests (tests 16 and 17), but also from one another. Chalcocite and bornite were the copper-containing phases in the residue from the low acid, low copper test (test 15). Pentlandite, troilite and bornite phases were present in the residue from test 15, but not in the residue from test 14, although copper and iron precipitation occurred in both tests. In the low acid, high copper test (test 14), covellite and digenite were formed due to copper leaching, while copper hydrolysis products (antlerite and malachite) formed as the pH increased and the solution became saturated with copper. The higher nickel extraction obtained in test 15 (in comparison to test 14) is reflected by the presence of polydymite in the residue.

Table 4-9 Mineralogical compositions of matte and residues from tests 14, 15, 16 and 17

 Test 14 conditions: 37 g/L acid, 40 g/L  $\text{Cu}^{2+}$ , 80 g solids / L, 1100 rpm, 0.89 % Fe

 Test 15 conditions: 37 g/L acid, 20 g/L  $\text{Cu}^{2+}$ , 80 g solids / L, 1100 rpm, 0.89 % Fe

 Test 16 conditions: 74 g/L acid, 40 g/L  $\text{Cu}^{2+}$ , 80 g solids / L, 1100 rpm, 0.89 % Fe

 Test 17 conditions: 74 g/L acid, 20 g/L  $\text{Cu}^{2+}$ , 80 g solids / L, 1100 rpm, 0.89 % Fe

Test:			14	15	16	17
Sample time:	Matte		240	240	240	240
Mineral	Mass %					
<b>Ni-Cu</b>	Ni-Cu	12.3	0	0	0	0
<b>Heazlewoodite</b>	$\text{Ni}_3\text{S}_2$	53.8	0	0.9	0	4.1
<b>Godlevskite</b>	$\text{Ni}_7\text{S}_6$	4.4	0	0	0	0
<b>Millerite</b>	NiS	0	35.4	46.7	52.5	51.3
<b>Polydymite</b>	$\text{Ni}_3\text{S}_4$	-	-	4.0	13.7	11.6
<b>Pentlandite</b>	$(\text{NiFe})_9\text{S}_8$	0.7	0	5.3	0	0
<b>Troilite</b>	FeS	0.9	0	4.0	0	0
<b>Magnetite</b>	$\text{Fe}_3\text{O}_4$	1.2	0	1.7	0	0
<b>Bornite</b>	$\text{Cu}_5\text{FeS}_4$	-	-	16.3	-	-
<b>Chalcocite</b>	$\text{Cu}_2\text{S}$	26.6	0	20.5	0	0
<b>Djurleite</b>	$\text{Cu}_{31}\text{S}_{16}$	-	-	-	-	-
<b>Digenite</b>	$\text{Cu}_9\text{S}_5$	0	9.2	-	-	-
<b>Covellite</b>	CuS	0	16.3	-	30.8	33.0
<b>Cuprite</b>	$\text{Cu}_2\text{O}$	0.2	0	0	0	0
<b>Antlerite</b>	$\text{Cu}_3\text{SO}_4(\text{OH})_4$	0	30.5	-	-	-
<b>Malachite</b>	$\text{Cu}_2\text{CO}_3(\text{OH})_2$	0	8.6	-	-	-
<b>Spertiniite</b>	$\text{Cu}(\text{OH})_2$	0	0	0.8	0	0

### Section review

The most important results discussed in the preceding text will be summarised in the following paragraphs. In tests with a solids content of 150 g/L, the rates and extents of nickel, cobalt and iron extractions were higher if the initial acid concentration was 74 g/L than when the initial acid concentration was 37 g/L. In 80 g solids/L tests, the initial acid concentration had a much less pronounced effect on the rates and extents of metal extractions.

Less copper was precipitated in tests with a high initial acid concentration. The effect of the initial acid concentration on the kinetics of copper precipitation was more pronounced during the second reaction stage, when heazlewoodite probably plays a more important role in copper precipitation than the alloy phase. In the high acid tests (16, 17 and 20), copper was leached to a large extent after an initial copper precipitation period. Provis et al. (2003) suggested that chalcocite will not be leached while heazlewoodite is still present in the matte. The current work shows

that the acid concentration should also be taken into consideration. Although heazlewoodite was leached out almost entirely (<5 % remaining in residue) in tests with a solids content of 80 g solids / L(14, 15, 16 and 17), copper leaching was limited in tests with a low initial acid concentration (14 and 15). Results from test 14 and 15 suggest that chalcocite will not be leached if the solution pH is above 2.

The results described in the previous paragraph are in contrast with results published by Llanos et al. (1974) and Hofirek and Kerfoot (1992). Llanos et al. (1974) found that Cu-precipitation accelerated when working at a high  $H^+/Cu^{2+}$  ratio. Hofirek and Kerfoot (1992) found that increasing the  $H^+$  concentration increased the rate of copper removal when using the non-metallic fraction of converter matte. Results from the current work suggested that a high initial copper concentration might promote copper leaching. This might serve as explanation for findings by Llanos et al. (1974): that copper precipitation decreased at lower acid to copper ratios.

Iron precipitation from solution is more likely to occur if the initial acid concentration is low, because the pH will increase more during the test. In tests with a solids content of 80 g solids/L, the reaction products from copper and iron precipitation depended on the initial copper concentration. When the initial copper concentration was 20 g/L, chalcocite and bornite were formed, while covellite, antlerite and malachite were formed in tests with an initial copper concentration of 40 g/L. At a high acid concentration, copper precipitation was limited and the copper concentration was consequently a less important factor than at low acid concentrations.

The effect of the initial copper concentration on metal extractions was limited. The percentage cobalt extraction increased when the initial copper concentration was higher. At a low acid concentration, the rate of nickel leaching was faster when the initial copper concentration was decreased from 40 g/L to 20 g/L. At a high acid concentration the initial copper concentration had no effect on the nickel extraction rate.

#### 4.2.4 Effect of the Fe-endpoint (OX)

The effect of the iron endpoint will be demonstrated by comparing test 20 (0.53 % Fe) with test 23 (5.72 % Fe), and test 19 (0.83 % Fe) with test 24 (5.72 % Fe). Tests 20 and 23 were carried out with a stirring rate of 1100 rpm and tests 19 and 24 were carried out with a stirring rate of 500 rpm. The initial acid concentration, initial copper concentration and solids content were 74 g/L, 20 g/L and 150 g/L, respectively, in all tests.

##### Comparison of tests 20 and 23

Operating conditions for tests 20 and 23 are given in Table 4-10. Metal extractions and copper concentrations with respect to time are compared in Figure 4-26. pH changes are illustrated in Figure 4-25. The high iron test was allowed to continue for 300 minutes after it was noticed that the solution pH increased very slowly. The pH in the high iron test reached a plateau at a value of 2.

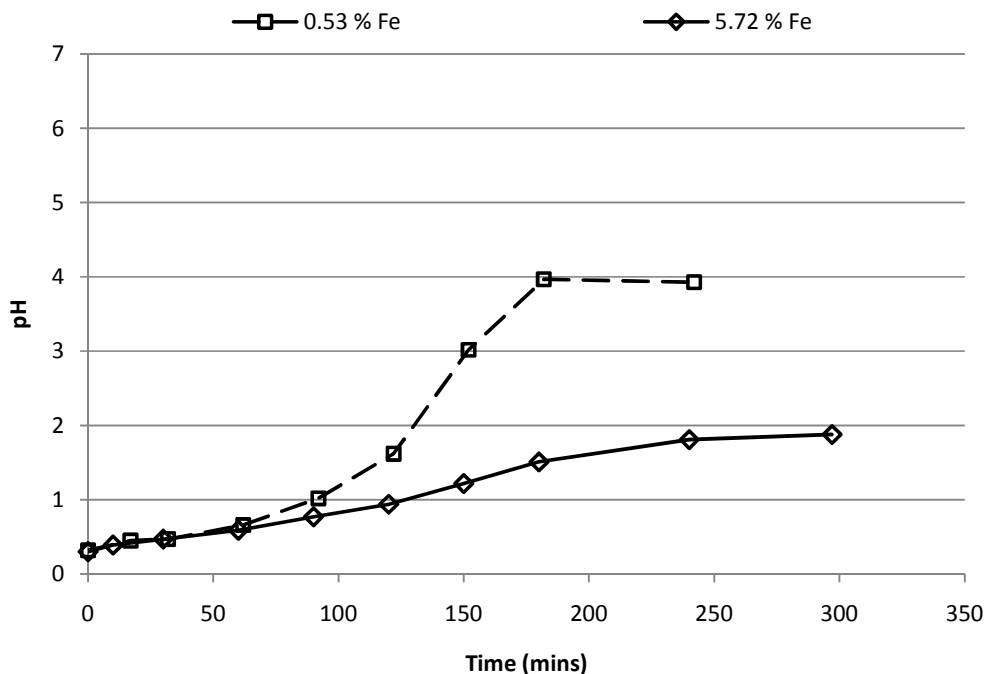


Figure 4-25 Comparison of pH changes during test 20 (0.53 % Fe) and test 23 (5.72 % Fe)

Figure 4-26 (graph a and b) shows that the rates and extents of nickel and cobalt leaching were higher when leaching the 0.53 % Fe matte than the 5.72% Fe matte. Nickel extraction slowed down dramatically after approximately 35 % of the nickel in the high iron matte had been extracted. The decreased leaching of metals in the high iron test explains the slower rise in solution pH. Copper precipitation was initially faster in the high iron than in the low iron test, but copper leaching in the high iron test started at an earlier time and progressed to a further extent. The low rates at which nickel and cobalt were leached in the high iron test led to a large amount of acid being available for copper leaching.

The rate and extent of iron extraction was higher in the low iron test, in terms of percentage extraction. In terms of moles extracted, less iron was extracted in the low iron test. At the time that iron precipitation started (120 minutes) 0.03 moles iron had been extracted in the low iron test and 0.39 moles had been extracted in the high iron test. The number of moles cobalt extracted were also higher in the high iron test: after 240 minutes 0.021 moles were extracted in the high iron test and 0.017 moles in the low iron test.

Table 4-10 Operating conditions for tests 20 and 23

Test	Solids/Liquid [g/L]	Gas	Fe-endpoint [Mass %]	Init. Cu conc [g/L]	Init. Acid conc. [g/L]	Stirring [rpm]
20	150	O <sub>2</sub>	0.53	20	74	1100
23	150	O <sub>2</sub>	5.72	20	74	1100

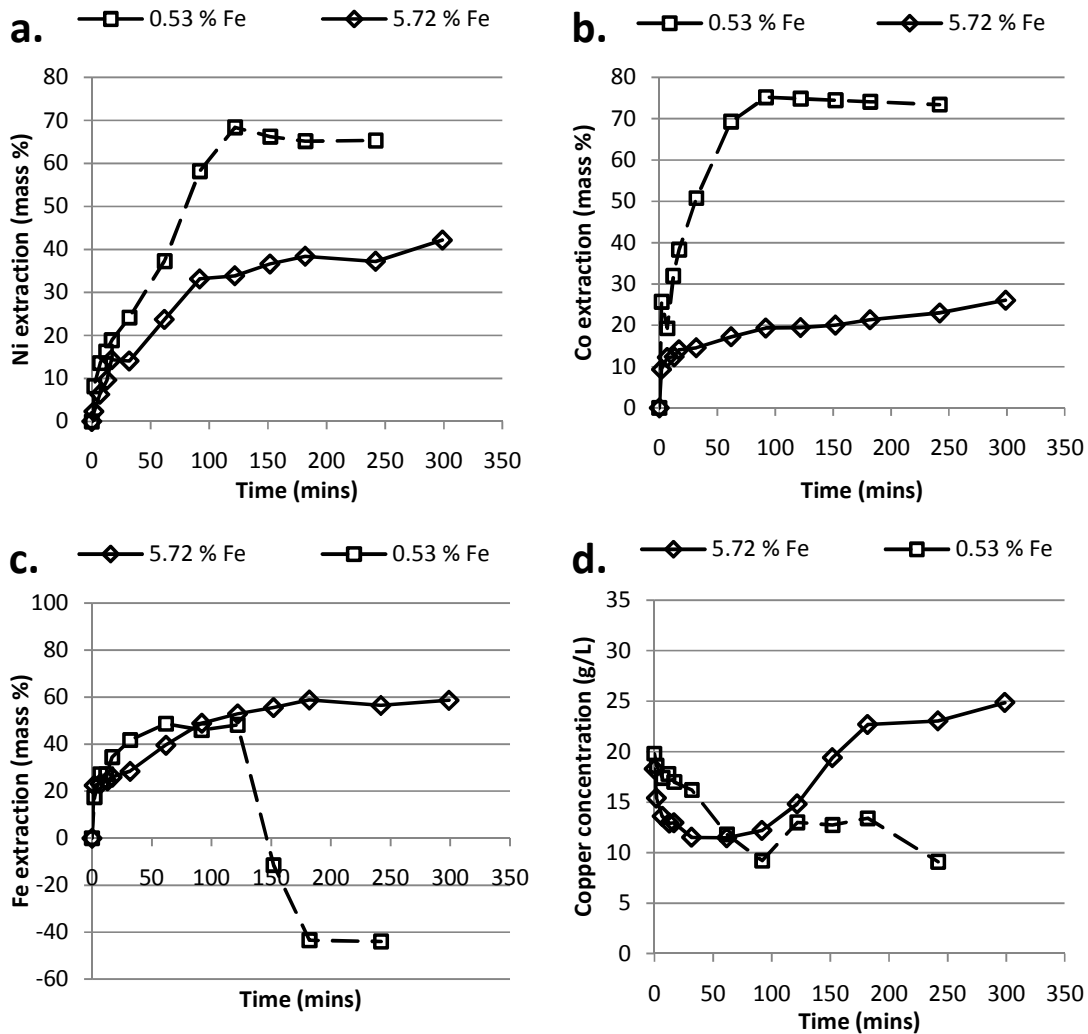


Figure 4-26 Comparison of metal extractions and copper precipitation during test 20 (0.53 % Fe) and test 23 (5.72 % Fe)

The concentration changes of iridium, rhodium and ruthenium for test 23 (5.72 % Fe) are shown in Figure 4-27. The behaviour of PGEs was similar to the behaviour of copper. After an initial fast period (0-30 mins) PGE precipitation slowed. After 120 minutes, iridium and rhodium concentrations increased, possibly due to a combination of leaching and evaporation effects. The percentages PGEs

precipitated in tests 6 and 12 are compared in Figure 4-28. The extent to which PGE precipitation took place was significantly lower in the high iron test.

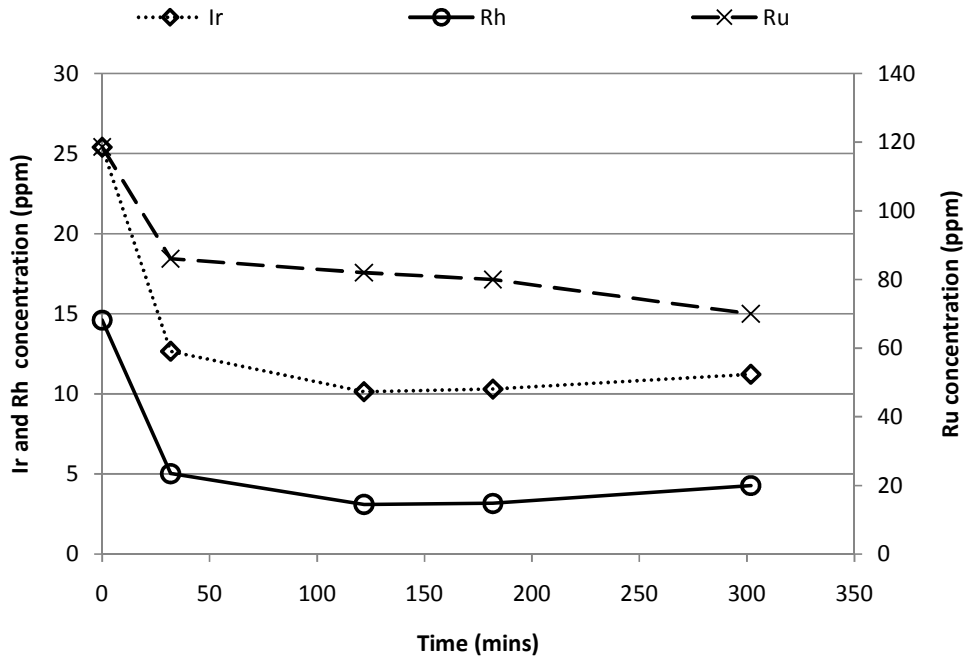


Figure 4-27 PGE concentration changes with time in test 23. 74 g/L acid, 20 g/L  $Cu^{2+}$ , 150 g solids/L, 1100 rpm, 5.72 % Fe

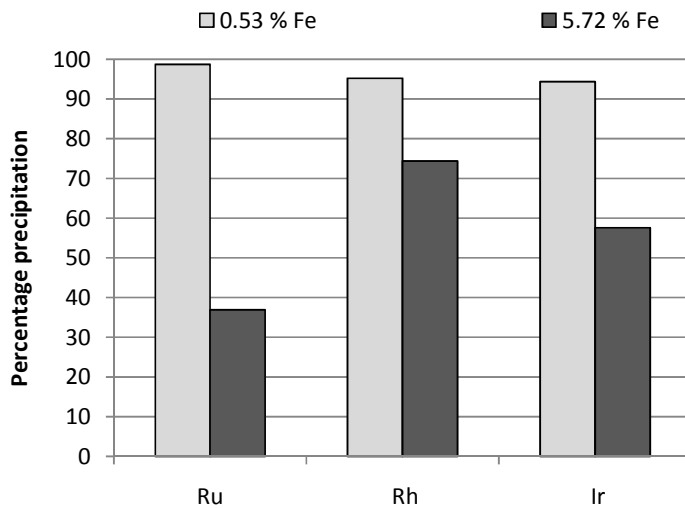


Figure 4-28 Comparison of percentages Ru, Rh and Ir precipitated from solution after 240 minutes in test 20 (0.83 % Fe) and test 23 (5.72 % Fe)



The mineralogical changes in the low iron test were discussed in Section 4.2.1. In order to compare results from the high and low iron tests, the phase mass changes for test 20 are shown again here (Figure 4-29). Mineral masses as a function of time for test 23 are shown in Figure 4-30. The mineralogical compositions of solid samples taken in test 23 are shown in Table 4-11.

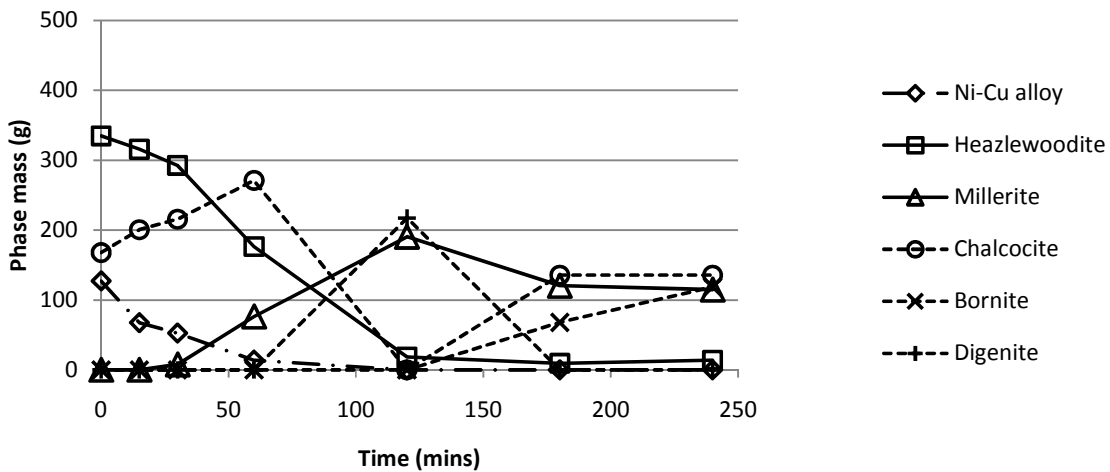


Figure 4-29 Masses of major phases as a function of time in test 20. 74 g/L acid, 20 g/L  $Cu^{2+}$ , 150 g solids/L, 1100 rpm, 0.53 % Fe

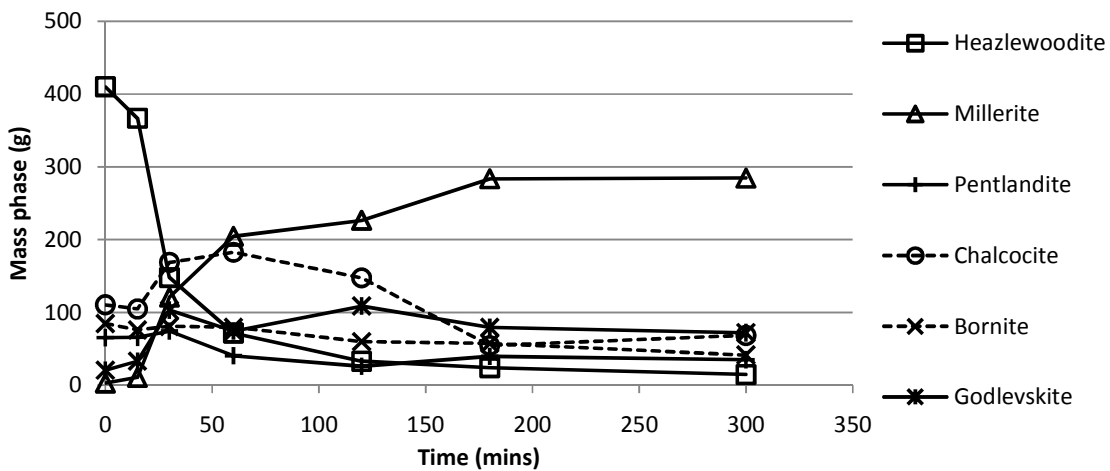


Figure 4-30 Masses of major phases as a function of time in test 23. 74 g/L acid, 20 g/L  $Cu^{2+}$ , 150 g solids/L, 1100 rpm, 5.72 % Fe

Table 4-11 Mineralogical changes during Test 23. 74 g/L acid, 20 g/L  $\text{Cu}^{2+}$ , 150 g solids / L, 1100 rpm, 5.72 % Fe

Mineral	Sample time	0	15	30	60	120	180	300
		Mass %						
Ni-Cu	Ni-Cu	2.1	3.1	0	0.5	0	0	0
Heazlewoodite	$\text{Ni}_3\text{S}_2$	56.9	53.2	21.3	10.8	5.4	4.3	2.7
Godlevskite	$\text{Ni}_7\text{S}_6$	2.9	4.8	14.8	11.3	17.9	14.3	13.5
Millerite	NiS	0.4	1.5	17.4	31.0	37.3	51.1	53.4
Polydymite	$\text{Ni}_3\text{S}_4$							
Pentlandite	$(\text{NiFe})_9\text{S}_8$	9.1	9.5	10.7	6.1	4.3	7.1	6.6
Troilite	FeS	0.4	0.4	0	0.1	1.0	1.2	1.3
Magnetite	$\text{Fe}_3\text{O}_4$	1.1	1.2	0	0.6	0	1.7	2.0
Bornite	$\text{Cu}_5\text{FeS}_4$	11.7	11.0	11.6	12.0	9.9	10.4	7.8
Chalcocite	$\text{Cu}_2\text{S}$	15.3	15.2	24.3	27.6	24.3	9.8	12.8
Djurleite	$\text{Cu}_{31}\text{S}_{16}$							
Digenite	$\text{Cu}_9\text{S}_5$							
Covellite	CuS							
Cuprite	$\text{Cu}_2\text{O}$							
Antlerite	$\text{Cu}_3\text{SO}_4(\text{OH})_4$							
Malachite	$\text{Cu}_2\text{CO}_3(\text{OH})_2$							

The high iron matte initially contained 2.1 % alloy, in comparison to 19.7 % in the low iron matte. (The alloy is not shown in Figure 4-30, due to the small amounts present in the high iron matte). During the first 15 minutes of the high iron test, the alloy content increased, presumably due to the formation of metallic copper. The alloy in the high iron test was completely leached out after 30 minutes.

An initial slow period of heazlewoodite leaching occurred in both tests, but continued for a longer time in the low iron test. The rate at which heazlewoodite was leached in the high iron test increased after 15 minutes. In the high and low iron tests, the mass of godlevskite and millerite increased and the mass of heazlewoodite decreased as nickel was leached from the nickel sulphide matrix. However, more godlevskite was formed in the high iron test. In the low iron test more nickel was leached and polydymite was formed. Pentlandite was abundant in the high iron matte and was less reactive than heazlewoodite. Lower nickel extractions in the high iron test can probably be linked to the lower alloy content and to nickel which remains locked up in pentlandite and godlevskite phases.

### Comparison of tests 19 and 24

Tests 19 and 24 show the effect of the Fe-endpoint at a stirring rate of 500 rpm. Results for tests 19 and 24 will not be presented here, but are respectively given in Appendix F and Appendix E. In terms of solution changes and mineralogical changes, the results from tests 19 and 24 supported results from tests 20 and 23.

### Section review

Results from both sets of tests (tests 20 and 23; tests 19 and 24), show that the iron endpoint significantly influence leaching behaviour and must be considered as a very important factor in the performance of the first stage leach. Previous works have reported that ferric and ferrous ions in solution have a catalytic effect by acting as oxygen carrier to increase the rate of nickel leaching (Mulak (1987), Hofirek and Kerfoot (1992) and Burkin (2001)). The results from the current work show that any increased catalytic activity which resulted from increased iron in the leaching system was negligible in comparison to the effect of the iron on matte mineralogy and leaching behaviour. Rather than increasing, nickel, cobalt and iron extractions were slower when leaching high iron mattes. The slower extraction rates can probably be linked to the mineralogy of the matte. High iron mattes contained less of the readily leachable Ni-Cu alloy than low iron mattes. High iron mattes also contained more pentlandite than low iron mattes, which was not readily leached. In high iron mattes, leaching of heazlewoodite led to the formation of large amounts of godlevskite.

When leaching high iron mattes, the slower rates of metal extractions meant that the rate at which the solution pH increased was slower. Decreased acid consumption with high iron mattes was previously reported by Llanos et al. (1974), Symmens et al. (1976) and Symmens et al. (1979). Symmens et al. (1976) noted that iron entered the nickel sulphide lattice to form  $(\text{Ni,Fe})_3\text{S}_4$  which does not readily react with acid. The formation of pentlandite  $(\text{Ni,Fe})_9\text{S}_8$  appeared to have a similar effect in the current work. Symmens et al. (1976) further noted that the pH stalled at a value of 4 for tests in which the matte contained more than 4 % iron, or where the initial iron concentration was higher than 8 g/L. In the current work, the pH reached

a plateau at a value of 4 in many oxidative tests, but in high iron tests the pH did not increase above a value of 2.

The initial copper precipitation rate was faster for high iron mattes, but copper leaching in high iron tests also took place to a greater extent after the initial copper precipitation period. The decreased rates of nickel and cobalt leaching in high iron tests presumably led to a higher availability of acid for copper leaching.

#### **4.2.5 Effect of stirring rate (OX)**

Stirring rate is an important indicator of the controlling mechanisms in reaction kinetics. In oxidative tests, the stirring rate will influence reactions in which boundary layer diffusion, or the rate of gas-liquid mass transfer is the rate limiting step. Chemical reaction controlled and pore diffusion controlled processes will not be influenced by the stirring rate.

Three pairs of tests will be discussed in this section: Tests 19 and 20 (low iron, 150 g solids/L), tests 17 and 18 (low iron, 80 g solids/L), and Tests 23 and 24 (high iron, 150 g solids/L) will respectively be compared. In each pair, the stirring rate was 1100 rpm in one test and 500 rpm in the other. The initial acid and copper concentrations were the same in all tests (74 g/L, 20 g/L)

The focus in discussions will be on initial reaction rates, although metal extractions and reaction rates during the second stages of reactions will also be discussed. When referring to copper removal from solution, the combined initial and second stage is implied.

##### Comparison of tests 19 and 20

Conditions for tests 19 and 20 are listed in Table 4-12. Tests 19 and 20 were carried out with a low iron matte and a solids content of 150 g/L. The rates and extents of nickel and cobalt extraction (Figure 4-31), as well as the rate of acid consumption (Figure 4-32), increased with stirring rate. Copper removal was initially faster at

1100 rpm, but copper leaching also started earlier. The rate of iron extraction was slower at 1100 rpm. The slower rate of iron extraction can probably be explained by increased acid consumption by nickel leaching and cobalt leaching reactions.

Table 4-12 Operating conditions for Tests 19 and 20

Test	Solids/Liquid [g/L]	Gas	Fe-endpoint [Mass %]	Init. Cu conc [g/L]	Init. Acid conc. [g/L]	Stirring [rpm]
19	150	O <sub>2</sub>	0.83	20	74	500
20	150	O <sub>2</sub>	0.53	20	74	1100

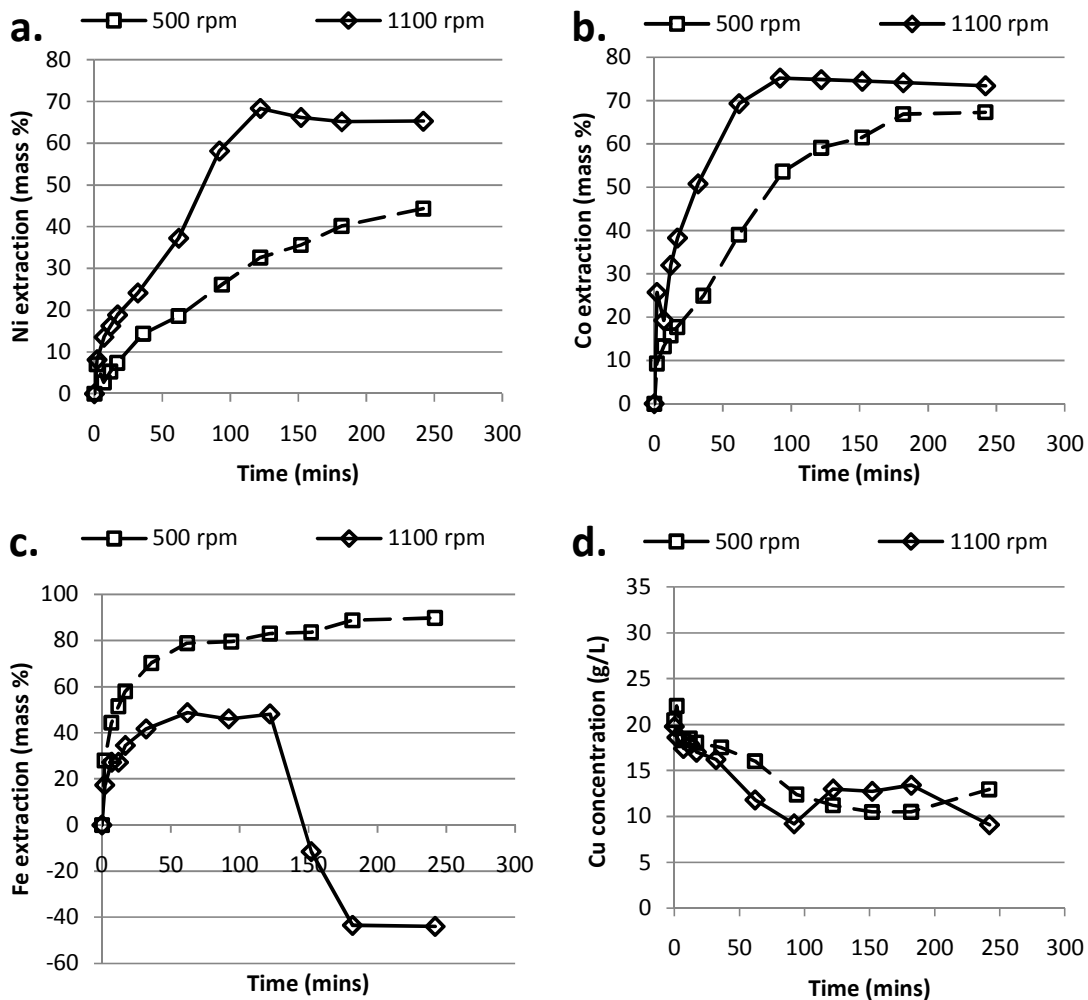


Figure 4-31 Comparison of metal extractions and copper precipitation during Test 19 (500 rpm) and Test 20 (1100 rpm)

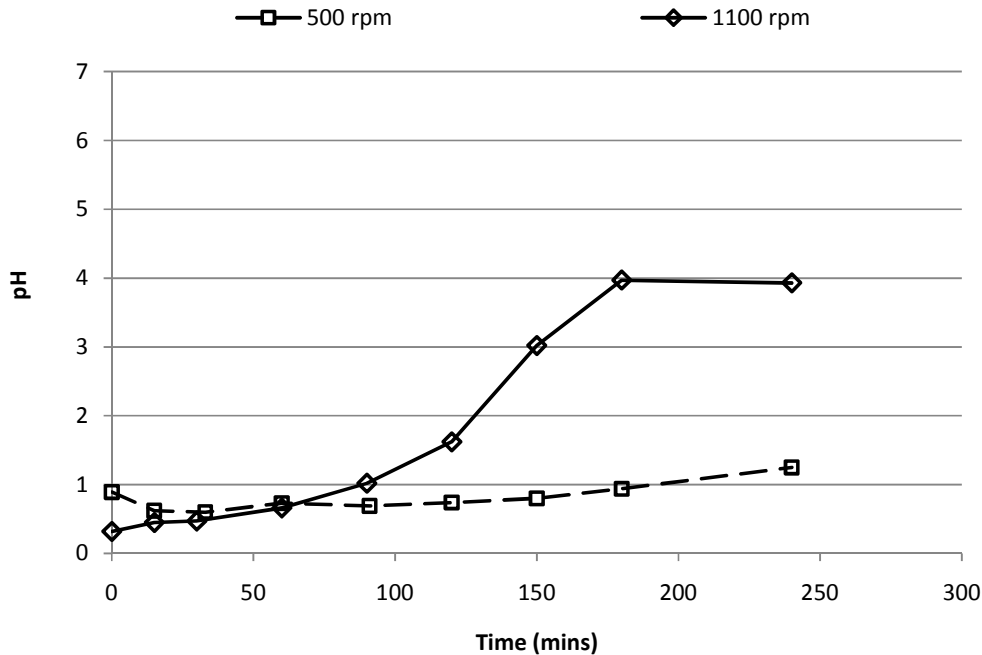


Figure 4-32 Comparison of pH changes during test 19 (500 rpm) and test 20 (1100 rpm)

#### Comparison of tests 17 and 18

Tests 17 and 18 were carried out with a low iron matte and a solids content of 80 g/L. The same effects were observed when comparing tests 17 and 18 that were observed when comparing tests 19 and 20. The exception is that iron hydrolysis did not take place at a solids content of 80 g/L and that the initial rate of iron extraction was unaffected by stirring rate. Results from tests 17 and 18 are compared in Appendix D.

#### Comparison of tests 23 and 24

Test 23 and test 24 were carried out with a high iron matte. Operating conditions are given in Table 4-13 and results are given in Figure 4-33 and Figure 4-34. Nickel and iron extraction rates were faster at 1100 rpm than 500 rpm, although the final extractions in the two tests were similar. The initial rate of cobalt extraction was not affected by stirring rate.

The initial rate of copper precipitation was not influenced by the stirring rate, but copper leaching started earlier when the stirring rate was 1100 rpm. The rate of copper leaching was also faster.

Table 4-13 Operating conditions for tests 23 and 24

Test	Solids/Liquid [g/L]	Gas	Fe-endpoint [Mass %]	Init. Cu conc [g/L]	Init. Acid conc. [g/L]	Stirring [rpm]
24	150	O <sub>2</sub>	5.7	20	74	500
23	150	O <sub>2</sub>	5.7	20	74	1100

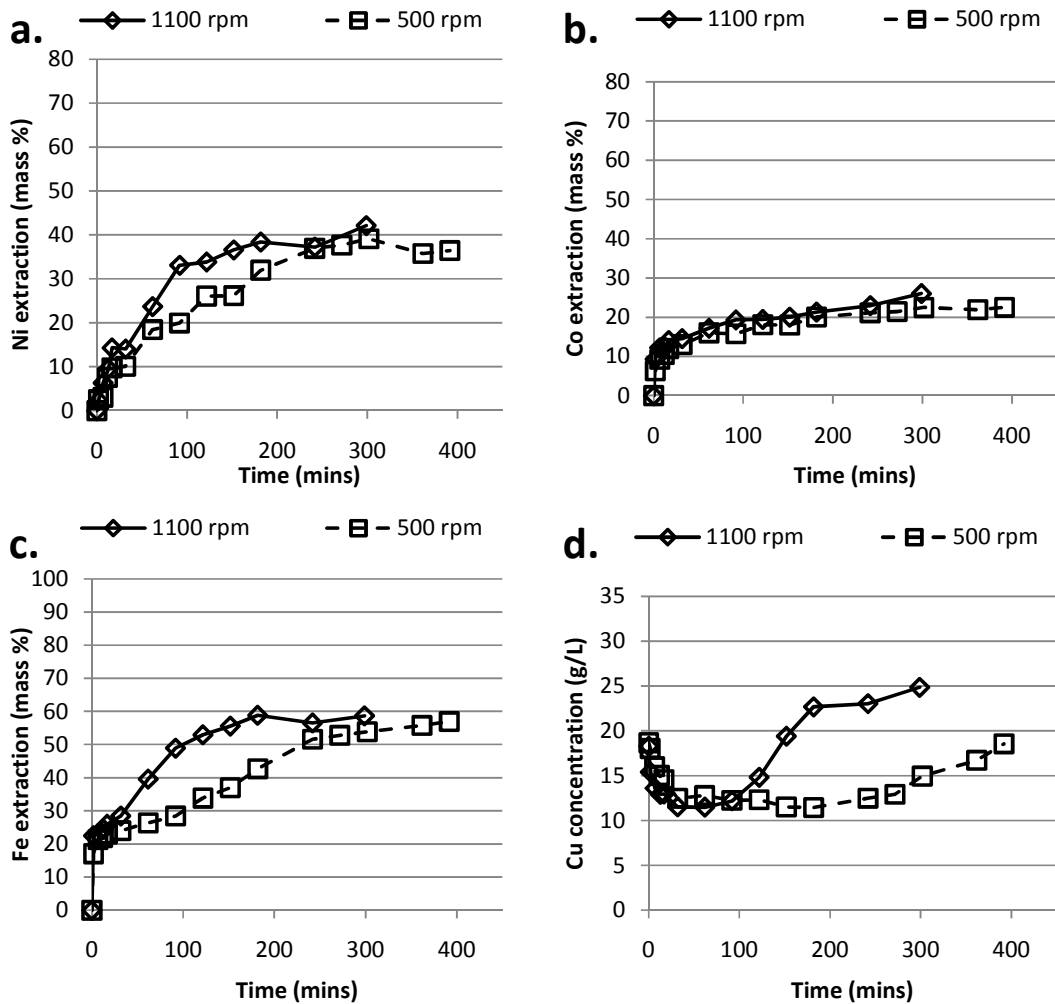


Figure 4-33 Comparison of metal extractions and copper precipitation during test 24 (500 rpm) and test 23 (1100 rpm)

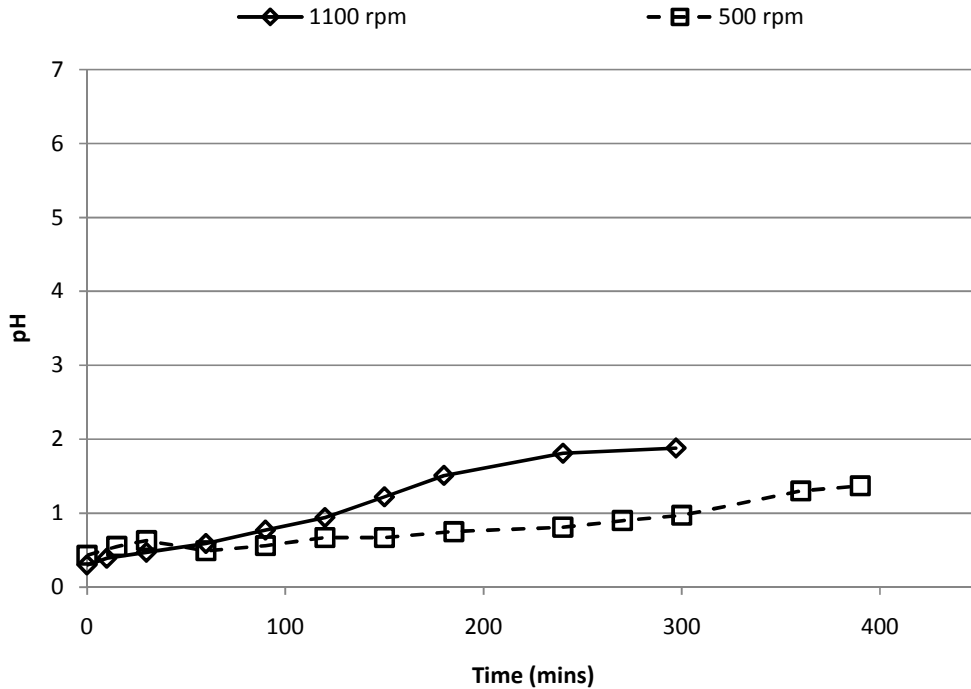


Figure 4-34 Comparison of pH changes in test 23 (1100 rpm) and test 24 (500 rpm)

The mineral changes during leaching for tests 23 and 24 were respectively given in Table 4-11 and Appendix E. In the 500 rpm test, the Ni-Cu alloy increased significantly between 0 and 120 minutes. In the 1100 rpm test, only a small increase in the Ni-Cu alloy can be seen in the first 15 minutes. Chalcocite formation during the first 120 minutes was slightly faster in the 1100 rpm test. These results indicate that the formation of metallic copper is more likely to take place at low stirring rates. Leaching of the Ni-Cu alloy and metallic copper might be advanced by higher gas/liquid mass transfer rates at higher stirring rates.

#### Section review

The results in the preceding text suggest that nickel, cobalt and copper leaching are mass transfer controlled processes when leaching low iron mattes (Gas/liquid or boundary layer diffusion controlled). The results also suggest that copper precipitation is a boundary layer diffusion controlled process. At a low density (80 g solids/L), the stirring rate did not have a significant influence on the leaching rate of iron from low iron matte, suggesting a chemically controlled reaction, or a pore



diffusion controlled reaction. At a solids content of 150 g/L, iron extraction was slower at higher stirring rates where the pH increased sufficiently for iron precipitation to take place.

In high iron tests, nickel and iron extraction rates increased with stirring rate, indicating that the reaction rate was controlled by boundary layer diffusion or gas/liquid mass transfer. The initial rate of cobalt extraction was not affected by stirring rate, indicating a chemically controlled or pore diffusion controlled reaction. Copper leaching was faster at a higher stirring rate, indicating gas/liquid or bulk solid/liquid mass transfer control. Gas/liquid mass transfer probably played an important role in the rates of iron, nickel and copper leaching reactions. The rate of copper precipitation was independent of stirring rate, indicating a chemically controlled process.

The mineralogy of samples from the high iron tests show that the alloy phase initially increased at a lower stirring rate, indicating that a low stirring rate is conducive to the formation of metallic copper when leaching high iron mattes.

## **4.3 Non-oxidative leaching (NOX)**

### **4.3.1 Leaching kinetics and mineralogical changes with time in non-oxidative tests (NOX)**

In the industrial process, the five tanks in series in the atmospheric leach consist of three oxidative and two non-oxidative tanks. The last two tanks are intended to provide residence time for copper precipitation. In this section, the mechanisms observed in non-oxidative leaching tests will be discussed.

The mineralogy of all test residues were analysed using quantitative XRD. Solid samples were also taken periodically during tests 5, 6, 7 and 9 for XRD analysis. Results from tests 5, 7 and 9 are given in Appendix F. Test 6 will be discussed as an example to show the mechanisms during non-oxidative leaching. Specific results from test 9, relating to the production of a large quantity of gas, are also included at the end of this section.

Concentration changes with time for test 6 are illustrated in Figure 4-35. The trends observed in tests 5, 7 and 9 were similar to that shown for test 6. The relative abundances of mineral phases in solid samples taken during test 6 are given in Table 4-14. The mass of the most abundant phases as a function of time is shown in Figure 4-36.

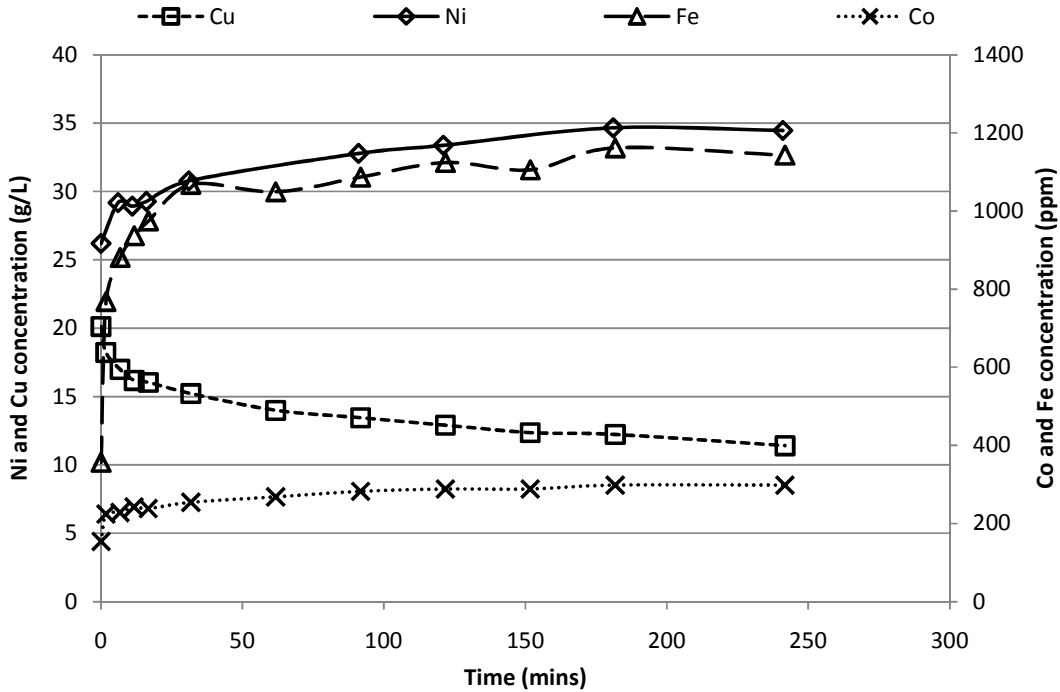


Figure 4-35 Concentration changes with time in test 6. 74 g/L acid, 20 g/L  $\text{Cu}^{2+}$ , 150 g solids/L, 1100 rpm, 0.83 % Fe

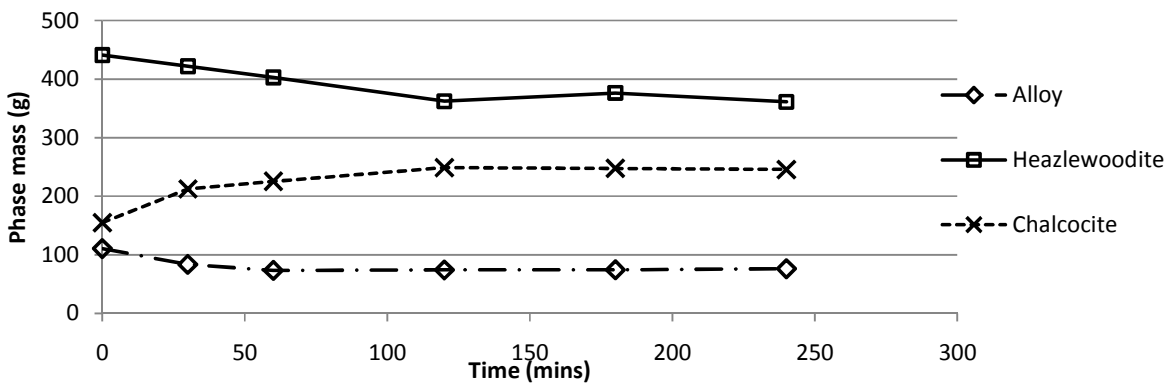


Figure 4-36 Masses of major phases in the solid state as a function of time in test 6. 74 g/L acid, 20 g/L  $\text{Cu}^{2+}$ , 150 g solids/L, 1100 rpm, 0.83 % Fe

In Figure 4-36, it can be seen that nickel, cobalt and iron extractions were very fast during the first 15 minutes of tests. Lamya (2007) noticed similar fast initial reaction periods and attributed these periods to the presence of small particles in the solids. According to Lamya (2007), metals were leached quickly from the small particles, after which the reaction rate slowed down. Another possible explanation for the initial fast reaction period is that some dissolved oxygen is initially present in solution that contributes to metal extractions by acting as oxidative leaching agent. This

theory is supported by redox potential measurements from experimental work, which show that the solution redox potential was typically in the range of 450 to 500 mV at the start of a test (relative to Ag/AgCl electrode), but then decreased to below 300 mV during the first 15 to 30 minutes of leaching.

In Figure 4-37, the number of moles nickel extracted are compared with the number of moles copper precipitated. From this comparison, it can be seen that nickel extraction can be accounted for by copper precipitation reactions (metathesis and cementation). Similar comparisons for tests 5, 7 and 9 (given in Appendix F) show that acid-leaching reactions must have taken place, but that copper-nickel exchange reactions were primarily responsible for nickel extraction.

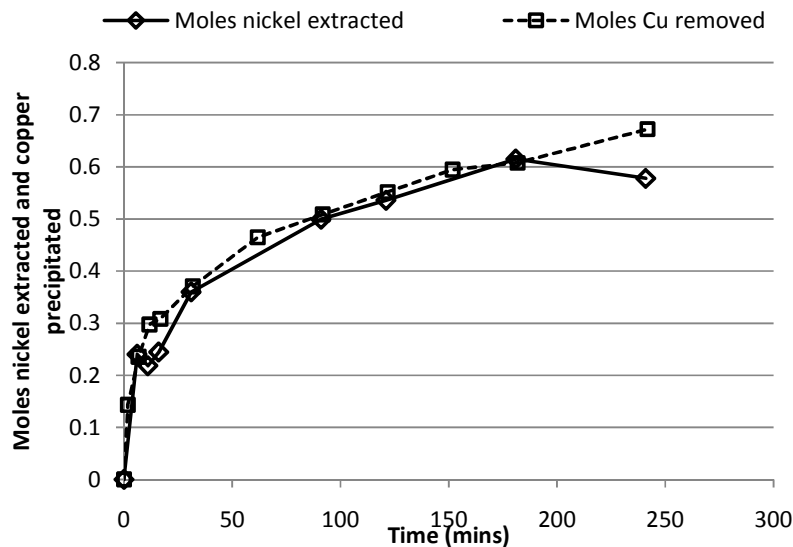


Figure 4-37 Comparison of the number of moles nickel extracted and number of moles copper precipitated in test 6.

Copper precipitation was found to be initially fast and gradually slowed down. Changes in the masses of mineral phases (Figure 4-36) suggest that reaction 2-12 describes the mechanism of copper removal. During the first 60 minutes of test 6, the rate of chalcocite growth was fast, while heazlewoodite and alloy masses decreased. Formation of metallic copper was generally not observed in non-oxidative tests, with the exceptions of tests 4 and 5, in which the stirring rate was lower than in other tests. Millerite formation in non-oxidative tests was limited (tests

1, 2, and 3), or absent (tests 4, 5, 6 and 7). All of these results suggest that copper precipitation can be described by reaction 2-12, rather than reaction 2-9 or reaction 2-11. Analysis of results from tests 5, 6 and 7 suggest that the reaction rate might be linked to the alloy content of the matte. Copper precipitation in tests 5, 6 and 7 slowed down after the alloy mass had decreased with respectively 33 %, 24 % and 28 %.

In oxidative tests, a second reaction period was characterised by increased nickel leaching rates and the formation of millerite. This second reaction period was mainly attributed to acid-oxygen leaching reactions. In non-oxidative tests, acid-leaching did not play an equally important role and copper precipitation and nickel extraction slowed down in the second period.

*Table 4-14 Mineralogical changes in Test 6. 74 g/L acid, 20 g/L Cu, 150 g solids / L, 1100 rpm, 0.83 % Fe*

Sample time:		0	30	60	120	180	240
Mineral		Mass %					
<b>Ni-Cu</b>	Ni-Cu	15.4	11.5	10.3	10.5	10.5	10.8
<b>Heazlewoodite</b>	Ni <sub>3</sub> S <sub>2</sub>	61.3	58.0	56.4	51.0	53.2	51.0
<b>Godlevskite</b>	Ni <sub>7</sub> S <sub>6</sub>	-	-	-	-	-	-
<b>Millerite</b>	NiS	0	0	0	1.8	0	1.5
<b>Polydymite</b>	Ni <sub>3</sub> S <sub>4</sub>	0	0	0	0	0	0
<b>Pentlandite</b>	(NiFe) <sub>9</sub> S <sub>8</sub>	0.5	0	0.4	0.5	0.3	0.6
<b>Troilite</b>	FeS	0	1.0	1.2	1.1	0.5	1.3
<b>Magnetite</b>	Fe <sub>3</sub> O <sub>4</sub>	1.4	0.4	0.2	0	0.5	0.2
<b>Bornite</b>	Cu <sub>5</sub> FeS <sub>4</sub>	-	-	-	-	-	-
<b>Chalcocite</b>	Cu <sub>2</sub> S	21.5	29.2	31.6	35.1	35.0	34.7
<b>Djurleite</b>	Cu <sub>31</sub> S <sub>16</sub>	-	-	-	-	-	-
<b>Digenite</b>	Cu <sub>9</sub> S <sub>5</sub>	-	-	-	-	-	-
<b>Covellite</b>	CuS	-	-	-	-	-	-

The solution concentrations of iridium, rhodium and ruthenium as a function of time during test 6 are shown in Figure 4-38. In all three cases a fast initial precipitation period (0 – 30 mins) was followed by a slower second period, similar to the trend observed in copper precipitation.

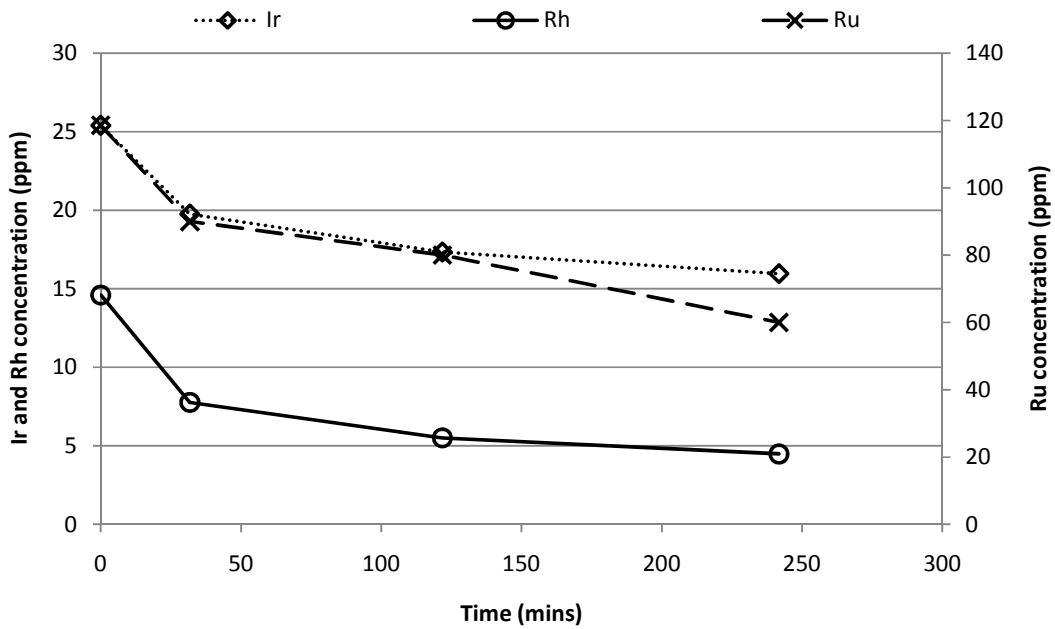


Figure 4-38 PGE Concentration changes with time in test 6. 74 g/L acid, 20 g/L  $\text{Cu}^{2+}$ , 150 g solids/L, 1100 rpm, 0.83 % Fe

Scanning electron microscopy was used to characterise the mineralogy of a sample of residue from test 6. SEM images of particles from the residue are presented in Figure 4-39. Quantitative XRD analysis showed that the residue contained 10.8 wt% Ni-Cu alloy, 51.0 wt% heazlewoodite, 34.7 wt% chalcocite and small amounts (<1.5 wt%) millerite, pentlandite, troilite and magnetite. The starting material for the test contained more alloy and heazlewoodite than the residue (15.4 wt% Ni-Cu alloy, 61.3 wt% heazlewoodite) and less chalcocite (21.5 wt%). The heazlewoodite matrix, as shown in Figure 4-39, does not show any clear signs of disintegration and contained very little copper. The average composition of the heazlewoodite matrix, as determined from analysis of seven different areas, was 62.5 at % Ni (58.8 – 65.5 at %), 33.3 at % S (29.9 – 36.7 %) and 2.8 at % Cu (0 – 6.1 at %). The lack of copper in the heazlewoodite matrix shows that precipitated copper was not incorporated into the heazlewoodite matrix at random, but rather led to growth of existing chalcocite grains. Very small chalcocite grains were also found that appear to be newly formed. The average composition of nine chalcocite grains was found to be 68.5 at % Cu (64.4 – 70.5 at %) and 28.6 at % S (25.7 – 30.8 at %). Although the mass of alloy decreased during test 6, leaching of the alloy phase did not lead to the formation of holes as it did in oxidative tests. In most alloy grains shown in Figure 4-39, a distinct boundary exists between the alloy and surrounding phases. In image (b), examples are shown where the grain boundaries faded and the alloy seemed to dissolve into the surrounding phases. The composition of four alloy grains were analysed, yielding an average composition of 69.7 at % Ni (68.6 – 71.5 at %), 25.4 at % Cu (23.9 – 26.9 at %) and 2.1 at % S (1.2 – 2.9 at %).

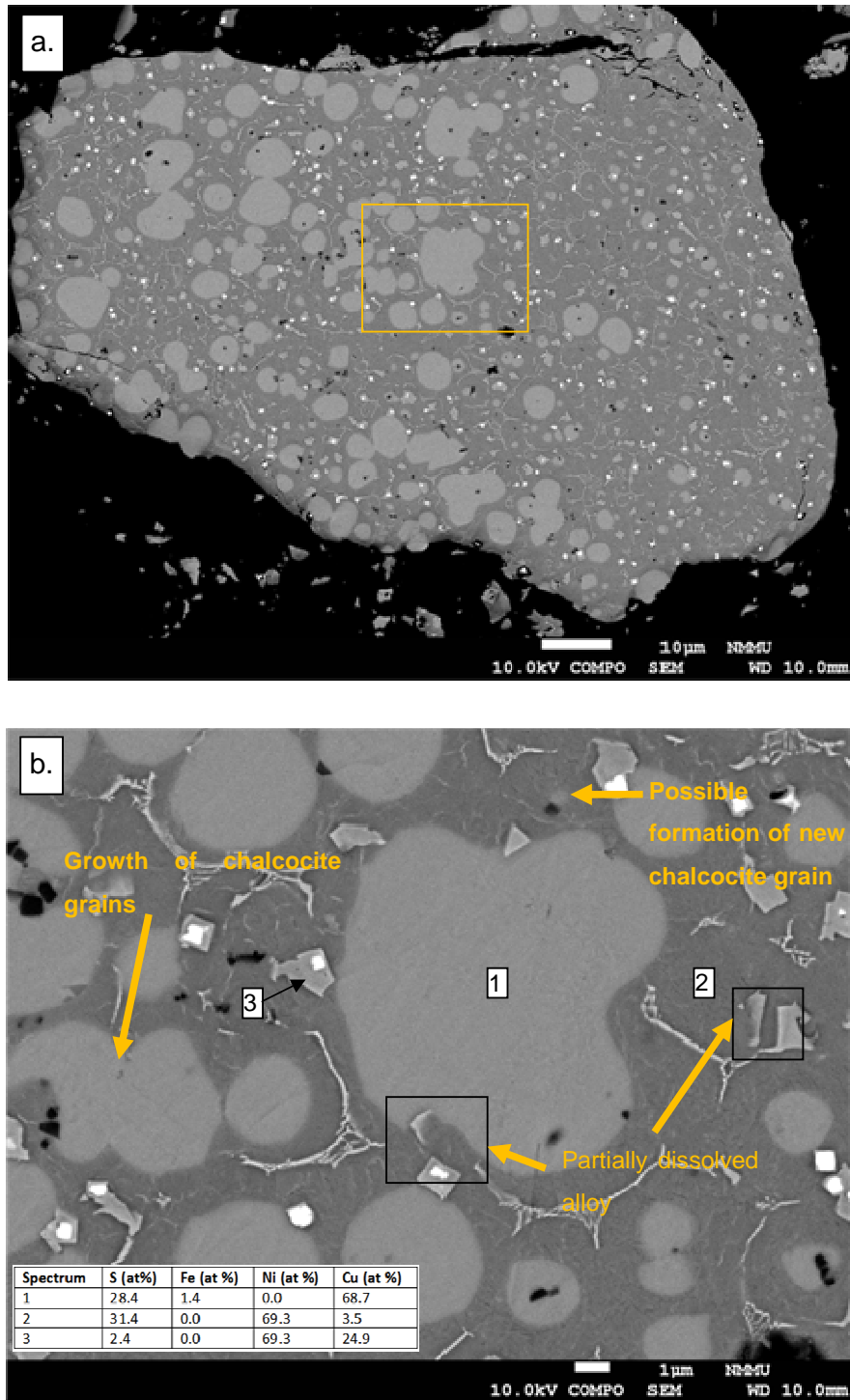


Figure 4-39 (a and b) SEM images of a residue particle from test), showing structure similar to starting material



Test 9 was carried out with the same conditions as test 6, with the exception that the solids content in test 9 was 540 g/L. Test 9 was stopped after 70 minutes, when foaming due to gas production caused the reactor to boil over (Figure 4-40). Some results from test 9 will be discussed here to expand on the phenomenon. Figure 4-41 shows that copper precipitation stopped after 60 minutes (when all the copper had been removed from solution). Foaming started at the same time and an increase in the rate of nickel extraction can be seen between 60 and 70 minutes. Figure 4-41 also shows that more moles nickel were extracted than the moles of copper precipitated, indicating that leaching by acid must have taken place. The gas that evolved did not have any noticeable smell, and was probably hydrogen which evolved due to direct leaching of nickel by acid (Reaction 2-2).



*Figure 4-40 Reactor boiling over during Test 9 due to hydrogen evolution*

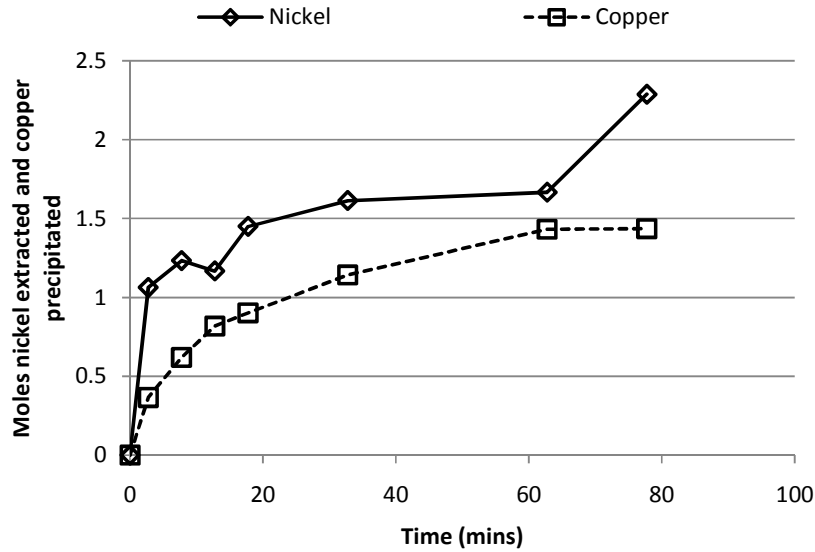


Figure 4-41 Comparison of the number of moles nickel extracted and number of moles copper precipitated in test 9

SEM images from test 9 are shown in Figure 4-42. Leaching of the Ni-Cu alloy clearly took place, as can be seen from the cracks around the alloy grains. Five alloy grains were analysed and showed an average composition of 61.8 at % Ni (58.2 – 72.7 at %), 32.8 at % Cu (24.0 – 38.2 at %) and 2.4 at % S (0.8 – 6.6 at %). When compared to alloy grains from test 6, the nickel content of alloy grains from test 9 is lower. Analysis of five chalcocite grains showed an average composition of 68.1 at % Cu (64.5 – 68.1 at %) and 28.5 at % S (28.1- 29.8 at %). Eleven spots were analysed on the heazlewoodite matrix, showing an average composition of 63.5 at % Ni (60.3 – 66.6 at %), 2.42 at % Cu (0 – 5.3 at %) and 31.7 at % S (29.3 – 34.3 at %). The compositions of heazlewoodite and chalcocite phases in the residue from test 9 were similar to the compositions which were measured in the residue from test 6.

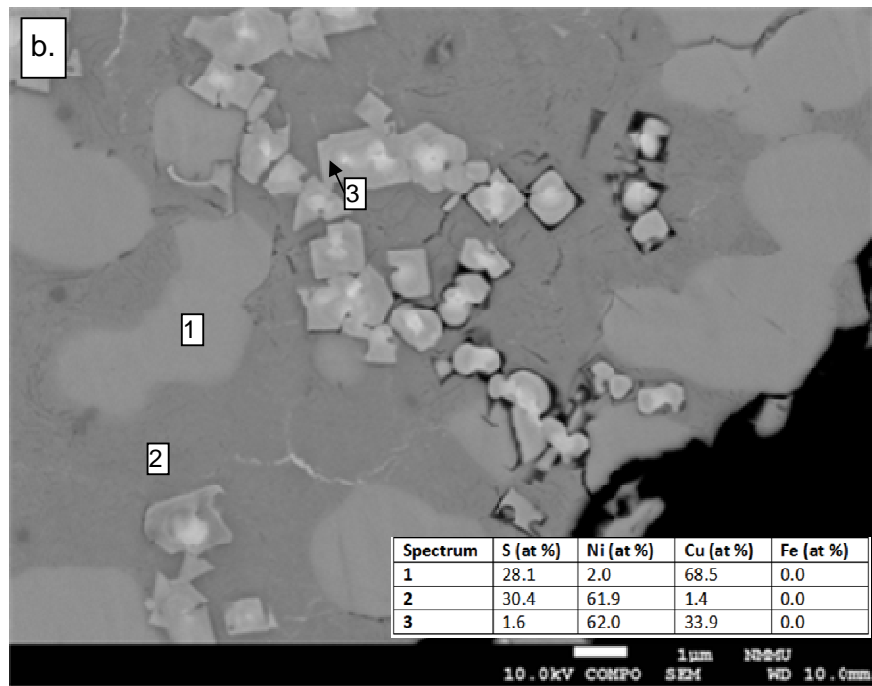
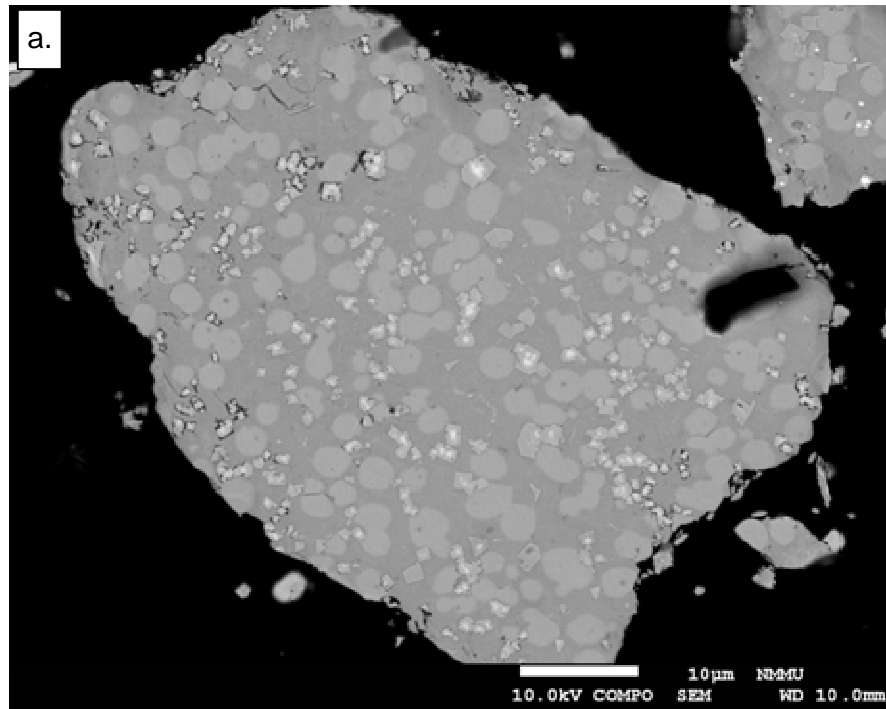


Figure 4-42 SEM images showing a particle from residue from test 9, with signs of alloy leaching at grain boundaries

From the results discussed in the preceding text, it can be seen that the non-oxidative leaching mechanism is characterised by an initial fast reaction period during which the masses of alloy and heazlewoodite phases decreased, while chalcocite phases grew. Copper precipitation and nickel extraction took place according to reaction 2-12. Reaction kinetics slowed down after the initial fast period. PGE precipitation followed similar two-stage kinetics, with an initial fast period and a second slower period.

### 4.3.2 Effect of solids/liquid ratio (NOX)

This section will deal with the effect of the solids/liquid ratio on non-oxidative leaching. Tests 6 and 9; Tests 2 and 7; and Tests 4 and 5 will be compared. The tests discussed in this section were conducted to be comparable with oxidative tests discussed under heading 4.2.2, rather than to highlight any specific interactions or effects.

#### Comparison of tests 6 and 9

In tests 6 and 9, the solids contents were respectively 150 g/L and 540 g/L. Other test conditions for tests 6 and 9 are given in Table 4-15. In Figure 4-43, the percentages nickel, cobalt and iron extracted in the first 60 minutes of the two tests are compared. Nickel extraction was not affected by the solids content. The extent of cobalt extraction was higher at the higher density, while iron extraction was lower. The copper concentrations as a function of time are shown in Figure 4-43. The rate at which copper was removed from solution, as well as the total amount of copper removed from solution increased with increasing solids content.

Table 4-15 Operating conditions for tests 6 and 9

Test	Solids/Liquid [g/L]	Gas	Fe-endpoint [Mass %]	Init. Cu conc [g/L]	Init. Acid conc. [g/L]	Stirring [rpm]
6	150	N <sub>2</sub>	0.83	20	74	1100
9	540	N <sub>2</sub>	1.05	20	74	1100

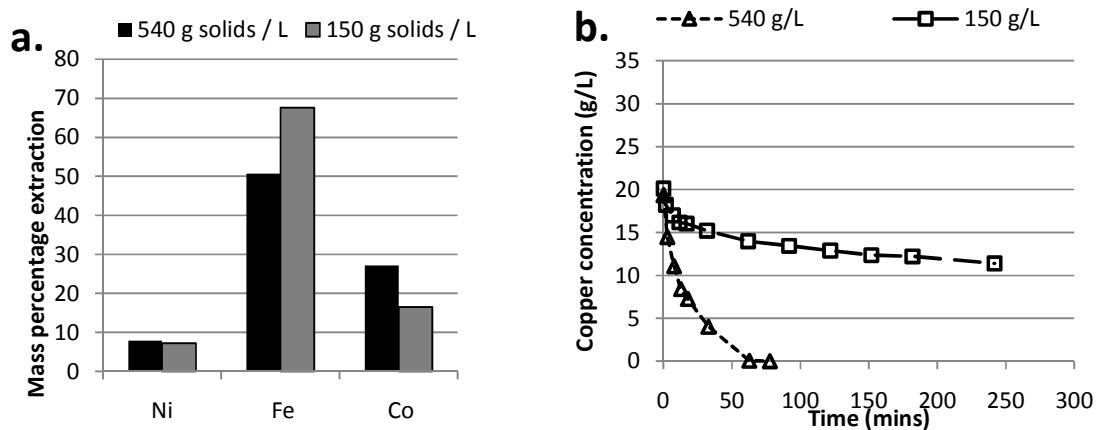


Figure 4-43 Comparison of (a) metal extractions in the first 60 minutes and (b) copper concentrations as a function of time, in test 6 (150 g solids/L) and test 9 (540 g solids/L)

Mineralogical analyses of solid samples from tests 6 and 9 are respectively given in Table 4-14 and Appendix F. Heazlewoodite and alloy phases decreased during leaching in both tests, but to a larger extent in the 540 g/L test (test 9), when the first 60 minutes are compared. The alloy phase was probably consumed to a larger extent in test 9 due to reaction 2-2 taking place.

#### Comparison of tests 2 and 7

In tests 2 and 7, the solids contents were 80 g/L and 150 g/L. The initial acid concentration was 37 g/L and the stirring rate was 1100 rpm. Operating conditions for tests 2 and 7 are given in Table 4-16 and results are illustrated in Figure 4-44. The difference in final nickel extractions was insignificant. Iron extraction was lower in the test with a higher solids content, while cobalt extraction was higher. More copper was removed from solution in the 150 g solids/L test (Figure 4-44). These results are in agreement with results from tests 6 and 9. In terms of mineralogical changes with respect to time (see Appendix F), the behaviours of the solid phases were similar in tests 2 and 7.

Table 4-16 Operating conditions for tests 2 and 7

Test	Solids/Liquid [g/L]	Gas	Fe-endpoint [Mass %]	Init. Cu conc [g/L]	Init. Acid conc. [g/L]	Stirring [rpm]
2	80	N <sub>2</sub>	0.89	20	37	1100
7	150	N <sub>2</sub>	0.89	20	37	1100

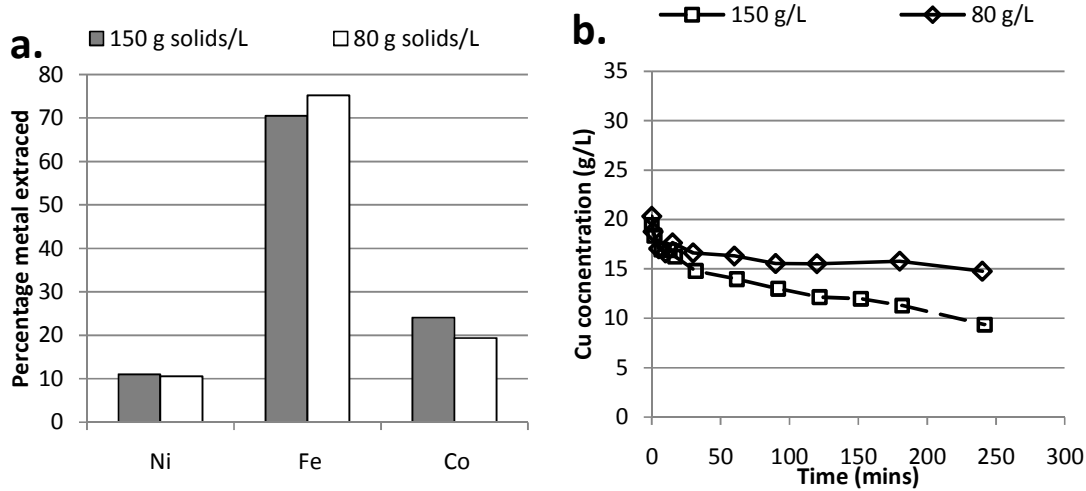


Figure 4-44 Comparison of (a) metal extractions after 240 minutes and (b) copper concentrations as a function of time, in test 2 (80 g solids/L), and test 7 (150 g solids/L)

#### Comparison of tests 4 and 5

In tests 4 and 5, the solids contents were respectively 80 g/L and 150 g/L. The initial acid concentration was 74 g/L and the stirring rate was 500 rpm. Operating conditions for tests 4 and 5 are given in Table 4-17. Results from the tests are shown in Figure 4-45. Only slight differences were visible in metal extractions when comparing test 4 and 5. With an increase in solids content, nickel extraction decreased, cobalt extraction was not significantly influenced and iron extraction increased. The rate as well as total copper removed from solution (Figure 4-45-b), increased with increased solids content. Mineralogical analyses of solid residues show very little difference between tests.

Table 4-17 Operating conditions for tests 4 and 5

Test	Solids/Liquid [g/L]	Gas	Fe-endpoint [Mass %]	Init. Cu conc [g/L]	Init. Acid conc. [g/L]	Stirring [rpm]
4	80	N <sub>2</sub>	0.83	20	74	500
5	150	N <sub>2</sub>	0.83	20	74	500

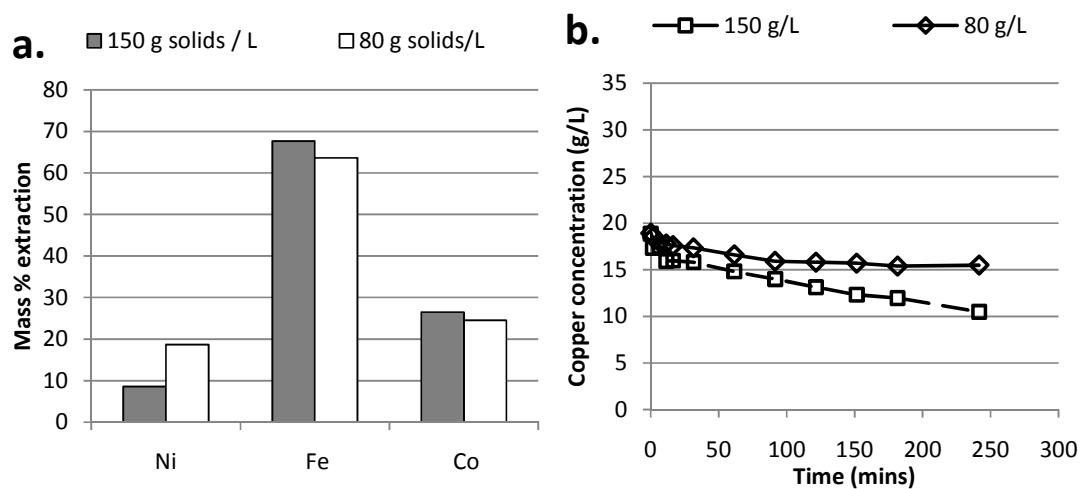


Figure 4-45 Comparison of (a) metal extractions after 240 minutes and (b) copper concentrations as a function of time, in test 4 (80 g solids / L) and 5 (150 g solids / L)

### Section review

In the current work, it was found that an increase in solids content leads to an increase in copper removal. The effect of the solids content on metal extractions was limited. This shows that the increased copper precipitation at higher solids contents is caused by increased reaction area and not by another factor in the kinetics of metal-copper exchange reactions.



### 4.3.3 Effect of initial acid and copper concentrations (NOX)

In this section, tests 6 and 7 will be compared to show some of the effects of initial acid concentration on non-oxidative leaching. Tests 1, 2 and 3 will be compared to demonstrate the effects of initial acid and copper concentrations. The first set of tests were carried out with a solids content of 150 g/L and the second set with a solids content of 80 g/L.

#### Comparison of tests 6 and 7

Operating conditions for tests 6 and 7 are given in Table 4-18. The solution pH in the low acid test (test 7) varied in a range between 0.8 and 0.9. In the high acid test (test 6), the pH remained between 0.3 and 0.4. Metal extractions in the two tests are compared in Figure 4-46-a, and copper concentrations as a function of time are compared in Figure 4-46-b. Metal extractions and copper precipitation in the two tests were not significantly different. Mineralogical changes with respect to time for test 6 are given in Table 4-14 and for test 7 in Appendix F. Although the stability of solid phases is a function of the acidity of the solution, the mineral phases which were formed in the two tests were similar, as were the changes in the masses of the phases with time. The most notable difference is that slightly more heazlewoodite dissolved in the high acid test (a decrease of 8.1 % in the mass percentage heazlewoodite during the first 180 minutes of test 6, vs a decrease of 3.9 % during the same period of test 7).

Table 4-18 Operating conditions in tests 6 and 7

Test	Solids/Liquid [g/L]	Gas	Fe-endpoint [Mass %]	Init. Cu conc [g/L]	Init. Acid conc. [g/L]	Stirring [rpm]
6	150	N <sub>2</sub>	0.83	20	74	1100
7	150	N <sub>2</sub>	0.89	20	37	1100

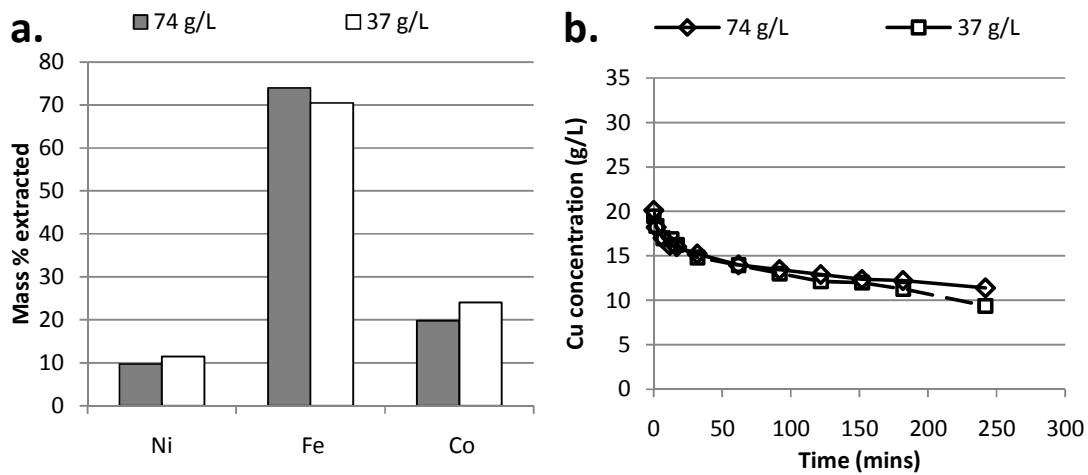


Figure 4-46 Comparison of metal extractions (a) and copper precipitation (b) in test 6 (74 g/L acid) and test 7 (37 g/L acid) and metal extractions after 240 mins

### Comparison of tests 1, 2 and 3

Tests 1, 2 and 3 were carried out with a solids/liquid ratio of 80 g/L. Operating conditions are given in Table 4-19 and results are shown in Figure 4-47. pH changes are not shown. The pH in the high acid test (test 3) remained in the range of 0.25 – 0.75 throughout the test, while the pH in the low acid tests (tests 1 and 2) was in the range of 0.9 – 1.1.

Table 4-19 Test conditions for tests 1 and 3

Test	Solids/Liquid [g/L]	Gas	Fe-endpoint [Mass %]	Init. Cu conc [g/L]	Init. Acid conc. [g/L]	Stirring [rpm]
1	80	N <sub>2</sub>	0.89	40	37	1100
2	80	N <sub>2</sub>	0.89	20	37	1100
3	80	N <sub>2</sub>	0.89	40	74	1100

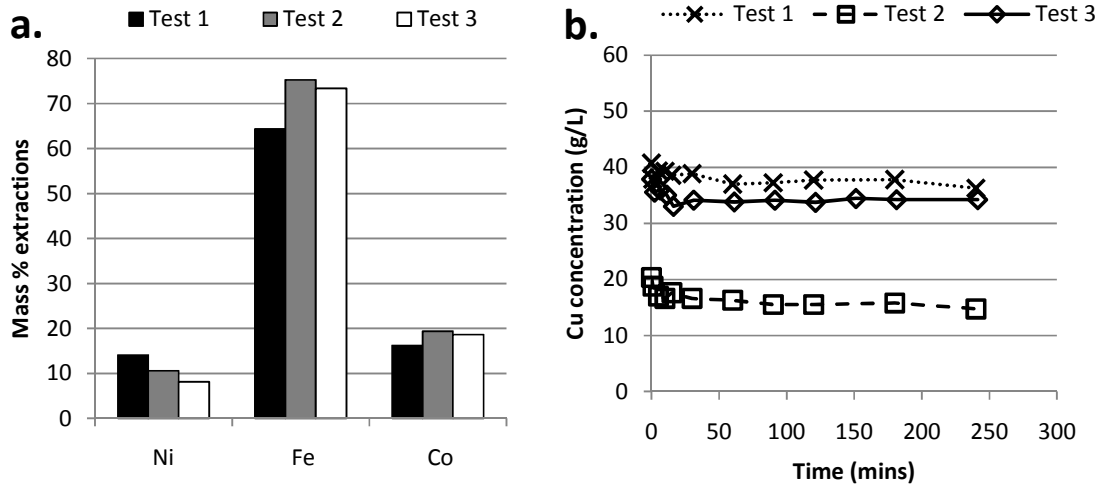


Figure 4-47 Comparison of copper precipitation and metal extractions after 240 minutes in test 1, test 2 and test 3. Operating conditions are listed in Table 4-22

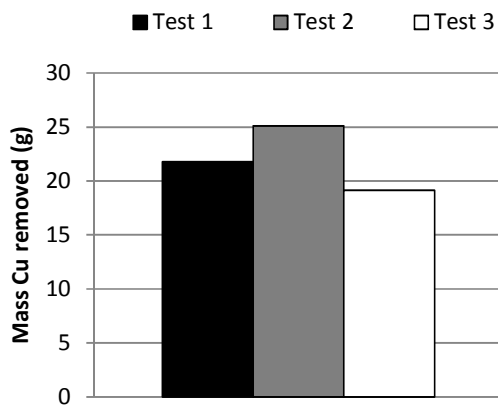


Figure 4-48 Comparison of copper precipitated (mass [g]) in tests 1, 2 and 3, for which operating conditions are listed in Table 4-22

The operating conditions for tests 1 and 3 only differed in terms of initial acid concentration. When comparing the percentages of metals extracted in tests 1 and 3, the most significant effect was on iron extraction, which was decreased from 75 % in the high acid test (test 3) to 64 % in the low acid test (test 1). When comparing copper precipitation during tests 1 and 3 (Figure 4-48-b), it can be seen that the initial rate of copper precipitation was faster at a higher acid concentration (test 3). This might be due to a particle surface activation effect, as noted by Mackinnon (1974). Mackinnon (1974) investigated cementation onto a Ni-powder substrate and found that acid was required to dissolve nickel oxides and activate the reaction surface for cementation to proceed.

Lamya (2007) investigated the non-oxidative leaching of Ni-Cu-S converter matte at 65 °C and three acid levels (90 g/L, 110 g/L and 125 g/L) and found that the amount of iron and cobalt extracted increased when the initial acid concentration was increased from 90 g/L to 110 g/L. The initial acid concentration had no effect on nickel extraction. Less copper was precipitated from solution when the initial acid concentration was increased from 90 g/L to 110 g/L. These effects were attributed to the direct attack of acid on iron, cobalt and copper. Leaching reactions in which acid and oxygen are involved probably played a less important role in this work than in Lamya's work (2007), because nitrogen was sparged into the leaching solution during non-oxidative tests.

The initial copper concentrations in tests 1 and 2 were different, while all other operating conditions were the same. Lamya (2007) found that the leaching of metals was independent of the copper concentration in the range of 25 – 48 g/L, but that the rate and degree of copper precipitation increased when the initial copper concentration was decreased from 36 g/L to 25 g/L.

The results for tests 1 and 2 reflect the findings of Lamya (2007) in terms of copper precipitation. Copper precipitation was faster in the 20 g/L Cu<sup>2+</sup> test (test 2) than in the 40 g/L Cu<sup>2+</sup> test (test 1) and a larger total amount of copper was precipitated (Figure 4-48). The effect of the initial copper concentration on nickel and cobalt extractions were negligible, but iron extraction was higher in the low copper test.

Differences in the mineralogical composition of residues from tests 1 and 2 were insignificant. (Appendix E)

### Section review

From the results of tests 6 and 7, as well as the results from tests 1 and 3, it can be seen that the effect of acid on non-oxidative kinetics (metal extractions and copper precipitation) is limited. From the results of tests 1 and 3 it can be seen that the effect of the initial acid concentration of copper precipitation kinetics and metal extractions was also very small.

In the context of the Lonmin atmospheric leach, these results show that the amount of acid and copper remaining in solution after the first three oxidative tanks will not influence the kinetics in the last two non-oxidative tanks significantly.

#### 4.3.4 Effect of the Fe-endpoint (NOX)

Literature dealing with the effect of iron on leaching is limited to oxidative leaching. Works by Llanos et al. (1974), Symmens et al. (1976) and Symmens et al. (1979) refer to the effect of the iron endpoint on acid consumption, but the effect on nickel dissolution by means of metathesis and cementation is not dealt with. Under non-oxidative conditions, the primary reaction mechanisms are exchange reactions between dissolved copper and metals in the solid phase.

The effect of the iron endpoint on non-oxidative leaching was investigated in two sets of tests, which were respectively carried out at a high stirring rate (1100 rpm) and a low stirring rate (500 rpm). Tests 6 and 12 were carried out with a stirring rate of 1100 rpm and mattes containing 0.83 % Fe and 5.72 % Fe. Tests 5 and 13 were carried out with a stirring rate of 500 rpm. The mattes used in tests 5 and 13 contained 0.8 % Fe and 5.72 % Fe mattes. All tests were done with an initial copper concentration of 20 g/L and an initial acid concentration of 74 g/L.

##### Comparison of tests 6 and 12

Operating conditions for tests 6 and 12 are summarised in Table 4-20. Results from the two tests are compared in Figure 4-49. The solution pH remained between 0.3 and 0.6 and did not change significantly in either test.

Table 4-20 Operating conditions for tests 6 and 12

Test	Solids/Liquid [g/L]	Gas	Fe-endpoint [Mass %]	Init. Cu conc [g/L]	Init. Acid conc. [g/L]	Stirring [rpm]
6	150	N <sub>2</sub>	0.83	20	74	1100
12	150	N <sub>2</sub>	5.72	20	74	1100

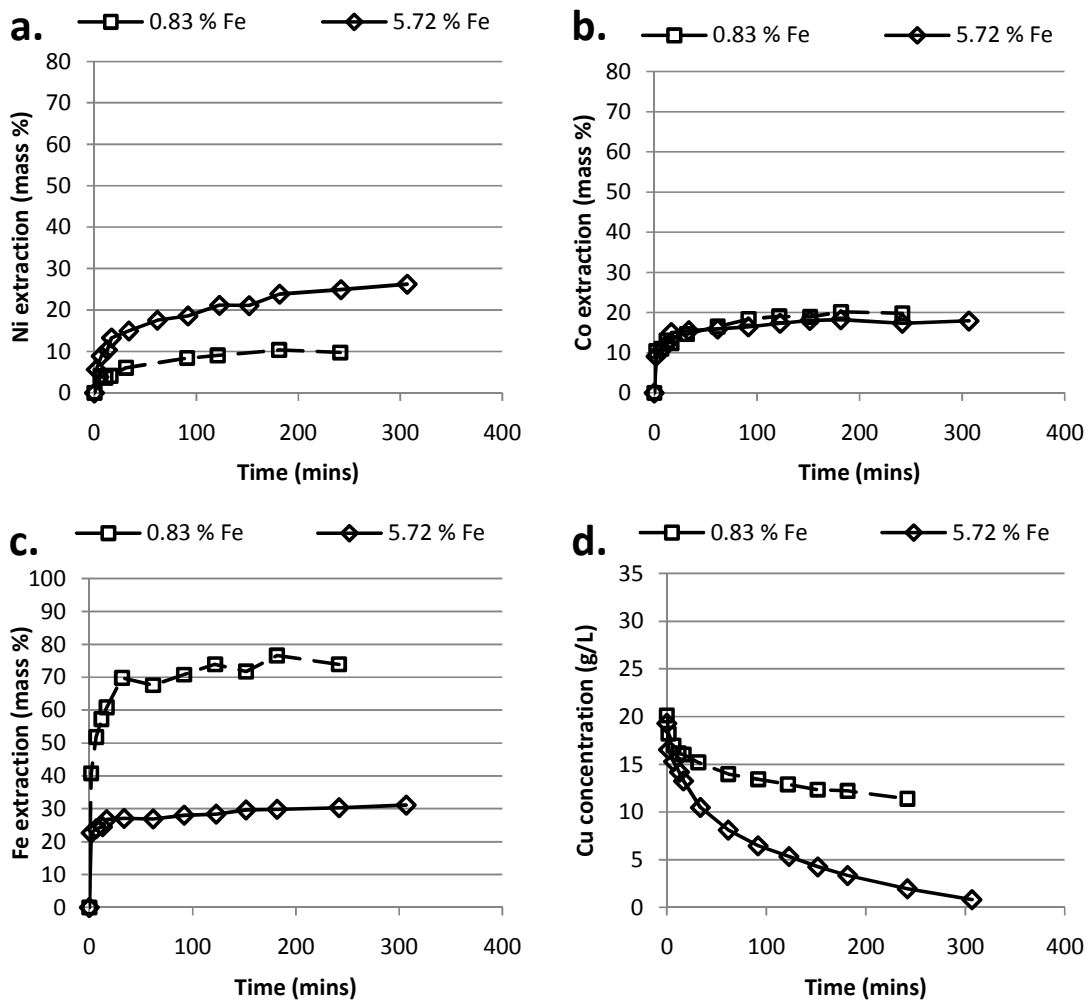


Figure 4-49 Comparison of metal extractions and copper precipitation in test 6 (0.83 % Fe) and test 12 (5.72 % Fe)

The rate and extent of nickel extraction, as well as the rate and extent of copper precipitation, were significantly larger in the high iron test.

Cobalt extraction in the high iron test was not significantly influenced in terms of percentage extraction, but it should be taken into account that the high iron matte

contained more cobalt than the low iron matte. In terms of moles extracted, cobalt extraction in the high iron test (0.016 moles) was higher than in the low iron test (0.011 moles)

Iron extraction was much lower in the high iron test (in terms of mass %), although more moles iron were extracted in the high iron test (0.224 moles) than the low iron test (0.064 moles)

In terms of PGE precipitation (Figure 4-50), more rhodium and iridium were precipitated in the high iron test, but less ruthenium was precipitated in the high iron than in the low iron test.

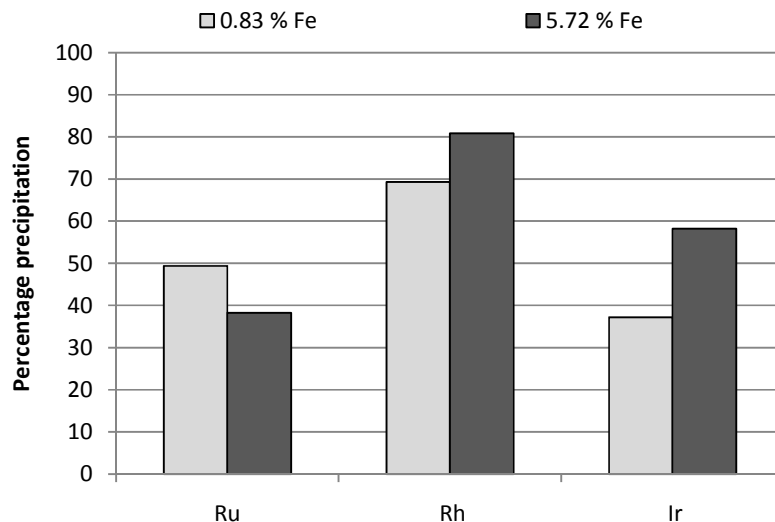


*Figure 4-50 Comparison of percentages Ru, Rh and Ir precipitated from solution after 240 minutes in test 6 (0.83 % Fe) and test 12 (5.72 % Fe)*

The mineralogical compositions of samples taken during test 12 (5.72 % Fe) are given in Table 4-21. The mineralogy of samples taken in test 6 (0.83 % Fe) was given in Table 4-14. Very little alloy was initially present in the high iron matte. The alloy and heazlewoodite contents of the high iron matte decreased in a gradual manner, with the alloy being almost completely depleted (< 1 %) after only 30 minutes. In the low iron test, the alloy phase stopped reacting after the initial fast stage of copper removal, when the solid phase still contained approximately 10 % alloy. Godlevskite formation is prominent in the high iron test, with godlevskite formation preceding millerite formation. Neither godlevskite nor millerite formed in



significant amounts in the low iron test. Bornite and pentlandite phases, that are characteristic of the high iron matte, did not show significant changes during leaching. In both tests, chalcocite was formed as a copper precipitation product.

*Table 4-21 Mineralogical changes during test 12. 74 g/L acid, 20 g/L Cu, 150 g solids / L, 1100 rpm, 5.72 % Fe*

Sample time		0	15	30	120	240	300
Mineral		Mass %					
<b>Ni-Cu</b>	Ni-Cu	2.1	1.9	0.5	0.6	0	0.4
<b>Heazlewoodite</b>	Ni <sub>3</sub> S <sub>2</sub>	56.9	48.0	46.1	35.6	29.6	27.6
<b>Godlevskite</b>	Ni <sub>7</sub> S <sub>6</sub>	2.9	7.1	3.9	10.2	12.3	13.1
<b>Millerite</b>	NiS	0.4	1.1	1.4	4.6	6.4	7.3
<b>Polydymite</b>	Ni <sub>3</sub> S <sub>4</sub>	-	-	-	-	-	-
<b>Pentlandite</b>	(NiFe) <sub>9</sub> S <sub>8</sub>	9.1	10.9	11.9	10.7	10.6	9.7
<b>Troilite</b>	FeS	0.4	0.5	0.1	0	0	0
<b>Magnetite</b>	Fe <sub>3</sub> O <sub>4</sub>	1.1	0.1	0	0	0	0
<b>Bornite</b>	Cu <sub>5</sub> FeS <sub>4</sub>	11.7	10.7	12.5	12.5	11.6	11.6
<b>Chalcocite</b>	Cu <sub>2</sub> S	15.3	20.0	23.6	25.7	29.7	30.2
<b>Djurleite</b>	Cu <sub>31</sub> S <sub>16</sub>	-	-	-	-	-	-
<b>Digenite</b>	Cu <sub>9</sub> S <sub>5</sub>	-	-	-	-	-	-
<b>Covellite</b>	CuS	-	-	-	-	-	-
<b>Cuprite</b>	Cu <sub>2</sub> O	-	-	-	-	-	-

SEM images and elemental mapping of a polished section of a solid particle from a sample taken after 240 minutes during test 12 are given in Figure 4-51. Image (a) shows a particle at 10 µm bar, with the marked area enlarged in image (b). Distinct pentlandite or bornite phases could not be distinguished. Rather, iron is incorporated into the nickel sulphide matrix and copper sulphide grains. Elemental mapping of the particle is provided in images (c) – (f). From image (c), (d) and (e) it can be seen that nickel and copper are concentrated in distinct phases, while iron occurred throughout the material. In the enlarged image (b), darker lines can be seen on the heazlewoodite and chalcocite phases. Although the darker lines were too small to determine the exact composition, it was found that these areas contained more iron than the surrounding nickel sulphide or copper sulphide grains.

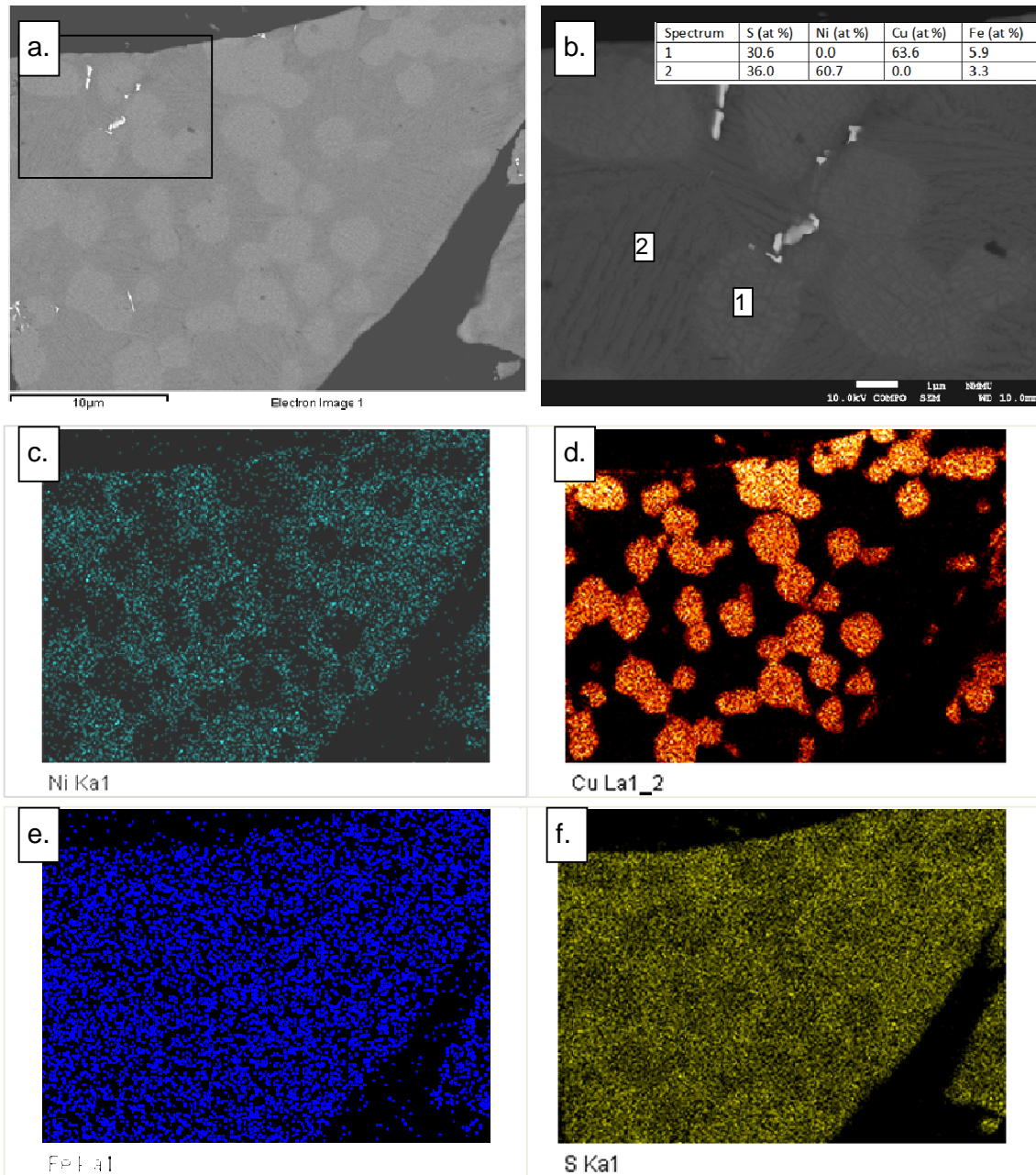


Figure 4-51 SEM images of a particle sampled after 240 minutes in test 12, showing (a) the intact nickel sulphide matrix with euhedral copper sulphide grains, (b) darker areas with high iron content and (c – f) elemental mapping for nickel, copper, iron and sulphur

Analysis of fourteen spots on the nickel sulphide matrix revealed an average composition of 58.5 at % Ni (54.0 – 65.6 at %), 35.9 at % S (30.0 – 41.8 at %), 1.9 at % Cu (0 – 4.1 at %) and 3.0 at % Fe (0.0 – 7.0 at %). The iron content in the nickel sulphide phase was considerably higher than observed in other residues. A similar

observation was made for the copper sulphide grains: 6 grains showed an average composition of 63.2 at % Cu (57.5 – 68.0 at %), 30.0 at % S (27.5 – 31.0 at %), 6.3 at % Fe (4.3 – 9.1 at %) and 0.4 at % Ni (0 – 2.6 at %)

### Comparison of tests 5 and 13

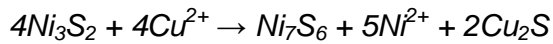
Results from tests 5 and 13 will not be given here, but are given in Appendix D. Test 5 and 13 were carried out at a lower stirring rate than tests 6 and 12. The same effects that were observed at a higher stirring rate were also observed at the lower stirring rate.

### Section review

Under non-oxidative conditions, nickel extraction takes place due to exchange reactions with copper in solution. The results discussed under the preceding paragraphs show that an increase in the iron endpoint leads to increased nickel extraction and copper precipitation. More moles iron and cobalt were extracted in high iron tests than in low iron tests, but in terms of percentages extracted, iron and cobalt extractions decreased with an increase in the iron endpoint. Iron has a higher anodic electropotential than nickel, so that iron is preferably oxidised by cupric ions from solution. In the high iron test, the faster rate of nickel extraction might be explained by the extraction of the large amount of iron which occurs in the heazlewoodite matrix. When iron is extracted, disintegration of the matrix also facilitates nickel extraction.

An initial fast stage and a second slower stage of copper precipitation can clearly be discerned when a low iron matte is leached. When a high iron matte is leached, the distinction cannot easily be made. The initial period of copper removal in low iron mattes is accompanied by a rapid decrease in the alloy content of the matte, which slows down in the second period. In high iron mattes, very little alloy is present in the starting material and the distinction between the two reaction stages is consequently less clear. Godlevskite formed in high iron tests, but was absent in low iron tests. Millerite formation also took place to a larger extent in high iron tests than in low iron tests. In the high iron tests, metathesis probably took place according to

reaction 2-9, or according to a reaction of the following form in which godlevskite is formed:



Bornite and pentlandite phases are abundant in high iron mattes but do not react readily.

### 4.3.5 Effect of stirring rate (NOX)

In order to determine the effect of stirring rate under non-oxidative conditions, tests 5 and 6 will be compared, as well as tests 12 and 13. The first two tests were carried out with low iron matte and the last two with high iron matte. In each set of tests, one test was carried out with a stirring rate of 500 rpm and the other with 1100 rpm. The solids content, initial acid concentration and initial copper concentrations were, respectively, 150 g/L, 74 g/L, 20 g/L, in all tests.

#### Comparison of tests 5 and 6

Test conditions for tests 5 and 6 are shown in Table 4-22 and results are compared in Figure 4-52. Nickel extraction and copper removal were not influenced by the stirring rate. Cobalt extraction was lower at a stirring rate of 1100 rpm and iron extraction was higher.

The mineralogy of solid samples from test 5 is given in Appendix F and from test 6 in Table 4-14. In terms of mineralogy, significant differences did not occur.

Table 4-22 Operating conditions in test 5 and test 6

Test	Solids/Liquid [g/L]	Gas	Fe-endpoint [Mass %]	Init. Cu conc [g/L]	Init. Acid conc. [g/L]	Stirring [rpm]
5	150	N <sub>2</sub>	0.83	20	74	500
6	150	N <sub>2</sub>	0.83	20	74	1100

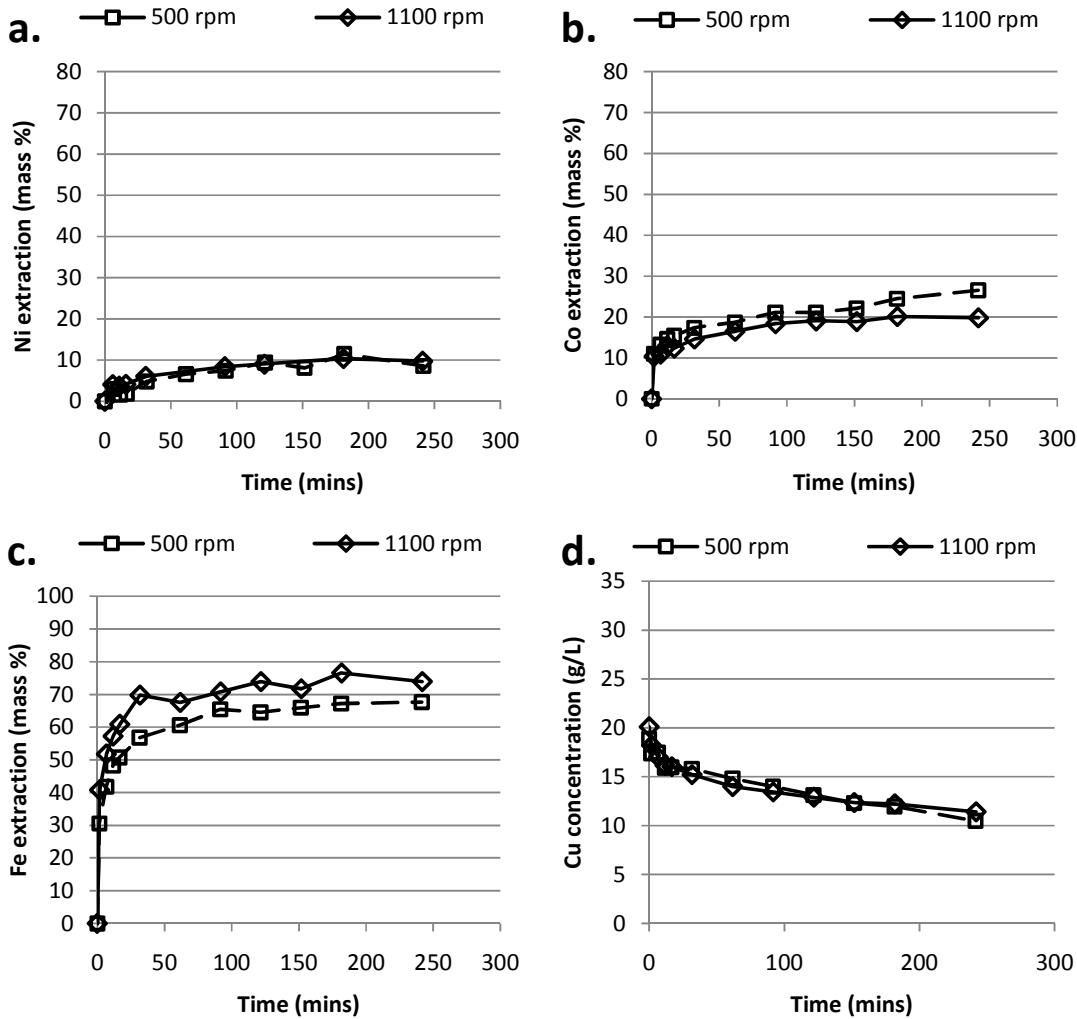


Figure 4-52 Comparison of metal extraction and copper precipitation during test 5 (500 rpm) and test 6 (1100 rpm)

The formation of pure copper on particles was observed in test 5 (Figure 4-53(d)). Figure 4-53(a) shows a large copper deposit which formed a coating on a matte particle. Image (b) shows evidence that these copper deposits nucleated at sites where the alloy grains were exposed to the solution at the particle surface. Although large copper deposits were formed, the relative abundance of alloy decreased during the test from 15.4 % to 9.5 %. Image (c) shows that while copper deposits were

forming, evidence can be found of the alloy phase dissolving. One possible explanation for this is that reaction 2-12 was also operative, in which nickel from the alloy, together with nickel from the heazlewoodite matrix reacts with copper from solution to form chalcocite as product. The relative abundance of chalcocite in the matte increased from 21.5 wt % at the start of the test to 33.9 wt % at the end of the test.

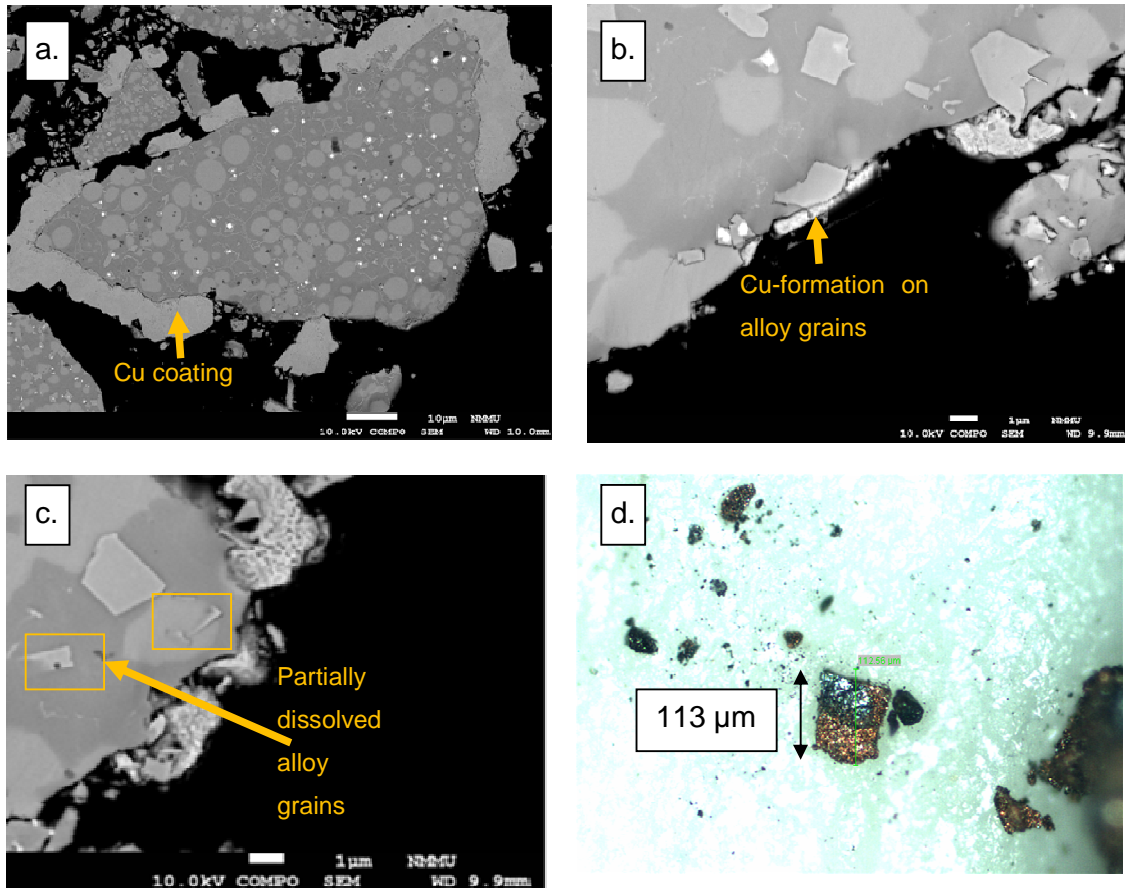


Figure 4-53 (a,b,c): SEM images of residue from test 5, showing (a) copper coating (b) nucleation sites (c) partially dissolved alloy phases. Image (d): photograph of copper coated particle, observed with optical microscope

Analysis of five grains of Ni-Cu alloy show an average composition of 69.1 at % Ni (60.0 – 74.2 at %), 24.4 at % Cu (21.4 – 27.5 at %) and 0.6 at % S (0.0 – 1.5 at %). The average composition of ten areas on the heazlewoodite matrix was found to be 59.4 at % Ni (49.2 – 65.0 at %), 5.5 at % Cu (1.4 – 9.7 at %) and 32.7 at % S (28.6 – 39.8 at %). Four chalcocite grains were analysed and had an average composition

of 67.3 at % Cu (62 – 70.4 at %), 25.7 at % S (16.7 – 29.6 at %) and 67.3 at % Ni (62.0 – 72.4 at %). The compositions of these phases were very similar to the compositions of phases in the residue from test 6.

#### Comparison of tests 12 and 13

The effect of stirring on reaction kinetics was more pronounced when leaching high iron mattes. Operating conditions and results from tests 12 and 13 are presented in Table 4-23 and Figure 4-54. The rates and extents of nickel extraction and copper precipitation increased with increased stirring rate. The effect of the stirring rate on iron and cobalt extraction was negligible.

Table 4-23 Operating conditions in test 12 and test 13

Test	Solids/Liquid [g/L]	Gas	Fe-endpoint [Mass %]	Init. Cu conc [g/L]	Init. Acid conc. [g/L]	Stirring [rpm]
12	150	N <sub>2</sub>	5.72	20	74	1100
13	150	N <sub>2</sub>	5.72	20	74	500

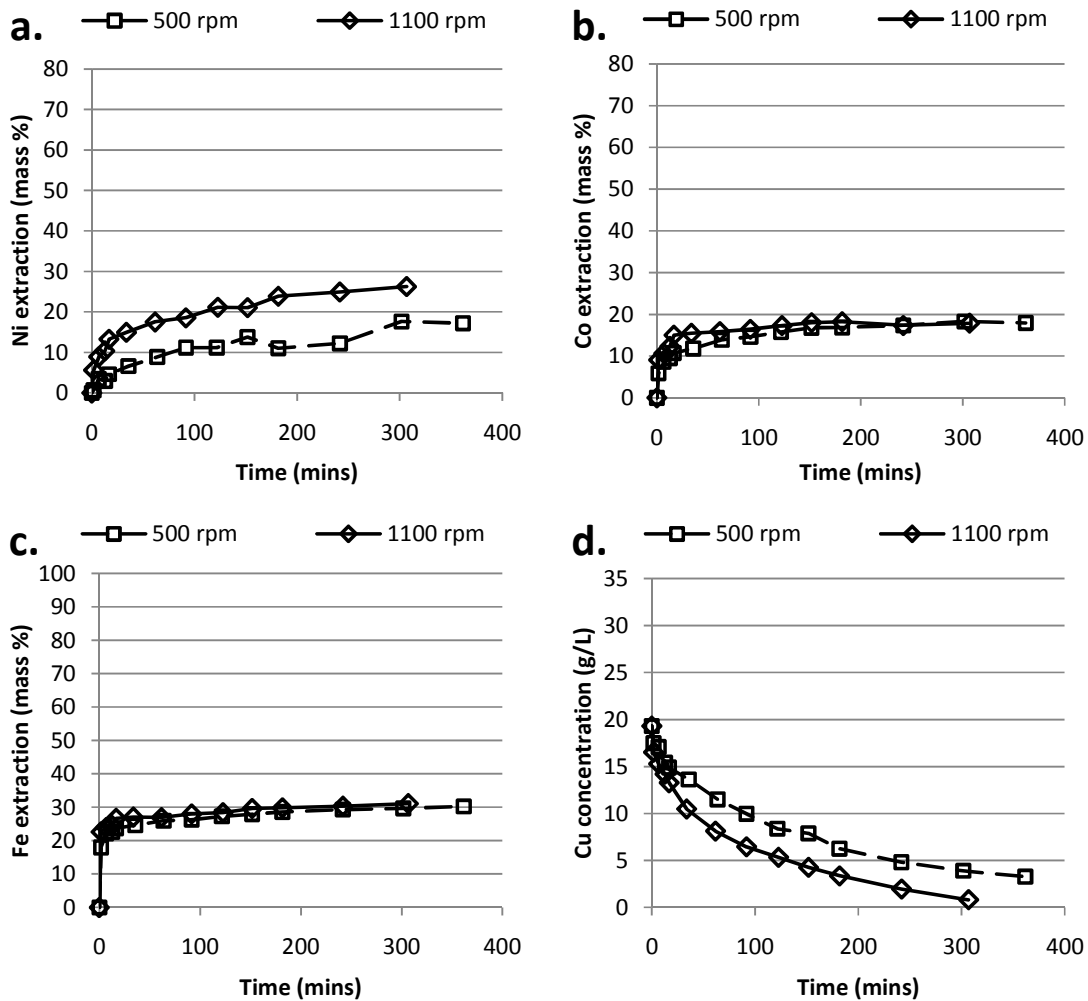


Figure 4-54 Comparison of metal extraction and copper precipitation during test 12 (1100 rpm) and test 13 (500 rpm)

In terms of mineralogy, the only significant difference between the tests was that the extent of heazlewoodite transformation to godlevskite and millerite was larger in the high stirring rate test than in the low stirring rate test, due to the larger percentage nickel extracted.



### Section review

The results show that different controlling mechanisms are applicable when leaching mattes with different iron endpoints. In high iron tests, cobalt and iron extractions were unaffected by stirring rates, indicating that the reaction rates must be either pore diffusion or chemical reaction controlled. Nickel extraction and copper removal rates increased with stirring rate, indicating that the rate of metathesis is controlled by diffusion in the bulk fluid when leaching high iron mattes.

When leaching low iron mattes, cobalt extraction decreased with an increase in stirring rate. Iron extraction increased, indicating a bulk diffusion controlled reaction. Nickel extraction and copper removal rates were unaffected, indicating a chemical reaction controlled or pore diffusion controlled process.

## **4.4 Effect of oxygen**

The tests discussed in this section were chosen to highlight differences and similarities in copper precipitation mechanisms during oxidative and non-oxidative leaching. The tests were also chosen to show the effect of oxygen on high iron and low iron mattes.

### Comparison of tests 9 and 22

Test 9 and test 22 were carried out with a solids content of 540 g/L. The conditions for the tests are given in Table 4-24 and the results are compared in Figure 4-55. Test 9 (non-oxidative) was stopped after 70 minutes due to hydrogen evolution which produced enough foam that the reactor boiled over. No foaming was observed in the test 22 (oxidative). Nickel, cobalt and iron extractions (Figure 4-55) were higher in the oxidative test than the non-oxidative test. On the other hand, the rate of copper precipitation was not affected by the availability of oxygen.

Table 4-24 Operating conditions for tests 9 and 22

Test	Solids/Liquid [g/L]	Gas	Fe-endpoint [Mass %]	Init. Cu conc [g/L]	Init. Acid conc. [g/L]	Stirring [rpm]
9	540	N <sub>2</sub>	1.05	20	74	1100
22	540	O <sub>2</sub>	1.05	20	74	1100

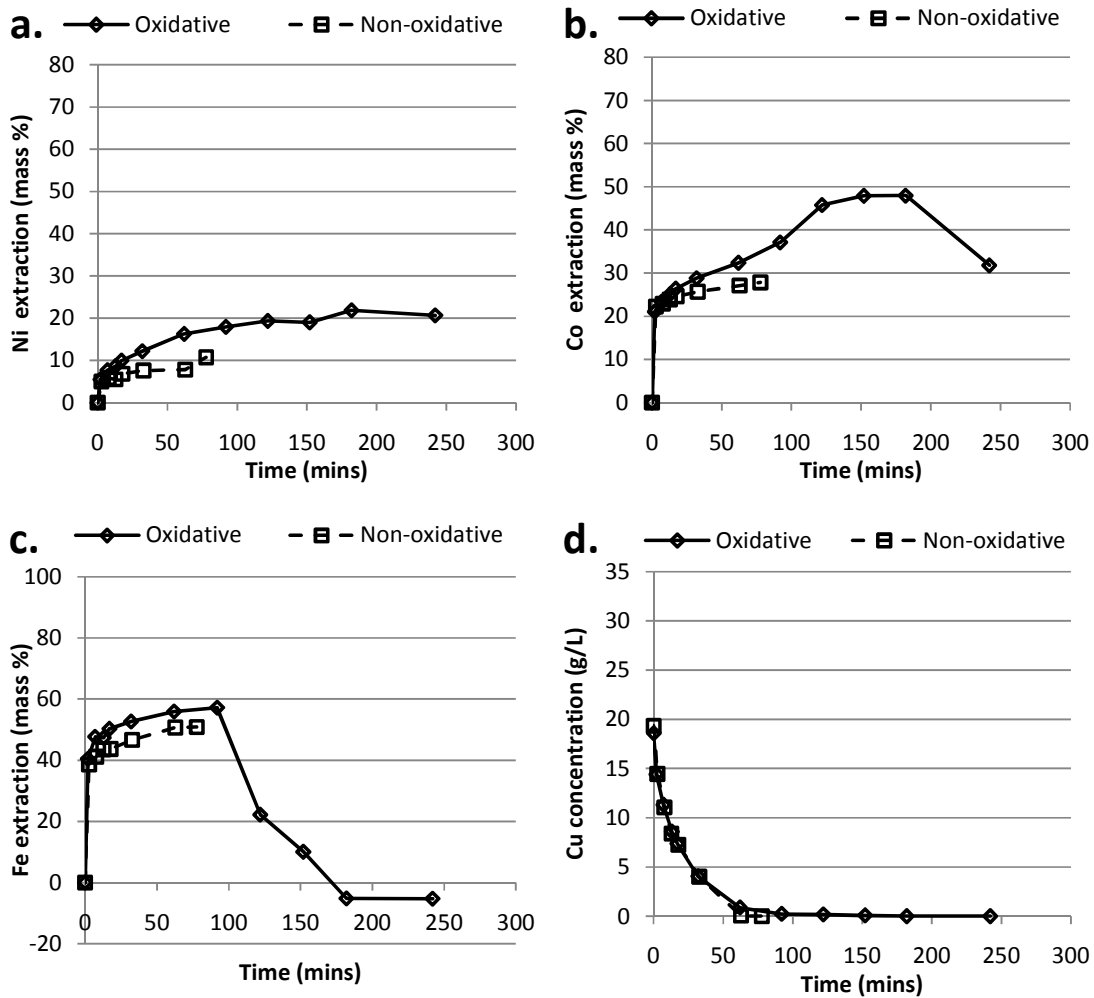


Figure 4-55 Comparison of metal extraction and copper precipitation during test 9 (non-oxidative), test 22 (oxidative)

Mineralogical analysis of solid samples taken during tests 9 and 22 are given in Appendix F. After 60 minutes, little distinction can be made between solid samples from the two tests.

Comparison of tests 6 and 20

Two oxidative tests during which copper was partially precipitated from solution were test 20 (150 g/L solids, 74 g/L acid) and test 15 (80 g/L solids, 37 g/L acid). The conditions for test 20 and the corresponding non-oxidative test (test 6) are given in Table 4-25.

Table 4-25 Operating conditions for tests 6 and 20

Test	Solids/Liquid [g/L]	Gas	Fe-endpoint [Mass %]	Init. Cu conc [g/L]	Init. Acid conc. [g/L]	Stirring [rpm]
6	150	N <sub>2</sub>	0.83	20	74	1100
20	150	O <sub>2</sub>	0.53	20	74	1100

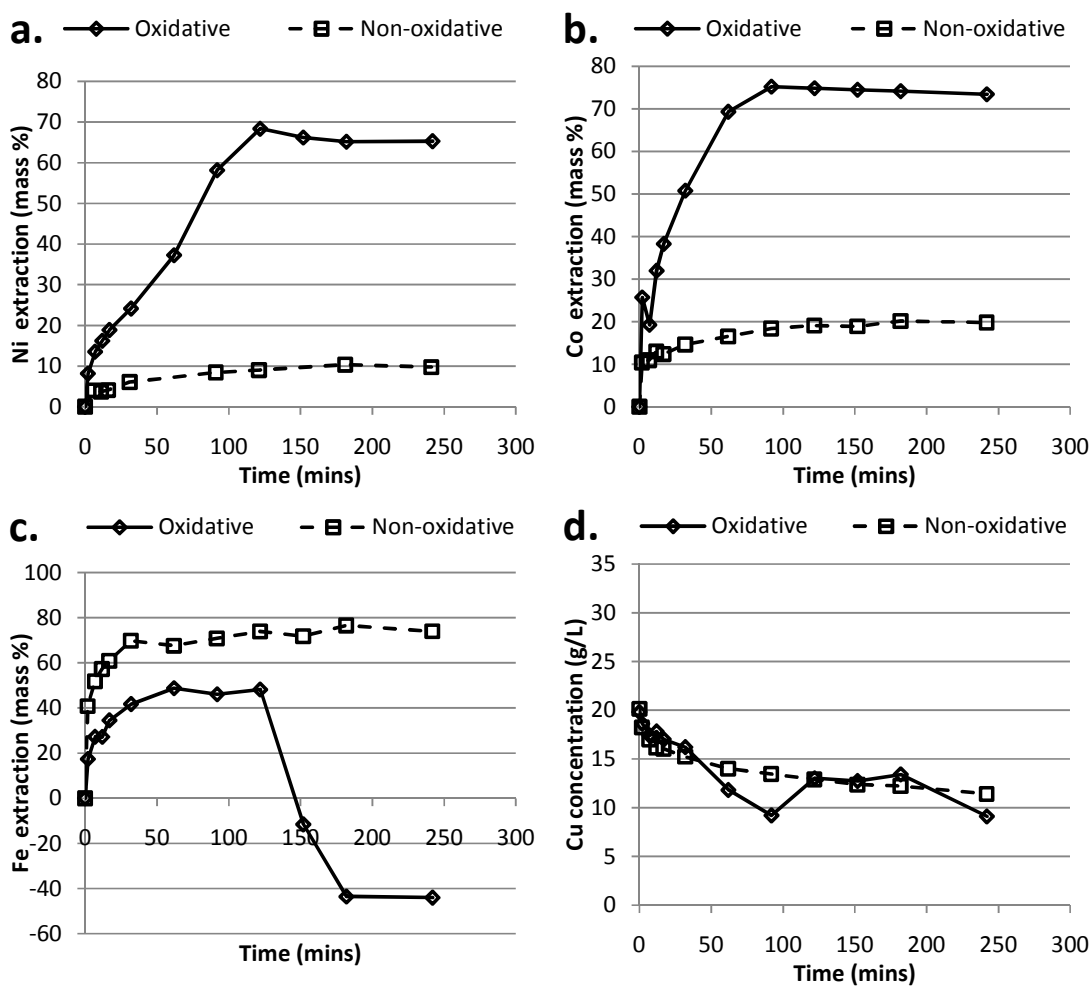


Figure 4-56 Comparison of metal extraction and copper precipitation during test 6 (non-oxidative), test 20 (oxidative)

Nickel and cobalt extractions are higher in the oxidative test. The higher extractions can be attributed to oxygen dependent leaching reactions that do not proceed under non-oxidative conditions. Under non-oxidative conditions, the primary mechanism of metal extraction was exchange reactions with copper. Iron extraction was lower in the oxidative test, where the pH increased and iron precipitation took place.

During the first stage of copper precipitation, the reaction rate was unaffected by the availability of oxygen. During the second stage, copper precipitation was faster under oxidative conditions. (Although not shown here, the same was seen when comparing test 7 with test 21.) After 90 minutes, copper leaching took place in the oxidative test (test 20), while copper leaching did not take place in any of the non-oxidative tests.

The percentages ruthenium, rhodium and iridium precipitated from solution in tests 6 and 20 are compared in Figure 4-57. More PGEs were precipitated in the oxidative test. The smaller extent of PGE precipitation in the non-oxidative test can probably be attributed to the fact that the kinetics slowed down after an initial fast period in non-oxidative tests (compare Figure 4-11 and Figure 4-38).

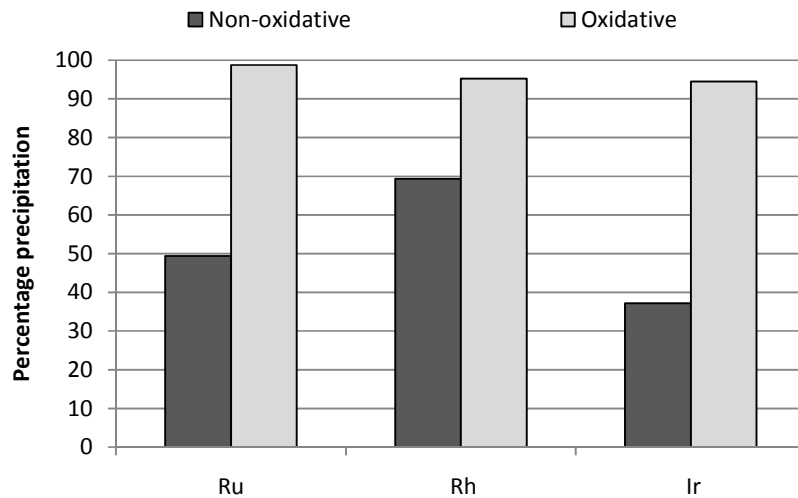


Figure 4-57 Comparison of percentages Ru, Rh and Ir precipitated from solution after 240 minutes in test 6 (non-oxidative) and test 20 (oxidative)

The mineralogy of samples from test 6 was given in Table 4-14 and from test 20 in Table 4-3. In the non-oxidative test, the alloy and heazlewoodite contents of the matte decreased during the first 30 minutes of the test, after which only the heazlewoodite decreased. In the oxidative test, the alloy contents decreased during the first 30 minutes while the heazlewoodite content did not change significantly. After 30 minutes, the heazlewoodite in the oxidative test was rapidly leached along with the remaining alloy. Chalcocite was produced in both tests and digenite was produced in the oxidative test where copper was leached.

#### Comparison of tests 12 and 13

The effect of oxygen on leaching of high iron mattes will be demonstrated by comparing test 12 and test 23. Operating conditions for the tests are given in Table 4-26. Results are illustrated in Figure 4-58.

In terms of metal extractions, the same trends were observed that were observed with low iron mattes. Nickel, cobalt and iron extractions were higher in oxidative tests due to the combined reactions with acid and dissolved copper. The rates of copper precipitation in the two tests were similar for the first 30 minutes, after which copper precipitation stopped in the oxidative test and copper was leached. Heazlewoodite leaching in both tests led to the formation of godlevskite and millerite. (Table 4-21 and Table 4-11)

Table 4-26 Operating conditions for tests 12 and 23

Test	Solids/Liquid [g/L]	Gas	Fe-endpoint [Mass %]	Init. Cu conc [g/L]	Init. Acid conc. [g/L]	Stirring [rpm]
12	150	N <sub>2</sub>	5.72	20	74	1100
23	150	O <sub>2</sub>	5.7	20	74	1100

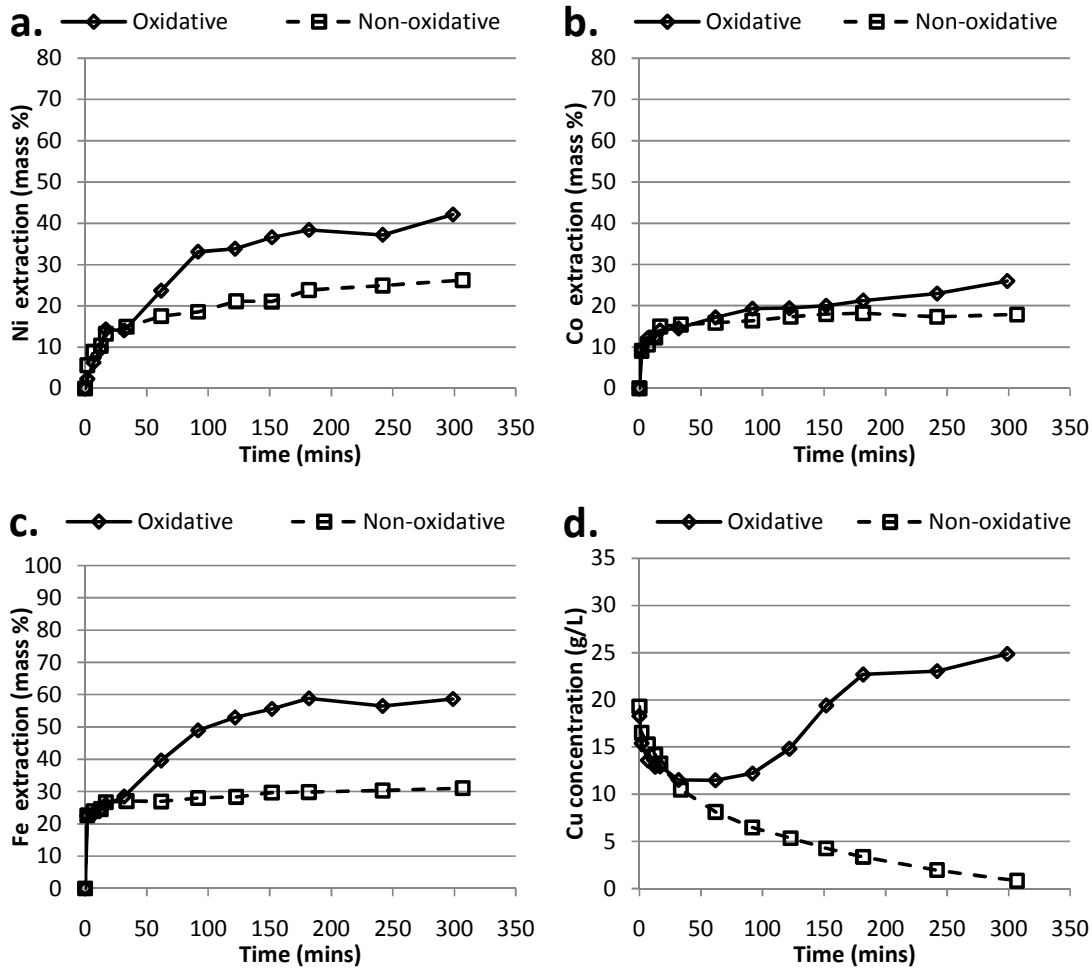


Figure 4-58 Comparison of metal extraction and copper precipitation during test 12 (non-oxidative), test 23 (oxidative)

### Section review

The comparison of oxidative and non-oxidative leaching shows that nickel and cobalt extraction increases when oxygen is available for leaching. This can be attributed to the availability of acid and copper for reaction. In non-oxidative leaching, metal extraction can primarily be attributed to reactions with copper and the rates are consequently slower. Significant increases in solution pH only occurred in oxidative

leaching tests. Consequently, iron precipitation only occurred in oxidative tests and iron extractions were lower under oxidative conditions.

In the first stage of copper precipitation, oxidative and non-oxidative copper-precipitation kinetics are very similar. The second stage of copper precipitation was faster under oxidative conditions, unless copper leaching took place. One explanation for this might be that the mineral structure opens up in oxidative tests due to increased leaching reactions, producing a larger reaction area. Another possibility is that evolved hydrogen sulphide, which can lead to passivation of reaction surfaces, is oxidised faster under oxidative conditions than non-oxidative conditions. The smell of hydrogen sulphide was detected in some non-oxidative tests.

The difference in copper precipitation rates under oxidative and non-oxidative conditions should be taken into account when considering the first three and last two tanks in the atmospheric leach. The rate of copper precipitation in the first three tanks of the atmospheric leach will differ from the rate of copper removal in the last two tanks. The results also suggest that the oxygen flowrate in the first three tanks need to be carefully controlled to prevent copper leaching. However, oxygen is important to create a large surface area.

## Chapter 5 Copper precipitation kinetics

---

In order to develop a control system for the first stage leach, a kinetic model first needs to be developed from experimental data. Such a model will have a structure similar to semi-empirical models developed by Provis et al. (2003) and Lamy (2007). Although the development of a kinetic model falls outside the scope of this work, the current work can assist in the development of a model in three ways:

1. Generating experimental data which can be used for modelling purposes.
2. Provide understanding of the reactions operative during different stages of leaching.
3. Gain understanding of the constraints controlling which reactions will take place.

The second point in the list was addressed under section 4.2.1 and section 4.3.1, where the mechanisms and reactions operative during oxidative and non-oxidative leaching were discussed. The third point can also be addressed to some extent, by defining the following constraints from experimental results:

- Provis et al. (2003) included galvanic interaction as a factor to increase the accuracy of his model. For example, in the model proposed by Provis et al. (2003), the first order reaction rate constant for the leaching of chalcocite was increased by 50 % once all the heazlewoodite was leached from the solid material. An attempt was made to identify specific values of heazlewoodite and alloy extraction at which the rate of copper precipitation or copper leaching would change, but the available data on mineralogy from tests 19, 20, 21 and 22 were insufficient to establish such a relationship.
- Results from tests 14, 15, 16 and 17 show that copper leaching did not take place at pH values above 2, even when nickel leaching had reached a maximum.
- In tests 14, 15, 16, 17 and 20, cobalt and nickel leaching reached a maximum, although enough acid was available for leaching to continue. These results show that 60 – 70 % of the nickel, as well as 60 – 70 % of the cobalt in the



matte is readily leachable. Extraction rates decreased substantially after these values were reached.

A full kinetic model of the system was not developed, but the kinetics of copper precipitation was investigated for selected tests, in which the solids/liquid ratio was sufficient for a significant amount of copper to be precipitated (oxidative tests: 20, 21, 22 and 23. non-oxidative tests: 6, 7, 9 and 12). The non-oxidative results will be discussed first.

Figure 5-1 shows the first order kinetic plot of  $\log([Cu^{2+}]_t/[Cu^{2+}]_0)$  with time for test 6. The reaction did not follow first order kinetics throughout the test, as can be seen from the poor fit given by the linear model.

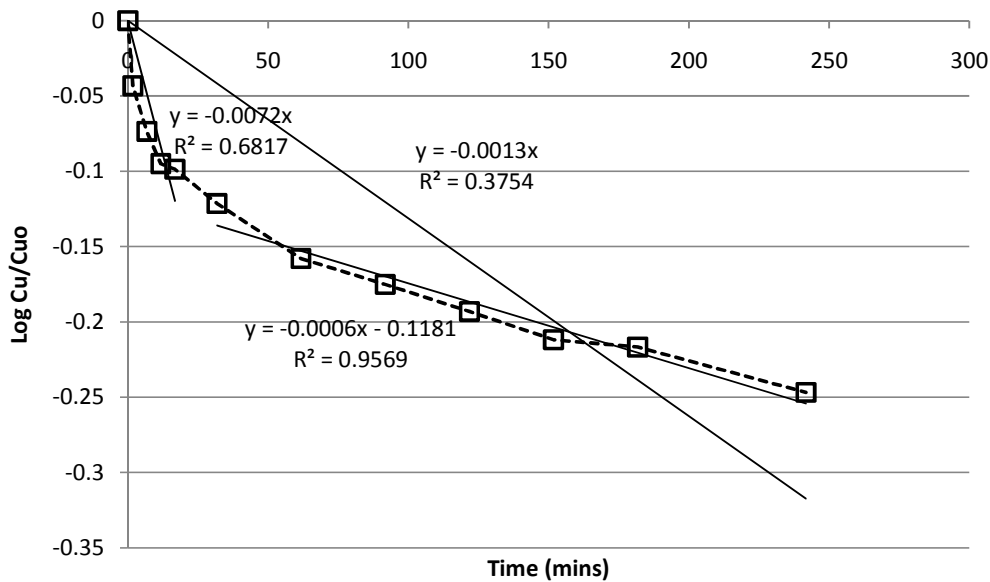


Figure 5-1  $\log([Cu^{2+}]_t/[Cu^{2+}]_0)$  as a function of time for a non-oxidative test (test 6)

Shrinking core effects might account for the decrease in reaction rate, as shown in Figure 5-2. In non-oxidative tests, nickel dissolution took place primarily due to the exchange reaction with copper (probably reaction 2-12). From a fundamental perspective, a shrinking core model should give a good description for non-oxidative leaching in which reaction 2-12 takes place: the decreasing mass of alloy grains that participate in the reaction can be seen as a 'shrinking core'. Equation 2-7 (given

again below) was used to determine whether a shrinking core model with ash diffusion gave a good fit to experimental data from test 6.

$$1-3(1-X_B)^{2/3} + 2(1-X_B) = k_d \cdot t = k_d' C_{Ab} t \tag{Equation 2-7}$$

In the equation above,  $X_B$  is the fraction nickel extracted from the solids and  $C_{Ab}$  is the concentration of copper in the bulk fluid. If the left hand side of the equation is divided by  $C_{Ab}$  and plotted against time, a straight line would indicate a good fit.

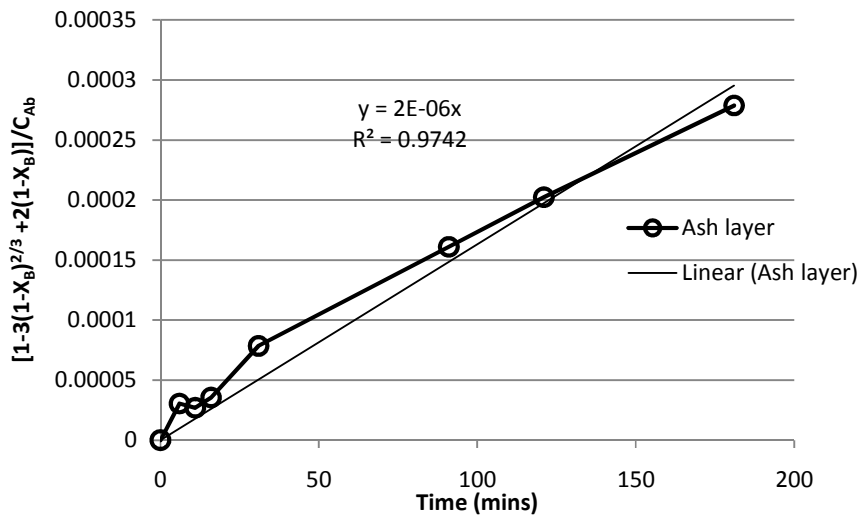


Figure 5-2 Shrinking core model with ash layer diffusion control fitted to data from test 6

For test 6, a shrinking core model with ash layer diffusion control was found to give a better fit than a shrinking core model with chemical or mixed control, or than a first order kinetic model. However, for test 5, a first order reaction model gave a fit equally good to a shrinking core with ash layer diffusion control. For tests 7 and 9, a first order model gave a better fit than a shrinking core model. The best empirical fit to experimental data could be obtained if precipitation was considered to take place in two stages which could each be described in terms of first order kinetics (such as shown in Figure 5-1). Copper precipitation in tests 6 and 7 slowed down, after the alloy mass had decreased, respectively, by 24 % and 28 %.

The reaction rate constants for the first and second reaction periods in test 6 were  $5.5 \times 10^{-6}$  cm/s and  $1.0 \times 10^{-6}$  cm/s. The rate constants obtained for the first and second reaction stages in test 7 were  $3.2 \times 10^{-6}$  cm/s and  $6.9 \times 10^{-7}$  cm/s. In test 6 and test 7, the second reaction period was slower than the first with a factor of approximately five. In test 9, only a single copper precipitation stage was observed, with a reaction rate constant was  $4.2 \times 10^{-6}$  cm/s. In a high iron test (test 12), first order kinetics gave a good fit over the entire test time. The reaction rate constant for test 12 was  $3.4 \times 10^{-6}$ .

Apparent first order rate constants for copper precipitation were calculated for oxidative tests (tests 20, 21, and 22), although copper leaching reactions were also operative and should be taken into account for more accurate results. A plot of  $\text{Log}([\text{Cu}^{2+}]_t/[\text{Cu}^{2+}]_0)$  with time did not give a linear result for test 23 (high iron test), so that a first order rate constant could not be calculated. Copper leaching probably played a more significant role in the high iron test than in other tests.

In oxidative tests, first and second stages of copper precipitation could clearly be observed. Unlike non-oxidative tests, the rate of copper precipitation in oxidative tests (specifically 20 and 21) was found to increase during a second reaction period. The first order  $\text{log}([\text{Cu}^{2+}]_t/[\text{Cu}^{2+}]_0)$  plot with time for test 20 is shown in Figure 5-3. The second reaction period followed 1<sup>st</sup> order kinetics more closely than the first reaction period (this was also true for test 21). The decreasing availability of alloy probably played an important role during the first reaction stage (reaction 2-12).

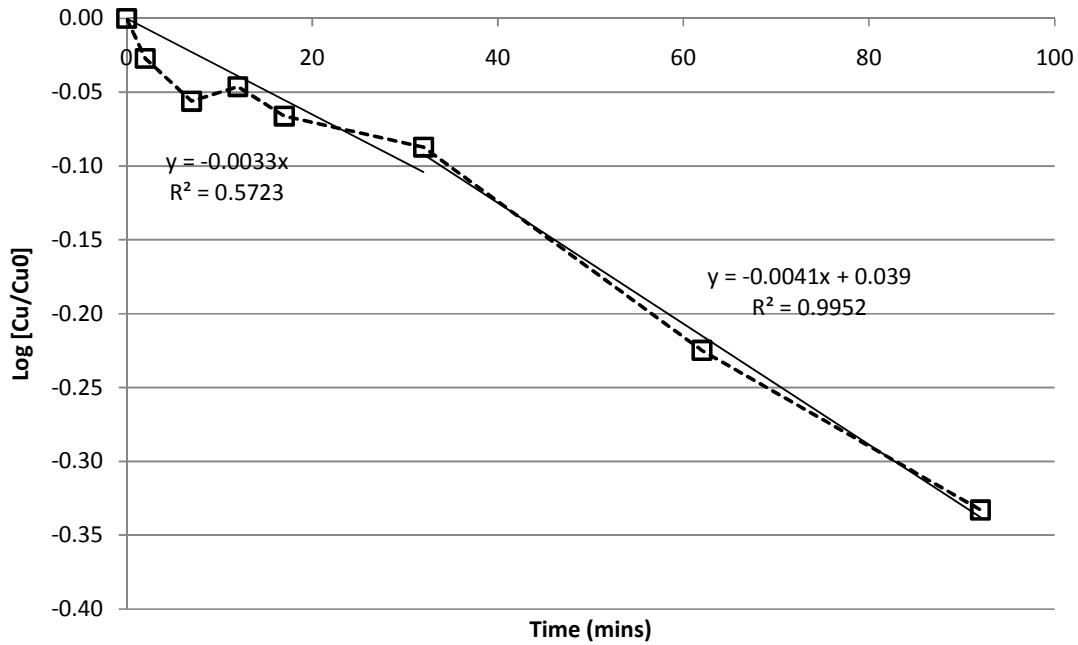


Figure 5-3  $\text{Log}([\text{Cu}^{2+}]/[\text{Cu}^{2+}]_0)$  as a function of time for two stages during an oxidative test (test 20).

The rate constant for the initial reaction period in test 20 was calculated as  $2.5 \times 10^{-6}$  cm/s and for the second period as  $3.1 \times 10^{-6}$  cm/s. The rate constants for the initial and second reaction stages in test 21 were respectively  $2.4 \times 10^{-6}$  cm/s and  $7.0 \times 10^{-6}$  cm/s. Copper precipitation in test 22 took place in a single stage and a first order reaction model gave an excellent fit, with a rate constant of  $4.3 \times 10^{-6}$  cm/s.

## Chapter 6 Conclusion

---

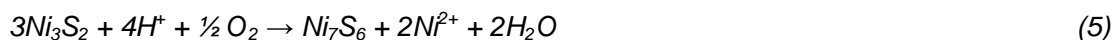
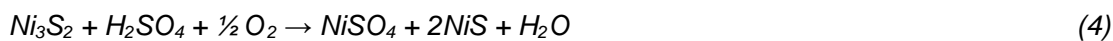
### 6.1 Oxidative leaching mechanism for low iron matte

A characteristic description of the progression of an oxidative leaching test was developed from changes in the mineralogy, along with changes in the concentrations of dissolved metals during leaching. The process is described and the most important reactions taking place at different stages of the process are proposed below.

In a first reaction stage, alloy was leached by acid (reaction 2-1). Metathesis in the first reaction stage took place according to reaction 2-12, which involves galvanic interaction between the alloy and heazlewoodite phases and leads to the formation of chalcocite. Cementation, or the formation of pure metallic copper from exchange reactions between nickel from the alloy and copper from solution, was limited. Leaching of heazlewoodite by acid was slow in this first reaction period, probably because heazlewoodite was galvanically inhibited by the alloy phase.



Inflection points in the rates of copper precipitation and nickel extraction indicated a second reaction stage. The rate of nickel extraction increased after the inflection point. Heazlewoodite leaching by acid was the prominent mechanism of nickel extraction in this stage (reaction 2-4) and millerite was formed. In some tests, godlevskite was also formed as an intermediate when heazlewoodite was leached. (reaction 2-5). Nickel leaching came to a stop or slowed down substantially when most of the nickel had been converted from heazlewoodite to phases with lower Ni:S ratios. Only 60 % - 70 % nickel was readily leachable.



The rate of copper precipitation during the second period was found to depend on the combination of available nickel in the matte and the available acid. If the acid concentration was high (pH < 2) and nickel leaching had reached a maximum, chalcocite leaching took place, leading to the formation of digenite or covellite. If the heazlewoodite was depleted, but the solution is not sufficiently acidic for copper leaching to take place, copper precipitation came to a stop. If heazlewoodite is available and the solution is not excessively acidic, copper will be removed from solution during the second period at a faster rate than during the initial reaction period.

If the solution pH rose sufficiently, iron precipitation occurred, accompanied by the formation of bornite and to a lesser extent troilite and pentlandite. In some instances it was found that the rate of copper precipitation increased when iron precipitation occurred and that a large quantity of bornite was formed at these times.

SEM images show that the nickel and copper contained in the alloy phase were leached out during oxidative tests, but that the PGE-containing core of the alloy phase remained intact. Ruthenium, rhodium and iridium, which were present in the starting leach solutions, were precipitated from solution completely when leaching low iron mattes. During the initial stage of copper precipitation, existing chalcocite grains in the matte increased in size. During later stages, copper was integrated into the heazlewoodite matrix, to produce a Ni-Cu-S structure with variable ratios of nickel to copper. The formation of a Ni-Cu-S structure is probably dependent on acid leaching of nickel-sulphide and alloy phases, which increases the particle porosity.

## 6.2 Non-oxidative leaching mechanism for low iron matte

In non-oxidative tests, nickel extraction could be accounted for by electrochemical exchange reactions between copper from solution and nickel in the matte. Nickel extraction primarily took place due to reaction 2-12, in which dissolved copper exchanges with nickel from the alloy and heazlewoodite phases to form chalcocite. The reaction rate is probably linked to the availability of alloy in the matte and slows down as the alloy content decreases. It was found that the reaction rate slowed down when 24 – 33 % of the alloy in the matte had been leached out. Precipitation of ruthenium, rhodium and iridium followed kinetics similar to copper precipitation kinetics, with an initial fast period followed by a slower second period. Leaching of nickel by acid was limited and millerite was not formed in non-oxidative tests.

SEM-images and EDS analysis of selected phases show that the heazlewoodite matrix remained intact during non-oxidative tests. Alloy grains also remained mostly intact, although examples could be found where the grain boundaries became less distinct and the alloy dissolved and blended into surrounding phases. Copper that was deposited during tests was not added to alloy or heazlewoodite phases, but led to the growth of existing chalcocite grains. The formation of metallic copper in non-oxidative tests was limited, unless the stirring rate was low, in which case metallic copper deposits were formed on the outside of particles.

## 6.3 Effect of solid/liquid ratio

### *Effect of solid/liquid ratio on non-oxidative leaching*

In non-oxidative tests, copper removal was enhanced by higher solids/liquid ratios. The extents of metal extractions were not significantly influenced by the solids/liquid ratio.

### ***Effect of solid/liquid ratio on oxidative leaching***

Under oxidative conditions, nickel and cobalt extraction rates decreased when the solid/liquid ratio was increased from 80 g/L to 150 g/L and to 540 g/L. This can be attributed to the lower ratio of acid to metals. The effect was less noticeable when the initial acid concentration was high (74 g/L rather than 37 g/L) and the solution was highly agitated (1100 rpm rather than 500 rpm).

Acid consumption increased with an increase in solids content, which meant that the pH increased to a higher value. This led to iron precipitation in tests with higher solids contents.

Less copper was precipitated at lower solids contents. The decreased copper precipitation in tests with lower solids contents can be attributed to a decrease in reaction area, the quicker leaching of heazlewoodite and copper leaching, which is caused by the excess acid available at lower solids contents.

Vydysh et al. (2005) found that copper removal decreased dramatically if the ratio of nickel in the matte to the initial copper in solution was smaller than 4.53 g Ni / g Cu<sup>2+</sup>. The decrease was attributed to a kinetic, rather than thermodynamic effect. Results from the current work show that complete copper removal was possible at a Ni/Cu<sup>2+</sup> ratio of 3.65 g/g (solids content of 150 g/L), but only if the initial acid concentration was low (37 g/L). If the Ni/Cu<sup>2+</sup> ratio was lowered further (solids content of 80 g / L), or the initial acid concentration was increased (74 g/L) copper precipitation became limited. This interaction demonstrates the difficulty of determining an exact solids/liquid ratio which will ensure copper precipitation.



## 6.4 Effect of initial acid concentration

### *Effect of initial acid concentration on non-oxidative leaching*

The effect of the initial acid concentration on metal leaching kinetics during non-oxidative tests was very limited. A higher initial acid concentration might lead to a slightly faster copper precipitation reaction due to activation of matte particles, but the effect of initial acid concentration on copper precipitation kinetics can probably be regarded as negligible.

### *Effect of initial acid concentration on oxidative leaching*

In oxidative tests with a solids content of 150 g/L, the rates and extents of nickel, cobalt and iron extractions were higher with an initial acid concentration of 74 g/L than in a test with an initial acid concentration of 37 g/L. In 80 g solids/L tests, an excess of acid was available and changes in the initial acid concentration did not have a significant effect on metal extractions.

Less copper was precipitated in tests with a high initial acid concentration. In high acid tests (16, 17 and 20), copper was leached to varying degrees after an initial copper precipitation period. Provis et al. (2003) suggested that chalcocite would not be leached while heazlewoodite is present in the matte. The current work shows that the acid concentration should also be taken into consideration. Results suggest that chalcocite will not be leached if the solution pH is above 2, even after more than 95 % of the heazlewoodite had been leached from the matte.

Iron precipitation from solution is more likely to occur if the initial acid concentration is low and the pH rises sufficiently for iron precipitation to occur.

## 6.5 Effect of initial copper concentration

### *Effect of the initial copper concentration on non-oxidative leaching*

The effect of the initial copper concentration on metal extractions and on copper precipitation was very limited. Although it is suspected that the effect of initial copper concentration is negligible, it is suggested that the effect of initial copper concentration should be investigated at a higher solids content than used in the current work, where copper precipitation will take place to a larger extent. In this work, the effect of the initial copper concentration was investigated at a solids content of 80 g/L.

### *Effect of initial copper concentration on oxidative leaching*

Results from the current work suggested that a high initial copper concentration might promote copper leaching and consequently lead to less copper being precipitated from solution. This can probably be explained by decreased diffusivity of copper ions in the boundary layer with increased copper concentration that leads to lower rates of nickel-copper exchange reactions.

The effect of the initial copper concentration on metal extractions was limited. Cobalt extraction was higher if the initial copper concentration was high. Results from tests with a solids/liquid ratios of 80 g/L suggest that decreasing the copper concentration from 40 g/L to 20 g/L might lead to higher nickel extraction rates. It is recommended that tests should be carried out at higher solids content, where copper precipitation takes place more readily, to confirm the effect of initial copper concentration on nickel leaching.

The reaction products from copper and iron precipitation in 80 g solids / L tests depended on the initial copper concentration. At an initial copper concentration of 20 g/L, chalcocite and bornite were formed, while covellite, antlerite and malachite were formed at an initial copper concentration of 40 g/L.

## 6.6 Effect of the Fe-endpoint

### *Effect of the Fe-endpoint on non-oxidative leaching*

High iron mattes were distinguished from low iron mattes by a lower alloy content (only 2.1 % in the starting material) and the presence of pentlandite and bornite phases. SEM images show that the iron in high iron matte was distributed throughout the material.

Under non-oxidative conditions, the rate of copper-nickel exchange reactions were faster when a high iron matte was leached. Consequently, more nickel was extracted and more copper was removed from solution in a high iron test than in a low iron test. The number of moles iron and cobalt extracted were more when a high iron matte was leached than when a low iron matte was leached. Extraction of iron from the heazlewoodite matrix might have facilitated nickel extraction in high iron tests.

An initial fast stage and a second slower stage of copper precipitation could be discerned when low iron mattes were leached, but when a high iron matte was leached, this distinction could not be made. Chalcocite was formed as copper precipitation product in low and high iron mattes. When leaching low iron mattes, reaction 2-12 best describes the metathesis reaction. The change in reaction kinetics in a low iron test can probably be associated with the alloy content of the matte. In high iron mattes, very little alloy (2.1 %) is present in the starting material. Millerite and godlevskite formed to a much larger extent in high iron than in low iron tests, indicating that metathesis took place due to reaction 2-9, or a similar reaction in which godlevskite is formed, when leaching high iron mattes.

Bornite and pentlandite phases, which were abundant in high iron mattes, did not react readily.

### ***Effect of the Fe-endpoint on oxidative leaching***

Under oxidative conditions, the initial rate of copper removal was faster in high iron tests than in low iron tests. This can probably be attributed to the same mechanism that caused an increase in the rate of copper precipitation in non-oxidative tests.

Nickel, cobalt and iron extractions were lower when leaching a high iron matte. In the case of nickel, the lower extraction can probably be attributed to the lack of alloy in the high iron matte, the amount of nickel locked up in the relatively inert pentlandite phase and the formation of godlevskite as leaching product when heazlewoodite is leached (rather than millerite, which formed in low iron tests). It is also possible that leaching of alloy phases from low iron mattes led to a more porous structure and consequently to faster leaching rates. In the case of cobalt and iron, the mass percentage extractions from high iron mattes were lower because the concentration in the starting material was higher.

The pH did not increase above a value of 2 in high iron tests and the excess availability of acid led to copper being leached after the initial fast copper precipitation stage. The behaviour of dissolved ruthenium, rhodium and iridium were similar to the behaviour of dissolved copper and precipitation of these elements stopped when copper leaching started in high iron tests. Consequently, less PGEs were precipitated in high iron tests than in low iron tests.

## **6.7 Effect of stirring**

### ***Effect of stirring on non-oxidative leaching***

The effect of stirring rate on reaction kinetics was used to determine possible rate controlling mechanisms. The stirring rate was increased from 500 rpm to 1100 rpm.

In low iron tests, cobalt extraction, as well as nickel extraction (together with copper precipitation), were chemical reaction or pore diffusion controlled (rate not influenced

by stirring). Iron extraction was controlled by boundary layer diffusion (increases with increased stirring).

In high iron tests, cobalt and iron extraction were found not to be influenced by stirring rate, indicating either pore diffusion or chemical reaction controlled kinetics. A metathesis reaction was responsible for nickel extraction and copper precipitation. The rate of the metathesis reaction increased with stirring rate (leading to higher nickel extractions and increased rates of copper precipitation), indicating kinetics controlled by boundary layer diffusion.

### ***Effect of stirring on oxidative leaching***

When leaching a low iron matte, the initial rates of nickel, cobalt and copper leaching increased with stirring rate, indicating that kinetics were controlled by the rate of gas/liquid mass transfer (oxygen dissolution) or boundary layer diffusion. The rate of copper precipitation was faster at higher stirring rates, indicating boundary layer diffusion control. The increased rate of copper precipitation at high stirring rates might also be attributed to an increase in particle porosity and effective surface area due to increased nickel leaching at higher stirring rates. Iron extraction did not increase when the stirring rate was increased, indicating chemically controlled kinetics or pore diffusion controlled kinetics. In a test with 150 g solids/L, the rate of iron extraction decreased when the stirring rate was increased, because more acid was consumed by nickel and cobalt leaching reactions. Due to the quicker pH rise, iron precipitation occurred at 1100 rpm, but not at 500 rpm.

When leaching high iron mattes under oxidative conditions, an increase in stirring rate from 500 rpm to 1100 rpm led to the following effects: the rates of nickel extraction, iron extraction and copper leaching increased, suggesting boundary layer diffusion or gas/liquid mass transfer controlled processes. The initial rate of copper precipitation and the rate of cobalt extraction were unaffected, suggesting chemically controlled kinetics.

## 6.8 Effect of oxygen

### *The effect of oxygen on non-oxidative leaching*

In the presence of oxygen, the rates and extents of nickel and cobalt extraction increased. Iron extraction rates also increased, unless the pH in the oxidative test rose sufficiently for iron precipitation to occur, in which case iron extractions were lower in oxidative tests.

It was found that the availability of oxygen did not have a significant influence on the initial period of copper removal. However, the rate of copper removal during the second period was faster under oxidative conditions, unless the solution was sufficiently acidic for copper leaching to take place. The higher copper precipitation rate in oxidative tests can probably be attributed to the fact that acid-leaching reactions caused particle disintegration to create a more porous structure and to increase the available reaction area. More ruthenium, rhodium and iridium were precipitated under oxidative conditions than under non-oxidative conditions.

## 6.9 Copper precipitation kinetics

### *Non-oxidative kinetics*

It was found that a first order kinetic model gave a reasonable fit to experimental data from non-oxidative tests ( $R^2 > 0.8$ ). Deviation from first order kinetics occurred because copper precipitation slowed down with time in most tests. In some tests, a shrinking core model with ash layer diffusion gave a better fit than a first order kinetic model, because the shrinking core model could account for the decrease in the copper precipitation reaction rate. However, for the majority of tests, first order kinetics described the data better than a shrinking core model. The most accurate description of experimental data was obtained by considering the precipitation reaction as a two stage process, in which both stages follow first order kinetics, with different rate constants.

Analysis of data from four tests showed that the rate constant for the first reaction period was in the range of  $3.2 \times 10^{-6}$  cm/s to  $5.5 \times 10^{-6}$  cm/s. Analysis of data from two tests, in which a distinct second period occurred, showed that the rate constant for the second reaction period was in the range  $6.9 \times 10^{-7}$  cm/s to  $1.0 \times 10^{-6}$  cm/s. In tests where two distinct reaction stages occurred, the rate constant for the initial reaction period was approximately five times larger than for the second reaction period.

### ***Oxidative kinetics***

Under oxidative conditions, two stages of copper precipitation could be distinguished. A first order rate equation could be fitted to each stage. The reaction rate was faster in the second stage than the first reaction stage. Analysis of data from three tests gave initial reaction rate constant as  $2.4 \times 10^{-6}$  cm/s to  $4.3 \times 10^{-6}$  cm / s and the rate constant for the second reaction period as  $3.1 \times 10^{-6}$  cm/s to  $7.0 \times 10^{-6}$  cm/s.

## Chapter 7 Recommendations

---

- The effect of the recycle stream, which is employed in industry to recycle solids from the last leach tank to the first leach tank, is not well-understood. In this work, copper precipitation kinetics were found to be highly dependent on the solids / liquid ratio. However, fresh matte was added to the mixture to obtain higher densities. It is not known what the effect of increasing the density by means of adding recycled solids will be. This can be determined by adding leach residue to fresh matte during batch tests.
- The current work suggests that only 60 – 70 % of the nickel in the matte is readily leachable. In industry, much higher yields are obtained (>85 %). It is suspected that the increased yield in industry can be attributed to increased residence time, which is the consequence of recycling a portion of solids from the last leach tank. In order to improve understanding of the recycle, it is suggested that the residue from the final leach tank should be characterised and that leach tests can be carried out to determine the reactivity of this material.
- Due to the nature of batch tests, the acid and  $\text{Cu}^{2+}$  concentrations employed in this work were much higher than used in industry. Industry conditions might be approximated more closely by controlling the pH and carrying out batch tests at a constant pH. This approach can improve understanding of the effects of  $\text{Cu}^{2+}$  and acid concentrations and also give a better understanding of how the changing character of the solid particle influences leaching kinetics, while the leach conditions remain fairly constant.
- The Fe-endpoint was found to have a significant influence on the leaching behaviour of the matte. It is recommended that the Fe-endpoint should be carefully controlled and that high Fe-matte should be avoided, to ensure that copper and PGE precipitation occurs in the first stage leach. If a high Fe-matte is leached, the oxygen feed to the first stage leached might be adjusted to a lower flowrate to assist copper and PGE precipitation.



- In this work, mattes containing <1.05 % Fe, or 5.72 % Fe were leached. It is recommended that test work on mattes with intermediate Fe-levels should also be leached as part of a sensitivity analysis.
- Literature suggests that high iron concentrations in solution can cause slow consumption of acid (similar to the effect of high iron concentrations in the matte) (Symmens et al., 1976). The effect of iron in solution was not explicitly investigated in this work, but might be a topic for further investigation.

## Chapter 8      References

---

Annamalai, V., Murr, L.E., 1979, Influence of deposit morphology on the kinetics of copper cementation on pure iron, *Hydrometallurgy*, 4, 57 – 82

Burkin, A.R., 2001, *Chemical Hydrometallurgy: Theory and Principles*. Imperial College Press, London. 414p.

Cawthorn, R.G., 1999, The platinum and palladium resources of the Bushveld Complex, *South African Journal of Science*, 95, Nov/Dec 1999, 481 - 489

Demirkiran, N.A., Ekmekyapar, A., Künkül, A., Baysar., A., 2007. A kinetic study of copper cementation with zinc in aqueous solutions. *International Journal of Mineral Processing*, 82, 80-85

Dönmez, B., Sevim, F., Saraç, H., 1999. A kinetic study of the cementation of copper from sulphate solutions onto a rotating aluminium disc. *Hydrometallurgy*, 53, 145-154

Dorfling, C., Akdogan, G., Bradshaw, S.M., Eksteen, J.J., 2011, Determination of the relative leaching kinetics of Cu, Rh, Ru and Ir during the sulphuric acid pressure leaching of leach residue derived from Ni-Cu converter matte enriched in platinum group metals, *Minerals engineering*, Vol 24, Issue 6, pp 583 - 589

Dutrizac, J.E., MacDonald, R.J.C., 1973, The effect of some impurities on the rate of chalcopyrite dissolution. *Canadian Metallurgical Quarterly*, 12(4), 409-420

Dutrizac, J.E., MacDonald, R.J.C., 1974, The kinetics of dissolution of covellite in acidified ferric sulphate solutions. *Canadian Metallurgical Quarterly*, 13, 423-433

Dutrizac, J.E., The kinetics of dissolution of Chalcopyrite in Ferric Ion media, *Metallurgical Transactions B*, Volume 9B, September 1978, 431 - 439

Dutrizac, J.E., Chen, T.,T. 1987, A mineralogical study of the phases formed during the  $\text{CuSO}_4\text{-H}_2\text{SO}_4\text{-O}_2$  leaching of nickel-copper matte, *Canadian metallurgical quarterly*, Vol. 26, No. 4, 265-276

Dutrizac, J.E., and Chen, T.T., 1995, The Leaching of Galena in Ferric Sulfate Media, *Metallurgical and Materials Transactions B*, 1995, 219 - 227

Fogler, H.S., 1998, *Elements of Chemical Reaction Engineering*, 4<sup>th</sup> Ed. Pearson Education Inc., New Jersey

Füglerberg, S., Hultholm, S.-E., Rosenback, L., Holohan, T. 1995., Development of the Hartley Platinum leaching process, *Hydrometallurgy*, 39, 1-10

Gbor, P.K., Ahmed, I.B., and Jia, C.Q., 2000. Behaviour of Co and Ni during aqueous sulphur dioxide leaching of nickel smelter slag. *Hydrometallurgy*, 57, 13-22

Grewal, I., Dreisinger, D.B., Krueger, D., Tyroler, P.M., Krause, E., Nissen, N.C. 1992, Total oxidative leaching of  $\text{Cu}_2\text{S}$ -containing residue at INCO Ltd.'s copper refinery: laboratory studies on the reaction pathways, *Hydrometallurgy*, 29, 319-333

Hayes, P.C., 2003. *Process Principles in Minerals and Materials Production*, 3rd Ed. Hayes Publishing, QLD, Australia.

Herreros, O., Quiroz, R., Hernández, M.C., Viñals, J., 2002, Dissolution kinetics of enargite in dilute  $\text{Cl}_2/\text{Cl}^-$  media, *Hydrometallurgy*, 64, 153 - 160

Hine, 1985, *Electrode processes and electrochemical engineering*, Plenum press, New York

Hiskey, J.B., Wadsworth, M.E., 1975, Galvanic conversion of chalcopyrite, *Metallurgical & materials transactions B*, Vol 6B, 183-190

Hiskey, J.B., Wadsworth, M.E., Electrochemical Processes in the leaching of metal sulphides and oxides. In: (2<sup>nd</sup> ed.), *Process and Fundamental Considerations of*

*Selected Hydrometallurgical Systems 303*, Society of Mining Engineers of AIMjE, New York, (1981)

Hofirek, Z., Kerfoot, D.G.E., 1992. The chemistry of the nickel-copper matte leach and its application to process control and optimisation, *Hydrometallurgy*, 29, 357-381

Holmes, P.R., Crundwell, F.K., 1995, Kinetic aspects of galvanic interactions between minerals during dissolution, *Hydrometallurgy*, 39, 353-375

Karavasteva, M., 2005, Kinetics and deposit morphology of copper cementation onto zinc, iron and aluminium, *Hydrometallurgy*, 76, (2005) 149 - 152

King, J.A., Burkin, A.R., Ferreira, R.C.H., Leaching chalcocite by acidic ferric chloride solutions. In: A.R. Burkin (Editor), *Leaching and reduction in hydrometallurgy*, Institute of Mining and Metallurgy., London (1975) pp. 36-45

Knuutila, K., Hultholm, S., Saxen, B., Rosenback, L., 1997. New nickel process increasing production at Outokumpu harjavalta Metals Oy, Finland. *ALTA Nickel/Cobalt Pressure Leaching and Hydrometallurgy Forum*, Perth. W. Australia

Lamya, R.M., Lorenzen, L., 2005. A study of factors influencing the kinetics of copper cementation during atmospheric leaching of converter matte. *Journal of SAIMM*, January, pp 21-27

Lamya, R.M., Lorenzen, L., 2006. Atmospheric acid leaching of nickel-copper matte from Impala Platinum Refineries. *Journal of SAIMM*, Vol. 106, 385-395

Lamya, R.M., 2007, *A fundamental evaluation of the atmospheric pre-leaching section of the nickel-copper matte treatment process*. PhD Dissertation, University of Stellenbosch, South Africa

Levenspiel, 1972, *Chemical reaction engineering*, 3rd Ed, John Wiley & Sons, Inc.

- Linge, H.G., 1976, Reactivity comparison of Australian chalcopyrite concentrates in acidified ferric solution, *Hydrometallurgy*, 2, 219-233
- Llanos, Z.R., Queneau, P.B., Rickard, R.S., 1974. Atmospheric leaching of matte at the Port Nickel Refinery, CIM bulletin, Vol 67, 74-81
- Mackinnon, D.J., Ingraham, T.R., 1970. Canadian Metallurgical Quarterly 9 (3), 443.
- Mackinnon, D.J., 1974, Recovery of copper by cementation on nickel powder, *Canadian Metallurgical Quarterly*, 13, 473 – 477
- Mao, M.H., Peters, E., 1983, Acid pressure leaching of chalcocite. In: K. Osseo-Asare & J.D. Miller (Editors), *Hydrometallurgy Research, Development and Plant Practice*. TMS/AIME, Warrendale Pa, USA, pp 243-260
- Muir, D.M., Ho, E., 1996, Composition and electrochemistry of Nickel Matte: Implications for Matte Leaching and Refining in Acid Solution, *Conference Series – Australian Institute of Mining and Metallurgy*, 291 - 297
- Muir, D.M., Ho, E., 2006, Process review and electrochemistry of nickel sulphides and nickel mattes in acidic sulphate and chloride media, *Mineral Processing and Extractive Metallurgy (Trans. Inst. Min Metall. C)*, Vol 115, No 2, 57 - 65
- Mulak, W., 1987, The catalytic action of cupric and ferric ions in nitric acid leaching of Ni<sub>3</sub>S<sub>2</sub>, *Hydrometallurgy*, 17, 201-214
- Nell, J., 2004, Melting of platinum group metal concentrates in South Africa, *Journal of SAIMM*, Vol. 104, No. 7, August, 423 - 428
- Pawlek, F., 1969, Research in pressure leaching, *Journal of SAIMM.*, Vol. 69, No. 12, 632–654.

Peters, E., 1984, Electrochemical mechanisms for decomposing sulphide minerals, in: P.E. Richardson, S.Srinivasan, R. Woods \_Eds., *Electrochemistry in Mineral and Metal processing, Proceedings of the International Symposium*, The Electrochemical Society, 343–361.

Plasket, R.P., Romanchuk, S., 1978. Recovery of nickel and copper from high-grade matte at Impala Platinum by the Sherrit Process, *Hydrometallurgy*, 3, 135-151

Provis, J.L., van Deventer, J.S.J., Rademan, J.A.M., Lorenzen, L., 2003. A kinetic model for the acid-oxygen pressure leaching of Ni-Cu matte, *Hydrometallurgy*, 70, 83-99

Rademan, J.A.M., 1995, *The simulation of a transient leaching circuit*, PhD Dissertation, University of Stellenbosch, South Africa, 423 pp.

Rademan, J.A.M., Lorenzen, L., van Deventer, J.S.J., 1999. The leaching characteristics of Ni-Cu matte in the acid-oxygen pressure leach process at Impala Platinum, *Hydrometallurgy*, 52, 231-252

Roine, A., 2002. *Outokumpu HSC Chemistry 5.11*. Outokumpu research Oy Pori, Finland

Sahoo, P.K., Rao, K.S., 1982. Cementation of copper from complex sulphide leach liquor. *Hydrometallurgy*, 8, 223-229

Sato, T., Lawson, F., 1983, Differential leaching of some lead smelter slags with sulphurous acid and oxygen, *Hydrometallurgy*, 11, 371 - 388

Sędzimir, J.A., 2002, Precipitation of metals by metals (cementation) – kinetics, equilibria, *Hydrometallurgy*, 64, 2002, 161 - 167

Sohn, H.Y., Wadsworth, 1979, M.E., *Rate processes of extractive metallurgy*, Plenum Press, New York

Steenekamp, N., Dunn, G.M., 1999, Operations of and improvements to the Lonrho Platinum Base Metal Refinery, EPD congress

Symens, R.D., Queneau, P.B., Chou, E.C., Clark, F.F., 1979, Leaching of iron-containing copper-nickel matte at atmospheric pressure, *Canadian Metallurgical Quarterly*, Vol. 18, 145 - 153

Thomas, G., Ingraham, T.R. , MacDonald, R.J.C., 1967, Kinetics of dissolution of synthetic digenite and chalcocite in aqueous acidic ferric sulphate solutions., *Canadian metallurgical Quarterly*, 6, pp 281-292

Thyse, E., Akdogan, G., Eksteen, J.J., 2010, The effect of changes in the iron-endpoint during Peirce Smith converting on PGE-containing nickel converter matte mineralization, *Minerals Engineering*, doi:10.1016/j.mineng.2010.09.022

Thyse, E., Akdogan, G., Taskinen, P., Eksteen, J.J., 2011, The distribution of metallic elements in granulated nickel converter matte phases, *South African Pyrometallurgy*, March

Van Schalkwyk, R.F., Eksteen, J.J., Petersen, J., Thyse, E.L., Akdogan, G., 2011, An experimental evaluation of the leaching kinetics of PGM-containing Ni-Cu-Fe-S Peirce Smith converter matte, under atmospheric leaching conditions, *Minerals Engineering*, Vol 24, Issue 6, pp 583 - 589

Vydysh, A.V., Naftal, M.N., Petrov, A.F., Batsunova, I.V., 2005, Specific features of chemical interactions in atmospheric purification of a nickel-cobalt solution to remove copper, *Russian Journal of Applied Chemistry*, Vol. 78, No. 5, 691-697

## Appendix A: Experimental procedure

---

### Preparation for leaching test

1. Calculate correct amounts of reactants to be used. Check that required amounts of matte, leaching solution, sulphuric acid, coppersulphate pentahydrate crystals, nitrogen and oxygen are available.
2. The following equipment should be clean and available for use:
  - Pipette for sampling
  - Buchner filters, flasks and filter paper to collect solid samples
  - Syringes and 2  $\mu\text{m}$  syringe filters to clean liquid samples
  - Pressure filter and 180 mm filter paper for filtering final slurry
  - Nitric acid solution for diluting samples
  - Sample bottles
3. The pH probe should be calibrated at a temperature of 45 °C (or the temperature at which samples will be held in the water bath), using pH buffers 1.68, 4 and 7.
4. The accuracy of the redox probe should be checked before each test, using standard solutions with known mV readings.

### Startup (takes approx 1.5 hrs)

5. Remove the vessel from the setup by releasing the handles at the top, while supporting the base plate, and then slowly lowering the plate with the vessel.
6. Fill the vessel with the required amount of liquid reactants.
7. Weigh the filled reactor.
8. Replace the vessel in position. Use the handles on the base plate to lift the reactor and to secure the vessel to the cover. Fasten the vessel to the cover by using 8mm wingnuts.
9. Fasten the heating band around the vessel.
10. Make sure that the temperature probe is inserted and making contact with the leach solution and that the temperature setpoint is ambient, before



connecting the heating element to the power supply and switching on the control system.

11. Turn on the stirrer motor at a low speed.
12. Turn on the cooling water at the tap, to supply water to the condenser. Keep the valve leading to the cooling coil closed.
13. Turn on the nitrogen or oxygen supply and adjust to the required flowrate.
14. Change the temperature setpoint to the required temperature.
15. When the final temperature is reached, open the valve to the cooling coil. Adjust the flowrate to the cooling coil to the required rate by using the valve. (150 mL/min is suggested)
16. Wait 15 minutes for the control system to stabilise
17. Measure pH and take one sample according to the sampling procedure described below.
18. Load powdered solids through the port in the reactor cover, using a sufficiently wide funnel. Replace plug in port after solids had been loaded.
19. Note down the time taken to load the reactor. The test will start once the reactor is loaded.
20. Slowly increase the stirring rate to the required setting.

### **Sampling procedure**

1. 15 mL samples will be taken with a pipette after 0, 5, 10, 15, 30, 60, 90, 120, 150, 180 and 240 minutes. If splashing through the sampling port is a problem, the stirring rate might temporarily need to be turned down.
2. If the solids content in the test is high, or if solid samples need to be collected, samples will be filtered using a Buchner filter. The filter cake will be washed with distilled water and dried at approximately 45 °C. The filtrate will be cleaned further, using 2 µm syringe filters, to produce clear liquid samples.
3. The pH and redox potential of liquid samples will be measured and documented at the start of the test, after 10 minutes and 30 minutes, and at 30 minute intervals after that. To prevent damage, pH and redox probes should not be directly inserted into the high temperature slurry in the reactor.
4. Liquid samples will be diluted with a HNO<sub>3</sub> solution to prevent precipitation.

5. All sample containers must be clearly marked.

### Test completion

6. Switch off the heater (using the switch on the control box).
7. Close off gas supply
8. Increase cooling water flowrate.
9. Remove heater carefully, using heat protective gloves.
10. Secure the reactor vessel in place by using the handles on the base plate, while loosening the wingnuts. Then carefully remove the vessel from the setup.
11. Weigh the reactor vessel with contents. Compare the initial mass with final mass to determine the mass evaporation.
12. Use a pressure filter to filter the slurry. Wash the filter cake with distilled water and collect solid samples for analysis.
13. Clean all equipment.

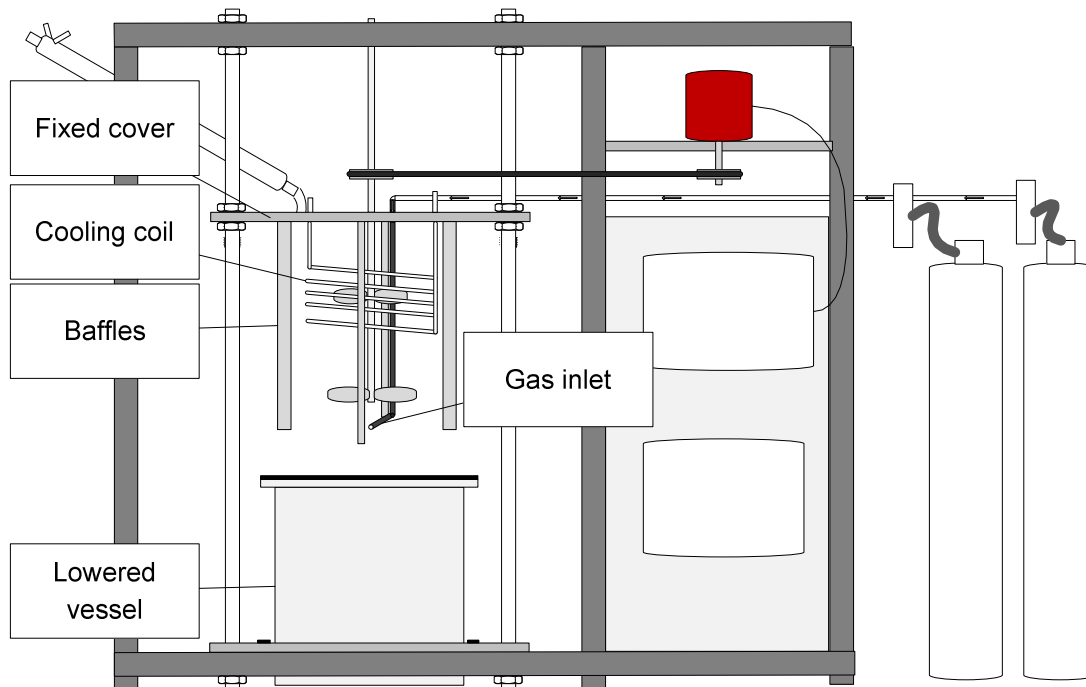


**Figure G.1 Setup when reactor vessel is lowered.**

## Appendix B: Calculations

---

In section 4.2 and 4.3, graphs were presented depicting the percentages copper, cobalt and iron extracted as a function of time.

The percentages extracted were calculated by utilising Equation 0-1.

$$\text{Percentage extraction}_{x,t} = \frac{C_{x,t}V_t + \sum_0^t C_{S_{x,t}}V_s - C_{x,0}V_0}{M_x m_{solids}} \times 100 \% \quad \text{Equation 0-1}$$

Where

$C_{x,t}$  = Concentration of element 'x' in solution at time 't' [g/L]

$C_{x,0}$  = Concentration of element 'x' in solution at the start of the test [g/L]

$C_{S_{x,t}}$  = the concentration of element 'x' in a sample taken at time 't' [g/L]

$V_t$  = the total solution volume at time 't' [L]

$V_0$  = The total solution volume at the start of the tests [L]

$V_s$  = Sample volume [L]

Changes in the solution volume due to sampling and evaporation were taken into account by incorporating equations Equation 0-2 and Equation 0-3.

$$V_t = V_0 - \sum_0^t V_s - \frac{r_{evap}t}{\rho_{water}} \quad \text{Equation 0-2}$$

Where

$r_{evap}$  = the rate of evaporation in [g/s]

$\rho_w$  = density of water [1000 g/L]

The rate of evaporation was determined from a mass balance for each test, as shown in Equation 0-3.

$$r_{evap} = \frac{M_i - M_f - \sum M_s}{t_f} \quad \text{Equation 0-3}$$

$M_i$  = Initial mass of solid and liquid mixture

$M_f$  = final mass of solid and liquid mixture

$\sum M_s$  = Mass of all samples

$t_f$  = total test time

The initial and final masses of the mixture were determined by weighing the reactor with its contents before and after tests. An average sample size of 15 mL was used together with the pulp density of the mixture for each test to determine the mass of a sample.

The mass of mineral phases present at different times in the test was calculated by means of a mass balance. Solution data was used to determine the mass of solids:

$$m_{solids,t} = m_{solids,0} - \sum m_{extracted,t} \quad \text{Equation 0-4}$$

Where

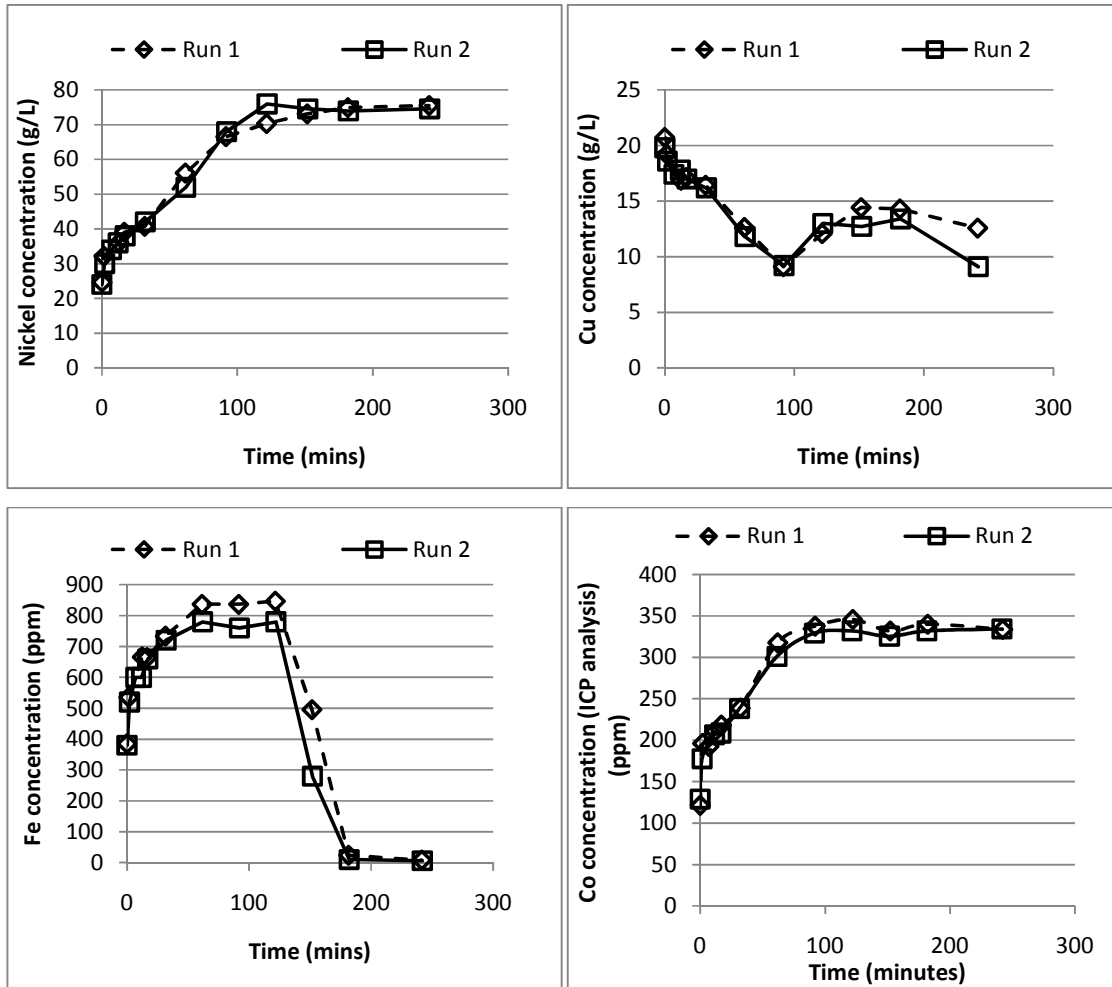
$m_{extracted,t}$  = mass of an element which has been extracted at time  $t$ .

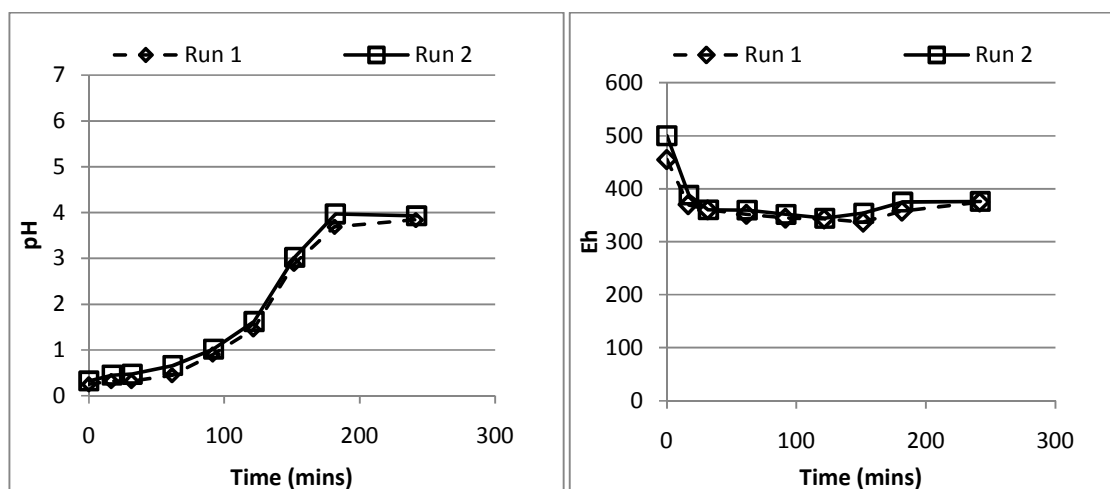
$$m_{extracted,t} = C_{x,t}V_t + \sum_0^t C_{s,x,t}V_s - C_{x,0}V_0 \quad \text{Equation 0-5}$$

When the mass of solids at a specific time was determined, the mass of each mineral phase could be determined by multiplying the relative abundance of the phase (from XRD data), with the total mass.

## Appendix C: Repeatability

Test 20 was carried out twice. Dissolved metal concentrations, solution pH and redox potential and the mineralogy of samples taken in the two tests are compared below and show very good agreement.





### Mineralogical composition of samples taken from Run 1

Sample time		0	30	60	120	180	240
Mineral	Mass %						
Ni-Cu	Ni-Cu	19.7	9.04	2.49	0	0	0
Heazlewoodite	Ni <sub>3</sub> S <sub>2</sub>	51.9	50.24	31.52	4.04	2.04	2.83
Godlevskite	Ni <sub>7</sub> S <sub>6</sub>	0	0	0	0.00	15.10	9.11
Millerite	NiS	0	1.32	13.64	41.67	25.65	23.64
Polydymite	Ni <sub>3</sub> S <sub>4</sub>	0	0	0	0	8.01	4.61
Pentlandite	(NiFe) <sub>9</sub> S <sub>8</sub>	0	0.46	1.96	4.30	4.05	4.83
Troilite	FeS	0.9	1.13	0.51	0.93	1.79	2.66
Magnetite	Fe <sub>3</sub> O <sub>4</sub>	1.5	0.81	1.43	1.51	0	0
Bornite	Cu <sub>5</sub> FeS <sub>4</sub>	0	0	0	0	14.50	24.41
Chalcocite	Cu <sub>2</sub> S	26.0	37.01	48.46	0.00	28.87	27.91
Digenite	Cu <sub>9</sub> S <sub>5</sub>		0	0	47.54	0	0

### Mineralogical composition of samples taken from Run 2

Sample time		0	30	60	120	180	240
Mineral	Mass %						
Ni-Cu	Ni-Cu	19.7	9.95	2.65	0.00	10.58	0
Heazlewoodite	Ni <sub>3</sub> S <sub>2</sub>	51.9	50.30	33.80	3.38	0	0
Godlevskite	Ni <sub>7</sub> S <sub>6</sub>	0	0	0	13.21	12.79	10.31
Millerite	NiS	0	0.07	11.64	35.50	33.10	24.77
Polydymite	Ni <sub>3</sub> S <sub>4</sub>	0	0	0	0	3.03	4.02
Pentlandite	(NiFe) <sub>9</sub> S <sub>8</sub>	0	0.25	1.33	4.77	5.97	6.07
Troilite	FeS	0.9	1.29	0.60	0.69	2.69	3.47
Magnetite	Fe <sub>3</sub> O <sub>4</sub>	1.5	0	0.62	1.21	0.55	0.00
Bornite	Cu <sub>5</sub> FeS <sub>4</sub>	0	0	0	0	2.52	24.64
Chalcocite	Cu <sub>2</sub> S	26.0	38.12	49.37	0	9.12	26.72
Digenite	Cu <sub>9</sub> S <sub>5</sub>	0	0		41.25	19.65	0

## Appendix D: Comparison of results not given in text

### Content:

D.1 Comparison of results from tests 17 and 18.

D.2 Comparison of results from tests 19 and 24

D.3. Comparison of results from tests 5 and 13

**D.1. Comparison of results from tests 17 and 18. Effect of stirring rate on low density, low iron tests.**

Operating conditions for Tests 17 and 18, which were conducted at low density (80 g solids / L) are given in Table D-1. Results from the two tests are compared in Figure D-1 and Figure D-2.

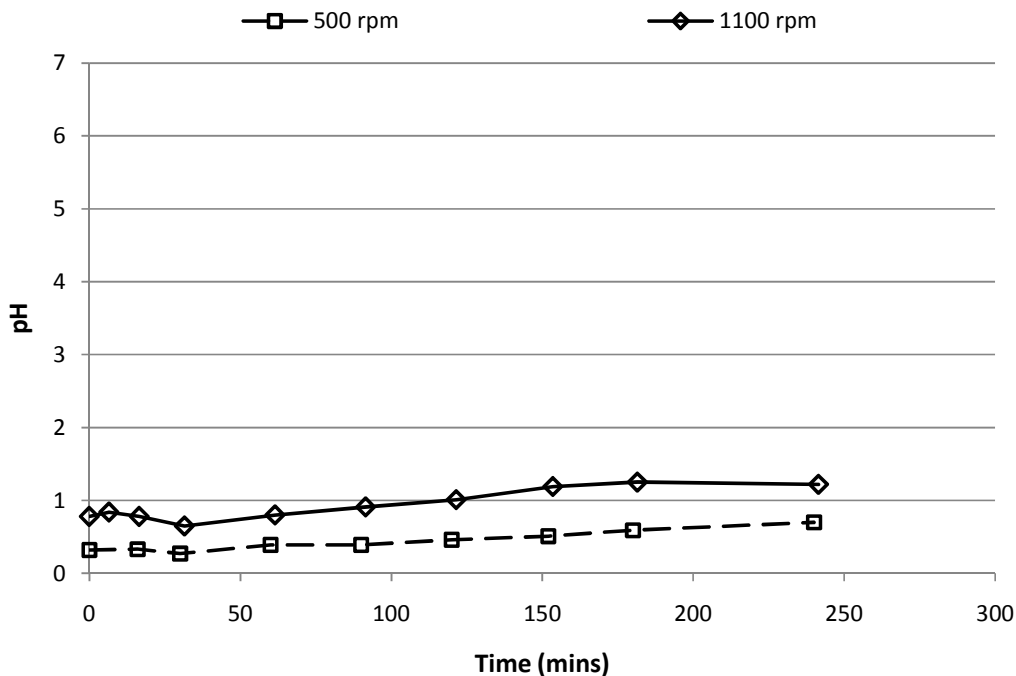


Figure D-1 Comparison of pH changes in tests 17 and 18 (respectively carried out at stirring rates of 1100 rpm and 500 rpm)

Table D-1 Operating conditions for tests 17 and 18

Test	Solids/Liquid [g/L]	Gas	Fe-endpoint [Mass %]	Init. Cu conc [g/L]	Init. Acid conc. [g/L]	Stirring [rpm]
18	80	O <sub>2</sub>	0.83	20	74	500
17	80	O <sub>2</sub>	0.86	20	74	1100

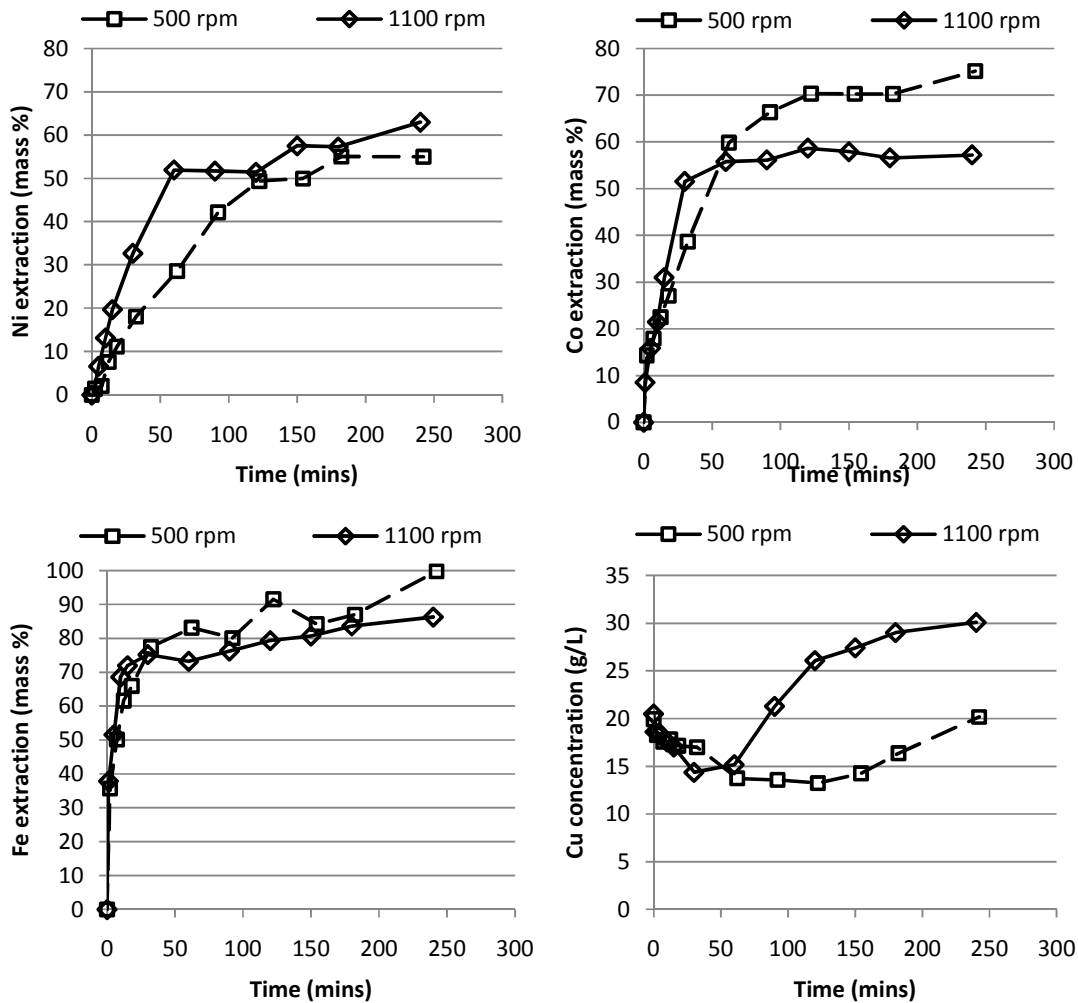


Figure D-2 Comparison of concentration changes in Test 18 (500 rpm) and Test 17 (1100 rpm)

The rate and extent of nickel extraction was higher in the 1100 rpm test (Test 17). Cobalt extraction was faster at 1100 rpm, but a lower final extraction was obtained. Iron behaviour was not significantly influenced by stirring rate. Acid was consumed to a larger extent in the 1100 rpm test.



Faster copper removal rates were obtained in the high stirring test, but copper leaching also started earlier. This might be due to increased gas/liquid mass transfer rates, or possibly due to the quicker dissolution of heazlewoodite, leading to a decreased reaction area for copper removal.

The mineralogy of residues from tests 17 and 18 differed. At a stirring rate of 500 rpm, heazlewoodite leaching led to the formation of godlevskite and millerite, while millerite and polydymite were formed at 1100 rpm. At 500 rpm, copper leaching was limited and the residue contained chalcocite and some digenite. At 1100 rpm, only covellite remained in the residue.

## D.2 Comparison of results from tests 19 and 24: Effect of Fe-endpoint on oxidative leaching

At 500 rpm (tests 19 and 24), the effect of the iron endpoint was less pronounced than at 1100 rpm, but results were consistent with results from Tests 20 and 23. The pH increased at a slower rate in the high iron test (Figure D-3) and the rates and extents of cobalt, nickel and iron extractions were lower (Figure D-4). Copper removal was initially faster for the high iron matte, but came to an end after a shorter period of time.

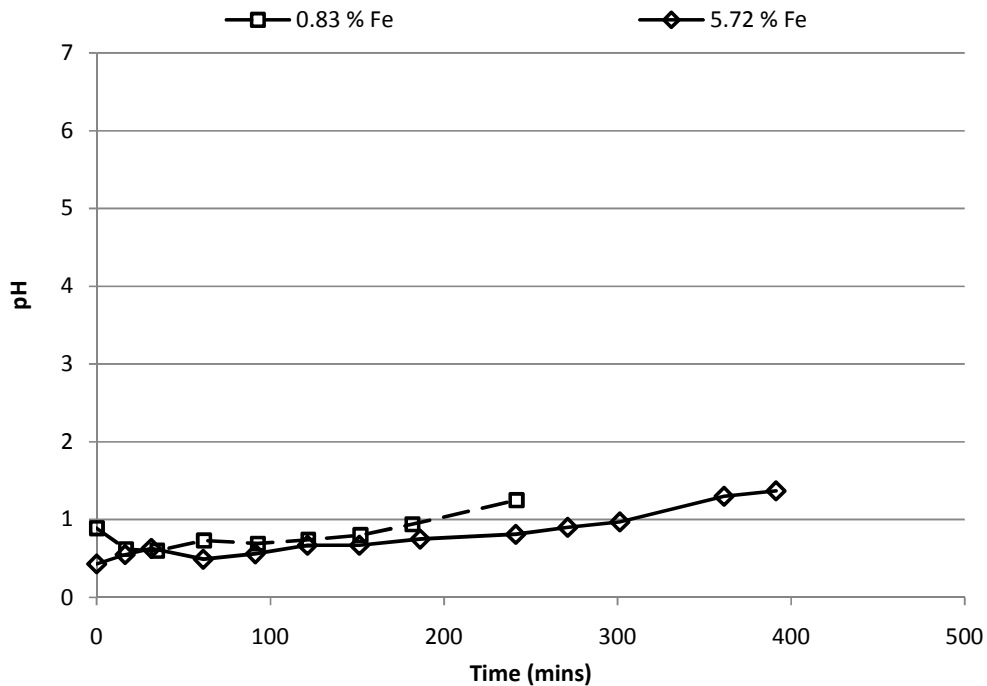


Figure D-3 Comparison of pH changes in test 19 (0.83 % Fe) and test 24 (5.72 % Fe)

Table D-2 Operating conditions for Tests 19 and 24

Test	Solids/Liquid [g/L]	Gas	Fe-endpoint [Mass %]	Init. Cu conc [g/L]	Init. Acid conc. [g/L]	Stirring [rpm]
19	150	O <sub>2</sub>	0.83	20	74	500
24	150	O <sub>2</sub>	5.72	20	74	500

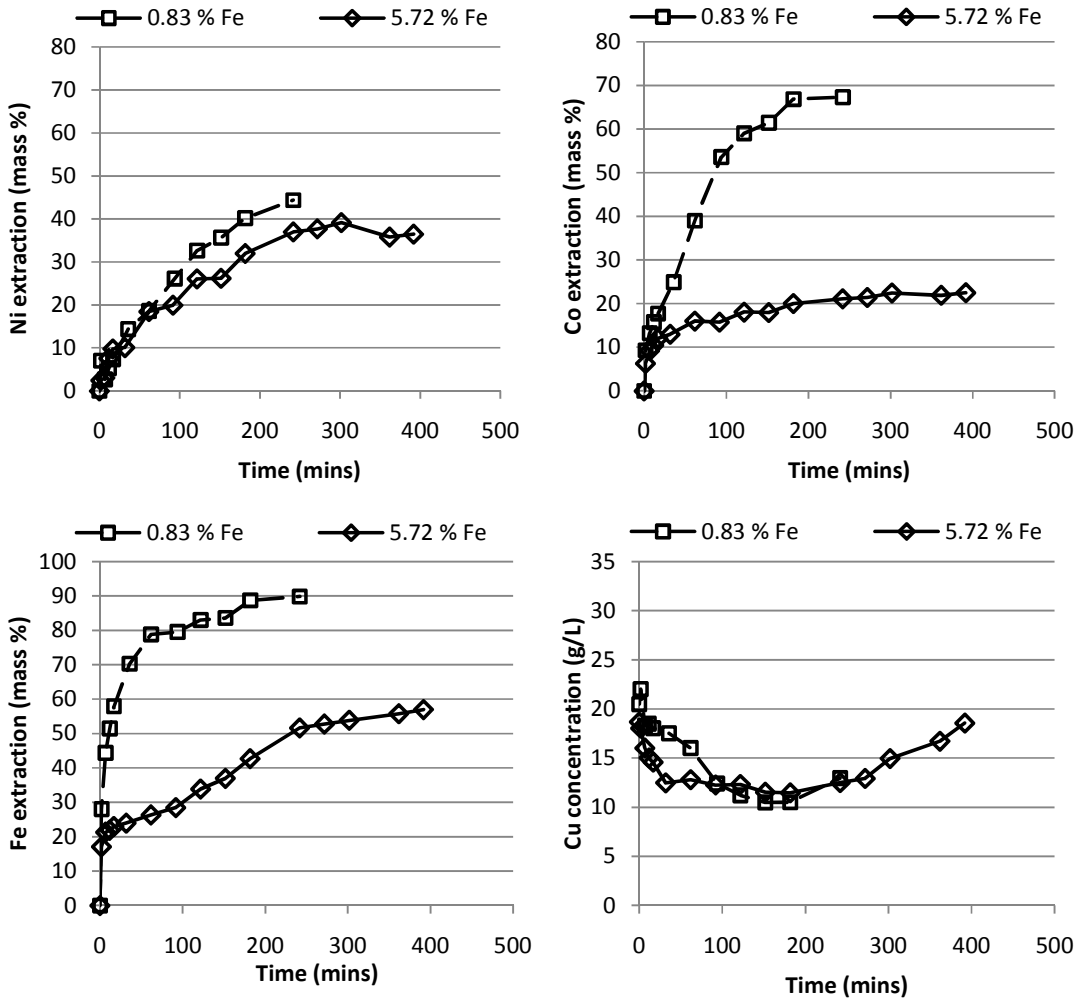


Figure D-4 Comparison of concentration changes for occurring in Test 19 (0.83 % Fe) and Test 24 (5.72 % Fe)

The mineralogy of the matte from test 24 and test 19 are respectively given in Appendix E and Appendix F. The relative abundance of alloy in the matte increased significantly for the first 120 minutes of the high iron test, while it was leached out in the low iron test. Heazlewoodite leaching in the high iron test led to the formation of godlevskite and millerite throughout the test, while godlevskite only took place at a later stage in the low iron test. Polydymite was formed only in the high iron test, but it should be noted that this occurred after 390 minutes, while the low iron test was stopped after 240 minutes. Pentlandite and bornite phases were much more prominent in the high iron matte. Pentlandite leaching took place, but only after 60 minutes. Copper leaching in the high iron test led to covellite formation, while digenite was formed in the low iron test.

### **D.3. Comparison of results from tests 5 and 13: Effect of Fe-endpoint on non-oxidative leaching**

The results from tests 5 and 13 are compared to accompany the discussion in Section 4.3.4, where tests 6 and 12 were compared. The rate of nickel extraction and copper removal were faster when using the high iron matte (Figure D-5). The rate and extent of iron extraction was lower for the high iron matte, although more moles were extracted after 240 minutes (0.216 moles vs 0.073 moles). The same applies to cobalt extraction, where a higher percentage was extracted in the low iron test although a smaller number of moles were extracted (0.015 moles vs 0.016 moles).

Table D-3 Operating conditions for test 5 and test 13

Test	Solids/Liquid [g/L]	Gas	Fe-endpoint [Mass %]	Init. Cu conc [g/L]	Init. Acid conc. [g/L]	Stirring [rpm]
5	150	N <sub>2</sub>	0.83	20	74	500
13	150	N <sub>2</sub>	5.72	20	74	500

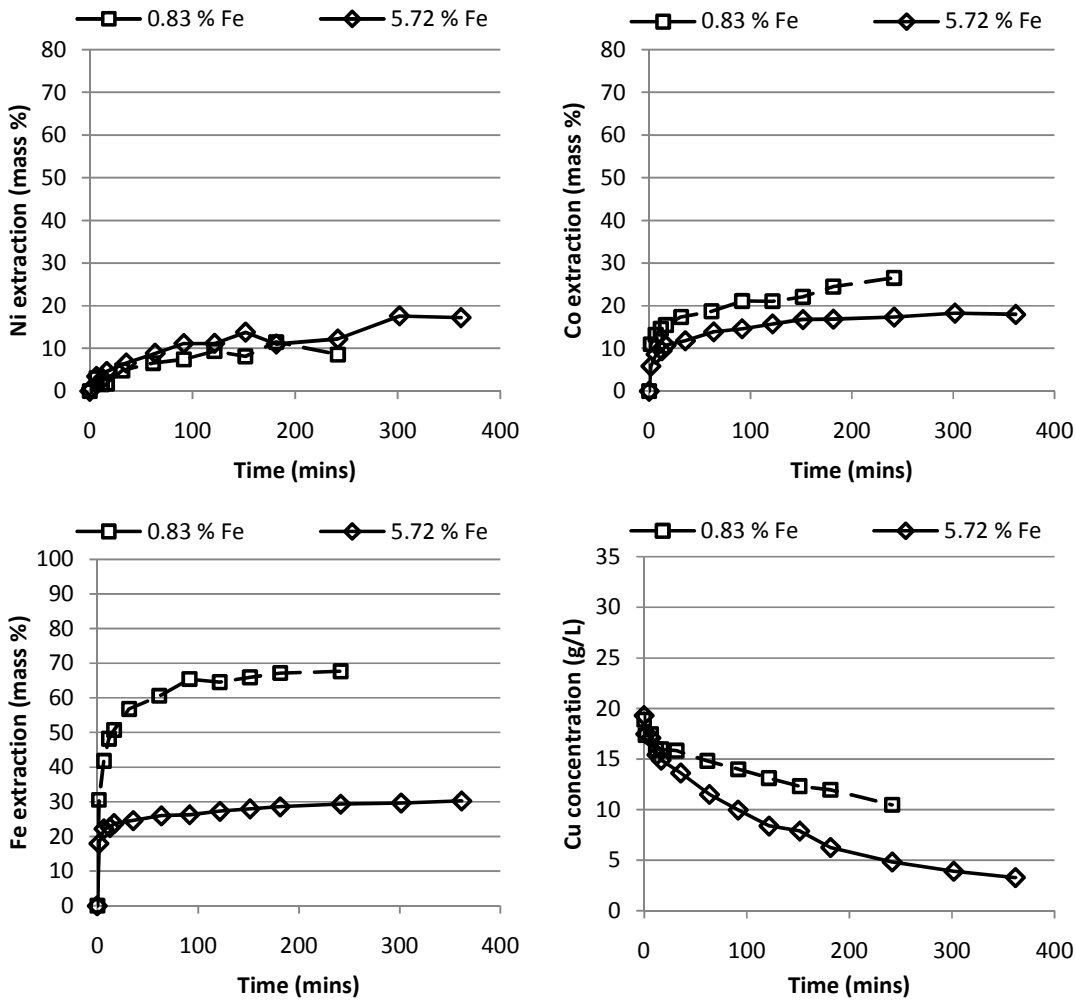


Figure D-5. Comparison of concentration changes in test 5 (0.83 % Fe) and test 13 (5.72 % Fe)

Mineralogical changes for the low stirring rate tests (tests 5 and 13, Given in Appendix E and Appendix F) reflect the same trends that were observed in the high density tests. The change in copper removal rate, from an initial fast stage to a second slower stage, was more prominent in the low iron test than the high iron test. In the low iron test, the alloy and heazlewoodite contents decreased at a fast rate during the first 30 minutes, after which the alloy content did not change and

heazlewoodite decreased slowly. In the high iron test, very little alloy was initially present and heazlewoodite decreased at a steady rate throughout the test. Heazlewoodite was converted to millerite in the low iron test, and to godlveskite and millerite in the high iron test. Chalcocite formation took place in both tests. Bornite and pentlandite were prominent in the high iron test, but were not reactive.

## Appendix E: Experimental data (concentrations, pH & XRD-analyses)

---

### Test 1

Time (mins)	Ni conc (ppm)	Cu conc (ppm)	Fe conc (ppm)	Co conc (ppm)
0	25880.0	36250.0	432.0	163.2
1	26260.0	35180.0	588.0	175.5
5	25940.0	32480.0	680.0	185.3
10	27440.0	34680.0	720.0	195.2
15	27820.0	34980.0	754.0	192.5
30	27680.0	34300.0	806.0	203.6
60	28640.0	33800.0	824.0	208.2
90	28280.0	32640.0	854.0	215.7
120	29640.0	33340.0	864.0	223.9
180	29480.0	33140.0	888.0	231.3
240	29200.0	31260.0	892.0	231.9
270	29860.0	32320.0	1110.0	233.4

Time (mins)	pH
0	1.07
15	0.93
30	1.18
60	0.92
90	1.07
120	0.95
180	1
240	0.96



*Mineralogical changes during test 1.*

Sample time:		0	270
Mineral		Mass %	
Ni-Cu	Ni-Cu	12.3	8.7
Heazlewoodite	Ni <sub>3</sub> S <sub>2</sub>	53.8	51.0
Godlevskite	Ni <sub>7</sub> S <sub>6</sub>	4.4	3.1
Millerite	NiS	-	-
Polydymite	Ni <sub>3</sub> S <sub>4</sub>	-	-
Pentlandite	(NiFe) <sub>9</sub> S <sub>8</sub>	0.7	0.6
Troilite	FeS	0.9	0.8
Magnetite	Fe <sub>3</sub> O <sub>4</sub>	1.2	0.1
Bornite	Cu <sub>5</sub> FeS <sub>4</sub>	-	-
Chalcocite	Cu <sub>2</sub> S	26.6	34.8
Djurleite	Cu <sub>31</sub> S <sub>16</sub>	-	-
Digenite	Cu <sub>9</sub> S <sub>5</sub>	-	-
Covellite	CuS	-	-
Cuprite	Cu <sub>2</sub> O	0.2	0.9
Antlerite	Cu <sub>3</sub> SO <sub>4</sub> (OH) <sub>4</sub>	-	-
Malachite	Cu <sub>2</sub> CO <sub>3</sub> (OH) <sub>2</sub>	-	-

## Test 2

Time (mins)	Ni conc (ppm)	Cu conc (ppm)	Fe conc (ppm)	Co conc (ppm)
0	25140.0	20340.0	446.0	137.8
1	25900.0	18780.0	690.0	167.4
5	25480.0	17040.0	782.0	170.2
10	26320.0	16620.0	826.0	173.8
15	27200.0	17640.0	868.0	176.0
30	27240.0	16620.0	898.0	186.4
60	27700.0	16300.0	936.0	193.2
90	28100.0	15540.0	966.0	193.4
120	28620.0	15520.0	984.0	201.8
180	30340.0	15780.0	998.0	210.8
240	30193.3	14753.3	1003.3	219.2

Time (mins)	pH
0	1.03
1.5	0.99
16.5	1.03
31.5	1.03
61.5	0.88
91.5	0.89
121.5	0.86
181.5	0.96
241.5	0.97

*Mineralogical changes in test 2.*

	<b>Mass %</b>	<b>Matte</b>	<b>240</b>
<b>Ni-Cu</b>	Ni-Cu	12.3	8.8
<b>Heazlewoodite</b>	Ni <sub>3</sub> S <sub>2</sub>	53.8	51.4
<b>Godlevskite</b>	Ni <sub>7</sub> S <sub>6</sub>	4.4	3.2
<b>Millerite</b>	NiS	-	-
<b>Polydymite</b>	Ni <sub>3</sub> S <sub>4</sub>	-	-
<b>Pentlandite</b>	(NiFe) <sub>9</sub> S <sub>8</sub>	0.7	0.4
<b>Troilite</b>	FeS	0.9	0.7
<b>Magnetite</b>	Fe <sub>3</sub> O <sub>4</sub>	1.2	-
<b>Bornite</b>	Cu <sub>5</sub> FeS <sub>4</sub>	-	-
<b>Chalcocite</b>	Cu <sub>2</sub> S	26.6	34.7
<b>Djurleite</b>	Cu <sub>31</sub> S <sub>16</sub>	-	-
<b>Digenite</b>	Cu <sub>9</sub> S <sub>5</sub>	-	-
<b>Covellite</b>	CuS	-	-
<b>Cuprite</b>	Cu <sub>2</sub> O	0.2	0.9
<b>Antlerite</b>	Cu <sub>3</sub> SO <sub>4</sub> (OH) <sub>4</sub>	-	-
<b>Malachite</b>	Cu <sub>2</sub> CO <sub>3</sub> (OH) <sub>2</sub>	-	-

**Test 3**

Time (mins)	Ni conc (ppm)	Cu conc (ppm)	Fe conc (ppm)	Co conc (ppm)
0	25260.0	37900.0	430.0	141.2
2.25	25300.0	35580.0	720.0	174.6
6.25	26860.0	35965.9	808.0	179.2
11.25	25500.0	35060.0	834.0	179.0
16.25	26580.0	33046.6	868.0	184.2
31.25	26520.0	34160.0	886.0	187.0
61.25	27100.0	33840.0	908.0	191.6
91.25	28620.0	34140.0	918.0	192.2
121.25	29430.7	33780.0	924.0	198.2
151.25	29460.0	34460.0	942.0	201.8
181.25	29700.0	34240.0	950.0	204.2
241.25	29260.0	34240.0	950.0	211.2

Time (mins)	pH
0	0.63
1.25	0.56
31.25	0.53
61.25	0.74
91.25	0.7
121.25	0.45
151.25	0.26
181.25	0.25
241.25	0.25

*Mineralogical changes during test 3.*

Sample time:		0	240
Mineral		Mass %	
Ni-Cu	Ni-Cu	12.3	8.1
Heazlewoodite	Ni <sub>3</sub> S <sub>2</sub>	53.8	51.5
Godlevskite	Ni <sub>7</sub> S <sub>6</sub>	4.4	3.0
Millerite	NiS	-	-
Polydymite	Ni <sub>3</sub> S <sub>4</sub>	-	-
Pentlandite	(NiFe) <sub>9</sub> S <sub>8</sub>	0.7	0.5
Troilite	FeS	0.9	0.6
Magnetite	Fe <sub>3</sub> O <sub>4</sub>	1.2	0.1
Bornite	Cu <sub>5</sub> FeS <sub>4</sub>	-	-
Chalcocite	Cu <sub>2</sub> S	26.6	35.4
Djurleite	Cu <sub>31</sub> S <sub>16</sub>	-	-
Digenite	Cu <sub>9</sub> S <sub>5</sub>	-	-
Covellite	CuS	-	-
Cuprite	Cu <sub>2</sub> O	0.2	0.9
Antlerite	Cu <sub>3</sub> SO <sub>4</sub> (OH) <sub>4</sub>	-	-
Malachite	Cu <sub>2</sub> CO <sub>3</sub> (OH) <sub>2</sub>	-	-

**Test 4**

<b>Time (mins)</b>	<b>Ni conc (ppm)</b>	<b>Cu conc (ppm)</b>	<b>Fe conc (ppm)</b>	<b>Co conc (ppm)</b>
0	24860.0	18920.0	402.0	146.0
1.375	26540.0	18480.0	582.0	180.0
6.375	26440.0	17940.0	672.0	192.0
11.375	26960.0	17760.0	698.0	198.0
16.375	27480.0	17580.0	726.0	204.0
31.375	28000.0	17340.0	760.0	208.0
61.375	28680.0	16600.0	788.0	216.0
91.375	28300.0	15900.0	802.0	222.0
121.375	29320.0	15800.0	806.0	224.0
151.375	30120.0	15700.0	806.0	230.0
181.375	30580.0	15380.0	824.0	224.0
241.375	32280.0	15500.0	832.0	240.0

<b>Time (mins)</b>	<b>pH</b>	<b>Eh (mV)</b>
0	0.55	490
16.375	0.6	346
31.375	0.63	343
66.375	0.54	268
91.375	0.43	323
121.375	0.42	240
151.375	0.48	336
181.375	0.53	290.5
241.375	0.47	200.5

*Mineralogical changes during test 4.*

Sample times:		0	240
Mineralogy		Mass %	
Ni-Cu	Ni-Cu	15.4	9.6
Heazlewoodite	Ni <sub>3</sub> S <sub>2</sub>	61.3	50.8
Godlevskite	Ni <sub>7</sub> S <sub>6</sub>	-	-
Millerite	NiS	0	1.5
Polydymite	Ni <sub>3</sub> S <sub>4</sub>	-	-
Pentlandite	(NiFe) <sub>9</sub> S <sub>8</sub>	0.5	0.5
Troilite	FeS		1.7
Magnetite	Fe <sub>3</sub> O <sub>4</sub>	1.4	0.1
Bornite	Cu <sub>5</sub> FeS <sub>4</sub>	-	-
Chalcocite	Cu <sub>2</sub> S	21.5	35.7
Djurleite	Cu <sub>31</sub> S <sub>16</sub>	-	-
Digenite	Cu <sub>9</sub> S <sub>5</sub>	-	-
Covellite	CuS	-	-
Cuprite	Cu <sub>2</sub> O	-	-
Antlerite	Cu <sub>3</sub> SO <sub>4</sub> (OH) <sub>4</sub>	-	-
Malachite	Cu <sub>2</sub> CO <sub>3</sub> (OH) <sub>2</sub>	-	-

**Test 5**

<b>Time (mins)</b>	<b>Ni conc (ppm)</b>	<b>Cu conc (ppm)</b>	<b>Fe conc (ppm)</b>	<b>Co conc (ppm)</b>
0	24660.0	18880.0	400.0	148.0
1.5	24440.0	17360.0	784.0	226.0
6.5	26860.0	17480.0	926.0	242.0
11.5	25820.0	15940.0	1008.0	252.0
16.5	25980.0	15980.0	1040.0	258.0
31.5	28240.0	15820.0	1118.0	272.0
61.5	29560.0	14820.0	1168.0	282.0
91.5	30240.0	14000.0	1232.0	300.0
121.5	31780.0	13120.0	1222.0	300.0
151.5	30860.0	12320.0	1242.0	308.0
181.5	33440.0	11960.0	1260.0	326.0
241.5	31320.0	10480.0	1270.0	342.0

<b>Time (mins)</b>	<b>pH</b>	<b>Eh (mV)</b>
0	0.67	457
15	0.67	180
30	0.6	275
60	0.57	190
90	0.61	222
120	0.65	153.2
150	0.5	225
180	0.44	145
240	0.44	133



## Test 6

Time (mins)	Ni conc (ppm)	Cu conc (ppm)	Fe conc (ppm)	Co conc (ppm)
0	26186.5	20123.4	356.0	154.0
1.75		18215.0	768.1	224.0
6.75	29170.5	16988.1	880.6	228.0
11.75	28917.3	16170.2	936.8	242.0
16.75	29260.9	16033.8	974.2	238.0
31.75	30761.9	15215.9	1067.9	254.0
61.75		13989.1	1049.2	268.0
91.75	32769.3	13443.8	1086.6	282.0
121.75	33366.1	12898.5	1124.1	288.0
151.75		12353.2	1105.4	288.0
181.75	34650.1	12216.9	1161.6	298.0
241.75	34453.0	11399.0	1142.8	298.0

Time (mins)	pH	Eh (mV)
0	0.31	480
15	0.5	285
30	0.46	350
60	0.36	334.8
90	0.35	276
120	0.37	336
150	0.32	207
180	0.36	292
240	0.61	250

**Test 7**

Time (mins)	Ni conc (ppm)	Cu conc (ppm)	Fe conc (ppm)	Co conc (ppm)
0	24380.0	19460.0	424.0	151.0
1.83	26700.0	18360.0	882.0	266.0
6.83	28280.0	16960.0	1068.0	285.2
12.83	29490.0	16890.0	1182.0	309.6
16.83	30540.0	16240.0	1192.0	293.4
31.83	29680.0	14800.0	1228.0	300.8
61.83	32200.0	13960.0	1270.0	316.0
91.83	32360.0	13000.0	1300.0	316.4
121.83	32540.0	12140.0	1350.0	316.0
151.83	33260.0	11980.0	1330.0	331.2
181.83	33500.0	11280.0	1320.0	329.6
241.83	34980.0	9360.0	1398.0	337.0
306.83	0.0	10300.0	1370.0	345.8

Time (mins)	pH	Eh (mV)
0	0.75	495
11.83	0.8	236
30.83	0.89	245
60.83	0.82	248
90.83	0.84	233
120.83	0.81	222
150.83	0.82	227
180.83	0.85	230
240.83	0.87	246.3
305.83	0.86	237

*Mineralogical changes during test 7*

		<b>0</b>	<b>15</b>	<b>100</b>	<b>180</b>	<b>300</b>
<b>Mineral</b>		<b>Mass %</b>				
<b>Ni-Cu</b>	Ni-Cu	12.4	9.2	8.9	7.6	6.7
<b>Heazlewoodite</b>	Ni <sub>3</sub> S <sub>2</sub>	53.8	53.9	52.4	49.9	48.4
<b>Godlevskite</b>	Ni <sub>7</sub> S <sub>6</sub>	4.4	4.0	3.8	3.2	3.0
<b>Millerite</b>	NiS	0	0.6	0	2.2	2.0
<b>Polydymite</b>	Ni <sub>3</sub> S <sub>4</sub>	-	-	-	-	-
<b>Pentlandite</b>	(NiFe) <sub>9</sub> S <sub>8</sub>	0.7	0.2	0	0.2	0.3
<b>Troilite</b>	FeS	0.9	0.6	0.6	0.8	0.8
<b>Magnetite</b>	Fe <sub>3</sub> O <sub>4</sub>	1.2	0	0	0	0
<b>Bornite</b>	Cu <sub>5</sub> FeS <sub>4</sub>	0	0.6	0.6	0.8	0.7
<b>Chalcocite</b>	Cu <sub>2</sub> S	26.8	31.0	33.9	35.4	38.1
<b>Djurleite</b>	Cu <sub>31</sub> S <sub>16</sub>	-	-	-	-	-
<b>Digenite</b>	Cu <sub>9</sub> S <sub>5</sub>	-	-	-	-	-
<b>Covellite</b>	CuS	-	-	-	-	-
<b>Cuprite</b>	Cu <sub>2</sub> O	0.2	0	0	0	0
<b>Antlerite</b>	Cu <sub>3</sub> SO <sub>4</sub> (OH) <sub>4</sub>	-	-	-	-	-
<b>Malachite</b>	Cu <sub>2</sub> CO <sub>3</sub> (OH) <sub>2</sub>	-	-	-	-	-

## Test 8

Time (mins)	Ni (ppm)	Cu (ppm)	Fe (ppm)	Co conc (ppm)
0	72159.0	9951.0	1824.0	771.0
3.5	85666.0	18.0	2644.0	1056.0
8.5	84099.0	6.0	2022.0	945.0
13.5	87885.0	6.0	2028.0	1002.0
26	86559.0	0.0	1992.0	1011.0
33.5	84054.0	27.0	1914.0	990.0
93.5	78564.0	27.0	1746.0	978.0
123.5	82920.0	9.0	1800.0	1053.0
183.5	87015.0	15.0	1866.0	1146.0
243.5	79749.0	0.0	1674.0	1095.0

Time (mins)	pH
0	2.5
8.5	5.29
13.5	5.27
18.5	5.36
33.5	5.25
63.5	5.37
93.5	5.35
123.5	5.25
183.5	5.29
243.5	5.2

**Test 9**

Time (mins)	Ni conc (ppm)	Cu conc (ppm)	Fe conc (ppm)	Co conc (ppm)
0	23620.0	19340.0	478.0	135.0
2.75	36760.0	14460.0	2698.0	640.0
7.75	38900.0	11060.0	2846.0	656.0
12.75	38120.0	8400.0	2988.0	678.0
17.75	41680.0	7260.0	3002.0	696.0
32.75	43840.0	4020.0	3180.0	722.0
62.75	44730.0	60.0	3435.0	759.0
77.75	52760.0	0.0	3452.0	778.0

Time (mins)	pH	Eh (mV)
0	0.52	470
10	0.9	329
15	0.9	
30	0.92	259
35	0.92	
60	1.01	305.6
65	0.94	302.7

**Test 10**

Time (mins)	Ni conc (ppm)	Cu conc (ppm)	Fe conc (ppm)	Co conc (ppm)
0	78832.0	18910.0	1804.0	744.0
2.15	82216.0	15300.0	2914.0	948.0
7.15	84746.0	10360.0	3106.0	992.0
12.15	94210.0	7742.0	3362.0	1096.0
17.15	94176.0	5900.0	3400.0	1082.0
32.15	95800.0	2160.0	3552.0	1116.0
62.15	97586.0	54.0	3420.0	1128.0
92.15	97906.0	80.0	3492.0	1150.0
122.15	94616.0	60.0	3456.0	1142.0
182.15	96116.0	70.0	3458.0	1198.0
242.15	97840.0	176.0	3380.0	1248.0

Time (mins)	pH
0	1.22
2.15	2.41
7.15	2.27
12.15	2.34
22.15	2.38
32.15	2.67
42.15	2.96
52.15	4.2
62.15	4.66
72.15	5.1
92.15	5.12
102.15	5.21
137.15	5.34
182.15	5.2
212.15	5.25
242.15	5.22

**Test 11**

Time (mins)	Ni conc (ppm)	Cu conc (ppm)	Fe conc (ppm)	Co conc (ppm)
0	24780.0	20680.0	826.0	143.8
9.5	59340.0	7240.0	7562.0	1210.0
14.5	58780.0	7260.0	7376.0	1202.0
19.5	62560.0	4540.0	7690.0	1254.0
34.5	64640.0	1800.0	7890.0	1288.0
64.5	70620.0	20.0	8110.0	1344.0
94.5	72720.0	0.0	8078.0	1356.0
124.5	75080.0	0.0	8392.0	1488.0
154.5	75060.0	100.0	8420.0	1526.0
184.5	78080.0	0.0	8628.0	1566.0
244.5	78360.0	0.0	8884.0	1676.0
304.5	79660.0	40.0	9138.0	1756.0

Time (mins)	pH	Eh (mV)
0	0	426
9.5	0.01	313.5
19.5	0.13	306.3
34.5	0.13	307.3
64.5	0.38	276.2
94.5	0.85	
124.5	1.14	290.4
156.6	1.03	262.8
184.5	1.06	280.2
244.5	1.05	286.4
304.5	1.24	284.4

**Test 12**

<b>Time (mins)</b>	<b>Ni conc (ppm)</b>	<b>Cu conc (ppm)</b>	<b>Fe conc (ppm)</b>	<b>Co conc (ppm)</b>
0	22980.0	19300.0	430.0	138.0
1.75	26740.0	16520.0	2388.0	244.0
6.75	28940.0	15280.0	2502.0	262.0
12.75	29940.0	14180.0	2556.0	282.0
16.75	31900.0	13260.0	2750.0	314.0
33.75	33120.0	10480.0	2786.0	320.0
61.75	35000.0	8120.0	2784.0	326.0
91.75	35840.0	6460.0	2892.0	334.0
122.75	37780.0	5340.0	2936.0	346.0
151.75	37860.0	4260.0	3062.0	356.0
181.75	39980.0	3360.0	3092.0	360.0
241.75	41060.0	1960.0	3162.0	352.0
306.75	42380.0	820.0	3262.0	362.0

<b>Time (mins)</b>	<b>pH</b>	<b>Eh (mV)</b>
0	0.26	469
10	0.34	351
32	0.43	
60	0.58	331.5
90	0.37	311
121	0.72	322
150	0.39	313
180	0.36	309.5
240	0.35	314
300	0.36	310



**Test 13**

Time (mins)	Ni conc (ppm)	Cu conc (ppm)	Fe conc (ppm)	Co conc (ppm)
0	24800.0	19300.0	402.0	136.4
1.65	25220.0	17480.0	1954.0	204.6
6.65	27100.0	17080.0	2322.0	236.8
12.65	26780.0	15420.0	2356.0	246.8
16.65	27900.0	14900.0	2456.0	261.8
35.65	29280.0	13620.0	2534.0	274.8
63.65	30880.0	11500.0	2660.0	300.0
91.65	32500.0	9960.0	2694.0	309.2
121.65	32600.0	8380.0	2788.0	323.6
151.65	34460.0	7880.0	2856.0	336.6
181.65	32620.0	6260.0	2916.0	338.4
241.65	33580.0	4820.0	3000.0	345.8
301.65	37540.0	3900.0	3044.0	358.8
361.65	37420.0	3280.0	3112.0	356.6

Time (mins)	pH	Eh
0	0.3	493
11	0.39	359
15	0.31	
34	0.41	327
62	0.36	323
90	0.36	327
120	0.38	329
150	0.46	322
180	0.4	318
240	0.41	315
300	0.38	313
360	0.39	307

Sample time:		0	15	30	60	120	180	300	360
Mineral		Mass %							
<b>Ni-Cu</b>	Ni-Cu	2.1	1.7	1.4	0.9	0.7	1.1	0.6	0.9
<b>Heazlewoodite</b>	Ni <sub>3</sub> S <sub>2</sub>	57.0	50.8	48.5	46.4	43.7	41.4	36.6	33.8
<b>Godlevskite</b>	Ni <sub>7</sub> S <sub>6</sub>	2.9	3.5	4.1	5.7	5.4	5.2	8.4	11.4
<b>Millerite</b>	NiS	0.4	0.9	0.5	0	1.7	0.8	3.0	3.6
<b>Polydymite</b>	Ni <sub>3</sub> S <sub>4</sub>	-	-	-	-	-	-	-	-
<b>Pentlandite</b>	(NiFe) <sub>9</sub> S <sub>8</sub>	9.1	11.7	10.8	10.6	10.4	10.6	10.0	9.3
<b>Troilite</b>	FeS	0.5	0.4	0.1	0	0	0.1	0	0
<b>Magnetite</b>	Fe <sub>3</sub> O <sub>4</sub>	1.1	0.2	0.2	0.1	0	0.0	0	0
<b>Bornite</b>	Cu <sub>5</sub> FeS <sub>4</sub>	11.7	12.0	11.6	11.5	12.4	11.9	12.0	11.3
<b>Chalcocite</b>	Cu <sub>2</sub> S	15.3	18.8	22.7	24.8	25.8	29.0	29.4	29.6
<b>Djurleite</b>	Cu <sub>31</sub> S <sub>16</sub>	-	-	-	-	-	-	-	-
<b>Digenite</b>	Cu <sub>9</sub> S <sub>5</sub>	-	-	-	-	-	-	-	-
<b>Covellite</b>	CuS	-	-	-	-	-	-	-	-
<b>Cuprite</b>	Cu <sub>2</sub> O	-	-	-	-	-	-	-	-
<b>Antlerite</b>	Cu <sub>3</sub> SO <sub>4</sub> (OH) <sub>4</sub>	-	-	-	-	-	-	-	-
<b>Malachite</b>	Cu <sub>2</sub> CO <sub>3</sub> (OH) <sub>2</sub>	-	-	-	-	-	-	-	-

### Test 14

Time	Ni conc. (ppm)	Cu conc. (ppm)	Fe conc (ppm)	Co conc (ppm)
0	24040.8	37680.0	376.1	146.6
1	27070.8	34980.0	624.5	188.8
5	29462.8	34460.0	763.6	240.4
10	30359.8	33780.0	803.3	247.9
15	30777.5	33620.0	862.9	303.5
30	36342.6	29880.0	882.8	362.1
60	44543.8	31940.0	932.5	377.5
90	45715.4	31680.0	773.5	392.8
120	46008.3	31340.0	217.2	394.8
155	48897.8	31520.0	68.2	435.0
180	47472.8	30000.0	58.3	392.3
240	48937.3	28920.0	48.3	392.0

Time (mins)	pH	T (ph)
0	0.93	60
5	0.94	54.8
15	1.09	56.1
31	1.28	54.2
60	1.88	56.3
91	3.1	55.5
121	3.57	53.6
150	3.66	54.9
180	3.61	55.4
240	3.58	51.7

**Test 15**

Time	Ni conc (ppm)	Cu conc. (ppm)	Fe conc (ppm)	Co conc. (ppm)
0	24040.8	37680.0	376.1	146.6
1	27070.8	34980.0	624.5	188.8
5	29462.8	34460.0	763.6	240.4
10	30359.8	33780.0	803.3	247.9
15	30777.5	33620.0	862.9	303.5
30	36342.6	29880.0	882.8	362.1
60	44543.8	31940.0	932.5	377.5
90	45715.4	31680.0	773.5	392.8
120	46008.3	31340.0	217.2	394.8
155	48897.8	31520.0	68.2	435.0
180	47472.8	30000.0	58.3	392.3
240	48937.3	28920.0	48.3	392.0

Time	pH	Sample temp (°C)
0	0.93	60
5	0.94	54.8
15	1.09	56.1
31	1.28	54.2
60	1.88	56.3
91	3.1	55.5
121	3.57	53.6
150	3.66	54.9
180	3.61	55.4
240	3.58	51.7

## **Test 16**

<b>Time</b>	<b>Ni conc (ppm)</b>	<b>Cu conc (ppm)</b>	<b>Fe conc (ppm)</b>	<b>Co conc (ppm)</b>
0	22869.2	35960.0	380.0	135.4
1	26966.5	35580.0	720.0	191.8
5	26969.8	34460.0	760.0	216.8
10	28434.3	33280.0	820.0	237.7
15	30484.6	33140.0	900.0	274.6
30	36928.4	31160.0	900.0	366.8
60	43079.3	35180.0	960.0	381.1
90	43372.2	39300.0	940.0	380.7
120	46594.1	43500.0	980.0	382.5
150	45422.5	44720.0	980.0	393.6
180	45715.4	44420.0	960.0	384.8
240	46301.2	44120.0	940.0	387.3

<b>Time</b>	<b>pH</b>	<b>Sample Temp (°C)</b>	<b>eh (Mv)</b>
<b>0</b>	0.69	57.4	490.3
15	0.68	46.8	329
30	0.82	42.9	351.4
60	0.6	39.4	357.2
90			383.3
120	1.17	48.7	404
150	0.91	40.5	408.8
180	1.11	41.1	412.2
240	1	43.3	417.5

**Test 17**

<b>Time</b>	<b>Ni conc (ppm)</b>	<b>Cu conc. (ppm)</b>	<b>Fe conc. (ppm)</b>	<b>Co conc. (ppm)</b>
0	26620.0	20497.4	363.0	143.0
1	26620.0	18634.0	629.2	176.0
5	29282.0	18367.8	726.0	204.6
10	31944.0	17569.2	847.0	226.6
15	34606.0	17036.8	871.2	264.0
30	39930.0	14374.8	895.4	345.4
60	47916.0	15173.4	883.3	363.0
90	47916.0	21296.0	907.5	365.2
120	47916.0	26087.6	931.7	376.2
150	50578.0	27418.6	943.8	374.0
180	50578.0	29015.8	968.0	369.6
240	53240.0	30080.6	992.2	374.0

<b>Time</b>	<b>pH</b>	<b>Sample Temp (°C)</b>
<b>0</b>	0.78	54.8
6	0.84	55.9
16	0.78	56
31	0.65	55.3
61	0.8	55.2
91	0.91	55.6
121	1.01	53.3
153	1.19	56.2
181	1.25	56.3
241	1.22	54.8

**Test 18**

Time (mins)	Nickel conc (ppm)	Cu conc (ppm)	Fe conc (ppm)	Co conc (ppm)
0	26960.0	19940.0	356.3	140.0
2.25	27520.0	18300.0	602.7	196.0
7.25	27760.0	17560.0	703.1	210.0
12.25	29960.0	17820.0	783.3	228.0
18.25	31380.0	17160.0	813.4	246.0
32.25	34140.0	17000.0	893.7	292.0
62.25	38360.0	13740.0	933.8	376.0
92.25	43820.0	13580.0	912.6	402.0
122.25	46740.0	13240.0	994.0	418.0
154.25	47000.0	14260.0	942.4	418.0
182.25	49080.0	16380.0	962.3	418.0
242.25	49080.0	20180.0	1054.2	438.0

Time (mins)	pH	Sample Temp (°C)	eh (Mv)
0	0.32	46	500
18.25	0.33	42.3	391
32.25	0.27	43	365
62.25	0.39	44.2	366
92.25	0.39	44.4	357
122.25	0.46	44	352
154.25	0.51	42.3	341
182.25	0.59	43.6	351
242.25	0.7	43.3	346.1

*Mineralogical changes during test 18.*

Sample time:		0	240
Mineral		Mass %	
<b>Ni-Cu</b>	Ni-Cu	15.4	0
<b>Heazlewoodite</b>	Ni <sub>3</sub> S <sub>2</sub>	61.3	2.6
<b>Godlevskite</b>	Ni <sub>7</sub> S <sub>6</sub>	0	16.0
<b>Millerite</b>	NiS	0	41.2
<b>Polydymite</b>	Ni <sub>3</sub> S <sub>4</sub>	-	-
<b>Pentlandite</b>	(NiFe) <sub>9</sub> S <sub>8</sub>	0.5	0
<b>Troilite</b>	FeS	0	3.2
<b>Magnetite</b>	Fe <sub>3</sub> O <sub>4</sub>	1.4	1.2
<b>Bornite</b>	Cu <sub>5</sub> FeS <sub>4</sub>	-	-
<b>Chalcocite</b>	Cu <sub>2</sub> S	21.5	25.4
<b>Djurleite</b>	Cu <sub>31</sub> S <sub>16</sub>	-	-
<b>Digenite</b>	Cu <sub>9</sub> S <sub>5</sub>	0	10.6
<b>Covellite</b>	CuS	-	-
<b>Cuprite</b>	Cu <sub>2</sub> O	-	-
<b>Antlerite</b>	Cu <sub>3</sub> SO <sub>4</sub> (OH) <sub>4</sub>	-	-
<b>Malachite</b>	Cu <sub>2</sub> CO <sub>3</sub> (OH) <sub>2</sub>	-	-



**Test 19**

Time (mins)	Ni conc (ppm)	Cu conc (ppm)	Fe conc (ppm)	Co conc (ppm)
0	26460.0	20480.0	444.0	156.0
1.83	31580.0	22020.0	796.0	222.0
6.83	28400.0	18280.0	1002.0	250.0
11.83	30300.0	18500.0	1092.0	268.0
16.83	31840.0	18040.0	1174.0	282.0
35.83	37020.0	17520.0	1332.0	334.0
61.83	40160.0	16020.0	1442.0	436.0
93.83	45780.0	12400.0	1452.0	542.0
121.83	50660.0	11220.0	1498.0	582.0
151.83	52960.0	10480.0	1506.0	600.0
181.83	56420.0	10500.0	1574.0	640.0
241.83	59640.0	12960.0	1590.0	644.0

Time (mins)	pH	Sample Temp (°C)	eh (Mv)
0	0.89	46.5	461
16.83	0.62	41.8	365
34.83	0.6	42	370
61.83	0.73	43.1	347
92.83	0.69	41.5	347
121.83	0.74	43	330
151.83	0.8	42.5	329
181.83	0.94	43	332.8
241.83	1.25	43	332

## **Test 20**

<b>Time (mins)</b>	<b>Ni conc (ppm)</b>	<b>Cu conc (ppm)</b>	<b>Fe conc (ppm)</b>	<b>Co conc (ppm)</b>
0	24000.0	19800.0	380.0	140.0
2	30000.0	18600.0	520.0	220.0
7	34000.0	17400.0	600.0	200.0
12	36000.0	17800.0	600.0	240.0
17	38000.0	17000.0	660.0	260.0
32	42000.0	16200.0	720.0	300.0
62	52000.0	11800.0	780.0	360.0
92	68000.0	9200.0	760.0	380.0
122	76000.0	13000.0	780.0	380.0
152	74573.3	12732.0	280.0	380.0
182	74000.0	13400.0	10.0	380.0
242	74573.3	9094.3	6.0	380.0

<b>Time (mins)</b>	<b>pH</b>	<b>Eh (mV)</b>
0	0.32	500
17	0.45	388
32	0.47	360
62	0.66	359.5
92	1.02	351.8
122	1.62	344.4
152	3.02	353.7
182	3.97	375
242	3.93	376

## Test 21

Time (mins)	Ni conc (ppm)	Cu conc (ppm)	Fe conc (ppm)	Co conc (ppm)
0	24300.0	19100.0	202.0	144.4
1.5	27100.0	18740.0	260.0	187.0
6.5	27840.0	17100.0	270.0	195.6
11.5	30040.0	16640.0	284.0	204.6
16.5	33540.0	16500.0	302.0	216.6
31.5	38040.0	16060.0	315.0	238.6
61.5	43300.0	14160.0	320.0	274.0
91.5	54020.0	4580.0	75.0	319.6
121.5	55000.0	0.0	13.0	319.6
151.5	59100.0	0.0	12.0	318.2

Time (mins)	pH	Eh (mV)
0	0.79	454
10	0.98	261
30	1.17	330
60	2.14	329
90	4.03	330
120	6.23	330
150	6.46	238

**Test 22**

<b>Time</b>	<b>Ni conc (ppm)</b>	<b>Cu conc (ppm)</b>	<b>Fe conc (ppm)</b>	<b>Co conc (ppm)</b>
0	23840.0	18600.0	398.0	150.0
2	38160.0	14420.0	2714.0	626.0
7	43940.0	11320.0	3128.0	678.0
13	46600.0	8600.0	3112.0	718.0
17	49920.0	7380.0	3282.0	748.0
32	55920.0	4060.0	3422.0	804.0
62	66980.0	880.0	3618.0	888.0
92	71580.0	240.0	3699.0	999.0
122	75440.0	180.0	1644.0	1202.0
152	74730.0	90.0	927.0	1254.0
182	82590.0	0.0	21.0	1257.0
242	79620.0	0.0	15.0	879.0

<b>Time (mins)</b>	<b>pH</b>	<b>Eh (mV)</b>
0	0.32	500
10	0.67	
31	0.93	332.2
60	1.22	317
90	2.99	290
120	3.86	270
145	4.00	281.5
180	6.26	193
240	6.36	181

**Test 23**

Time (mins)	Ni conc (ppm)	Cu conc (ppm)	Fe conc (ppm)	Co conc (ppm)
0	24860.0	18280.0	390.0	136.0
1.83	26380.0	15400.0	2332.0	244.0
6.83	29060.0	13600.0	2384.0	278.0
12.83	31280.0	12920.0	2498.0	280.0
16.83	34440.0	12960.0	2636.0	300.0
31.83	34300.0	11520.0	2856.0	306.0
61.83	40900.0	11480.0	3842.0	338.0
91.83	47380.0	12200.0	4676.0	364.0
121.83	47980.0	14820.0	5042.0	366.0
151.83	49960.0	19400.0	5288.0	374.0
181.83	51300.0	22680.0	5590.0	390.0
241.83	50680.0	23040.0	5402.0	412.0
298.83	54320.0	24860.0	5620.0	451.0
331.83	56760.0	25420.0	6002.0	490.0
361.83	60260.0	26600.0	5952.0	556.0
391.83	60820.0	26900.0	5986.0	618.0
421.83	61720.0	26460.0	5968.0	642.0

Time (mins)	pH	Eh (mV)
0	0.3	487
10	0.39	346
30	0.47	338
60	0.59	336
90	0.77	320
120	0.94	322
150	1.22	334
180	1.51	344
240	1.81	355
297	1.88	353
330	1.9	350.4
360	1.88	349.1
390	1.89	346
420	1.88	346.9

**Test 24**

Time (mins)	Ni conc (ppm)	Cu conc (ppm)	Fe conc (ppm)	Co conc (ppm)
0	23640.0	18680.0	402.0	137.0
1.75	25280.0	18040.0	1874.0	210.2
6.75	25680.0	16020.0	2244.0	244.4
11.75	28700.0	15020.0	2294.0	258.8
16.75	30180.0	14580.0	2390.0	277.2
31.75	30420.0	12480.0	2478.0	288.8
61.75	36140.0	12800.0	2692.0	325.2
91.75	37220.0	12260.0	2884.0	322.8
121.75	41480.0	12320.0	3368.0	351.2
151.75	41640.0	11520.0	3652.0	350.4
181.75	45700.0	11460.0	4174.0	376.4
241.75	49360.0	12500.0	4996.0	390.6
271.75	49960.0	12920.0	5110.0	395.0
301.75	51060.0	14960.0	5220.0	408.8
361.75	48880.0	16720.0	5416.0	403.6
391.75	49460.0	18560.0	5536.0	411.8

Time (mins)	pH	Eh
0	0.43	468
15	0.55	334
30	0.63	323
60	0.49	320
90	0.56	301
120	0.67	322
150	0.67	320
185	0.75	305
240	0.81	311
270	0.9	308
300	0.97	310
360	1.3	318
390	1.37	332

*Mineralogical changes during Test 24*

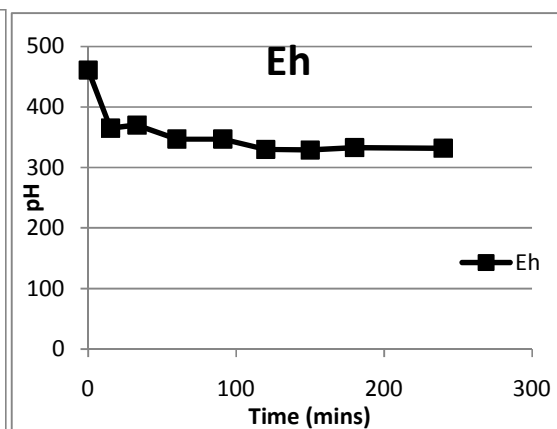
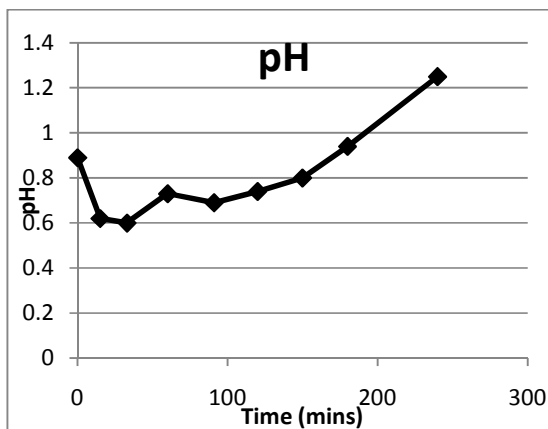
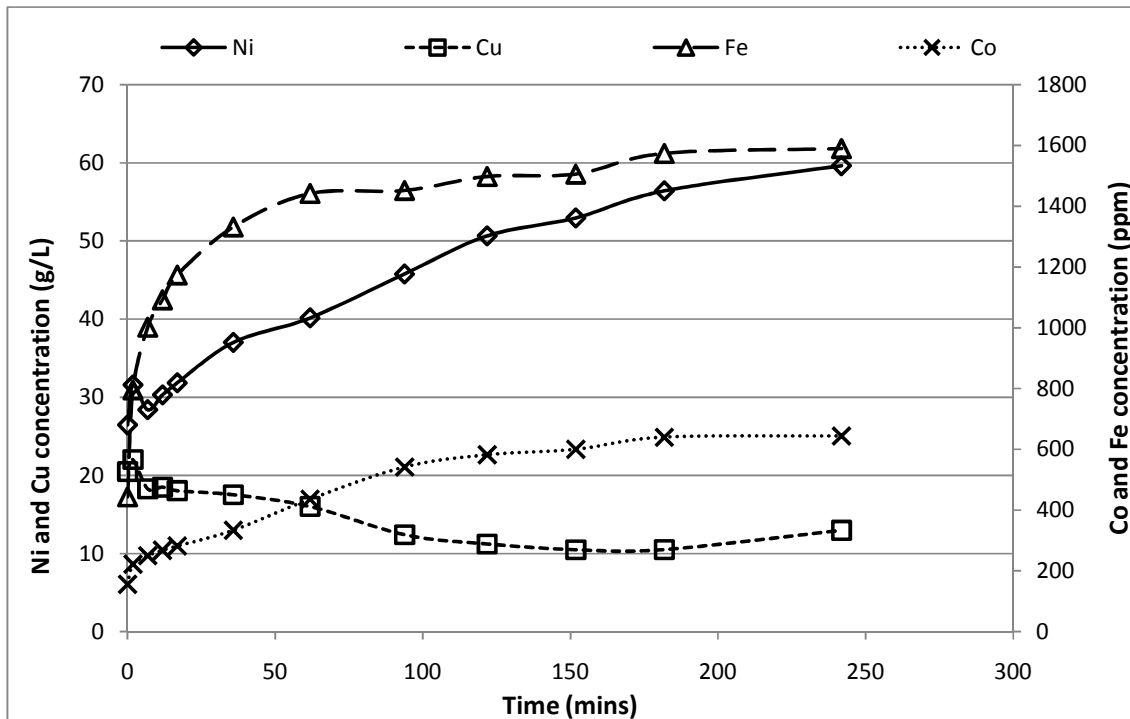
Sample times:		0	15	30	60	120	240	300	390
Mineral		Mass %							
<b>Ni-Cu</b>	Ni-Cu	2.1	1.2	2.8	3.9	8.3	0.0	0.3	0.0
<b>Heazlewoodite</b>	Ni <sub>3</sub> S <sub>2</sub>	56.9	45.8	35.6	24.1	10.8	11.5	4.5	2.5
<b>Godlevskite</b>	Ni <sub>7</sub> S <sub>6</sub>	2.9	3.6	11.5	13.5	18.1	21.3	14.0	9.0
<b>Millerite</b>	NiS	0.4	3.3	6.3	14.5	29.3	32.9	28.0	37.8
<b>Polydymite</b>	Ni <sub>3</sub> S <sub>4</sub>	0	0	0	0	0	0	0	11.1
<b>Pentlandite</b>	(NiFe) <sub>9</sub> S <sub>8</sub>	9.1	12.5	11.0	10.7	7.5	4.6	2.4	2.7
<b>Troilite</b>	FeS	0.4	0	0	0	0	0.3	0	0
<b>Magnetite</b>	Fe <sub>3</sub> O <sub>4</sub>	1.1	0.2	0.3	0	0.2	0	0	1.4
<b>Bornite</b>	Cu <sub>5</sub> FeS <sub>4</sub>	13.1	13.1	11.1	11.3	9.0	6.8	17.2	7.3
<b>Chalcocite</b>	Cu <sub>2</sub> S	15.3	18.7	19.8	20.0	16.8	22.8	21.6	8.4
<b>Djurleite</b>	Cu <sub>31</sub> S <sub>16</sub>	-	-	-	-	-	-	-	-
<b>Digenite</b>	Cu <sub>9</sub> S <sub>5</sub>	-	-	-	-	-	-	-	-
<b>Covellite</b>	CuS	0	1.6	1.7	2.1	0	0	12.1	19.9
<b>Cuprite</b>	Cu <sub>2</sub> O	-	-	-	-	-	-	-	-
<b>Antlerite</b>	Cu <sub>3</sub> SO <sub>4</sub> (OH) <sub>4</sub>	-	-	-	-	-	-	-	-
<b>Malachite</b>	Cu <sub>2</sub> CO <sub>3</sub> (OH) <sub>2</sub>	-	-	-	-	-	-	-	-

# Appendix F: Results from selected tests

## F.1 Oxidative tests

### Results from Test 19

Test conditions: 74 g/L acid, 20 g/L copper, 150 g solid / L, 500 rpm, 0.83 % Fe



Results from test 19 continued on next page



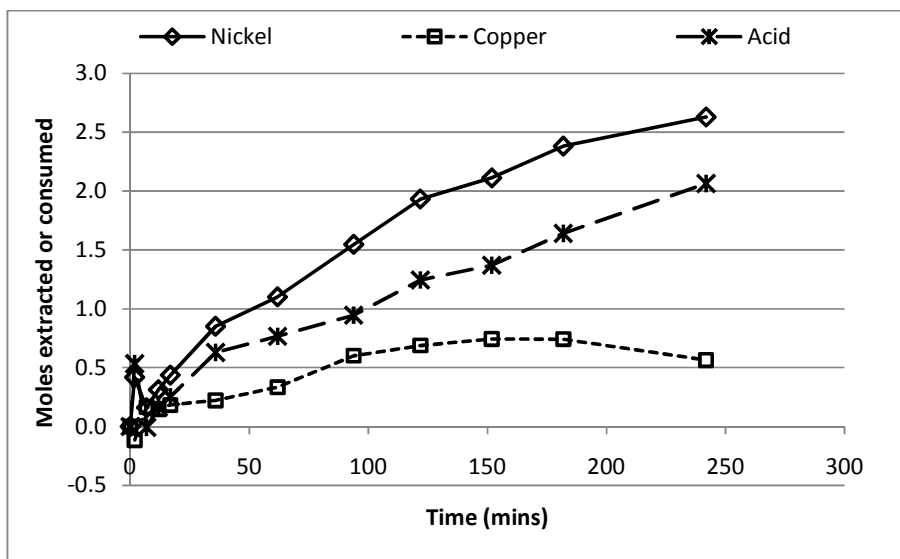
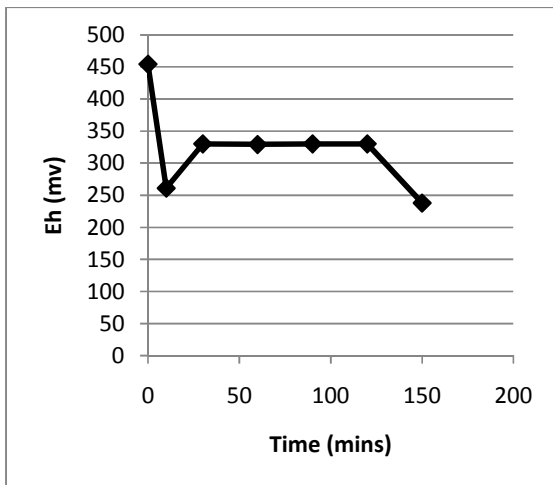
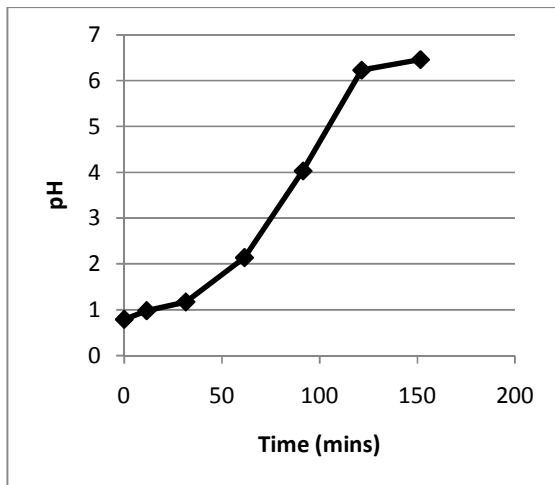
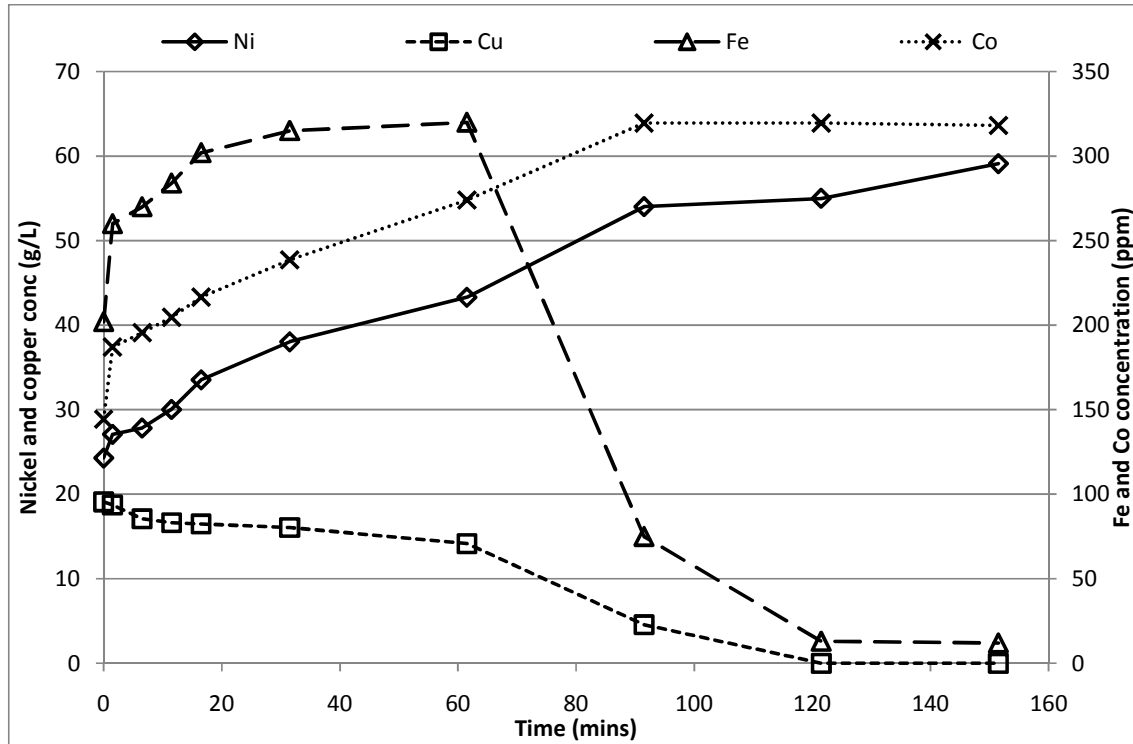


Table F-1 Mineralogical changes during Test 19: 74 g/L acid, 20 g/L copper, 150 g solid / L, 500 rpm, 0.83 % Fe

Sample time:		0	30	60	120	180	240
Mineral		Mass %					
Ni-Cu	Ni-Cu	15.4	5.2	1.1	0	0	0
Heazlewoodite	Ni <sub>3</sub> S <sub>2</sub>	61.3	56.3	51.4	10.9	2.8	3.1
Godlevskite	Ni <sub>7</sub> S <sub>6</sub>	0	0	0	16.8	15.8	11.8
Millerite	NiS	0	1.4	6.8	45.7	40.7	46.9
Polydymite	Ni <sub>3</sub> S <sub>4</sub>	-	-	-	-	-	-
Retgersite	NiSO <sub>4</sub> ·6H <sub>2</sub> O	-	-	-	-	-	-
Pentlandite	(NiFe) <sub>9</sub> S <sub>8</sub>	0.5	0.4	1.8	0	4.5	4.6
Troilite	FeS	0	1.7	1.9	1.7	2.5	1.1
Magnetite	Fe <sub>3</sub> O <sub>4</sub>	1.4	0.2	0.2	0.9	1	1.1
Bornite	Cu <sub>5</sub> FeS <sub>4</sub>	-	-	-	-	-	-
Chalcocite	Cu <sub>2</sub> S	21.5	34.9	36.9	0	0	0
Djurleite	Cu <sub>31</sub> S <sub>16</sub>	-	-	-	-	-	-
Digenite	Cu <sub>9</sub> S <sub>5</sub>	0	0	0	18.6	32.8	31.5
Covellite	CuS	0	0	0	5.5	0	0
Cuprite	Cu <sub>2</sub> O	-	-	-	-	-	-
Antlerite	Cu <sub>3</sub> SO <sub>4</sub> (OH) <sub>4</sub>	-	-	-	-	-	-
Malachite	Cu <sub>2</sub> CO <sub>3</sub> (OH) <sub>2</sub>	-	-	-	-	-	-

## Results from Test 21

Test conditions: 37 g/L acid, 20 g/L  $\text{Cu}^{2+}$ , 150 g solids / L, 1100 rpm, 0.53 % Fe



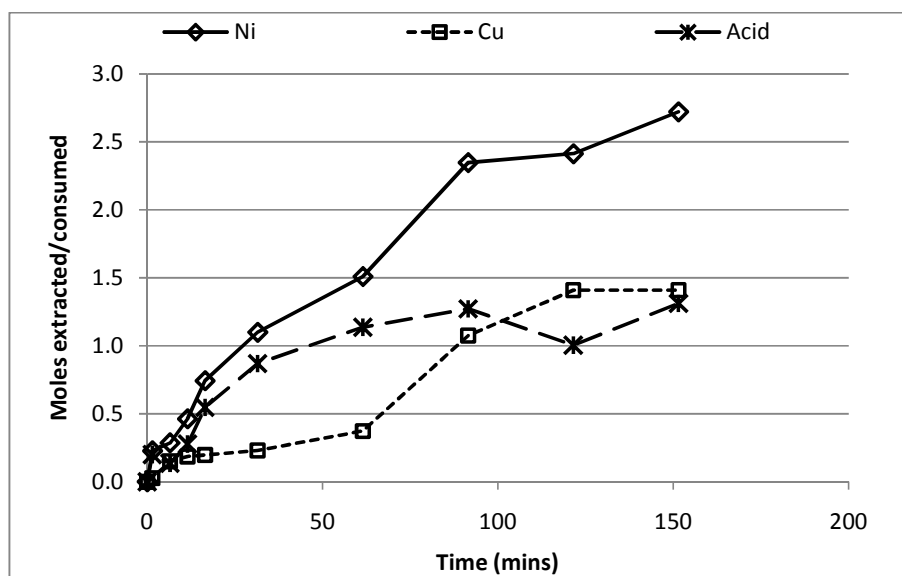
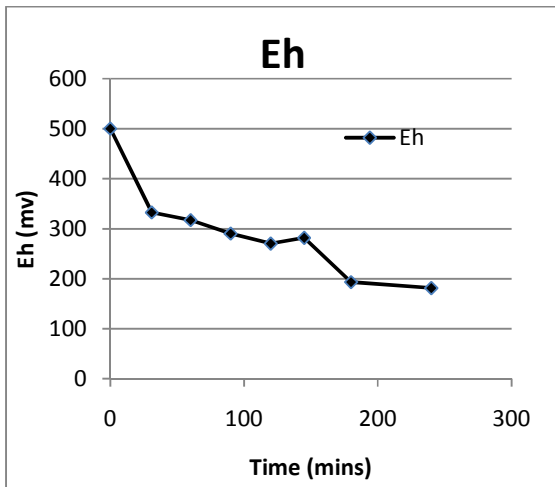
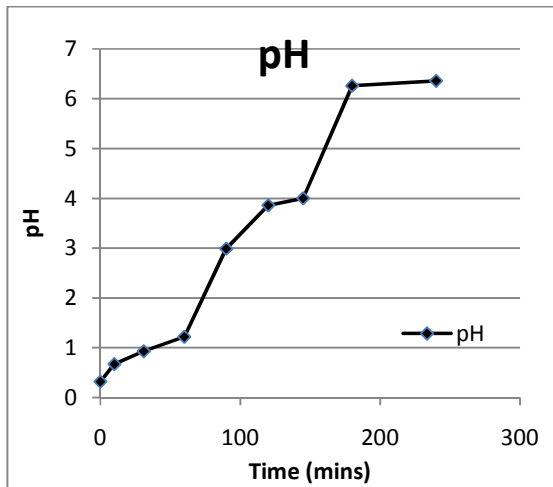
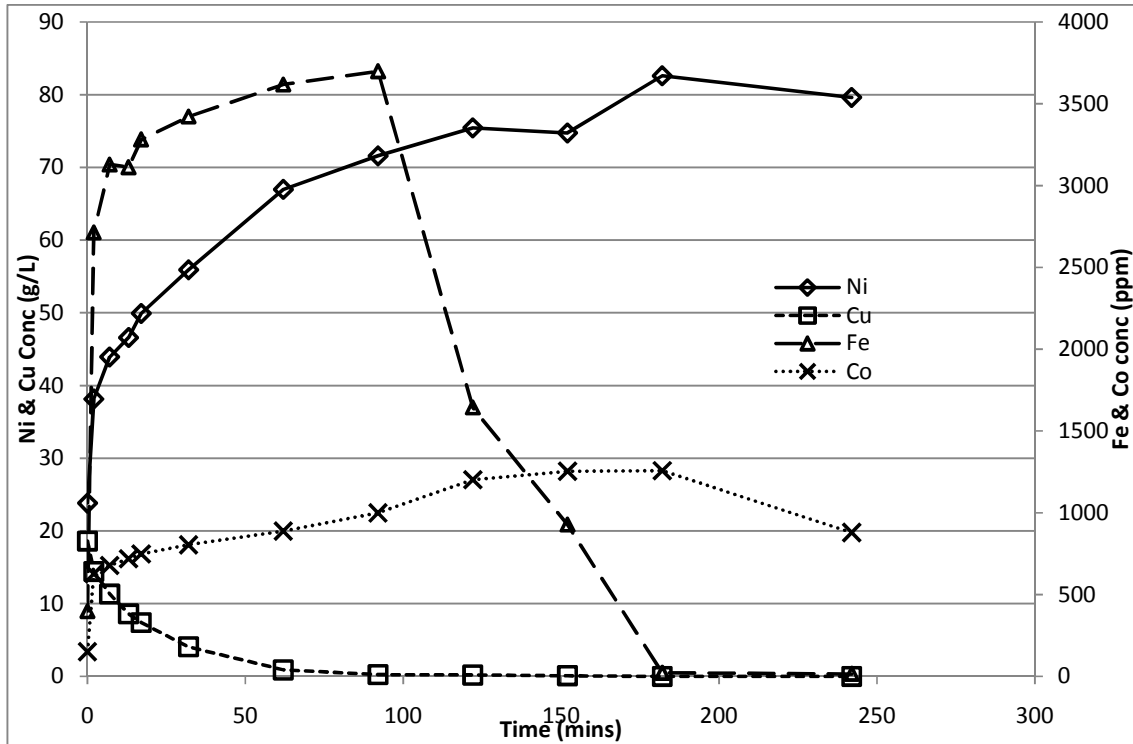


Table F.2 Mineralogical changes occurring during test 21.

Mineral	Sample time:	Mass %				
		0	15	30	60	150
Ni-Cu	Ni-Cu	19.7	12.4	10.8	4.7	2.0
Heazlewoodite	Ni <sub>3</sub> S <sub>2</sub>	51.9	47.7	48.8	50.6	4.7
Godlevskite	Ni <sub>7</sub> S <sub>6</sub>	0	3.2	3.2	1.7	5.2
Millerite	NiS	0	2.3	1.7	1.6	17.0
Polydymite	Ni <sub>3</sub> S <sub>4</sub>	-	-	-	-	-
Pentlandite	(NiFe) <sub>9</sub> S <sub>8</sub>	0	0.5	0	0	5.9
Troilite	FeS	0.9	0.7	0.8	1.5	2.8
Magnetite	Fe <sub>3</sub> O <sub>4</sub>	1.5	0.8	0.8	0.8	1.0
Bornite	Cu <sub>5</sub> FeS <sub>4</sub>	0	0.4	0.5	0.7	25.2
Chalcocite	Cu <sub>2</sub> S	26.0	32.0	33.4	38.5	36.4
Djurleite	Cu <sub>31</sub> S <sub>16</sub>	-	-	-	-	-
Digenite	Cu <sub>9</sub> S <sub>5</sub>	-	-	-	-	-
Covellite	CuS	-	-	-	-	-
Cuprite	Cu <sub>2</sub> O	-	-	-	-	-
Antlerite	Cu <sub>3</sub> SO <sub>4</sub> (OH) <sub>4</sub>	-	-	-	-	-
Malachite	Cu <sub>2</sub> CO <sub>3</sub> (OH) <sub>2</sub>	-	-	-	-	-

## Results from Test 22

Test conditions: 74 g/L acid, 20 g/L  $\text{Cu}^{2+}$ , 540 g solids/L, 1100 rpm, 1.05 % Fe



Results from test 22 continued on next page

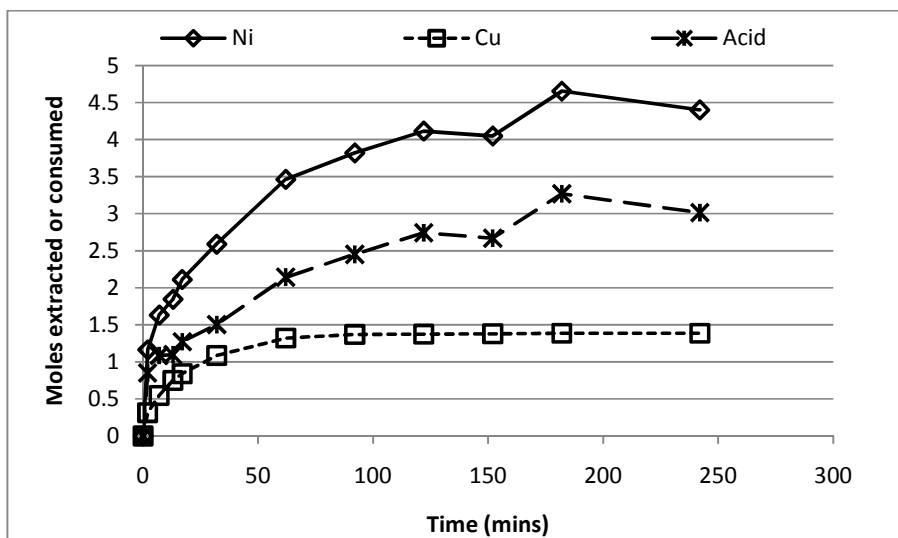


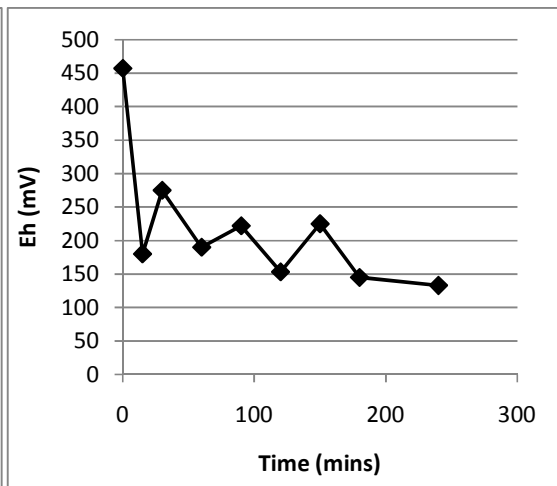
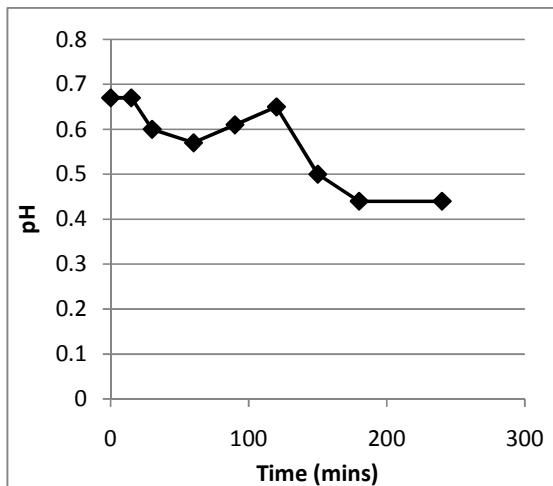
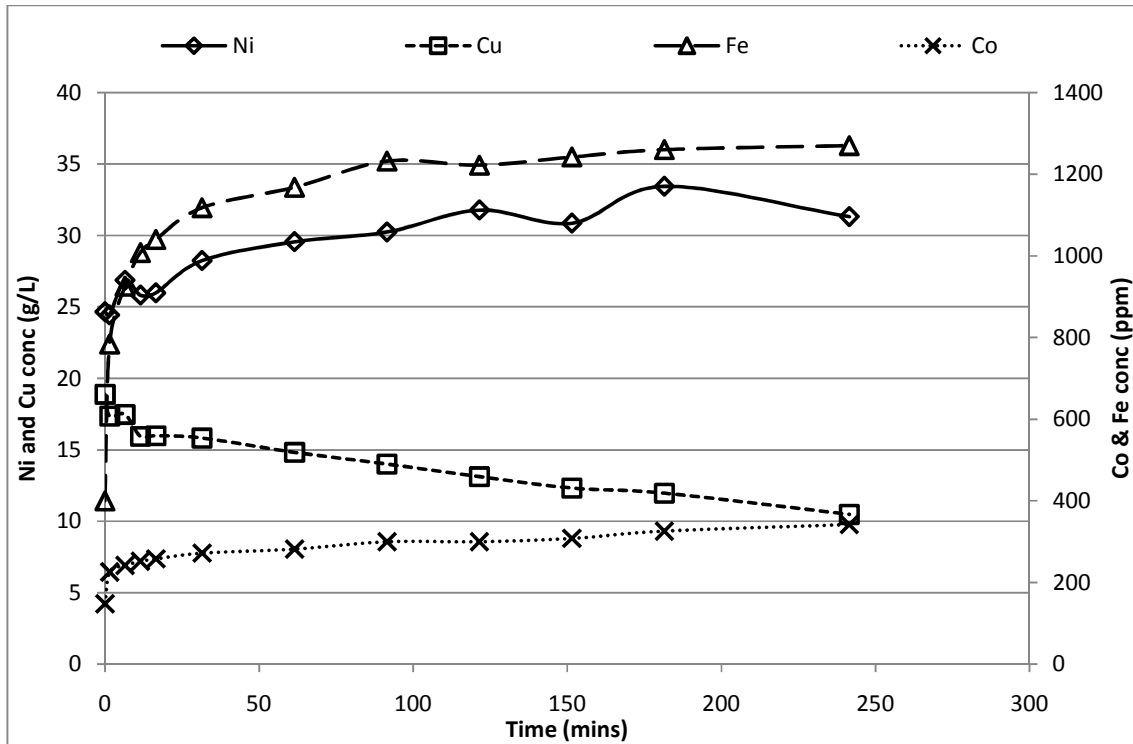
Table F.3 Mineralogical changes during test 22

Sample time:		0	15	60	120	180	240
Mineral		Mass %					
<b>Ni-Cu</b>	Ni-Cu	12.0	9.2	6.8	5.0	3.7	3.4
<b>Heazlewoodite</b>	Ni <sub>3</sub> S <sub>2</sub>	53.7	52.5	52.4	46.3	35.9	28.8
<b>Godlevskite</b>	Ni <sub>7</sub> S <sub>6</sub>	2.6	1.5	1.8	3.9	9.4	11.7
<b>Millerite</b>	NiS	2.7	2.3	2.2	6.7	11.3	16.2
<b>Polydymite</b>	Ni <sub>3</sub> S <sub>4</sub>	-	-	-	-	-	-
<b>Pentlandite</b>	(NiFe) <sub>9</sub> S <sub>8</sub>	0.4	0.4	0.3	0.2	0.2	0.3
<b>Troilite</b>	FeS	0.8	1.2	0.9	0.7	1.3	1.5
<b>Magnetite</b>	Fe <sub>3</sub> O <sub>4</sub>	1.7	0.1	0	0.2	0.2	0.1
<b>Bornite</b>	Cu <sub>5</sub> FeS <sub>4</sub>	0.7	0.4	1.1	1.1	1.7	2.6
<b>Chalcocite</b>	Cu <sub>2</sub> S	25.5	32.5	34.5	36.0	36.3	35.4
<b>Djurleite</b>	Cu <sub>31</sub> S <sub>16</sub>	-	-	-	-	-	-
<b>Digenite</b>	Cu <sub>9</sub> S <sub>5</sub>	-	-	-	-	-	-
<b>Covellite</b>	CuS	-	-	-	-	-	-
<b>Cuprite</b>	Cu <sub>2</sub> O	-	-	-	-	-	-
<b>Antlerite</b>	Cu <sub>3</sub> SO <sub>4</sub> (OH) <sub>4</sub>	-	-	-	-	-	-
<b>Malachite</b>	Cu <sub>2</sub> CO <sub>3</sub> (OH) <sub>2</sub>	-	-	-	-	-	-

## F.2. Results from non-oxidative tests

### Results from Test 5

Test conditions: 74 g/L acid, 20 g/L Cu, 150 g solids / L, 500 rpm, 0.83 % Fe



Results from test 5 continued on next page

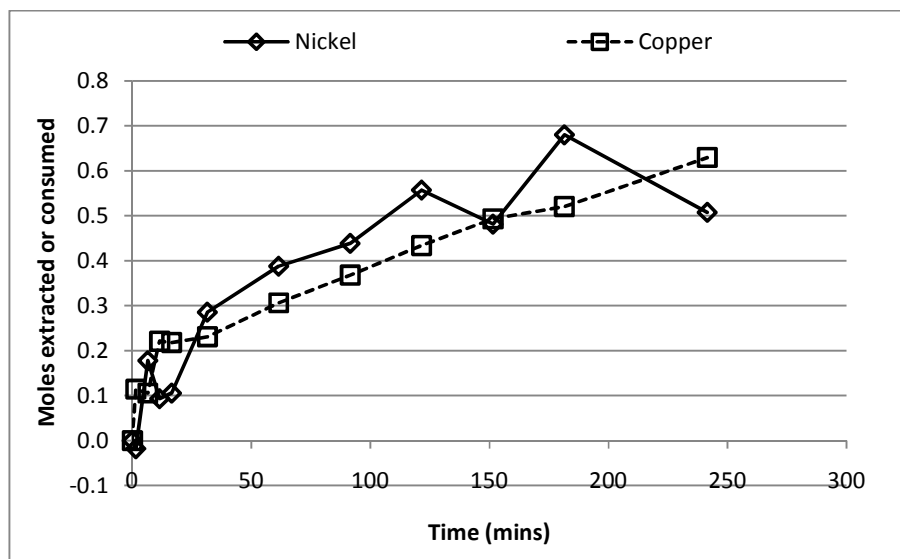
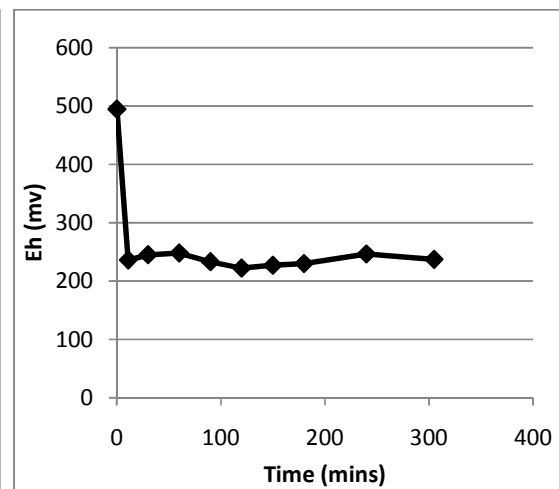
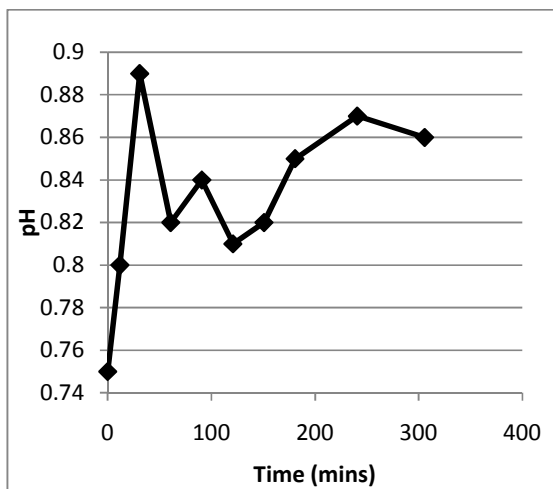
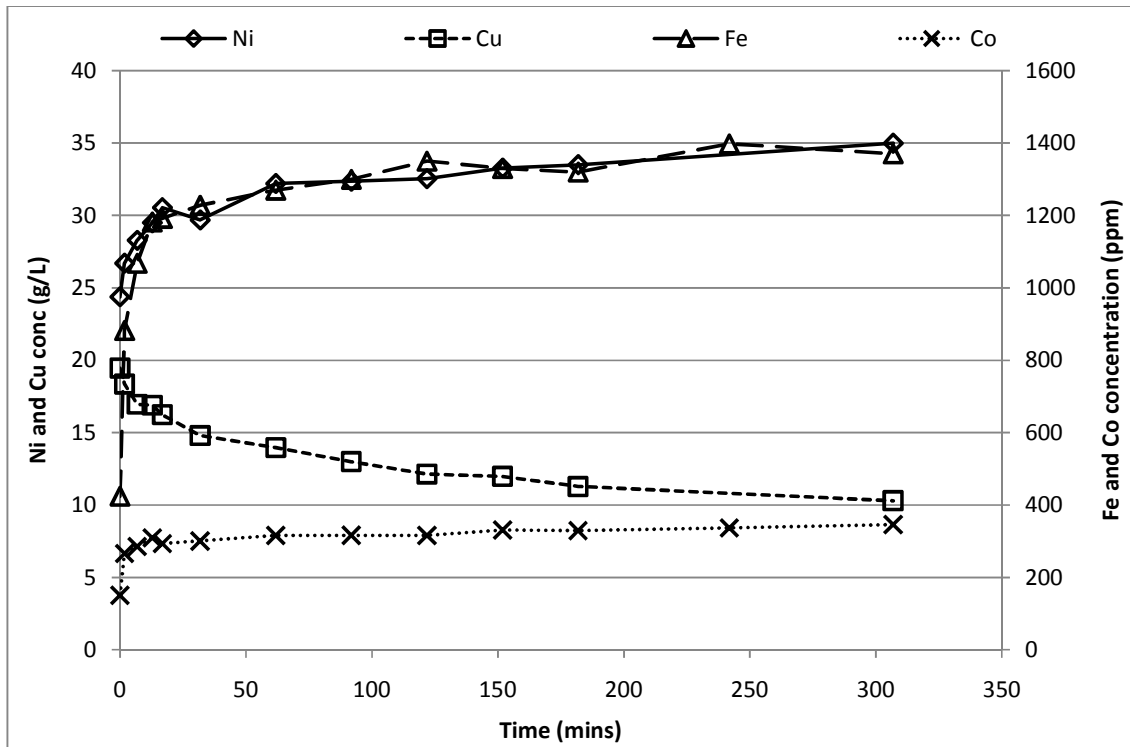


Table F.4 Mineralogical changes during test 5.

Sample times		0	30	60	120	180	240
Mineralogy		Mass %					
Ni-Cu	Ni-Cu	15.4	10.4	10.1	9.7	7.8	9.5
Heazlewoodite	Ni <sub>3</sub> S <sub>2</sub>	61.2	53.3	53.9	51.4	50.1	50.9
Godlevskite	Ni <sub>7</sub> S <sub>6</sub>	-	-	-	-	-	-
Millerite	NiS	0	1.5	0	1.3	2.2	2.9
Polydymite	Ni <sub>3</sub> S <sub>4</sub>	-	-	-	-	-	-
Pentlandite	(NiFe) <sub>9</sub> S <sub>8</sub>	0.5	0.4	0	0.6	0.6	0.6
Troilite	FeS	0	1.1	0.9	0.9	1.8	2.2
Magnetite	Fe <sub>3</sub> O <sub>4</sub>	1.4	0	0	0	0.1	0.1
Bornite	Cu <sub>5</sub> FeS <sub>4</sub>	-	-	-	-	-	-
Chalcocite	Cu <sub>2</sub> S	21.5	33.3	35.1	36.0	37.4	33.9
Djurleite	Cu <sub>31</sub> S <sub>16</sub>	-	-	-	-	-	-
Digenite	Cu <sub>9</sub> S <sub>5</sub>	-	-	-	-	-	-
Covellite	CuS	-	-	-	-	-	-
Cuprite	Cu <sub>2</sub> O	-	-	-	-	-	-
Antlerite	Cu <sub>3</sub> SO <sub>4</sub> (OH) <sub>4</sub>	-	-	-	-	-	-
Malachite	Cu <sub>2</sub> CO <sub>3</sub> (OH) <sub>2</sub>	-	-	-	-	-	-

## Results from Test 7

Test conditions: 37 g/L acid. 20 g/L Cu, 150 g solids / L, 1100 rpm, 0.89 % Fe



Results from test 7 continued on next page



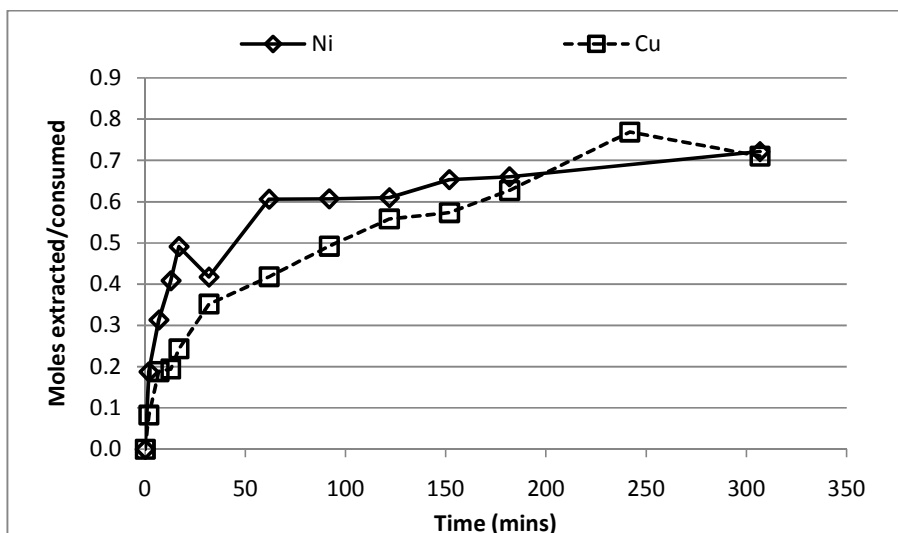
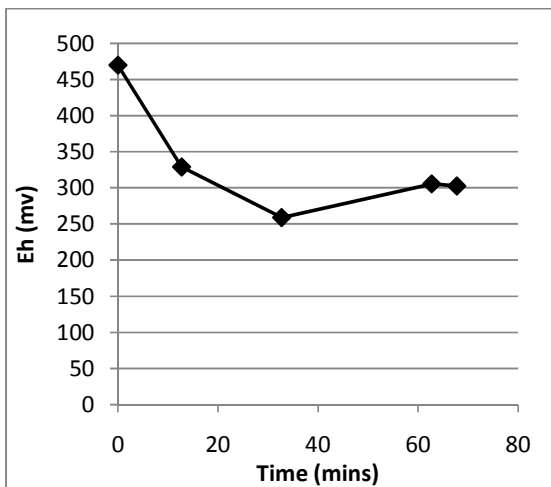
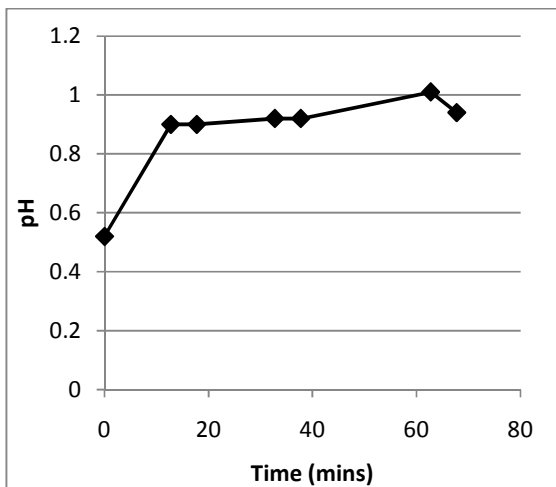
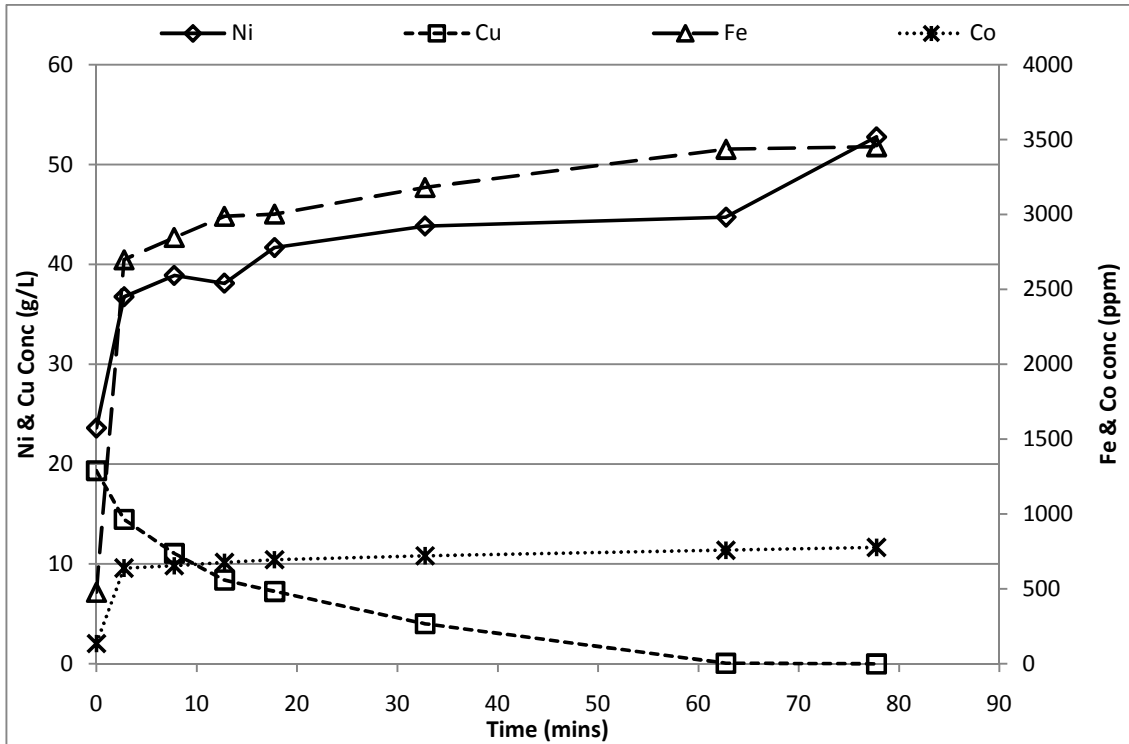


Table F.5 Mineralogical changes during test 7

Mineral		Mass %				
		0	15	100	180	300
<b>Ni-Cu</b>	Ni-Cu	12.4	9.2	8.9	7.6	6.7
<b>Heazlewoodite</b>	Ni <sub>3</sub> S <sub>2</sub>	53.8	53.9	52.4	49.9	48.4
<b>Godlevskite</b>	Ni <sub>7</sub> S <sub>6</sub>	4.4	4.0	3.8	3.2	3.0
<b>Millerite</b>	NiS	0	0.6	0	2.2	2.0
<b>Polydymite</b>	Ni <sub>3</sub> S <sub>4</sub>	-	-	-	-	-
<b>Pentlandite</b>	(NiFe) <sub>9</sub> S <sub>8</sub>	0.7	0.2	0	0.2	0.3
<b>Troilite</b>	FeS	0.9	0.6	0.6	0.8	0.8
<b>Magnetite</b>	Fe <sub>3</sub> O <sub>4</sub>	1.2	0	0	0	0
<b>Bornite</b>	Cu <sub>5</sub> FeS <sub>4</sub>	0	0.6	0.6	0.8	0.7
<b>Chalcocite</b>	Cu <sub>2</sub> S	26.8	31.0	33.9	35.4	38.1
<b>Djurleite</b>	Cu <sub>31</sub> S <sub>16</sub>	-	-	-	-	-
<b>Digenite</b>	Cu <sub>9</sub> S <sub>5</sub>	-	-	-	-	-
<b>Covellite</b>	CuS	-	-	-	-	-
<b>Cuprite</b>	Cu <sub>2</sub> O	0.2	0	0	0	0
<b>Antlerite</b>	Cu <sub>3</sub> SO <sub>4</sub> (OH) <sub>4</sub>	-	-	-	-	-
<b>Malachite</b>	Cu <sub>2</sub> CO <sub>3</sub> (OH) <sub>2</sub>	-	-	-	-	-

**Test 9**

Test conditions: 74 g/L acid, 20 g/L Cu, 520 g solids / L, 1100 rpm, 1.05 % Fe



Results from test 9 continued on next page

Table F.6. Mineralogical changes in test 9

Sample time		0	15	30	60
Mineral		Mass %			
<b>Ni-Cu</b>	Ni-Cu	11.5	9.0	7.3	8.3
<b>Heazlewoodite</b>	Ni <sub>3</sub> S <sub>2</sub>	53.6	55.3	54.8	52.3
<b>Godlevskite</b>	Ni <sub>7</sub> S <sub>6</sub>	3.0	1.5	0	2.6
<b>Millerite</b>	NiS	2.5	0.3	2.5	2.2
<b>Polydymite</b>	Ni <sub>3</sub> S <sub>4</sub>	-	-	-	-
<b>Pentlandite</b>	(NiFe) <sub>9</sub> S <sub>8</sub>	0.5	0.4	1.2	0.6
<b>Troilite</b>	FeS	0.8	0.7	0.5	0.5
<b>Magnetite</b>	Fe <sub>3</sub> O <sub>4</sub>	1.8	0.2	0.4	0.0
<b>Bornite</b>	Cu <sub>5</sub> FeS <sub>4</sub>	0.5	0.7		0.8
<b>Chalcocite</b>	Cu <sub>2</sub> S	25.8	32.0	33.3	32.7
<b>Djurleite</b>	Cu <sub>31</sub> S <sub>16</sub>	-	-	-	-
<b>Digenite</b>	Cu <sub>9</sub> S <sub>5</sub>	-	-	-	-
<b>Covellite</b>	CuS	-	-	-	-
<b>Cuprite</b>	Cu <sub>2</sub> O	-	-	-	-

## Appendix H: Size distribution of milled matte

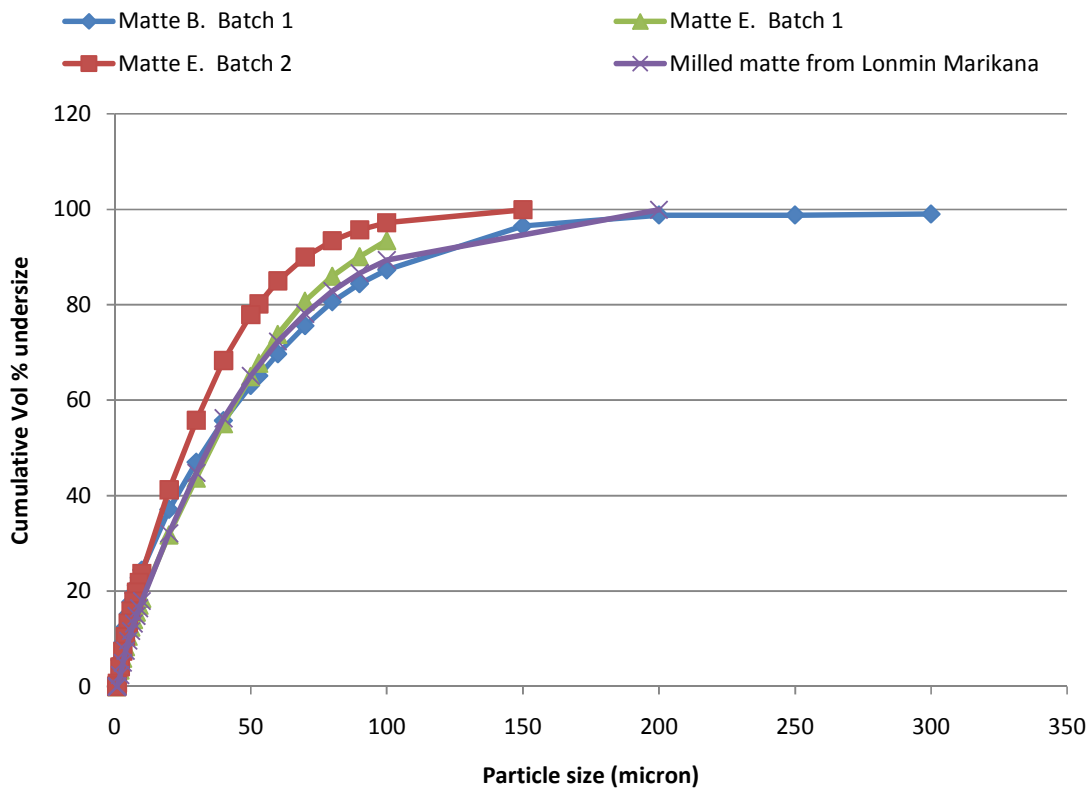


Figure 0-1 Comparison of size distributions of three batches of matte milled in the laboratory with milled matte received from Lonmin Marikana. Experimental data determined with Saturn Digisizer 5200 V1.10, using the Fraunhofer model.